

DISCOVERY OF NEW REACTIVITY AT COMPLEXES OF RHENIUM SUPPORTED BY
PCP, PNN, AND PNP PINCER LIGANDS AND THE STUDY OF PINCERS CONTAINING
ANCILLARY ANTIMONY DONORS

A Dissertation

by

ALEX JOAQUIM KOSANOVICH

Submitted to the Office of Graduate and Professional Studies of
Texas A&M University
in partial fulfillment of the requirements for the degree of

DOCTOR OF PHILOSOPHY

Chair of Committee,	Oleg V. Ozerov
Committee Members,	Michael Nippe
	Lei Fang
	Hung-Jue Sue
Head of Department,	Simon W. North

May 2019

Major Subject: Chemistry

Copyright 2019 Alex J. Kosanovich

ABSTRACT

The chemistry of pincer ligands is such that a wide variety of transition metals and main group elements are capable of being supported, stabilized, and isolated in often, highly reactive forms. The pincer ligands which have found the most utility are those based on the 1,3-*bis*(dialkylphosphinomethyl)benzene and 2,2'-*bis*(dialkylphosphine)diphenylamine ligand backbones. Herein, we have taken steps and report on the development of complexes of rhenium supported by PCP and PNP-related pincer ligands.

Described is the formation and characterization of the first complexes of rhenium supported by the parent PCP pincer ligand and the subsequent formation of multiple *polyhydrides*. The substitution of dihydrogen allowed access to mixed ligand species supported by the PCP pincer. The general salt metathesis reactivity as well as the generation of supposed five-coordinate (PCP)Re⁺ cations and their insertion reactivity was explored. Attention was then turned to the unusual and counter-intuitive reactivity of a novel rhenium-oxo-acetate supported by the PCP pincer. Against expected pK_a values, the rhenium-acetate undergoes completely irreversible hydrolysis to form a highly fluxional rhenium dioxo with an acetic acid adduct, featuring a significant hydrogen-bonding interaction. Aside from the substitution chemistry at (PCP)Re, the parent ligand was also found to, for the first time, be capable of undergoing a base-assisted dearomatization forming a “pseudo-carbene” which performs a metal-ligand cooperative activation of small molecules such as carbon dioxide. The nature of the rhenium-carbon bonding was studied spectroscopically, crystallographically, and computationally to determine significant Re-C π -bonding interactions.

PNP and proton-responsive PNN-type pincers were introduced into the coordination sphere of high-valent rhenium as well. They exhibited pronounced rotameric isomerism which was able to be studied on the NMR timescale. The reduction of high-valent (PNP)Re fragments also allowed for the isolation of Re(I)/Mn(I) dicarbonyls which exhibit metal-ligand cooperativity in the activation of acidic substrates such as formic acid. Finally, pincer ligands containing antimony donors in varying oxidation states were examined and their direct comparisons to phosphorous were made as well as their possible application in the binding of small molecules and formation of novel aromatics.

DEDICATION

To my father, Jerry, whose example of hard work, leadership, love, and intellect has helped to inspire and drive my journeys in life.

ACKNOWLEDGEMENTS

Thank you to Dr. Martha Low and Scott Sieling, who started me on this path. To Dr. Matt Whited, thank you for ensuring that I had the resources, mentorship, and education to explore this passion for chemistry. I cannot express enough gratitude to my Ph.D. advisor, Dr. Oleg Ozerov, who has put up with my questions, my over-the-top energy, and my foibles with compassion and guidance. Through your consistent patience, encouragement, and our many, many chemistry talks you have helped me to become a successful, independent organometallic chemist. I would also like to thank my committee members Dr. Michael Nippe, Dr. Lei Fang, and Dr. Hung-Jue Sue.

I would like to thank all the Ozerov group members past and present for their friendship. To Olivia, Ming-Uei, and Yihan, it has been a pleasure getting lunch and seeing your appreciation for rhenium chemistry. To Bryan Foley, who has been like a brother to me, thank you for your steady belief in God and what is right, I've appreciated it immensely these last few years. To Kelsey Schulte and David Kempe for helping keep fun alive. To Tom Malinski, thank you for being an incredible VP and helping things to run smoothly. Thank you also, to GSAC and NOBCCChE for allowing me to lead and to Dr. Batteas for facilitating my leadership. Also, to Ryan Smith, Christian Chaheine, and Joseph Baker: thank you for your enduring friendship.

I would like to thank my sisters Jana and Stephanie for their consistent love. To my best man, Tim Dugan and my duo partner, Terry Lund, I have nothing but love, and thank you for being there for me. To my father, Jerry Kosanovich who is the most excellent person I have ever known, you inspire me to greatness and have taught me how to effectively love people where they are at. To Josephine Patton, my future and my love, you are amazing and your support has been integral. I look forward to our life together and what we will make of it.

CONTRIBUTORS AND FUNDING SOURCES

This work was supervised by a thesis committee consisting of Professor Oleg V. Ozerov, Professor Michael Nippe, and Professor Lei Fang of the Department of Chemistry, and Professor Hung-Jue Sue of the department of Materials Science and Engineering.

The XRD structures in Chapter 2 were solved by Dr. Joseph Reibenspies (Department of Chemistry, TAMU). The XRD structures in Chapters 3, 5, and 6 were solved by Dr. Wei-Chun Shih during his time as a graduate student in the Department of Chemistry at Texas A&M. The XRD structures in Chapters 4, 7, and 8 were solved by Dr. Nattamai Bhuvanesh (Department of Chemistry, TAMU).

Cyclic voltammetry data in Chapter 7 was collected with assistance from Siyoung Sung during his time as a graduate student in the Nippe group at Texas A&M. IR spectroscopic data in Chapter 3 was in part collected with assistance from David Kempe during his time as a graduate student in the Dunbar group at Texas A&M. PNSb ligand syntheses in Chapter 7 were completed in part with assistance from Aldo M. Jordan during his time as an REU student at Texas A&M. Computational results in Chapter 4 were calculated by Christopher Komatsu during his time as a graduate student in the Wooley group at Texas A&M, and by Dr. Lisa M. Perez (Laboratory for Molecular Simulation at Texas A&M). The Initial synthesis of **501** in Chapter 5 was completed by Dr. Rodrigo Ramirez during his time as a graduate student in the Ozerov group at Texas A&M.

All other work conducted for this dissertation was completed by the student independently.

This work was made possible in part by support from the Welch Foundation (grant A-1717 to O. V. O.), the US National Science Foundation (HRD-1406755 to A. J. K.; CHE-1610311; CHE-1565923 to O. V. O.), and the National Institutes of Health (MARC-T34GM008048 to A. M. J.). Its contents are solely the responsibility of the authors and do not necessarily represent the official view of the U.S. National Science Foundation, the Welch Foundation, or the National Institutes of Health.

NOMENCLATURE

Ar	Aryl
BArF ₂₀	Tetrakis(pentafluorophenyl)borate
Cp	Cyclopentadienyl
Cp*	1,2,3,4,5-Pentamethylcyclopentadienyl
COD	1,5-Cyclooctadiene
COE	Cyclooctene
Chloranil	3,4,5,6-tetrachloro <i>ortho</i> quinone
DFT	Density Functional Theory
DHBTA	Dehydrogenative Borylation of Terminal Alkynes
dmap	4-Dimethylaminopyridine
Et	Ethyl
HOAc	Acetic acid, ethanoic acid
iPr	<i>Isopropyl</i>
LAH	Lithium Aluminum Hydride
Me	Methyl
Mes	Mesityl
NaOAc	Sodium Acetate
NBO	Natural Bond Orbital
nBu	<i>n</i> -butyl
NMR	Nuclear Magnetic Resonance
OAc	Acetate

OTf	Trifluoromethanesulfonate, triflate
PCP ^{iPr}	1,3-Bis(diisopropylphosphinomethyl)benzene
PCP ^{tBu}	1,3-Bis(ditertbutylphosphinomethyl)benzene
Ph	Phenyl
tBu	<i>Tert</i> butyl
TBE	<i>Tert</i> butylethylene
THF	Tetrahydrofuran
TMS	Trimethylsilyl
XRD	X-ray diffraction

TABLE OF CONTENTS

	Page
ABSTRACT.....	ii
DEDICATION.....	iv
ACKNOWLEDGEMENTS.....	v
CONTRIBUTORS AND FUNDING SOURCES.....	vi
NOMENCLATURE.....	viii
TABLE OF CONTENTS.....	x
LIST OF SCHEMES.....	xiv
LIST OF FIGURES.....	xx
CHAPTER I INTRODUCTION AND LITERATURE REVIEW.....	1
1.1 Introduction and Overview.....	1
1.2 Pincer Ligands.....	1
1.3 PCP-Type Pincer Ligands.....	4
1.3.1 Different Types of PCP Ligands.....	4
1.3.2 Late Transition Metal Chemistry with Aryl Based PCP Pincer Ligands.....	7
1.4 Pincer Ligands Based on a Diarylamine Backbone.....	12
1.4.1 Diverse Pincer Ligands Based on Diarylamines.....	12
1.4.2 PNP Pincer Ligands in Catalysis.....	15
1.5 An Introduction to the Chemistry of Rhenium.....	18
1.5.1 Metal-Ligand Multiple Bonding in Complexes of Rhenium.....	18
1.5.2 Catalytic Applications of High-Valent Rhenium Species.....	20
1.5.3 Chemistry of Rhenium in a Pincer Ligand Context.....	22
1.5.4 Rationale for Exploring the Chemistry of Pincer-Supported Rhenium.....	25
1.6 Antimony Based Ligands for Transition Metal Complexes.....	26
1.6.1 Stibine-Transition Metal Complexes.....	26
1.6.2 Redox Activity of Antimony.....	29
1.6.3 Antimony as a Potent Lewis Acid for Anion Binding.....	32
1.7 Conclusion and Overview.....	36

CHAPTER II COMPLEXES OF HIGH-VALENT RHENIUM SUPPORTED BY THE PCP PINCER	37
2.1 Introduction.....	37
2.2 Results and Discussion	38
2.2.1 Synthesis of Re(V) Oxo Complexes	38
2.2.2 Synthesis of a Rhenium <i>Polyhydride</i> Complex	43
2.2.3 Reactivity of the (PCP)Re <i>Polyhydride</i>	45
2.2.4 Metathesis Reactivity of (PCP ^{iPr})ReOCl ₂	51
2.2.5 Generation and Reactivity of the (PCP ^{iPr})ReOMe ⁺ Cation.....	53
2.3 Conclusion	55
2.4 Experimental	56
2.4.1 General Considerations.....	56
2.4.2 Synthesis and Characterization of Rhenium Complexes.....	57
 CHAPTER III THE IRREVERSIBLE HYDROLYSIS OF PCP-SUPPORTED RHENIUM(V) ACETATES	 68
3.1 Introduction.....	68
3.2 Results and Discussion	69
3.2.1 Synthesis of (PCP ^{tBu})ReOCl ₂ and Formation of the Hexahydride	69
3.2.2 Installation and Observed Hydrolysis of a Rhenium-Acetate Bond.....	71
3.2.3 Accessing (PCP)ReO(OAc) ₂ and Mechanistic Inquiry	71
3.2.4 Structural and Spectroscopic Study of (PCP)ReO(OAc)(OH)	72
3.2.5 Isolation and Reactivity of a Relevant (PCP)ReO ₂ Species	74
3.3 Conclusion	75
3.4 Experimental	75
3.4.1 General Considerations.....	75
3.4.2 Synthesis and Characterization of Rhenium Complexes	76
3.4.3 Reactivity of Rhenium Complexes	82
 CHAPTER IV DEAROMATIZATION OF THE PCP PINCER LIGAND IN A RHENIUM(V) OXO COMPLEX.....	 89
4.1 Introduction.....	89
4.2 Results and Discussion	91
4.2.1 Initial Observations of PCP Ligand Dearomatization	91
4.2.2 Spectroscopic Study of a Dearomatized P*CP-Re Complex.....	91
4.2.3 Structural Study of (P*CP)ReOCl	92
4.2.4 Computational Analysis of (P*CP)ReOCl.....	93
4.2.5 Cycloaddition Reactivity of (P*CP)ReOCl with CO ₂	96
4.2.6 Halide Metathesis and Structural Study of CO ₂ Cycloaddition Product	98
4.3 Conclusion	99
4.4 Experimental	100

4.4.1 General Considerations	100
4.4.2 Computational Details and Optimization.....	100
4.4.3 Synthesis and Characterization of the (P*CP)Re Complexes.....	101
 CHAPTER V N-H CLEAVAGE AS A ROUTE TO NEW Pincer COMPLEXES OF HIGH-VALENT RHENIUM.....	 108
5.1 Introduction.....	108
5.2 Results and Discussion	110
5.2.1 Synthesis and Metalation of Diarylamido Ligands.....	110
5.2.2 Structural and Spectroscopic Study of PNP and PNN Complexes.....	111
5.2.3 Dehydrohalogenation of (PNN ^H)ReOX ₂ complexes	116
5.2.4 Reaction with Trimethylphosphine.....	117
5.2.5 Chloride Metathesis Reactivity of (PNN)ReOCl.....	119
5.2.6 Structural and Isomerism Analysis	120
5.3 Conclusion	124
5.4 Experimental.....	124
5.4.1 General Considerations.....	124
5.4.2 Synthesis and Characterization of PNP and PNN Complexes.....	125
 CHAPTER VI SYNTHESIS AND REACTIVITY OF UNSATURATED CARBONYL COMPLEXES OF RHENIUM AND MANGANESE SUPPORTED BY THE PNP Pincer.....	 138
6.1 Introduction.....	138
6.2 Results and Discussion	140
6.2.1 Synthesis of (PNP)M(CO) ₃ (M = Mn, Re)	140
6.2.2 Hydrobrominative Decarbonylation of (PNP)M(CO) ₃ (M = Mn, Re)	141
6.2.3 Synthesis of Unsaturated (PNP)M(CO) ₂ (M = Mn, Re).....	142
6.2.4 Structural Study of (PNP)Re(CO) ₂	144
6.2.5 Carbonyl Reactivity of (PNP)M(CO) ₂ (M = Mn, Re)	145
6.2.6 Further Reactivity of (PNP)Re(CO) ₂ (606)	146
6.3 Conclusion	150
6.4 Experimental.....	151
6.4.1 General Considerations.....	151
6.4.2 Synthesis and Reactivity of Manganese and Rhenium Complexes	151
 CHAPTER VII Pincer LIGANDS CONTAINING ANCILLARY ANTIMONY DONORS	 161
7.1 Introduction.....	161
7.2 Results and Discussion	163
7.2.1 Synthesis and Spectroscopic Characterization of PNSb Ligands.....	163
7.2.2 Metalation of the PNSb Ligand to Rhodium, Palladium, and Iridium	164
7.2.3 Spectroscopic Analysis of PNSb ^{Ph} Complexes.....	165

7.2.4 Infrared and Electrochemical Analysis of PNSb^{Ph} Complexes	166
7.2.5 Structural Characterization and Analysis of the PNSb^{Ph} Ligand.....	168
7.2.6 Metalation of PNSb^{tBu} to Rhodium, Iridium, and Palladium.....	170
7.2.7 Catalytic Activity of PNSb -Iridium Complexes in DHBTA	171
7.3 Conclusion	173
7.4 Experimental	173
7.4.1 General Considerations.....	173
7.4.2 Synthetic Details for Antimony-Containing Complexes	175
 CHAPTER VIII OXIDATION OF A BIS-STIBINO AMINE AND SPONTANEOUS FORMATION OF A STIBAACRIDINIUM.....	 183
8.1 Introduction.....	183
8.2 Results and Discussion	184
8.2.1 Synthesis of SbNSb	184
8.2.2 Oxidation of SbNSb with MeOTf	185
8.2.3 Oxidation of SbNSb with Chloranil.....	186
8.2.4 Structural Consideration of 804	190
8.2.5 Reaction with Fluoride and Reformation of Stibaacridinium Cation	192
8.3 Conclusion	195
8.4 Experimental	195
8.4.1 General Considerations.....	195
8.4.2 Synthesis of Sb -complexes	196
 CHAPTER IX CONCLUSIONS	 205
 REFERENCES	 207
 APPENDIX A LIST OF PUBLICATIONS RESULTING FROM PHD WORK.....	 225

LIST OF SCHEMES

	Page
Scheme I-1. Examples of L, X, and Z-type ligand interactions with a generic metal center	2
Scheme I-2. Examples of bidentate ligands containing oxygen, nitrogen, and phosphorous donors	2
Scheme I-3. Representation of generic metal complexes supported by Tp and PCP ligands in facial and meridional fashion, respectively	3
Scheme I-4. Array of named pincer ligands and relative <i>trans</i> influence and pi donicity properties.....	4
Scheme I-5. Photochemical dehydrogenation and subsequent carbenic rearrangement at an alkyl-based PCP iridium	5
Scheme I-6. (A) Double C-H activation of a dipyrrolyl methane type PCP ligand results in formation of a (PC=P)Ru(II) species. (B) A highly reactive central carbene donor is capable of acting in concert with an iridium center to extrude N ₂ from N ₂ O and efficiently abstract the O-atom to form a novel iridaepoxide species	6
Scheme I-7. Formation of a nucleophilic PCP-type Pd-carbene species. Reactions are shown with carbon based and protic electrophiles involving metal-ligand cooperation	7
Scheme I-8. Schematic showing different types of generic arene based PCP complexes	8
Scheme I-9. Catalytic alkyne dimerization, Kumada coupling, and C-S bond formation mediated by a (POCOP)Rh(H)(Cl) precatalyst.....	9
Scheme I-10. Catalytic arene C-H borylation and boryl transfer to small molecules (ethylene) mediated by POCOP supported complexes of Ir.....	10
Scheme I-11. (A) (PCP)Ir-catalyzed transfer dehydrogenation of aliphatic substrates (B) Tandem Ir/Mo catalysis to achieve a “net alkane metathesis”	11
Scheme I-12. General scheme for the <i>ortho</i> functionalization of the diarylamine backbone	12

Scheme I-13. (A) Reversible electrochemical oxidation of a diarylamine based pincer ligand to form an aminyl radical cation (B) Examples of redox active pincer complexes based on various diarylamine cores	13
Scheme I-14. (A) (PNP)Ti activation of the C=N bond in pyridine (B) First lutetium (Lu) phosphinidene (C) Divergent C-H/C-X oxidative addition to (PNP)M (M =Ir, Rh) species.....	14
Scheme I-15. (A) Catalytic Heck coupling mediated by a PNP-supported Pd complex with a possible by unlikely Pd(IV) species shown (B) Typical Heck coupling mechanism mediated by Pd(0)	15
Scheme I-16. Generation of a 14-electron (PNP)Ir fragment and generation of active catalysts for alkene hydrosilylation and C-H borylation of terminal alkynes	17
Scheme I-17. Common rhenium starting materials in the +7, +5, and +1 oxidation states.....	19
Scheme I-18. Diagram showing orbital interactions of rhenium-oxo multiple bonding and progression of electrons filling a generic d-orbital manifold to create a pseudo d ⁶ rhenium center	19
Scheme I-19. Schematic of Re ₂ O ₇ catalyzed olefin metathesis on a Al ₂ O ₃ solid support.....	21
Scheme I-20. Representation of Re(V) catalyst formation and subsequent activation of Si-H bond.....	21
Scheme I-21. Deoxydehydration (DODH) catalyzed by Re ₂ O ₇ at high temperature	22
Scheme I-22. (A) Redox active ONO-Re complex (B) FLP-type alkene hydrogenation catalysis using a Lewis basic Re-oxo fragment in concert with a triarylborane Lewis acid (C) Direct insertion of CO into a Re-Me, notable for not proceeding <i>via</i> pre-coordination.....	23
Scheme I-23. Thermal rearrangement of a (PNP)ReOCl ₂ species <i>via</i> double silyl migration to form a new, (POP)Re(N)Cl ₂ complex.....	24
Scheme I-24. Reaction of an operationally unsaturated <i>tetrahydride</i> , (PNP ^R)ReH ₄ with cyclohexane resulting in formation of a 1,1-cyclohexylidene. Reaction of either the <i>tetrahydride</i> or the previously acquired carbene with a methyl-containing reagent results in C-H activation and formation of a rhenium hydridocarbene species.....	25

Scheme I-25. Pnictogen donors with bulky <i>tert</i> butyl substituents. Stibine and phosphine varieties are stable and isolable, whereas the corresponding amine degrades <i>via</i> alkene elimination.....	27
Scheme I-26. Increasing s-character of the lone pair moving from amine to phosphine to stibine	28
Scheme I-27. (A) Coordination of triarylstibines to Au(I) (B) Bidentate stibine coordination to Ru(II) (C) tris(<i>isopropyl</i>)stibine coordination to Ir(I) and Ir(III) centers and observable ligand isomerism	29
Scheme I-28. General reactions that form Sb(V) products from SbPh ₃ as an Sb(III) example	30
Scheme I-29. Examples of photoreductive elimination of chlorine from PSbP pincer ligated Pt and Pd species to form counter-intuitive mixed-valence species	31
Scheme I-30. Oxidation of a trialkyl stibine, Sb(III) to Sb(V) and subsequent thermal elimination of an alkyl halide to form the desired Sb(III) complex	32
Scheme I-31. Si/B-based Lewis acid mediated hydrodefluorination and hydroarylation	33
Scheme I-32. Fluoride anion binding to highly Lewis acidic Sb(III) and Sb(V) species. Epoxide/isocyanate cyclization catalyzed by an Sb(V) cation. Intramolecular Sb Lewis acid stabilization of a terminal Sb=O moiety	34
Scheme I-33. Deepening of the “σ-hole” by oxidation to Sb(V) and “Magic acid” generation	35
Scheme II-1. Examples of rhenium complexes supported by pincer ligands Featuring central amido and pyridyl donors	38
Scheme II-2. Synthesis of PCP-rhenium 1:1 adduct (201) and subsequent C-H activation to access (PCP ^{iPr})ReOCl ₂ (202).....	39
Scheme II-3. Halide metathesis reactivity of 202 with trimethylsilylhalide reagents	42
Scheme II-4. Reduction of 202 using an excess of LAH to form the hexahydride 205 ...	44
Scheme II-5. Synthesis of (PCP)ReH ₄ (L) species <i>via</i> introduction of PMe ₃ or DMAP...46	
Scheme II-6. Synthesis of the rhenium(I) tricarbonyl, 208 , by addition of CO to 205	49
Scheme II-7. Dehydrogenative dimerization of 202 <i>via</i> loss of 3/2 H ₂	51

Scheme II-8. Salt metathesis reactivity of 202 with PhLi, NaOMe, and MeMgCl	52
Scheme II-9. Generation and preliminary reactivity of the (PCP ^{iPr})ReOMe ⁺ fragments.....	54
Scheme III-1. (A) Hydrolysis of a generic metal acetate (B) Equilibrium hydrolysis of a Pd-OAc bond in Pd(OAc) ₂	69
Scheme III-2. Synthesis and reactivity of PCP-supported rhenium complexes	70
Scheme III-3. Possible interconversion between degenerate C _s -symmetric structures of 303 . H-bonding interaction is shown between OAc and OH ligands	74
Scheme IV-1. Generic depiction of HX loss from pyridine-based PNP complexes and an example of dearomatization of a hydroxyl-substituted PCP complex	90
Scheme IV-2. Dearomatization of 301 <i>via</i> base mediated dehydrochlorination	91
Scheme IV-3. Graphical representation of (P*CP)ReOCl (401) showing experimentally (black) and computationally (blue) determined bond distances	95
Scheme IV-4. Reactions of 401 with H ₂ and CO ₂ and the synthesis of iodo derivatives 403 and 404	97
Scheme V-1. (top) Examples of pincer-supported rhenium with a central amido-, amino-, or pyridyl-type donor (bottom) ligands utilized in this study ...	109
Scheme V-2. Synthesis of PNN ^H proligand 501	110
Scheme V-3. Synthesis of PNP and PNN complexes of rhenium	111
Scheme V-4. Two different rotamers/enantiomers possible for (PNP)ReOCl ₂ (502)	115
Scheme V-5. Alternate view of (PNN ^H)ReOCl ₂ (503) and representative schematic of observed proximity of benzylic methyl protons with PNN ^H ligand's aromatic backbone, leading to ring current effects	116
Scheme V-6. Reversible deprotonation of (PNN ^H)ReOX ₂ (503/504) to give (PNN)ReOX (505/506).....	117
Scheme V-7. Reaction of (PNN)ReOCl (505) with PMe ₃ to form (PNN)ReOCl(PMe ₃) (507) in isomeric ratios. One possible isomer is shown	118

Scheme V-8. Chloride metathesis reactions with (PNN)ReOCl (505).....	119
Scheme V-9. Representation of different possible rotameric diastereomers envisioned for the PNN-type framework	123
Scheme VI-1. (A) Examples of saturated pincer-supported rhenium <i>polycarbonyls</i> (B) unsaturated PNP-supported Mn <i>dicarbonyls</i> and (C) PNP supported Re <i>di-carbonyls</i>	139
Scheme VI-2. Synthesis of saturated PNP-supported Mn and Re <i>poly-carbonyls</i>	141
Scheme VI-3. Hydrobrominative decarbonylation of <i>tricarbonyls</i>	142
Scheme VI-4. Facile dehydrohalogenation to access unsaturated, <i>dicarbonyl</i> species ...	143
Scheme VI-5. Reaction to gauge preliminary carbonyl affinity of (PNP)Re(CO) ₂	146
Scheme VI-6. Catalytic alkyne dimerization of trimethylsilylacetylene	147
Scheme VI-7. Possible origins of fluxionality observed in reaction of HOAc addition to 606	148
Scheme VI-8. Formation and presumed, selective thermal decomposition of rhenium-formate	149
Scheme VII-1. Comparison of ⁱ PrPNP ^{Ph} and ⁱ PrPNSb ^{Ph} complexes.....	162
Scheme VII-2. Synthesis of PNSb Pincer Ligands.....	163
Scheme VII-3. Metalation of the ⁱ PrPNSb proligand.....	165
Scheme VII-4. Selected metrics from the X-ray structures of (ⁱ PrPNSb ^{Ph})Rh(CO) (702) and (ⁱ PrPNP ^{Ph})Rh(CO)	169
Scheme VII-5. Metalation of the ⁱ PrPNSb ^{tBu} proligand.....	171
Scheme VII-6. Catalytic dehydrogenative borylation of terminal alkynes by PNSb complexes of iridium	172
Scheme VIII-1. Examples of multidentate, Sb-containing ligands.....	183
Scheme VIII-2. Synthesis of SbNSb (801).....	184
Scheme VIII-3. Oxidation of 801 to 802 using an excess of MeOTf.....	185

Scheme VIII-4. Oxidation of 801 with chloranil leading to crystallographic Observation of <i>bis</i> -stiboranyl amine-THF adduct 803	187
Scheme VIII-5. Rearrangement of <i>bis</i> -stiboranyl amine to ionic isomer 804	189
Scheme VIII-6. Previous examples of ionizing rearrangements of stiborane catecholates to stibonium antimonate salts	190
Scheme VIII-7. Possible resonance contributors for 804 cation.....	192
Scheme VIII-8. Synthesis of neutral fluorostiborane and net anion metathesis with TMSOTf.....	193

LIST OF FIGURES

	Page
Figure II-1. ORTEP drawing (50% probability ellipsoids) of (PCP ^{iPr})ReOCl ₂ (202). H atoms and a disordered molecule of cocrystallized toluene omitted for clarity. Selected distance (Å) and angles (°) follow: Re1-O1, 1.692(2); Re1-P1, 2.365(1); Re1-P2, 2.346(1); Re1-C6, 2.116(3); Re1-Cl1, 2.4539(7); Re1-Cl2, 2.4248(8); P1-Re-P2, 158.53(3); P1-Re1-C6, 81.04(8); P2-Re1-C6, 80.31(8); O1-Re1-C6, 99.15(10); O1-Re1-Cl2, 177.34(7); C6-Re1-Cl1, 164.78(8); C6-Re1-Cl2, 81.71(7); Cl1-Re1-Cl2, 83.36(3); O1-Re1-Cl2, 177.34(7).....	41
Figure II-2. ORTEP drawing (50% probability ellipsoids) of (PCP ^{iPr})ReH ₄ (dmap) (207). All ligand (PCP ^{iPr}) based H atoms omitted for clarity. Selected distance (Å) and angles (°) follow: Re1-C8, 2.207(4); Re1-N1, 2.289(4); Re1-P1, 2.3645(14); Re1-P2, 2.3454(15); Re1-H46, 1.51(4); Re1-H47, 1.57(4); Re1-H48, 1.50(5); Re1-H49, 1.66(4); N1-Re1-C8, 85.17(14); P1-Re1-P2, 153.54(4); C4-N2-C5, 117.4(4); P2-Re1-C8, 79.28(12); P1-Re1-C8, 77.37(12).....	48
Figure III-1. ORTEP drawing (50% probability ellipsoids) of (PCP ^{iPr})ReO(OAc)(OH) (303a). Selected H atoms are omitted for clarity. Selected Distances (Å) and angles (deg): Re1-O1, 1.719(2); Re1-O2, 1.908(3); Re1-O3, 2.241(3); O2-Re1-O3, 83.9(1); C7-O3, 1.258(5); C7-O4, 1.255(6); O1-Re1-O2, 171.4(1).....	73
Figure IV-1. ORTEP drawing (50% probability ellipsoids) of (P*CP)ReOCl (401). Select H atoms and a second molecule in the unit cell are omitted for clarity. Selected distance (Å) and angles (°): Re1-C1, 2.026(5); C2-C7, 1.472(13); C6-C8, 1.399(13); Re1-O1, 1.686(5); P1-Re1, 2.445(3); P2-Re1, 2.460(3); P1-Re1-P2, 149.87(15); P1-Re1-C1, 80.5(4); P2-Re1-C1, 79.1(3).....	93
Figure IV-2. Calculated Wiberg Bond Index and Delocalization Index values	94
Figure IV-3. (left) DFT (B3LYP/BSI) optimized structure of 401 (right) Highest Occupied Molecular Orbital (HOMO) of 401 (isovalue = 0.04)	96
Figure IV-4. ORTEP structures of CO ₂ cycloaddition products (left) 402 and (right) 404	99
Figure V-1. ORTEP drawing (50% probability ellipsoids) of (PNN ^H)ReOCl ₂ (503). H atoms are omitted for clarity. Selected distance (Å) and angles (deg): Re1-N1, 1.984(2); Re1-N2, 2.2126(2); Re1-O1, 1.684(2); P1-Re1-N2, 155.62(6).....	113

- Figure V-2. ORTEP drawing (50% probability ellipsoids) of (PNP)ReOCl₂ (**502**). O1/Re1/Cl1 disorder and H atoms are omitted for clarity. Selected distance (Å) and angles (deg): Re1-N1, 2.028(4); Re1-O1, 1.67(2); P1-Re1-P2, 155.79(3).114
- Figure V-3. ORTEP drawing (50% probability ellipsoids) of (PNN)ReOCl (**505**). H atoms are omitted for clarity. Selected distance (Å) and angles (deg): Re1-N1, 1.955(3); Re1-N2, 1.997(4); Re1-O1, 1.684(3); P1-Re1-N2, 80.3(1); N1-Re1-N2, 87.1(1); O1-Re1-N1, 117.1(1); O1-Re1-N2, 103.4(1); P1-Re1-O1, 106.6(1); P1-Re1-N1, 136.2(1); Cl1-Re1-N2, 154.1(1).....121
- Figure V-4. ORTEP drawing (50% probability ellipsoids) of (PNN)ReO(OTf) (**508**). H atoms are omitted, and mirror image of original structure is shown for clarity and ease of comparison. Selected distance (Å) and angles (deg): Re1-N1, 1.958(3); Re1-N2, 1.949(3); Re1-O1, 1.698(3); P1-Re1-N2, 123.73(8); P1-Re1-O1, 105.68(9); O1-Re1-N2, 130.6(1); N1-Re1-O2, 164.5(1); P1-Re1-N1, 80.89(8); N1-Re1-N2, 86.70(1); Re1-N2-C16, 122.0(2).....122
- Figure VI-1. ORTEP drawing (50% probability ellipsoids) of (PNP^{iPr})Re(CO)₂ (**606**). H atoms are omitted for clarity. Selected distance (Å) and angles (deg): N1-Re1, 2.078(6); Re1-P1, 2.388(17); Re1-C1, 1.874(6); C1-Re1-C2, 82.6(4), P1-Re1-P2, 158.65(7); C1-Re1-N1.....145
- Figure VII-1. ATR-IR spectrum of (^{iPr}PNSb^{Ph})Rh(CO) (**702**) featuring a diagnostic CO stretch at 1951 cm⁻¹167
- Figure VII-2. Cyclic voltammogram of (^{iPr}PNSb^{Ph})PdCl (**703**) in CH₂Cl₂ at 25 °C. The scan rate was 100 mV/s in the positive direction. The cyclic voltammogram was obtained with 0.1 M [Bu₄N][PF₆] as the supporting electrolyte and resulted in a measured potential (E_{1/2}) equal to 0.0 V vs. [Cp₂Fe]/[Cp₂Fe]⁺167
- Figure VII-3. ORTEP drawing (50% probability ellipsoids) of (^{iPr}PNSb^{Ph})Rh(CO) (**702**). H atoms are omitted for clarity. Selected distance (Å) and angles (deg): Rh1-N1, 2.105(4); Rh1-P1, 2.263(1); Rh1-Sb1, 2.5539(5); P1-Rh1-Sb1, 161.30(4).169
- Figure VIII-1. ORTEP drawing (50% probability ellipsoids) of Me₂PhSbNHSb^{Me,Ph}(OTf)₂ (**802**). H atoms are omitted for clarity.....186
- Figure VIII-2. ORTEP drawing (50% probability ellipsoids) of **803**. Selected H atoms are omitted for clarity. Selected Distances (Å): C19-Sb1, 2.161(5); C48-Sb2, 2.130(4); C24-N1, 1.438(7); C49-N1, 1.442(6). 188

Figure VIII-3. ORTEP drawing (50% probability ellipsoids) of **804**.
All H atoms and one molecule of THF are omitted for clarity. Selected Distances
(Å): Sb1- C19, 2.131(3); Sb2-C45, 2.091(2); Sb2-C25, 2.063(2);
Sb2-C32, 2.067(2); C30-N1, 1.386(3); C33-N1, 1.389(3). 191

Figure VIII-4. ORTEP drawing (50% probability ellipsoids) of **806**. Selected H atoms
are omitted for clarity. Selected Distances (Å): Sb1-C1, 2.093(5);
Sb1-C12, 2.094(5); N1-C6, 1.376(7); N1-C7, 1.392(7); O2-H1, 2.039(14). 194

CHAPTER I

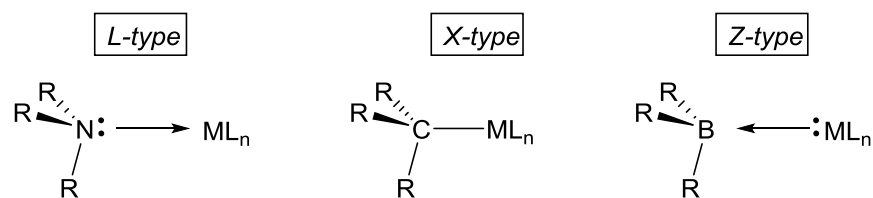
INTRODUCTION AND LITERATURE REVIEW

1.1 Introduction and Overview

Transition metals offer a rich variety of stoichiometric and catalytic chemistries which have found utility and relevance across academia and industry, from the benchtop to the production plant scale.¹ These reactivities are often supported by a litany of ligands which bind in different fashions to the metal center.² Rational synthetic design, paired with judicious ligand selection allows chemists to tune the steric and electronic environments of transition metal centers. Paired together, ligands and metals in concert can permit access to any number of bond-making and bond-breaking processes. This chapter will introduce the concept and application of tridentate pincer ligands, specifically the PNP and PCP-types, which have allowed transition metals and main group elements across the periodic table to exhibit incredible reactivity. The chemistry of rhenium both in and out of a pincer ligand context will be discussed, as well as background information on the main group chemistry of antimony as a ligand and a functional lewis acid.

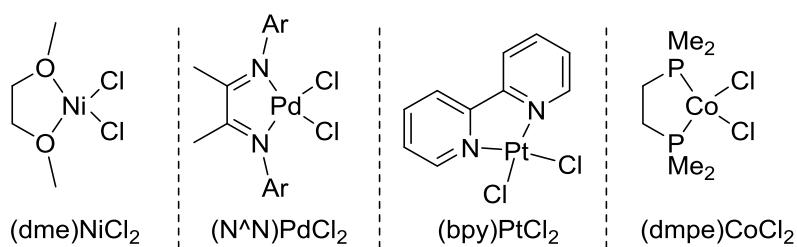
1.2 Pincer Ligands

Ligands allow for a functional tuning and design of the steric and electronic parameters of the transition metal and its chemical environment. Ligands can bind to a metal center in three different ways which can be described using “LXZ” notation.³ Where the ligand can bind covalently, in which one electron is donated from the ligand and the other from the metal, it is referred to as being “X-type”. Binding *via* lone pair, or two-electron donation to the metal center is categorized as an “L-type” interaction, and the reverse, a two-electron donation from the metal to an empty lewis acidic orbital of the ligand is assigned as being “Z-type” (Scheme I-1).



Scheme I-1. Examples of L, X, and Z-type ligand interactions with a generic metal center

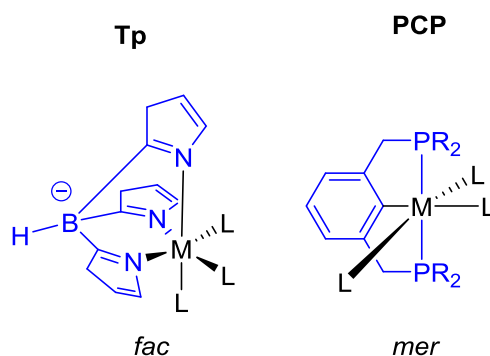
Generally, the bonding shown in Scheme I-1 consists of σ -bonding interactions which involve electrons residing in p- and d-orbitals of σ -symmetry in the ligand and metal, respectively. Common monodentate ligands can include L-type donors, such as phosphines (PR_3)⁴ and amines (NR_3)⁵ as well as X-type donors such as hydrocarbyls (CR_3)⁶, boryls (BR_2)⁷ and silyls (SiR_3)⁸. Bidentate ligands in organometallic chemistry usually contain oxygen, phosphorous, or nitrogen donors (Scheme I-2).⁹



Scheme I-2. Examples of bidentate ligands containing oxygen, nitrogen, and phosphorous donors

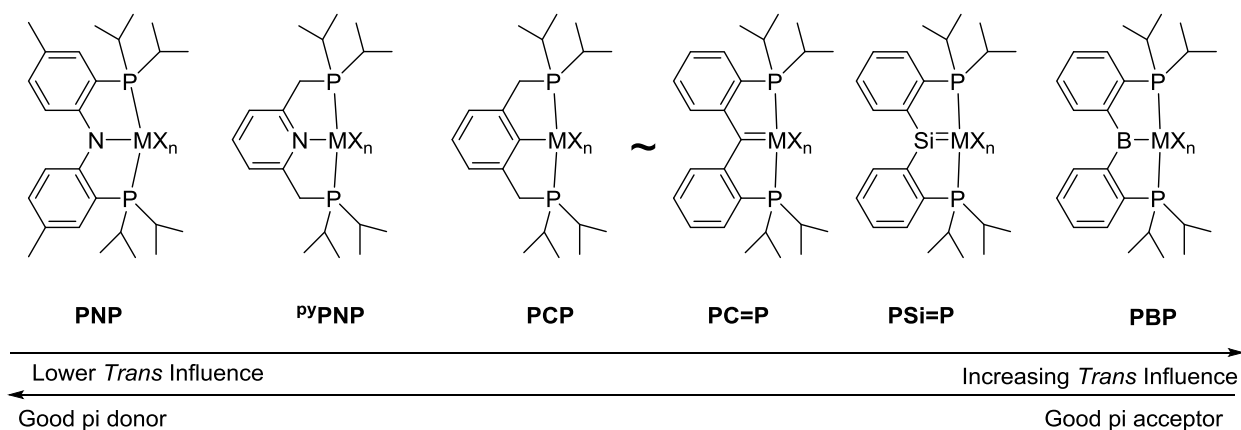
The main studies in this work were performed utilizing tridentate pincer ligands. Tridentate ligands can exhibit meridional (*mer*) or facial (*fac*) binding to a metal center, and depending on their inherent molecular flexibility, may be capable of switching between them. Those tridentate

ligands which bind facially are often referred to as “scorpionates” and include ligands like *tris*-pyrazolylborate (Tp) whereas those that show preference for meridional binding, we refer to as “pincer” ligands such as the 1,3-dialkylphosphinomethyl benzene, or PCP ligand (Scheme I-3).



Scheme I-3. Representation of generic metal complexes supported by Tp and PCP ligands binding in facial and meridional fashion, respectively

Pincer ligands confer greatly heightened thermal stability while enforcing rigid and predictable geometries about the metal center. They are synthetically variable and are thus able to be tuned for designer steric and electronic environments about the metal center. Pincer complexes utilized in this study were mainly constructed utilizing either a *m*-xylylenyl or *o*-ditolylamido backbone, easily functionalized with appropriate halogenations and subsequent nucleophilic substitutions to furnish the desired pincer-type proligands. Metalation of these ligands was then able to be achieved *via* selective C-H activation or N-H cleavage to form the tridentate ligated species. Pincers are named according to their two flanking (typically L-type) and single central (typically X-type) donors. Scheme I-4 presents a small sampling of the possible central donors and some of their key electronic features.

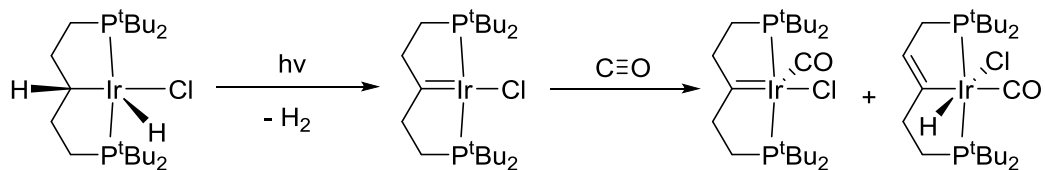


Scheme I-4. Array of named pincer ligands and relative *trans* influence and pi donicity properties

1.3 PCP-Type Pincer Ligands

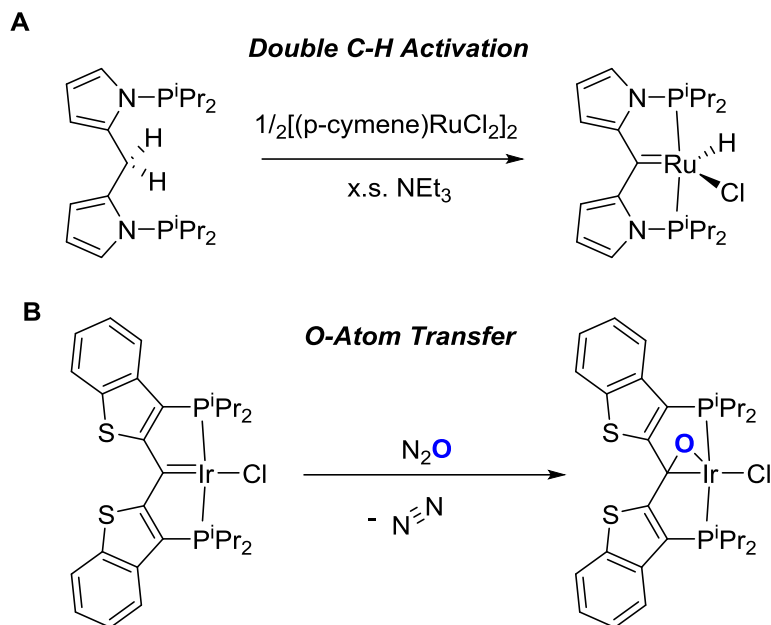
1.3.1 Different Types of PCP Ligands

PCP ligands are aptly named for their two flanking phosphino-type donors and the central carbon-donor. Though the first PCP-type ligand was discovered in 1976 and based on the 1,3-*bis*(dialkylphosphinomethyl)benzene scaffold disclosed by Moulton and Shaw,¹⁰ multiple other PCP ligands have found their way into the literature and exhibit different types of reactivity.¹¹ Though an aryl donor provides a certain amount of rigidity, PCP ligands based on aliphatic backbones have found differing reactivity. The 1,5-*bis*(dialkylphosphino)pentane ligand can be metalated to iridium, forming an alkyl-central donor. The alpha C-H bond can then be lost dehydrogenatively or *via* radical processes to produce a reactive, carbenic center (Scheme I-5).¹²



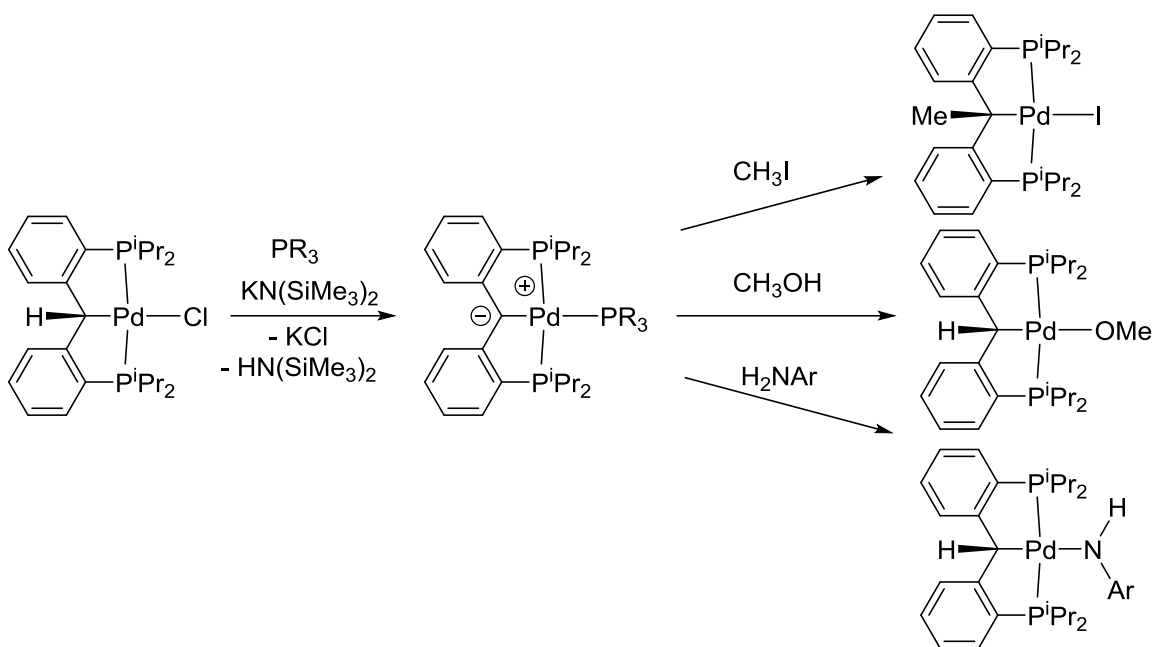
Scheme I-5. Photochemical dehydrogenation and subsequent carbenic rearrangement at an alkyl-based PCP iridium

Aside from being incidentally generated, PCP ligands with a central carbene donor can be intentionally designed and installed. In this vein, the Ozerov group reported that a dipyrrolylmethylene based pincer was able to be introduced to the coordination sphere of ruthenium (Ru) *via* double C-H activation in the presence of excess base.¹³ Though reactivity in this case was observed to occur primarily at ruthenium, other, more reactive carbene-type donors have been isolated and their reactivities explored further. For an example it can be seen that the Piers group revealed the ability of a dithiophenylmethylene, PCP-type ligand to be metalated to iridium and undergo O-atom transfer reactions (Scheme I-6).¹⁴



Scheme I-6. (A) Double C-H activation of a dipyrrolyl methane type PCP ligand results in formation of a (PC=P)Ru(II) species. (B) A highly reactive central carbene donor is capable of acting in concert with an iridium center to extrude N_2 from N_2O and efficiently abstract the O-atom to form a novel iridaepoxide species.

The Iluc group at the University of Notre Dame has developed an impressively reactive PCP-carbene type system based on an *ortho*-bis(dialkylphosphino)diphenylmethane core. They have succeeded in introducing this ligand *via* direct C-H activation and concomitant dehydrohalogenation at (COD)PdCl₂ in THF to form an alkyl PCP-palladium chloride complex which can then undergo another dehydrohalogenation involving both the ligand and metal cooperatively to form a nucleophilic PCP-carbene Pd(II) (Scheme I-7). This carbene, which carries a primarily anionic contribution, is effectively capable of participating in reactivity as the nucleophilic partner to the electrophilic Pd(II) cation, acting almost as a pseudo-frustrated lewis pair.¹⁵

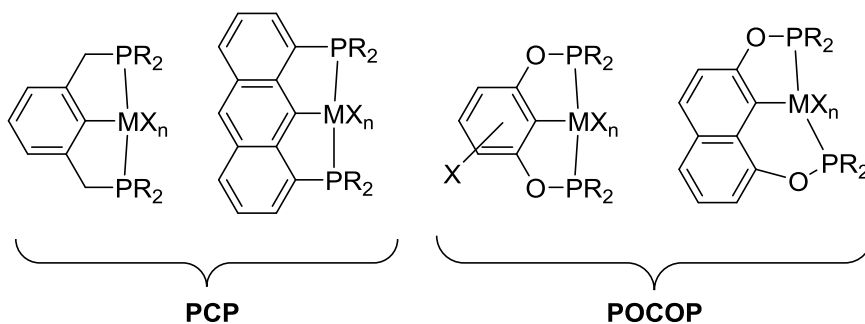


Scheme I-7. Formation of a nucleophilic PCP-type Pd-carbene species. Reactions are shown with carbon based and protic electrophiles involving metal-ligand cooperation.

Though PCP pincer ligands featuring ostensibly neutral, central N-heterocyclic carbene (NHC) type donors exist in the literature, they will not be covered here.¹⁶ Other types of aliphatic PCP pincers generally act as strong electron donors to the metal center, but tend not to participate directly in the chemistry reported thus far.

1.3.2 Late Transition Metal Chemistry with Aryl Based PCP Pincer Ligands

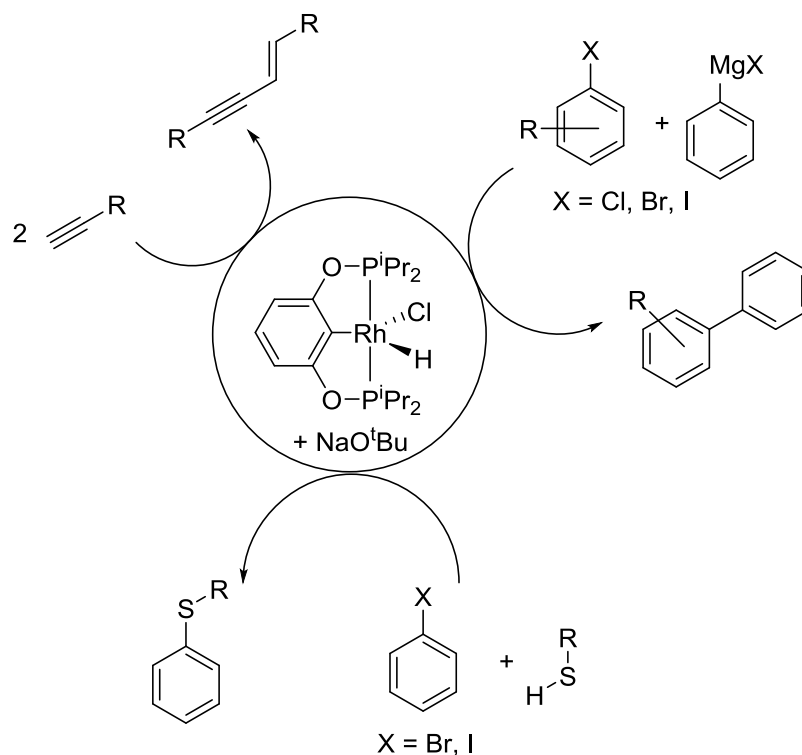
Despite the many types of PCP ligands featuring aliphatic and carbenic donor types, the PCP ligands with a central, anionic aryl donor remain the most popular choice. Within this subgroup are multiple arene backbones including those based on benzene, naphthalene, anthracene, and resorcinol (Scheme I-8).¹⁷



Scheme I-8. Schematic showing different types of generic arene based PCP complexes

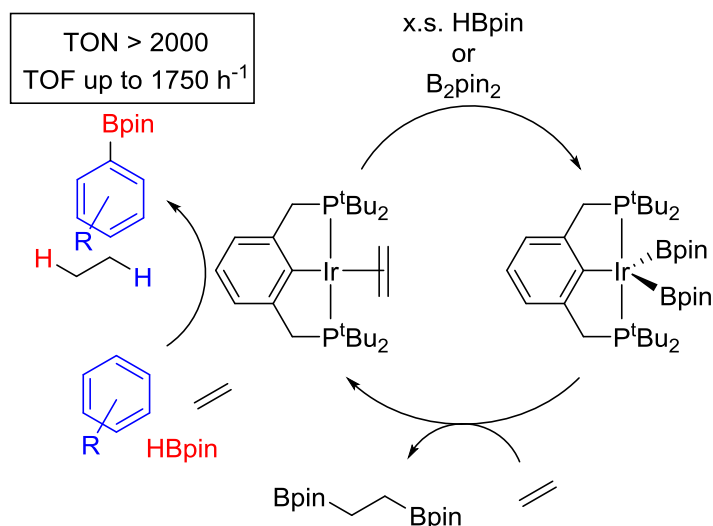
Late transition metals (groups 8-10) have a notable history of C-H activation chemistries.¹⁸ Complexes of Pd supported by PCP-type ligands are relatively easy to make and have garnered a large amount of attention and study and have been looked at specifically for their catalytic C-H functionalization abilities. They have been explored by our group as catalysts for the dehydrogenative borylation of terminal alkynes (DHBTA)¹⁹, by the Guan group for the hydroboration/reduction of CO₂²⁰ and also in the study of catalytic Suzuki coupling by Bedford and coworkers.²¹

The chemistry of rhodium (Rh) and iridium(Ir) have allowed access to developments which center on efficient C-H activation and subsequent functionalization. Supported by PCP ligands, both have shown exceptional activity in catalytic and stoichiometric transformations of interest. Our group has studied the ability of Rh supported by the POCOP ligand to affect high turnover, catalytic alkyne dimerization²² as well as catalytic C-C²³ and C-S²⁴ coupling of aryl halides and C/S-based nucleophiles (Scheme I-9).



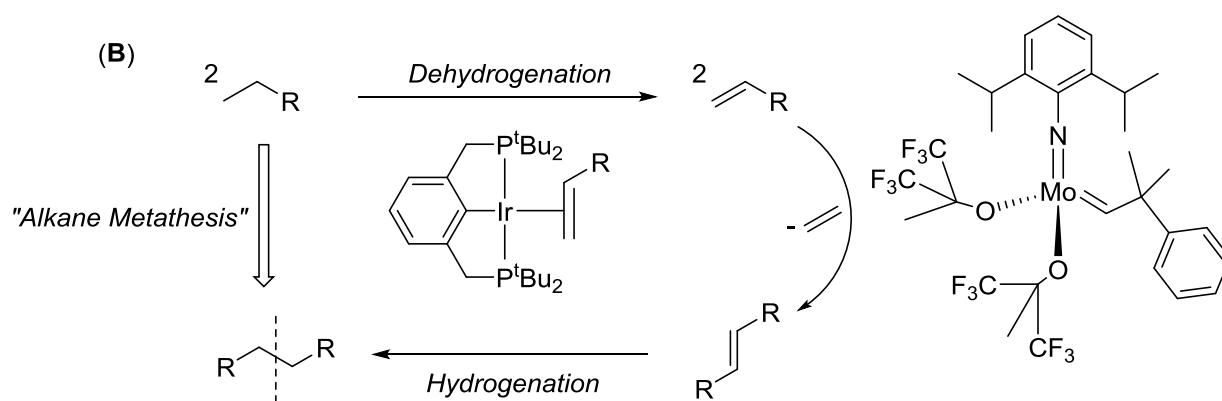
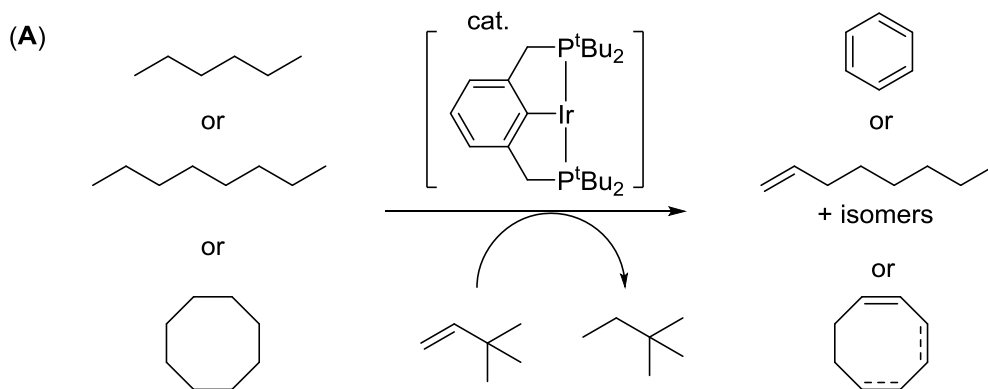
Scheme I-9. Catalytic alkyne dimerization, Kumada coupling, and C-S bond formation mediated by a (POCOP)Rh(H)(Cl) precatalyst

Chemistry with rhodium utilizing the parent PCP pincer ligand is a bit rarer, though recently Mayer, Goldman and coworkers studied the electrochemical reduction and protonation of monomeric and dimeric (PCP)Rh(N₂) complexes.²⁵ The chemistry of iridium supported by the PCP and POCOP ligands has been developed to a much greater degree. This is largely due to the high activity of PCP and POCOP iridium complexes in direct C-H activation of typically unreactive substrates. We have examined and reported the capability of POCOP-supported complexes of iridium to mediate high turnover, catalytic arene C-H borylation as well as boryl transfer to small molecules (Scheme I-10).²⁶



Scheme I-10. Catalytic arene C-H borylation and boryl transfer to small molecules (ethylene) mediated by POCOP supported complexes of Ir

Perhaps most famous, is the reactivity of PCP-type complexes of iridium in the catalytic dehydrogenation of aliphatic and other substrates to furnish olefins and other unsaturated reagents for further functionalization. First disclosed in a report by Jensen, it was shown that complexes of (PCP)Ir are capable of acting as efficient catalysts for the dehydrogenation of alkanes to produce olefins.²⁷ The Goldman group has expanded this reactivity into a large body of work²⁸ showing elegantly designed reactivity which includes the transfer dehydrogenation of long-chain alkanes with *tert*butylethylene to make aromatics or alpha olefins, and the pairing of (PCP)Ir and molybdenum imido catalysts for net “alkane metathesis” system (Scheme I-11).²⁹



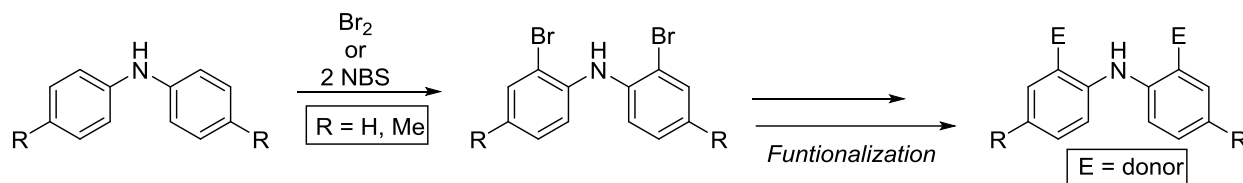
Scheme I-11. (A) (PCP)Ir-catalyzed transfer dehydrogenation of aliphatic substrates (B) Tandem Ir/Mo catalysis to achieve a “net alkane metathesis”

Overall, the chemistry of late transition metal complexes supported by PCP-type pincer ligands is brought together by a few salient features, those being: 1) Stabilization of highly reactive fragments 2) Preservation of the ligand’s meridional geometry about the metal center and 3) Access to modes of C-H activation and subsequent functionalization. It stands to reason that such a privileged ligand platform which provides high reactivity to late transition metals, should it be incorporated into other, earlier d-block elements, may provide access to novel and useful expansions of fundamental reactivity that could inform future catalytic applications.

1.4 Pincer Ligands Based on a Diarylamine Backbone

1.4.1 Diverse Pincer Ligands Based on Diarylamines

Diarylamines such as diphenyl- or ditolyl-amine have found great utility in the synthesis of pincer ligands which seek to incorporate a central, anionic amido donor. Due to the high reactivity of the *ortho* and *para* C-H positions to halogenation reactions, they can be subsequently functionalized with a variety of nucleophiles which make attractive flanking donors in the resultant pincer ligands (Scheme I-12).

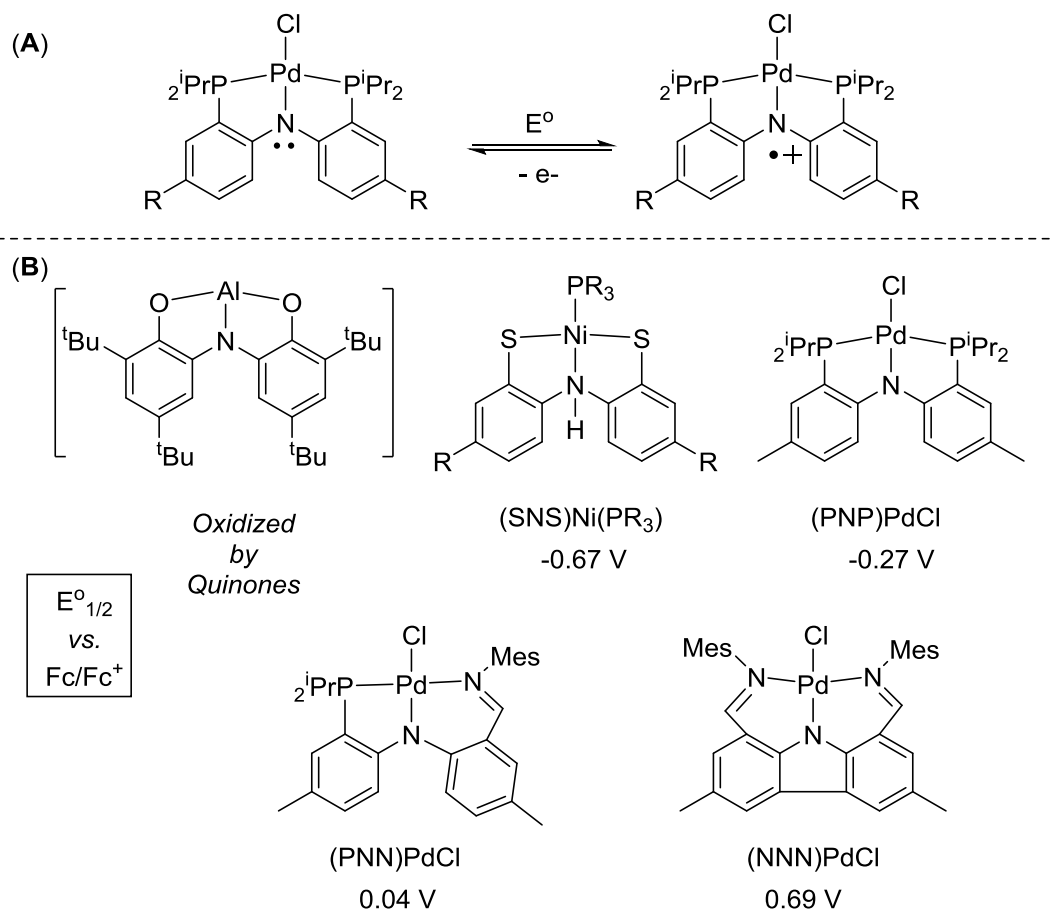


Scheme I-12. General scheme for the *ortho* functionalization of the diarylamine backbone

Another attractive feature of the diarylamine core in a pincer framework is the lack of redox innocence, or rather, its ability to be readily oxidized either chemically or by an applied electrochemical potential. The redox functionality of the backbone can be tuned largely by the *para*-substituent with more electron donating groups, leading to a lower oxidation potential, and more electron-withdrawing groups, giving higher oxidation potentials. The oxidation of the diarylamine backbone leads to formation of an aminyl radical cation which could potentially be leveraged for further reactivity.

The redox activity of the diarylamine backbone has been observed and studied in complexes of nickel (Ni) supported by an SNS ligand,³⁰ aluminum (Al) supported by an ONO

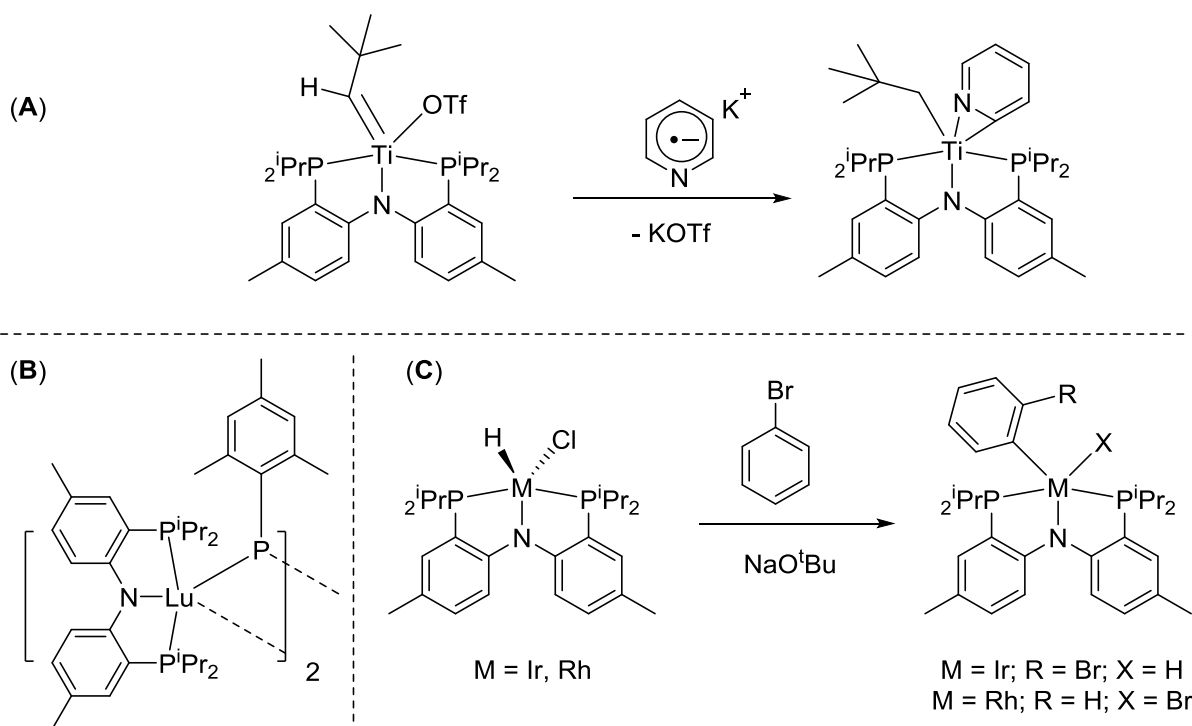
pincer,³¹ and within our group with complexes of Pd supported by NNN, PNP, and PNN pincers (Scheme I-13).³²



Scheme I-13. (A) Reversible electrochemical oxidation of a diarylamine based pincer ligand to form an aminyl radical cation (B) Examples of redox active pincer complexes based on various diarylamine cores

The major focus of much of the chemistry in our group has been on the reactivity imbued by the PNP pincer ligand featuring *isopropyl* phosphine substituents and a central amido donor. The PNP ligand can be easily metalated to almost every transition metal and larger main group

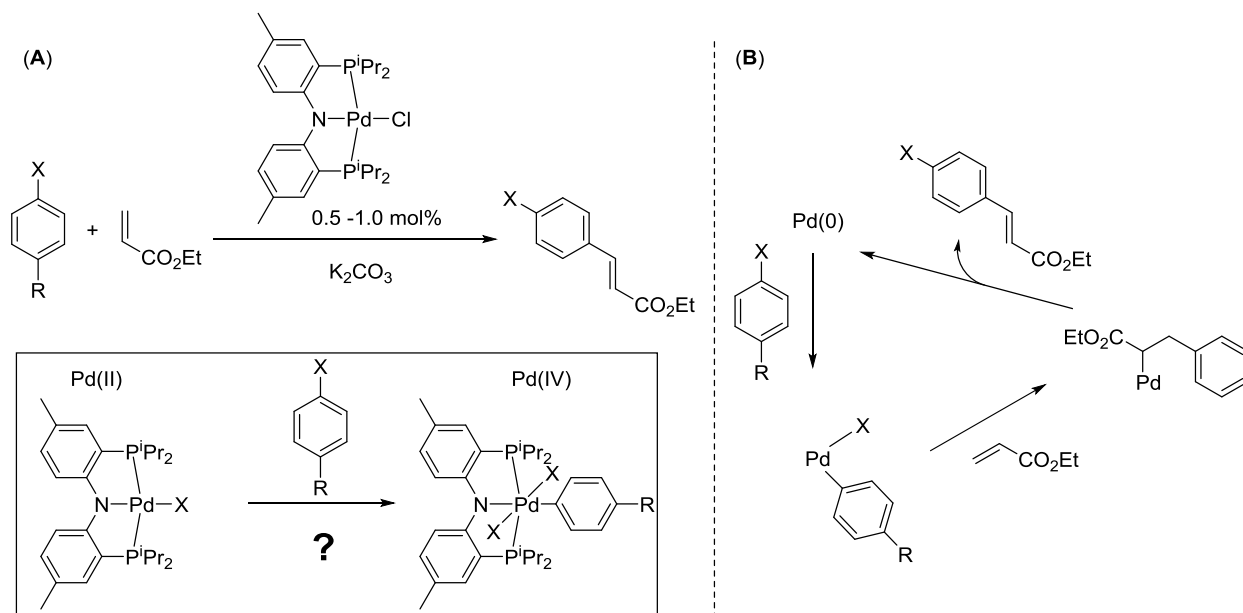
element due to a privileged mixture of the hard central nitrogen donor with two soft flanking phosphine donors. With this combination, PNP complexes of early, mid, and late transition metals have been isolated and their novel reactivities tested. Most notably, the PNP ligand has supported a bevy of bond-making and bond-breaking reactivities. As a few key examples of its utility across the periodic table, Mindiola has utilized the PNP ligand to unlock powerful pyridine activation chemistry with a reduced titanium species (Ti),³³ Kiplinger has isolated and characterized a lanthanide phosphinidene,³⁴ and our group has reported on the divergent initial reactivity of PNP Ir/Rh complexes in the activation of aryl C-H and C-X bonds (Scheme I-14).³⁵



Scheme I-14. (A) (PNP)Ti activation of the C=N bond in pyridine (B) First lutetium (Lu) phosphinidene (C) Divergent C-H/C-X oxidative addition to (PNP)M (M=Ir,Rh) species

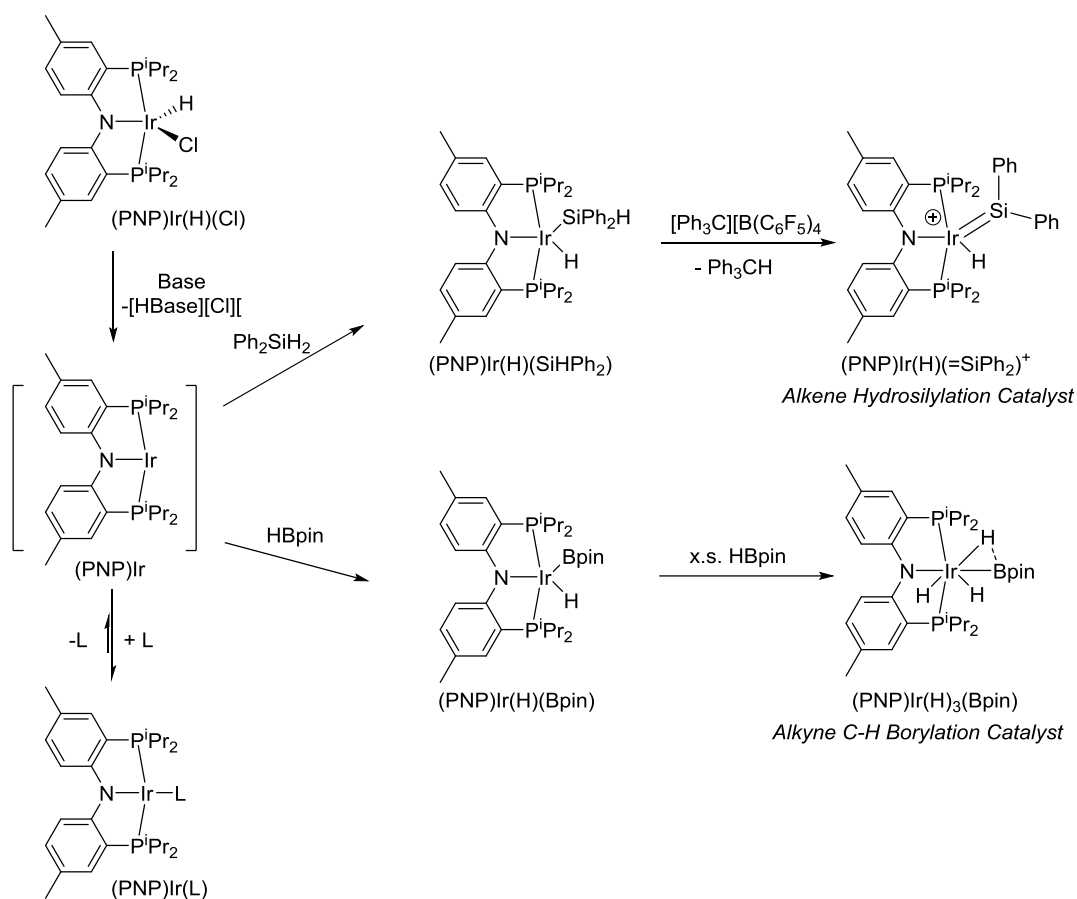
1.4.2 PNP Pincer Ligands in Catalysis

Though the PNP pincer has been utilized for multiple stoichiometric reactions, much of the catalytic chemistry has been observed with the late transition metals such as Pd and Ir. Our group has developed (PNP)Pd species as catalysts for the Heck coupling reaction of aryl halides with ethyl acrylate, though the oxidation state of Pd during catalysis (Pd(II) or Pd(IV)?) is a matter of continued question.³⁶ In the previously mentioned systems of Pd supported by PCP ligands, it was noted that Pd nanoparticles were formed *via* serendipitous liberation of the Pd from the ligand. However, it appears that regardless, given its continuous bearing of a PNP-pincer framework, the mechanism in this case should differ from that of the typical Pd(0/II) cycle (Scheme I-15).



Scheme I-15. (A) Catalytic Heck coupling mediated by a PNP-supported Pd complex with a possible, but unlikely Pd(IV) species shown (B) Typical Heck coupling mechanism mediated by Pd(0)

Iridium complexes of PNP offer a wide variety of reactivity that depends mainly on the generation of the highly unsaturated, three-coordinate, 14-electron (PNP)Ir fragment. The generation of this reactive fragment can be achieved either *via* dehydrohalogenation at the Ir(III) species, (PNP)Ir(H)(Cl), or by thermal ligand dissociation from a suitable Ir(I) precursor of the type (PNP)Ir(L) (where L= COE, C₂H₄, N₂, etc). Much of the catalytic reactivity that has been leveraged both by the Tilley group³⁷ and our own has focused on hydrofunctionalization using silanes or catalytic C-H borylation using hydroboranes.³⁸ The active catalysts in each of these cases is derived from the (PNP)Ir fragment undergoing some series of Si-H and B-H activations with hydrosilanes and boranes (Scheme I-16).



Scheme I-16. Generation of 14-electron (PNP)Ir fragment and generation of active catalysts for alkene hydrosilylation and C-H borylation of terminal alkynes

Pincers based on the diarylamine backbone come with a variety of synthetic features and variations that allow for a seemingly never ending stream of innovation and discovery. The combination of hard amido and soft phosphine donors allows for strong binding and geometry enforcement of multiple transition metals and main group elements. The chemistry of the PNP pincer has given access to multiple catalytic transformations at late transition metals, and supports stoichiometric transformations of academic interest across the board. Aside from its redox reactivity, the diarylamine backbone is impressively unreactive given its high level of rigidity/planarity and its lack of beta hydrogens which precludes ligand participation and

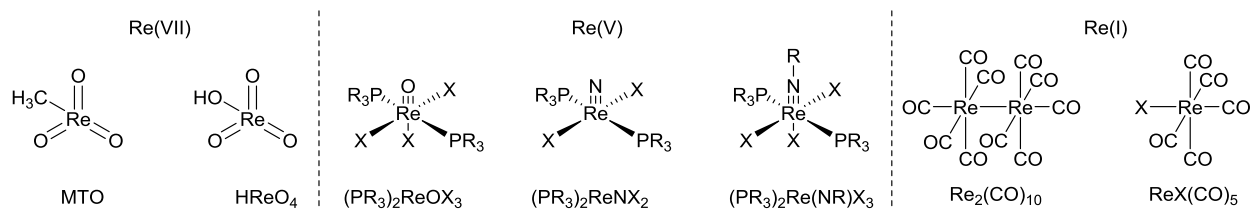
degradation by more reactive transition metals. For these reasons, it can be reasonably expected that the development of PNP-supported chemistry will continue to be seen for many more years.

1.5 An Introduction to the Chemistry of Rhenium

Many of the initial discoveries in organometallic chemistry were first made with complexes of rhenium (Re) and were then applied to later transition metals with either higher reactivity or greater abundance. Rhenium is a 5d, group VII transition metal which has a range of available, formal oxidation states ranging from -1 to +7. Found in trace amounts during platinum mining, Re is incredibly scarce. However, due to its relatively low demand and industrial usage, the costs of rhenium are still comparatively low enough to warrant further exploration of its chemistries.

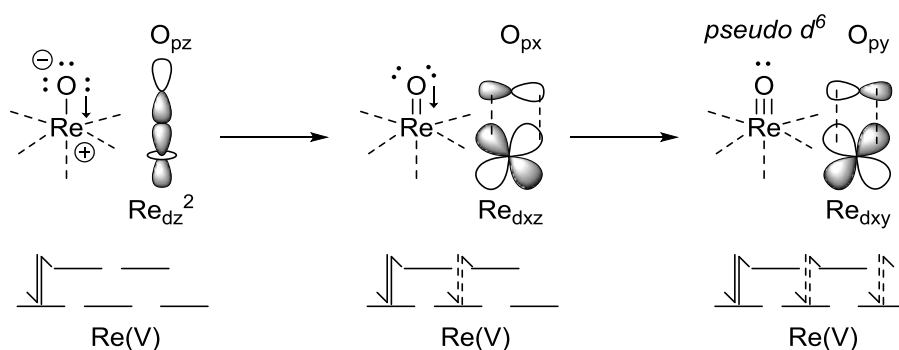
1.5.1 Metal-Ligand Multiple Bonding in Complexes of Rhenium

Rhenium, being a mid-transition, 5d-metal is most often found in the +1, +5, and +7 oxidation states and is a fairly π -basic metal center which also is good at accepting additional lone pair donations from suitable ligands. Common starting materials for rhenium in the +7 oxidation state are perrhenic acid (HReO_4) and methyltrioxorhenium or MTO (MeReO_3). In the +5 oxidation state rhenium starting materials generally take on the formula $\text{L}_2\text{Re}(=\text{X})\text{Y}_3$ where L= phosphines, pyridines, or sulfides; X = O, NR, or CR_2 ; Y = Cl, Br, I, or alkoxide. In the +1 oxidation state there is less variety and $\text{ReX}(\text{CO})_5$ or $\text{Re}_2(\text{CO})_{10}$ are the dominant starting materials for further synthesis (Scheme I-17).



Scheme I-17. Common rhenium starting materials in the +7, +5, and +1 oxidation states

Most often, the multiple bonding in rhenium is seen in oxo, imido, and nitrido species of Re(V) containing phosphine ligands with a d^2 electron configuration at Re. Despite being d^2 , the rhenium center is often a diamagnetic, octahedral, 18-electron complex. The diamagnetism arises from the high *trans* influencing terminal, multiply bound ligand donating not only into the dz^2 but also having 4 additional electrons to donate into other orbitals of π -symmetry, those being the dxz and dyz . In this way it behaves akin to a d^6 octahedral metal complex and thus presents as a diamagnetic species (Scheme I-18).

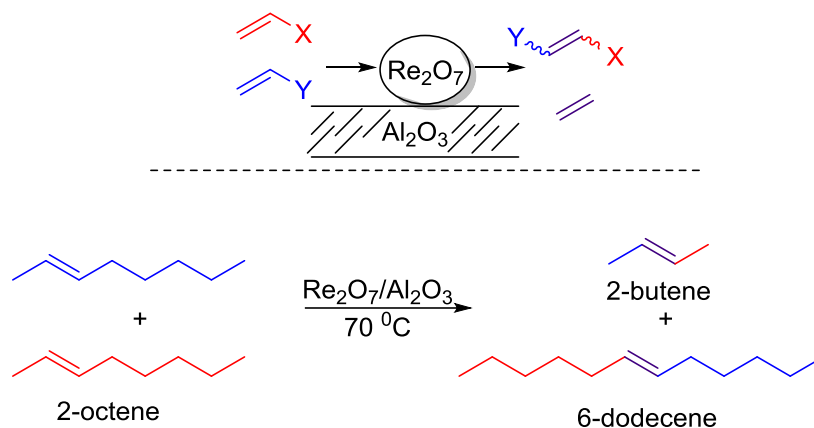


Scheme I-18. Diagram showing orbital interactions of rhenium-oxo multiple bonding and progression of electrons filling a generic d-orbital manifold to create a pseudo d_6 rhenium center

The side effect of rhenium being so effective at forming and retaining multiple bonds is that they become highly stable and are difficult to functionalize further. However, reduction of rhenium oxo moieties is possible and a topic of consideration in chapter 2 of this dissertation. Though rhenium oxo species have proven to be quite robust, they have been developed into a number of catalytic transformations.

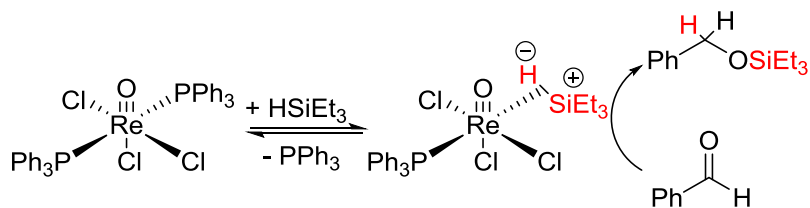
1.5.2 Catalytic Applications of High-Valent Rhenium Species

Given their inertness, oxophilicity, and robust nature under highly oxidizing conditions, high-valent rhenium species have found utility in the oxidation of various organic substrates to produce value added chemicals. The polyolefins business is one which brings in billions of dollars (USD) per year and is driven largely by forcing conditions and organometallic/inorganic catalysis. In that vein, the Eldridge group has recently reported a detailed study showing that Re_2O_7 supported on an Al_2O_3 support is capable of mediating efficient olefin metathesis reactions to form heavy olefins utilizing lower temperatures and flow rates than other solid state industrial catalysts.³⁹ This reactivity, paired with proper technology can allow for the creation of multiple internal olefins such as 2-butene, 6-dodecene, and higher order C_n olefins (Scheme I-19).



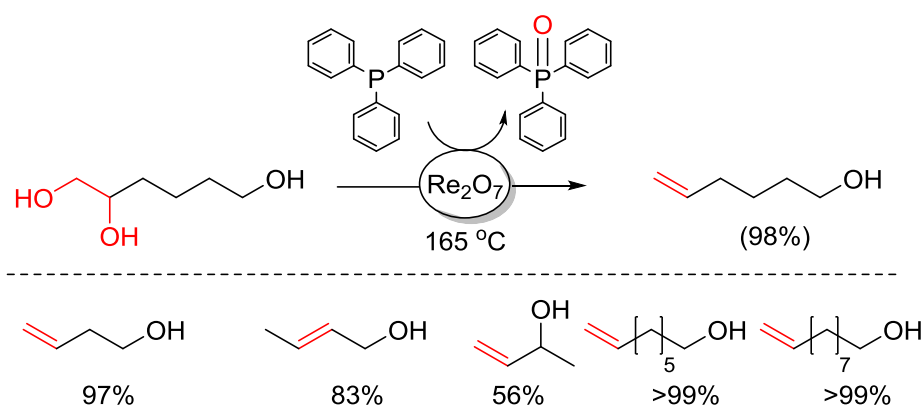
Scheme I-19. Schematic of Re_2O_7 catalyzed olefin metathesis on a Al_2O_3 solid support

Abu-Omar and coworkers reported a cationic rhenium(V) oxo-hydride species capable of performing the hydrosilylation of aldehydes. In that study they showed that hydrosilane Si-H bonds do not add across the $\text{Re}=\text{O}$ bond as was previously assumed, but rather, get electrophilically activated *via* σ -complexation for subsequent formal hydride and silylium transfer equivalents (Scheme I-20).⁴⁰



Scheme I-20. Representation of $\text{Re}(\text{V})$ catalyst formation and subsequent activation of Si-H bond

Finally, de Vries and coworkers explored Re(VII) oxide in the catalytic deoxydehydration (DODH) of aliphatic diols to give olefin products. Multiple Re(VII) precatalysts worked efficiently such as MTO, Re_2O_7 and ammonium perrhenate (NH_4ReO_4) to achieve selective DODH products in high yields. Though conducted at 165 °C, the reactions were run under neat conditions using PPh_3 as the terminal reductant (Scheme I-21).⁴¹

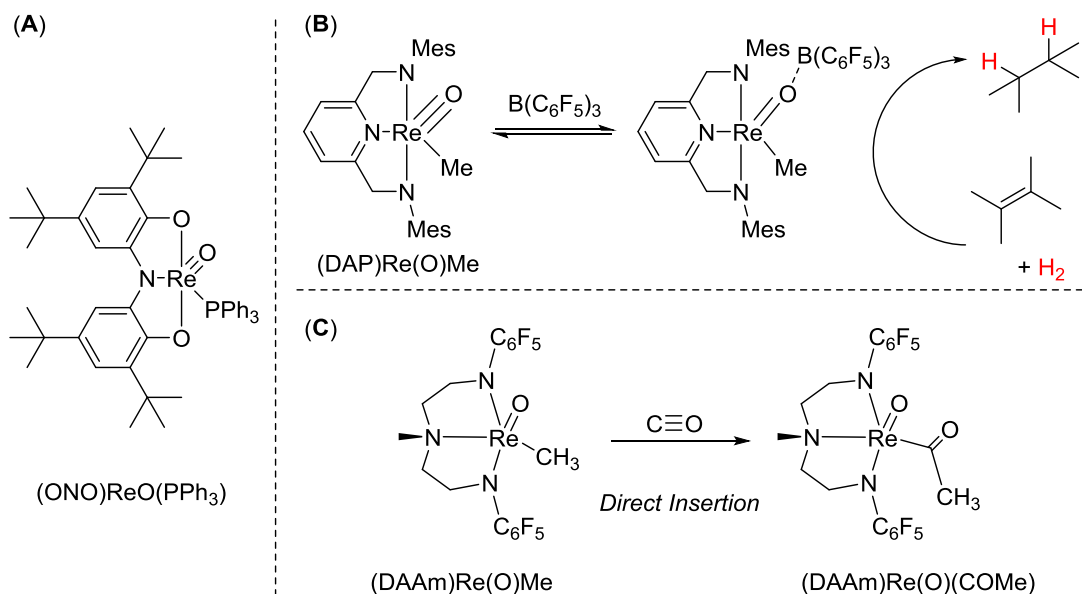


Scheme I-21. Deoxydehydration (DODH) catalyzed by Re_2O_7 at high temperature

1.5.3 Chemistry of Rhenium in a Pincer Ligand Context

Though the chemistry of rhenium ligated by *mono*- and *bidentate* ligands has been well developed, the analogous chemistry of rhenium in a pincer ligand context has remained less so. As a result of this, the literature retains a general paucity of pincer-rhenium complexes, and even moreso when it comes to explorations of novel, fundamental reactivity and catalysis. This does not mean, however, that no chemistry has been done or disclosed on pincer-supported complexes of rhenium. Most of the ligands utilized feature central, nitrogenous donors with flanking group XV donors (amido, amino, phosphine), though there is some variety to be found.

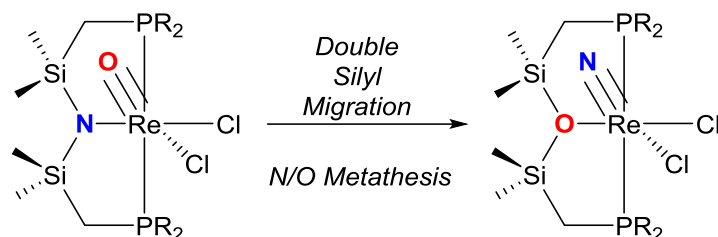
For examples of the rhenium pincer complexes available we can begin by looking at those from the Brown laboratories where a redox-active (ONO)Re(O)(PPh₃) complex was disclosed which mediates catalytic O-atom transfer.⁴² We can then look to the Ison group where a diamidopyridine (DAP), NNN-type pincer, was reported which allows for frustrated Lewis pair-type reactivity with B(C₆F₅)₃ to hydrogenate unactivated alkenes to alkanes, and where studies of a diamidoamine (DAAm) supported rhenium complex allows for direct insertion of CO to a Re-C bond (Scheme I-22).⁴³



Scheme I-22. (A) Redox active ONO-Re complex (B) FLP-type alkene hydrogenation catalysis using a Lewis basic Re-oxo fragment in concert with a triarylborane Lewis acid (C) Direct insertion of CO into a Re-Me bond, notable for not proceeding *via* pre-coordination

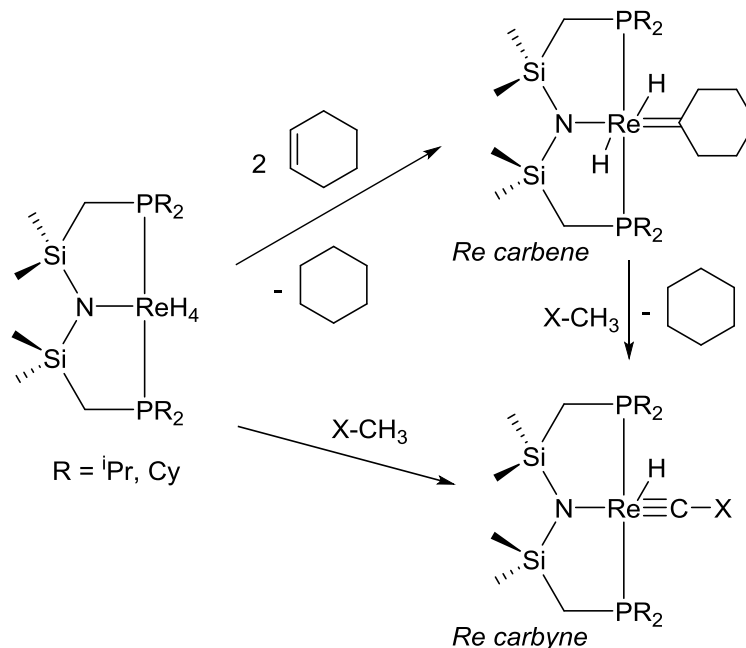
Though terminal oxo ligands are most common in pincer-rhenium chemistry as stable moieties, there are instances where they can react, such as in the thermal rearrangement of Fryzuk's PNP ligand as observed by Caulton and coworkers. In this case, a series of 1,3-silyl-to-oxo

migrations causes a thermal isomerization of the formerly L₂X PNP ligand to an L₃ POP ligand with a newly installed terminal rhenium nitride (Scheme I-23).⁴⁴



Scheme I-23. Thermal rearrangement of a (PNP)ReOCl₂ species *via* double silyl migration to form a new, (POP)Re(N)Cl₂ complex

The previous rearrangement puts the sensitivities of the silyl-linked PNP pincer on stark display. However, Caulton and coworkers showed that despite the lability of the N-Si bond, interesting C-H activation and dehydrogenative isomerization chemistries could be readily accessed. Generation of the *polyhydride*, (PNP)ReH₄ was able to be achieved by magnesium (Mg) reduction of the (PNP)ReOBr₂ species, formed *in situ*, under an atmosphere of hydrogen. Subsequent hydrogenation of an alkene furnished a proposed, transient *dihydride* species, (PNP)ReH₂ which would perform C-H activation of an alkane or cycloalkane, and isomerize them in stepwise fashion into π -acidic hydrido-carbynes and *dihydrido* carbenes (Scheme I-24).⁴⁵



Scheme I-24. Reaction of an operatively unsaturated *tetrahydride*, $(\text{PNP}^{\text{R}})\text{ReH}_4$ with cyclohexane resulting in formation of a 1,1-cyclohexylidene carbene. Reaction of either the *tetrahydride* or the previously acquired carbene with a methyl-containing reagent results in C-H activation and formation of a rhenium hydridocarbene species

1.5.4 Rationale for Exploring the Chemistry of Pincer-Supported Rhenium

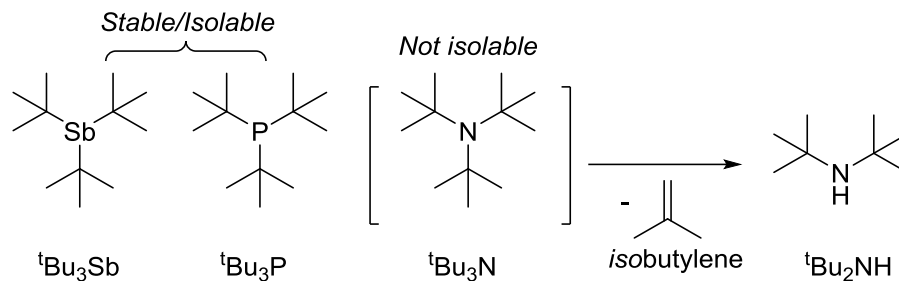
Given the already established reactivity of various pincer-supported rhenium complexes, it remained of interest to us to determine what kinds of novel reactions might become accessible with *polyhydrides* or rhenium-oxos supported by other, perhaps more robust ligand sets. The PCP pincer provides a rigid scaffold with a highly electron-donating central aryl which could reasonably allow for easier C-H activation of aliphatic substrates. The lack of additional π -donation from the aryl ligand may be expected to raise the energy of resultant species, but may also preclude formation of carbene/carbyne species (i.e.; π acids), and allow future catalytic alkane dehydrogenation to be kinetically accessible.

The diarylamine-based ligand backbone offers no moisture or oxo-sensitivities in contrast to the Fryzuk disilylamido-based pincer. Unlike the flexible diamidoamine, our PNP retains the rigidity and amido donicity that's prized in many of the shown systems, while avoiding potential pitfalls that can arise from the presence of hydrogens beta to an amide. Given the synthetic variability of diarylamine-based pincers, taken with previous discoveries in the literature, it stands to reason that such potential is worthy of continued exploration. With our more rigid and robust PNP pincer, thermal C-H activations of substrates with different functional groups may prove accessible. On top of this, the redox capabilities of the diarylamine core may also end up being leveraged in a currently unidentified but potentially serendipitous way.

1.6 Antimony Based Ligands for Transition Metal Complexes

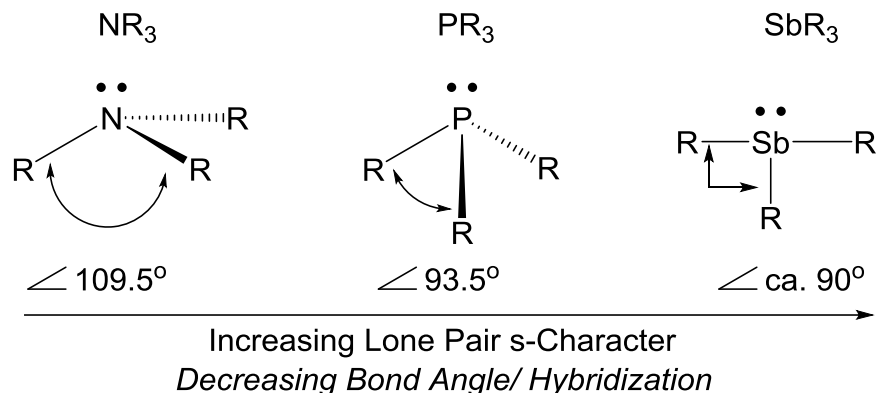
1.6.1 Stibine-Transition Metal Complexes

Group 15, pnictogen donors are ubiquitous in organotransition metal chemistry. Amine (NR_3) and phosphine (PR_3) ligands feature widely as hard and soft analogues of each other as they bind to mainly early and later transition metals, respectively. Stibines (SbR_3) can be thought of as heavier, main group analogues of phosphine donors, with some key differences. The larger size of phosphorous and antimony versus that of nitrogen allows for the isolation and utilization of large *tri*-substituted substituents. For that reason, ${}^t\text{Bu}_3\text{P}$ and ${}^t\text{Bu}_3\text{Sb}$ are isolable species, whereas the analogous ${}^t\text{Bu}_3\text{N}$ species does not exist. Though it has been sought after and progress has been made recently, even potentially transient generation of ${}^t\text{Bu}_3\text{N}$ leads to formation of ${}^t\text{Bu}_2\text{NH}$ and isobuylene arising from beta-hydrogen elimination.⁴⁶ In this case, the steric environment around the smaller nitrogen atom is so great that previously unexpected pathways of degradation become accessible (Scheme I-25).



Scheme I-25. Pnictogen donors with bulky *tert*butyl substituents. Stibine and phosphine varieties are stable and isolable, whereas the corresponding amine degrades *via* alkene elimination

Electronically, amines, phosphines, and stibines vary greatly. In terms of hard/soft acid/base theory, antimony remains the softest donor, with nitrogen being the hardest. However, in terms of electronic donation, sterics briefly aside, amine donors are the strongest as the lone pair resides in an accessible p-orbital. Phosphines are excellent, strong donors, though they tend to bind more efficiently to larger 4d and 5d transition metals beyond group 6. Stibines, on the other hand would be expected to bind best to late transition metals, but would be expected to be the weakest donor in the group. Assuming steric considerations do not preclude binding to a metal center, this phenomenon is due largely to the angles between the substituents becoming more compressed as we move down the periodic table. This angular compression has the effect of increasing the s-character of the accessible lone pair, causing it to be less donating (Scheme I-30). At bond angles that are essentially 90° we can functionally assign the stibine as being unhybridized, as it utilizes P_x , P_y , and P_z orbitals to bond with substituents, forcing the lone pair to reside in an s-orbital and becoming less accessible for donation to a metal.

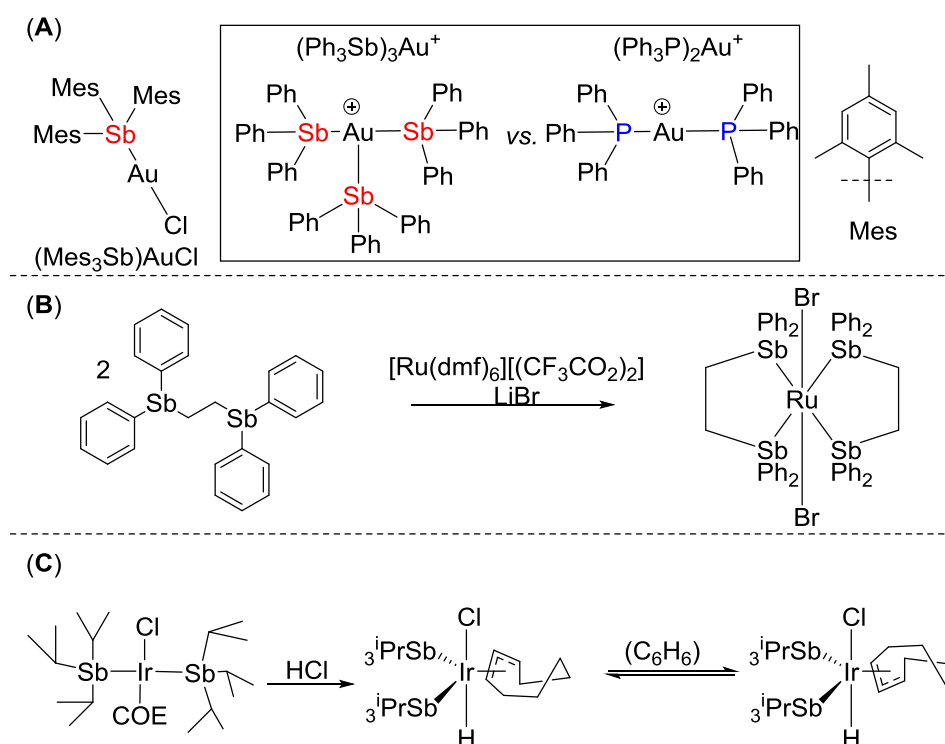


Scheme I-26. Increasing s-character of the lone pair moving from amine to phosphine to stibine

A search of the literature indicates that organostibine donors (SbR_3) have been utilized to synthesize a variety of molecules, though their applications in the support of catalysis and further reactivity appears to be relatively underdeveloped. In the chemistry of gold (Au), Mes_3Sb was shown to bind easily to the Au-Cl fragment to form $(\text{Mes}_3\text{Sb})\text{AuCl}$. However, as a cation, it was found to prefer a higher coordination number versus that of the corresponding phosphine.⁴⁷ What this means is that as $(\text{PPh}_3)_2\text{Au}^+$ is formed, $(\text{SbPh}_3)_3\text{Au}^+$ is able to form where SbPh_3 is available. The reasoning behind this is that as a less electron-donating ligand, Au shows a preference to bind a third equivalent versus the more electron-donating phosphorous analogue (Scheme I-31).

Similar to the chemistry of bidentate amines or phosphines, bidentate stibines based on a 1,2-difunctionalized ethane backbone have been utilized. Levason and coworkers showed that using 1,2-*bis*(diphenylstibino)ethane up to two equivalents could be bound to a RuBr_2 fragment to produce an octahedral complex of the general formula $(\text{L}^{\wedge}\text{L})_2\text{RuBr}_2$ (Scheme I-31). Though further chemistry beyond its solid and solution state structures was not elucidated they note that analysis of structural metrics relating to the Sb-C bond lengths upon coordination reveals that stibine donors

are poor π -acceptors.⁴⁸ Finally, a *tris(isopropyl)*stibine was coordinated to Ir(I) and Ir(III) for the formation of $(^i\text{Pr}_3\text{Sb})_2\text{IrCl}$ and $(^i\text{Pr}_3\text{Sb})_2\text{Ir(H)(Cl)}$ complexes. The Werner group studied the molecular motion of the various ligands attached to iridium on the NMR timescale. Though providing an interesting spectroscopic study, the reactivity of these complexes was not further developed or leveraged into any transformative application (Scheme I-27).⁴⁹

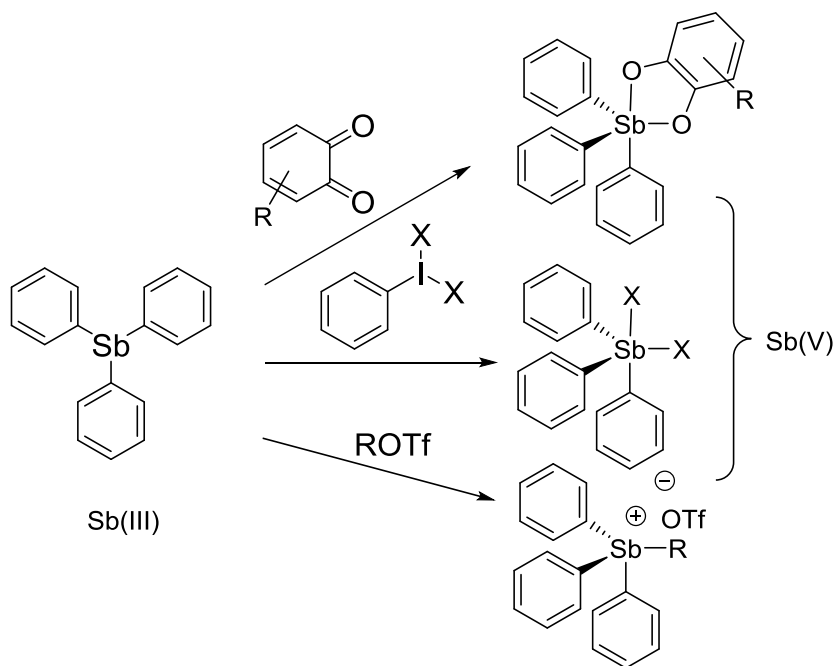


Scheme I-27. (A) Coordination triarylstibines to Au(I) (B) Bidentate stibine coordination to Ru(II) (C) *tris(isopropyl)*stibine coordination to Ir(I) and Ir(III) centers and observable ligand isomerism

1.6.2 Redox Activity of Antimony

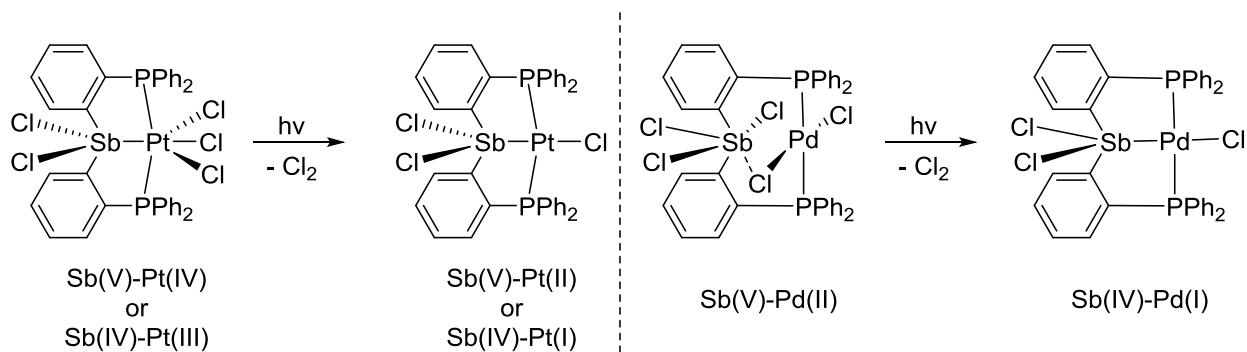
One of the primary potential benefits of utilizing antimony as a ligand in organotransition metal chemistry is the ability of antimony to cycle between oxidation states in a relatively facile

manner. Amines have shown reactivity for single electron chemistries as previously discussed in the formation of aminyl radical cations. The Radosevich group has recently shown, in a beautifully designed study, the ability of phosphorous in a strictly rigid, tridentate ligand environment to cycle between P(III) and P(V) oxidation states.⁵⁰ Despite this, however, each case of redox reactivity requires specifically designed constraints on the system employed. With Sb, this is not necessarily the case, as two electron chemistry is readily available *via* the Sb(III)/Sb(V) redox pairings. Even simple species such as Ph₃Sb are capable of being oxidized to Sb(V) *via* treatment with an *ortho*quinone, X₂ equivalent, or alkyl triflate (R-OTf) to form stiboranes or stiboniums, respectively (Scheme I-28).



Scheme I-28. General reactions that form Sb(V) products from SbPh₃ as an Sb(III) example

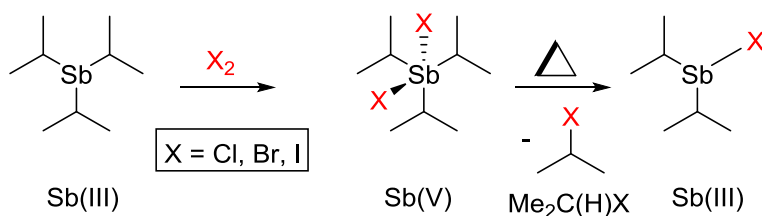
The Gabbai group has shown that redox cycling is possible between Sb(III) and Sb(V) in the coordination sphere of a transition metal. Utilizing a (PSbP)Pt complex it was discovered that photoreductive elimination of chlorine followed by subsequent, redox non-innocent rearrangements could furnish a clean transformation to a Sb(V)-Pt(II) species which can also be formulated as Sb(IV)-Pt(I).⁵¹ They have also shown a similar phenomenon of photoreductive chlorine elimination in a (PSbP)Pd complex where a Sb(V)-Pd(II) species is transformed into what is assigned as a Sb(IV)-Pd(I) species (Scheme I-29).⁵²



Scheme I-29. Examples of photoreductive elimination of chlorine from PSbP pincer ligated Pt and Pd species to form counter-intuitive mixed-valence species

The privileged pincer framework in these cases proves to not be necessary in the redox capabilities of Sb. Other, simpler Sb species are also capable of undergoing an elimination from an Sb(V) center to form a desired Sb(III) product. The synthesis of ${}^i\text{Pr}_2\text{SbX}$ ($\text{X} = \text{Cl}, \text{Br}, \text{I}$) is one such example. Since substitution at SbX_3 reagents is easily performed to get *tris*-functionalized stibines, in order to get the mixed variant, some synthetic creativity is necessary. First ${}^i\text{Pr}_3\text{Sb}$ is made by action of ${}^i\text{PrMgCl}$ and SbCl_3 . Then, ${}^i\text{Pr}_3\text{Sb}$ is oxidized by treatment with the suitable X_2

reagent (Cl_2 , Br_2 , or I_2) to generate the Sb(V) species, ${}^i\text{Pr}_3\text{SbX}_2$. This Sb(V) reagent can then undergo a thermal elimination of $\text{Me}_2\text{C}(\text{H})\text{X}$ to cleanly produce ${}^i\text{Pr}_2\text{SbX}$ species (Scheme I-30).⁵³

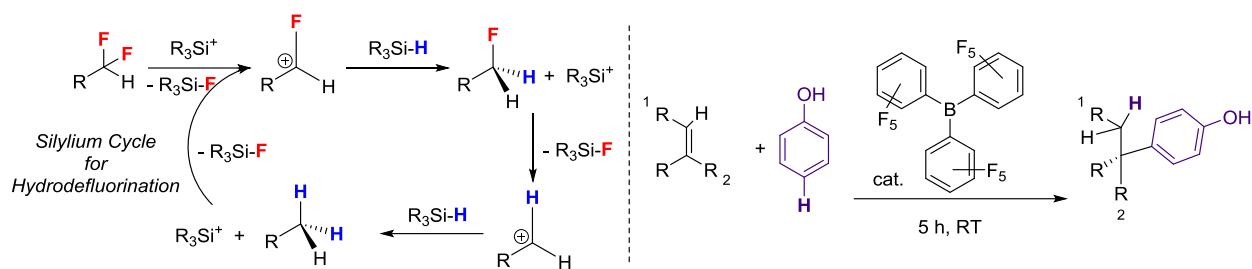


Scheme I-30. Oxidation of a trialkyl stibine, Sb(III) to Sb(V) and subsequent thermal elimination of an alkyl halide to form the desired Sb(III) complex

1.6.3 Antimony as a Potent Lewis Acid for Anion Binding

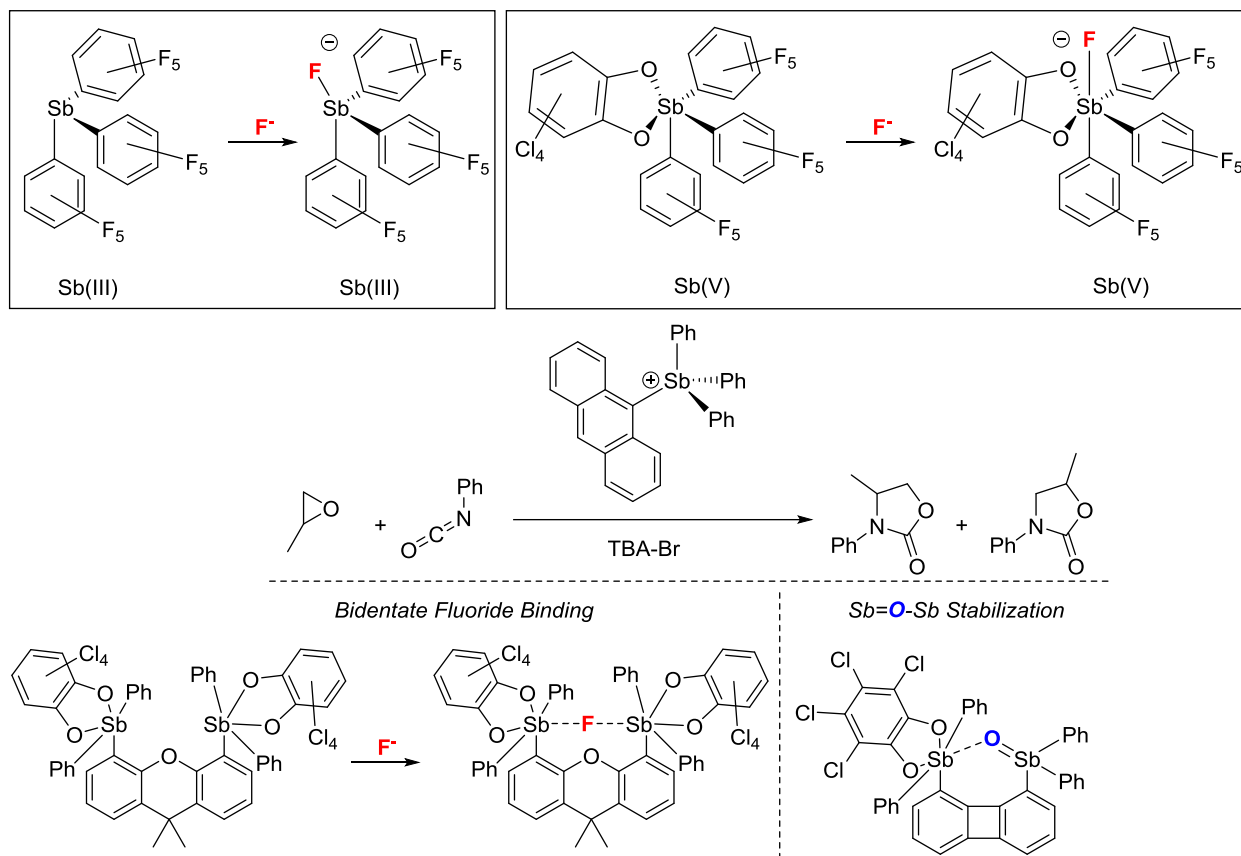
So long as chemists have sought to activate unsaturated species, they have worked to develop more potent, selective, and useful lewis acids. Lewis acids are defined primarily by their electrophilicity and available, empty orbitals into which lone pair or σ -bonding electrons can be donated. Largely, transition metals act as Lewis acids towards Lewis basic ligands, though the intentional synthesis and application of Lewis acids is a worthy endeavor in its own rite.

Typical main group Lewis acids have centered on boranes, such as $\text{B}(\text{C}_6\text{F}_5)_3$ which feature high Lewis acidity due to a low-lying, empty p-orbital. $\text{B}(\text{C}_6\text{F}_5)_3$ has been utilized to generate highly reactive H^+ equivalents but also other electrophilic main group lewis acids, such as silylium *via* its reaction with HSiR_3 species to give $[\text{R}_3\text{Si}^+][\text{HB}(\text{C}_6\text{F}_5)_3]^-$ equivalents. Borane and silane-based lewis acids have found great utility in the recently reported hydroarylation of phenols with alkenes, and also in the hydrodefluorination of aliphatic C-F bonds (Scheme I-31).⁵⁴



Scheme I-31. Si/B-based Lewis acid mediated hydrodefluorination and hydroarylation

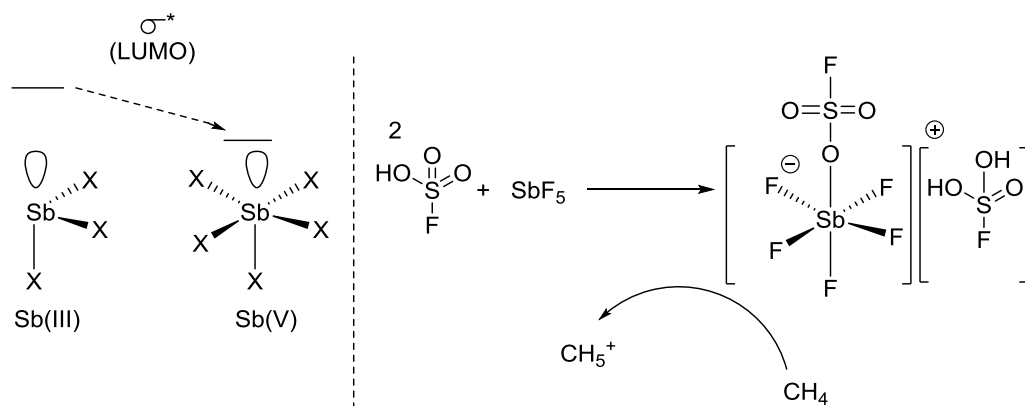
Antimony, as heavy, more electrophilic congener of phosphorous has the ability to exhibit enhanced Lewis acidic properties even while in the Sb(III) oxidation state. It was shown by the Gabbai group that certain Sb(III) compounds are able to behave as Lewis acids for the binding of fluoride anion (F^-) as well as certain electrophilic P(V) compounds (Scheme I-32).⁵⁵ They have also shown the electrophilicity of stibonium species (SbR_4^+) and their subsequent activity in catalytic cyclizations of epoxides with isocyanates,⁵⁶ as well as the bidentate Lewis acidic binding of fluoride anion and Lewis acid stabilization of a Sb(V)-oxo species by an intramolecular Sb=O-Sb interaction (Scheme I-32).⁵⁷



Scheme I-32. Fluoride anion binding to highly Lewis acidic $Sb(III)$ and $Sb(V)$ species. Epoxide/isocyanate cyclization catalyzed by an $Sb(V)$ cation. Intramolecular Sb Lewis acid stabilization of a terminal $Sb=O$ moiety

Strong nucleophiles are defined by those molecules which have a lone pair of electrons in a high-lying HOMO that are accessible for donation. Strong electrophiles, being the opposite, are defined by those molecules which contain unfilled orbitals, or LUMOs which are lower in energy and can effectively accept lone pair donation from an appropriate nucleophile. The combination of a strong nucleophile and a strong electrophile generally necessitates interaction and quenching of reactivity, steric parameters aside. However, a strong nucleophile or electrophile can often interact with weaker complementary partners to quench reactivity, or potentially “activate” those complexes it interacts with.

The high Lewis acidity of antimony can be traced mainly to the presence of a low-lying σ^* which can accept lone pairs of electrons from suitable nucleophiles. This “ σ -hole” as it has been termed allows for a tuning of the Lewis acidic properties at Sb. By oxidizing to Sb(V), this lowers the energy of the LUMO, thereby increasing effective electrophilicity and a deepening of the “ σ -hole.”⁵⁵ This high electrophilicity has been leveraged in the generation of highly electrophilic species such as “magic acid” or HSbF_6 which is generated by the action of SbF_5 on fluorosulfinic acid (FSO_3H) to generate a highly reactive “naked” proton source, being formally $[\text{H}][\text{SbF}_5(\text{SO}_3\text{F})]$ that is capable of protonating even methane (Scheme I-33).⁵⁸



Scheme I-33. Deepening of the “ σ -hole” by oxidation to Sb(V) and “Magic acid” generation

For these reasons and more, we are interested in exploring the ability of Sb in the +5 oxidation state to act as a strong Lewis acid. By utilizing chemical principles to inform the rational synthetic design of stronger, multidentate Lewis acids, it is expected that the binding and subsequent activation of weakly nucleophilic/reactive small molecules will be achieved.

1.7 Conclusion and Overview

Contained in this chapter was a brief foray into the chemistry of pincer ligands and the reactivities, both stoichiometric and catalytic, that they're capable of supporting. Acting as tridentate, rigid scaffolds, they can stabilize highly reactive species for in depth mechanistic analysis. Different types of pincer ligands were explored with an intentional focus on the PCP and PNP variants, based on diarylamine backbones. The combination of various σ - and π -donor effects engender unusual reactivity and the combination of hard and soft donors allows for the isolation of pincer complexes of various elements across the periodic table. The catalytic dehydrogenation and hydrofunctionalization reactivities supported by the PCP and PNP pincer, respectively, were discussed. The general chemistry of redox active rhenium was introduced as well as concepts involving metal-ligand multiple bonding. Pincer-supported complexes of rhenium were disclosed which notably tend to feature a central nitrogenous donor and support a wealth of oxidation chemistries. Finally, the general chemistry of antimony was shown as a neutral Sb(III) donor to transition metal complexes, a redox active participant in photochemical transition metal reactions, and a potent Lewis acid for anion binding and catalysis. Taken together this chapter provides a solid, cursory basis from which further chemistries can and will be leveraged and developed into innovation and hopefully application.

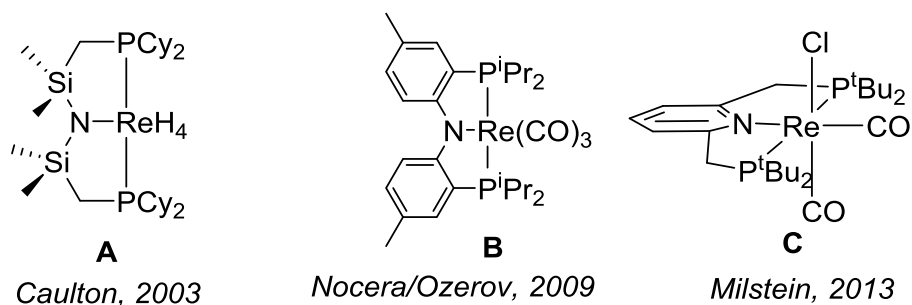
CHAPTER II

COMPLEXES OF HIGH-VALENT RHENIUM SUPPORTED BY THE PCP PINCER*

2.1 Introduction

Pincer ligands bind to transition metals in tridentate, meridional fashion, enforcing rigid geometries. They confer formidable thermal stability and have allowed for the study of multiple, challenging stoichiometric, and sometimes catalytic applications to be discovered and further developed.⁵⁹⁻⁶¹ A large advantage of pincer frameworks lies in the robust nature and preservation of the meridionally bound coordination mode under forcing conditions. Since their conception in 1976 by Shaw and coworkers,¹⁰ no pincer ligand has retained quite as much attention throughout the years⁶² as the aryl/bis(trialkylphosphine) PCP scaffold based on bis(*ortho*-phosphinomethyl)benzene. Seeking to further expand upon the chemistry accessed via the use of PCP-supported transition metals, we aimed to synthesize its rhenium complexes.

* Reprinted in part with permission from “Complexes of High-Valent Rhenium Supported by the PCP-Pincer” Kosanovich, A. J.; Reibenspies, J. H.; Ozerov, O. V. *Organometallics* **2016**, 35, 513-519. Copyright 2016 by American Chemical Society. DOI: 10.1021/acs.organomet.5b00935



Scheme II-1. Examples of rhenium complexes supported by pincer ligands featuring central amido and pyridyl donors. Reprinted with permission from [107]

The known chemistry of rhenium in the pincer context primarily involves pincer ligands with a central nitrogenous donor (examples **A-C** in Scheme II-1), either a neutral amine- or pyridine-type,⁶³⁻⁶⁶ or an anionic amido site.⁶⁷⁻⁷¹ We surmised that encapsulation of rhenium in a PCP scaffold may provide different reactivity avenues by virtue of stronger σ -donation from the aryl donor. Given the history of rhenium polyhydrides in C-H bond activation reactions,^{72,73} we were particularly interested in accessing rhenium polyhydrides supported by the PCP ligand. In this report, we describe synthetic routes to PCP complexes of Re(V) oxo fragments, their conversion to various polyhydrides, and other metathesis reactivity, including generation of reactive, cationic species.

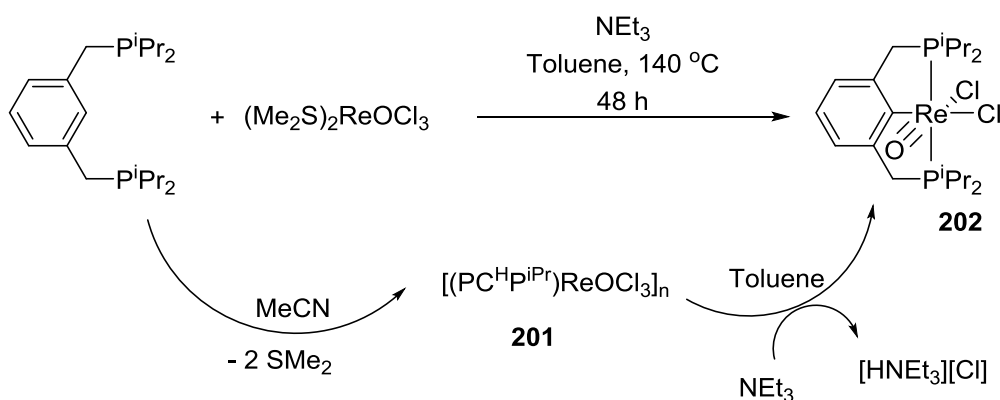
2.2 Results and Discussion

2.2.1 Synthesis of Re(V) Oxo Complexes

The work by the Caulton group^{67a} with Re complexes of the Fryzuk^{74, 75} disilylamido/bis(phosphine) PNP ligand (e.g. Scheme II-1 A) showed that $(\text{Me}_2\text{S})_2\text{ReOCl}_3$ is an

easily accessible and convenient precursor due to the apparent ease of replacement of the Me_2S ligands and because of the volatility of the released, free Me_2S . Targeting the reaction of $(\text{Me}_2\text{S})_2\text{ReOCl}_3$ with PCP^{iPr} , we surmised that the phosphine donors would readily displace Me_2S , creating a setup for an intramolecular metalation of the central pincer C-H bond.

Indeed, reaction of PCP^{iPr} with $(\text{Me}_2\text{S})_2\text{ReOCl}_3$ in acetonitrile resulted in the precipitation of the “unmetallated” adduct $(\text{PC}^{\text{H}}\text{P}^{\text{iPr}})\text{ReOCl}_3$ (**201**), isolated in 64% yield as a bright, yellow-green powder of 85 - 90% purity, which could be used without further purification. Pure **201** could be obtained by recrystallization from CH_2Cl_2 and pentane in 10% yield. **201** gives rise to a singlet resonance by $^{31}\text{P}\{^1\text{H}\}$ NMR (δ -4.1) spectroscopy, while the ^1H NMR spectrum contains the expected resonances of the coordinated $\text{PC}^{\text{H}}\text{P}^{\text{iPr}}$ ligand, including resonances corresponding to the four aromatic C-H protons. The presence of the rhenium-oxo moiety was confirmed by IR spectroscopy ($\nu_{\text{Re}=\text{O}} = 978 \text{ cm}^{-1}$), though the exact structure and connectivity of **201** could not be determined.



Scheme II-2. Synthesis of PCP-rhenium 1:1 adduct (**201**) and subsequent C-H activation to access $(\text{PCP}^{\text{iPr}})\text{ReOCl}_2$ (**202**)

Metallation of PCP ligands is very common at many late transition metals. The Takai group has reported multiple instances of successful, directed C-H activation at rhenium(I) ⁷⁶, and there are important examples of intermolecular C-H activation at Re centers in various oxidation states.^{72,73} Although examples of aryl C-H activation at oxo rhenium(V) complexes are rare, metalation of PCP^{iPr} seemed very plausible. Thermolysis of the crude **201** with Et₃N in toluene (Scheme II-2) led to the elimination of triethylammonium chloride and formation of the metallated pincer complex **202**. Interestingly, utilization of other neutral nitrogenous (2,6-lutidine, HNⁱPr₂, EtNⁱPr₂, HN(SiMe₃)₂) or anionic (LiN(SiMe₃)₂, KO^tBu) bases was less effective and led to little to no formation of (PCP^{iPr})ReOCl₂. Isolation of **201** proved unnecessary for the synthesis of **202**. Thermolysis of (Me₂S)₂ReOCl₃ in toluene or *p*-xylene in the presence of Et₃N led to predominant formation of **202** (³¹P NMR evidence in situ). **202** was isolated in a pure form as a bright green powder in 51% isolated yield after workup. NMR spectra of **202** indicated C_s-symmetry on the NMR timescale. A lone singlet resonance was detected in the ³¹P{¹H} spectrum. In the ¹H NMR spectrum, four resonances for the isopropyl methyl groups, two resonances for the isopropyl methines, as well as two resonances for the benzylic protons showing strong geminal (²J = 16 Hz) coupling were observed in the aliphatic region. These ¹H NMR resonances and the corresponding ¹³C NMR resonances all displayed virtual coupling to the two ³¹P nuclei, as is common for complexes with *trans*-disposed phosphines.

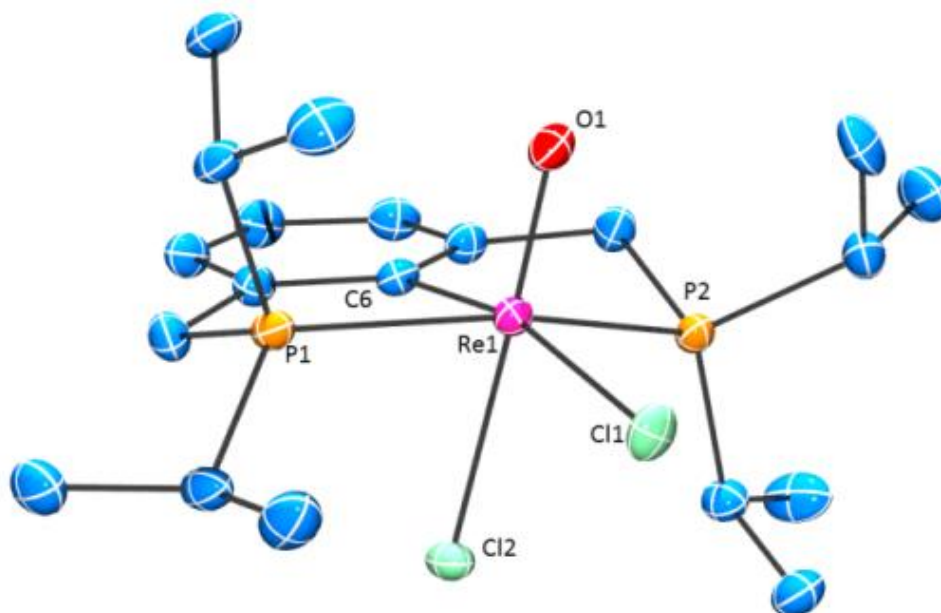
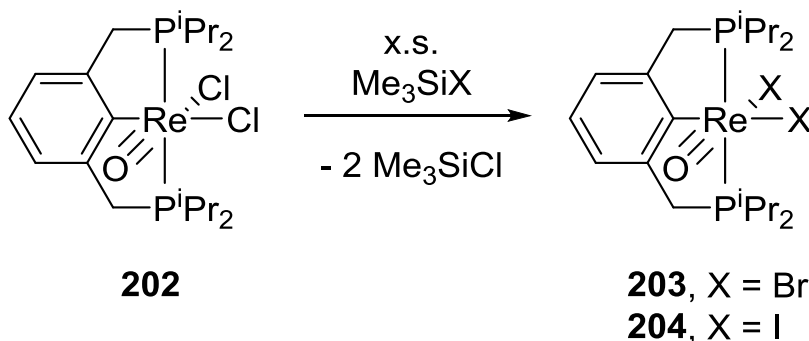


Figure II-1. ORTEP⁷⁷ drawing (50% probability ellipsoids) of (PCP^{iPr})ReOCl₂ (**202**). H atoms and a disordered molecule of cocrystallized toluene omitted for clarity. Selected distance (Å) and angles (°) follow: Re1-O1, 1.692(2); Re1-P1, 2.365(1); Re1-P2, 2.346(1); Re1-C6, 2.116(3); Re1-Cl1, 2.4539(7); Re1-Cl2, 2.4248(8); P1-Re-P2, 158.53(3); P1-Re1-C6, 81.04(8); P2-Re1-C6, 80.31(8); O1-Re1-C6, 99.15(10); O1-Re1-Cl2, 177.34(7); C6-Re1-Cl1, 164.78(8); C6-Re1-Cl2, 81.71(7); Cl1-Re1-Cl2, 83.36(3); O1-Re1-Cl2, 177.34(7). Reprinted with permission from [107]

An X-ray diffraction study unambiguously confirmed the identity and symmetry of **202**, with a pseudooctahedral configuration about Re featuring an oxo ligand *cis* to the central C of PCP (Figure II-1). As expected for a d^2 rhenium species, a typically short rhenium-oxo bond (1.692(2) Å) is noted, allowing its assignment as a formal triple bond.^{78,79} The structure features a rhenium-aryl bond length (Re1-C6, 2.116(3) Å) similar to the structurally characterized rhenium(V)-oxo-aryl species $\text{Tp}^*\text{Re}(\text{O})\text{Ph}(\text{OTf})$, reported by Mayer et al. (Re-Ph, 2.111(5) Å).⁸⁰ The PNP-supported systems by Caulton gave rise to both the C_s and C_{2v} -symmetric (in which oxo lies *trans* to the amido nitrogen) isomers of (PNP)ReOCl₂ in equilibrium but we saw no evidence of the presence of the putative C_{2v} -symmetric isomer of **202**. It is likely that the more strongly *trans*-influencing nature of the central C_{sp^2} -aryl donor strongly disfavors positioning of it *trans* to the oxo ligand in **202**.



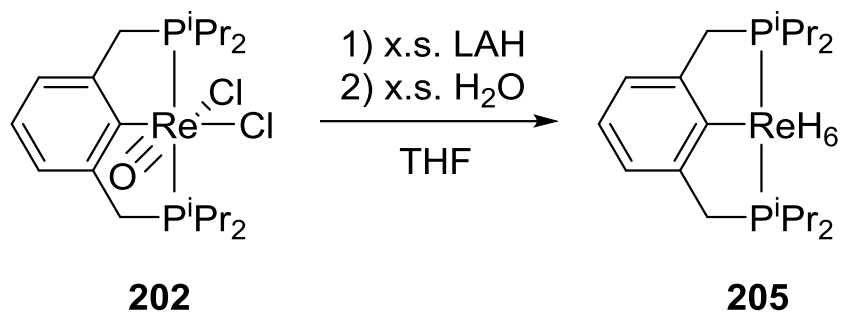
Scheme II-3. Halide metathesis reactivity of **202** with trimethylsilylhalide reagents. Reprinted with permission from [107]

Reaction of **202** with a large excess (20 equiv.) of bromotrimethylsilane (Me_3SiBr) in toluene led to the clean formation of $(\text{PCP}^{\text{iPr}})\text{ReOBr}_2$ (**203**) after 24 h (Scheme II-3). **203** was

isolated in 88% yield as a dark green powder. With the addition of only 10 equiv. of Me₃SiBr, 64% of an intermediate, assumed to be (PCP^{iPr})ReOBrCl, could be seen by ³¹P{¹H} NMR (δ 45.1) spectroscopy after 12 h, along with 33% of **203**. Addition of another 10 equiv. Me₃SiBr led to the full conversion to **203** (δ 38.9) after 12 h. Similarly, reaction of **202** with five equivalents of iodotrimethylsilane (Me₃SiI) in toluene produced (PCP^{iPr})ReOI₂ (**204**) in minutes, as observed by ³¹P{¹H} NMR spectroscopy (δ 23.9). The product was isolated as a dark red-brown, microcrystalline powder in 70% yield. All (PCP^{iPr})ReOX₂ (X = Cl, Br, I) species were found to be air and moisture stable. Only C_s-symmetric isomers were evident in NMR spectra of **203** and **204**. **202**, **203**, and **204** featured characteristic rhenium-oxo stretches in their IR spectra at similar frequencies (**202**, 978 cm⁻¹; **203**, 976 cm⁻¹; **204**, 974 cm⁻¹).

2.2.2 Synthesis of a Rhenium Polyhydride Complex

Amongst high valent rhenium, there are multiple reported examples of isolable, neutral polyhydrides including (PPh₃)₃ReH₅, Tp*ReH₆, (PNP)ReH₄,⁸¹ and (triphos)ReH₅,⁸² to name a few. By analogy to the synthesis of (PPh₃)₂ReH₇,⁸³ treatment of **202** with an excess of LiAlH₄, followed by aqueous workup, resulted in the isolation of (PCP^{iPr})ReH₆ (**205**) as an ashy gray solid in 72% yield (Scheme II-4).



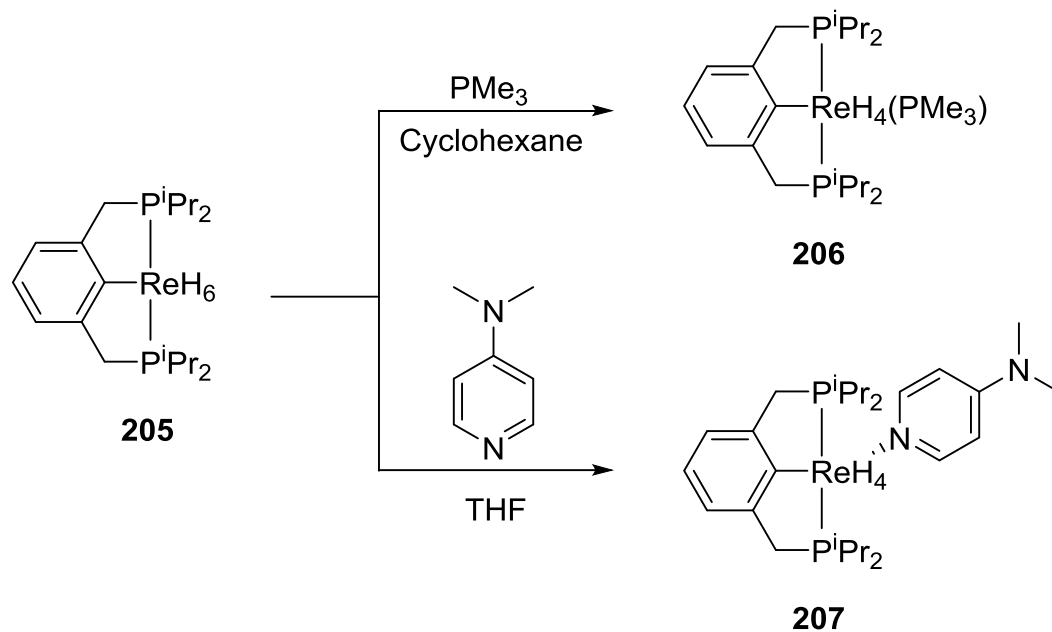
Scheme II-4. Reduction of **202** using an excess of LAH to form the hexahydride, **205**. Reprinted with permission from [107]

The $^{31}\text{P}\{^1\text{H}\}$ NMR spectrum of **205** features a sharp, singlet resonance (δ 72.1). Similar to $(\text{PPh}_3)_2\text{ReH}_7$,⁸⁴ facile H/D exchange occurred in solutions of deuterated benzene, even at 22 °C, resulting in initial scrambling and the eventual loss of the hydride resonance by ^1H NMR. Thus, more inert deuterated solvents (C_6D_{12} , $\text{THF-}d_8$) were utilized for spectroscopic studies. The ^1H NMR spectrum in cyclohexane- d_{12} showed clear doublet and triplet resonances ($J_{\text{H-H}} = 7.3$ Hz) of 2:1 ratio in the aromatic region, corresponding to the PCP^{iPr} backbone. Based on two doublet of virtual triplet resonances for each set of isopropyl methyl (12H each) groups, as well as single multiplets for methine (4H) and benzylic (4H) resonances, **205** appears to adopt C_{2v} symmetry in solution on the NMR timescale. All six (by ^1H NMR integration) hydride ligands are chemically equivalent at room temperature, giving rise to an upfield triplet resonance in the ^1H NMR spectrum (δ - 6.2, $J_{\text{P-H}} = 16.9$ Hz). A selectively decoupled $^{31}\text{P-}^1\text{H}$ NMR spectrum allowed the observation of a clear septet, showing the ligand phosphines are split by six chemically equivalent hydrides. T_1 inversion recovery experiments at low temperature allow for the observation of hydride bonding modes,⁸⁵ and have even led to the reformulation of the heptahydride, $(\text{PPh}_3)_2\text{ReH}_7$, as the pentahydride, dihydrogen species: $(\text{PPh}_3)_2\text{ReH}_5(\text{H}_2)$.⁸⁶ At low temperatures, *poly*hydrides can

“freeze out”, breaking their symmetry and allowing for the resolution of multiple hydride resonances by ^1H NMR spectroscopy.⁸⁷ Variable temperature T_1 measurements conducted on the triplet hydride resonance of **205** (- 6.2 ppm, ^1H NMR, {500 MHz, THF- d_8 }) showed that even at -75 °C, the symmetry of the hexahydride is maintained, providing a single triplet resonance, and a T_1 minimum measurement of 225 ms. Although this measurement is most consistent with a classical hexahydride formulation, some ambiguity remains, as fast hydride exchange between classical and non-classical hydrogen positions could account for these observations, even at low temperature.⁸⁸

2.2.3 Reactivity of the (PCP)Re polyhydride

Reactions of **205** with PMe_3 in cyclohexane or with 4-dimethylaminopyridine (dmap) in THF were found to proceed in a facile manner at ambient temperature with loss of H_2 to provide the adducts $(\text{PCP}^{\text{iPr}})\text{ReH}_4(\text{L})$ ($\text{L} = \mathbf{206}, \text{PMe}_3; \mathbf{207}, \text{dmap}$). **206** and **207** were isolated in moderate to good yields. (Scheme II-5).



Scheme II-5. Synthesis of (PCP)ReH₄(L) species *via* introduction of PMe₃ or DMAP. Reprinted with permission from [107]

The ³¹P{¹H} NMR spectrum of **206** shows two broad resonances (δ 65.5, -40.9) in a 2:1 ratio, corresponding to the ligand phosphines and coordinated trimethylphosphine (shifted downfield from free trimethylphosphine (δ -62)). **207** features a singlet resonance (³¹P{¹H} NMR) at 68.1 ppm, corresponding to the metallated PCP^{iPr}. The hydride resonances for **206** and **207** present as singular, broad, upfield humps at -5.5 and -6.24 ppm, respectively, and each integrate to four hydrogens. Unlike **205**, **206** and **207** do not undergo H/D exchange in solutions of C₆D₆ at ambient temperature. **207** features two resonances (2H each) for the pyridyl *ortho* and *meta* protons (¹H NMR, δ 8.35 and 5.43, respectively), as well as a singlet resonance for the NMe₂ moiety (δ 1.94), indicating unrestricted rotation about the Re-N_{dmap} bond. The most obvious spectroscopic difference between **206** and **207** at ambient temperature is the apparent C_{2v} symmetry for **206**, contrasted with C_s-symmetry for **207**. An X-ray structural study on a suitable crystal of **207**

confirmed the C_s symmetry observed in solution, with the dmap ligand bound to Re perpendicularly to the PCP/Re plane (and thus *cis* to the central C of PCP). It was not clear whether the higher apparent symmetry for **206** in solution by NMR spectroscopy reflected positioning of the PMe_3 ligand trans to C of PCP or is a result of a rapid fluxional process exchanging two degenerate C_s structures. Therefore, variable temperature NMR experiments were carried out. By $^{31}P\{^1H\}$ NMR spectroscopy, low temperatures (below 0 °C) allowed for the resolution of the coupling constant ($J_{P-P} = 9.7$ Hz) shown as the doublet splitting of the PCP resonance from the PMe_3 moiety, though the corresponding PMe_3 resonance remained broad. From room temperature down to -40 °C, the higher C_{2v} -symmetry appeared to be maintained, though broadening of resonances was observed (1H NMR evidence). Cooling a d_8 -toluene solution of **206** to -75 °C resulted in the clear resolution of two separate multiplet hydride resonances (-4.07 and -7.83 ppm, 1H NMR, {500 MHz}), as well as the resolution of two separate resonances for the benzylic C-H protons, indicative of C_s -symmetry. Though it remains ambiguous whether **206** is truly a fluxional C_s -symmetric molecule that merely appears to be of higher symmetry, it is clear that a C_s -symmetric isomer dominates as the major constituent in solution at low temperatures. Unlike **205** and **206** which turn purple and give rise to unidentified products upon exposure to air, **207** could be handled in open air as either a solid, or in solution, for brief periods of time without visible decomposition.

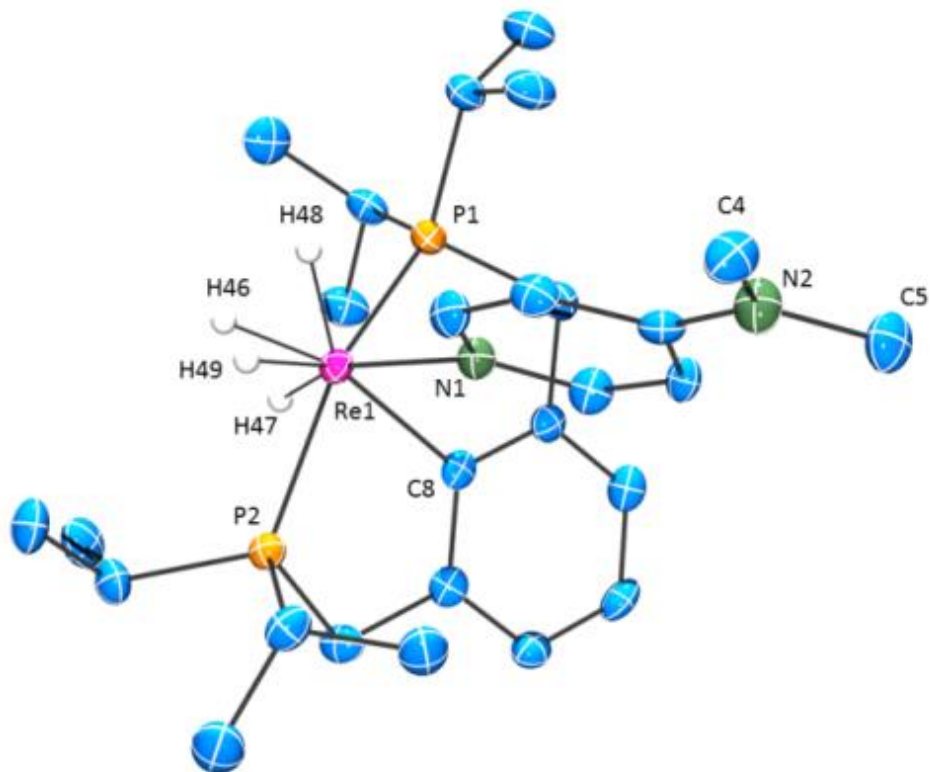
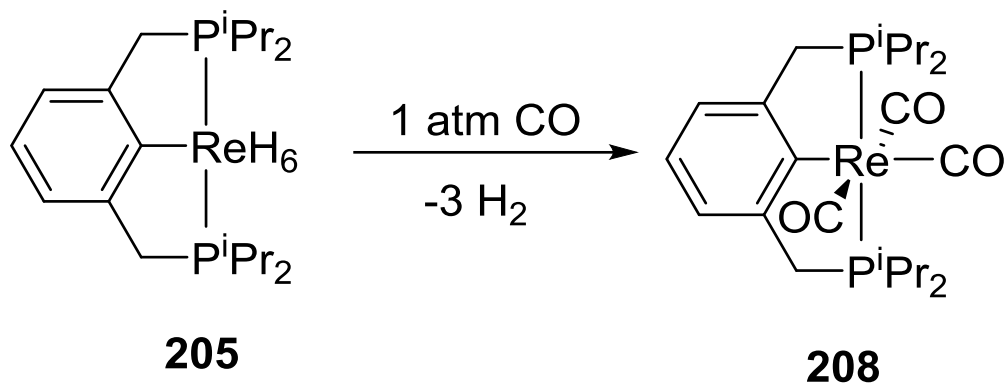


Figure II-2. ORTEP drawing (50% probability ellipsoids) of $(PCP^{iPr})ReH_4(dmap)$ (**207**). All ligand (PCP^{iPr}) based H atoms omitted for clarity. Selected distance (Å) and angles ($^\circ$) follow: Re1-C8, 2.207(4); Re1-N1, 2.289(4); Re1-P1, 2.3645(14); Re1-P2, 2.3454(15); Re1-H46, 1.51(4); Re1-H47, 1.57(4); Re1-H48, 1.50(5); Re1-H49, 1.66(4); N1-Re1-C8, 85.17(14); P1-Re1-P2, 153.54(4); C4-N2-C5, 117.4(4); P2-Re1-C8, 79.28(12); P1-Re1-C8, 77.37(12). Reprinted with permission from [107]

The structure of **207** (Figure II-2) shows the pincer bound in a T-shaped geometry. Four hydrogen atoms were located on the electron difference map, but significant uncertainty in positional determination precludes us from drawing conclusions with regards to possible H-H bonding. Of note is the significantly longer rhenium-aryl bond (Re1-C8, (2.207(4) Å)) and a smaller P-Re-P angle (153.54(4) $^\circ$) for **207** versus those of $(PCP^{iPr})ReOCl_2$ (2.116(3)Å and 158.53(3) $^\circ$). It is possible that the lengthening of the Re-C is a reflection of being situated *trans* to two hydrides (or perhaps a dihydrogen ligand) in **207** vs *trans* to a chloride in **202**.

As observed for other rhenium-*polyhydrides*,^{89,90} reaction of **205** with CO in C₆D₆ resulted in the expulsion of H₂ and HD (result of H/D exchange) with quantitative formation over 24 h of (PCP^{iPr})Re(CO)₃ (**208**), isolated as an off-white powder in 93% yield (Scheme II-6).

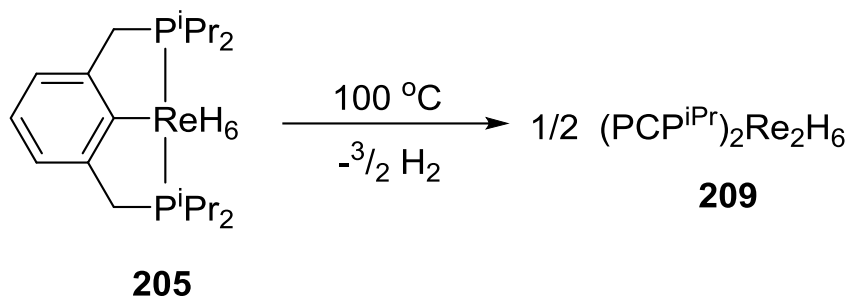


Scheme II-6. Synthesis of the rhenium(I) tricarbonyl, **208**, by addition of CO to **205**. Reprinted with permission from [107]

208 shows a sharp, singlet resonance by ³¹P{¹H} NMR (δ 53.2) and features C_{2v} symmetry, as evidenced by four broad, ligand based multiplet resonances (¹H NMR) in a 3:4:4:24 ratio. The presence of three coordinated carbonyls was confirmed by elemental analysis, IR spectroscopy (ν_{Re-CO} = 1901, 1911, 2015 cm⁻¹), and ¹³C{¹H} NMR spectroscopy, as two downfield resonances of roughly 2:1 intensity (δ 197.93, 197.86). The frequencies of the IR bands of **208** are similar to those of (MePNP^{iPr})Re(CO)₃,⁶⁸ which is somewhat surprising given that PCP is a more donating ligand than MePNP^{iPr}. Alternatively, **208** could also be accessed in good yields by reaction of **206** with CO over 72 h at 80 °C in C₆D₆. Initial expulsion of H₂ is noted by ¹H NMR spectroscopy, as

a new intermediate product is observed in the $^{31}\text{P}\{^1\text{H}\}$ NMR spectrum, assumed to be $(\text{PCP}^{\text{iPr}})\text{Re}(\text{CO})_2(\text{PMe}_3)$, with resonances at 48.2 and -53.1 ppm, in a 2:1 ratio, respectively.

Thermolysis of **205** in cyclohexane- d_{12} (90 °C, 48 h) gave rise to a mixture of products with the major product showing two phosphine resonances by $^{31}\text{P}\{^1\text{H}\}$ NMR, each shifted downfield from those of **205**. A new, quintet hydride resonance was observed (δ -7.13, $J_{\text{P-H}} = 7.2$ Hz) in the ^1H NMR spectrum. Heating a degassed *cyclo*- C_6H_{12} solution of **205** in a J. Young tube for 4 h at 100 °C led to observation of a single thermolysis product ($^{31}\text{P}\{^1\text{H}\}$ NMR evidence). Filtration of the solution and subsequent drying under reduced pressure allowed for the isolation of this product in moderate yield as a dark purple, air-sensitive, microcrystalline powder. A lack of H/D exchange allowed for spectroscopic characterization of the dimerized species in C_6D_6 . The isolated product produced two broad resonances in its $^{31}\text{P}\{^1\text{H}\}$ NMR spectrum (δ 82.4, 77.4) in 1:1 ratio. By ^1H NMR spectroscopy, the aromatic resonances of the PCP^{iPr} backbone could be clearly resolved as a doublet and triplet ($J_{\text{H-H}} = 7.3$ Hz) in 2:1 ratio, respectively. Broadened resonances for the benzylic, isopropyl methine, and isopropyl methyl protons presented as large humps in the spectrum which integrated 4:4:24, respectively. The hydride resonance, which integrates to three hydrogens per PCP ligand, showed a clear, quintet splitting pattern (δ -6.95, $J_{\text{P-H}} = 7.2$ Hz) analogous to that seen in the dimeric $(\text{PPhEt}_2)_4\text{Re}_2\text{H}_8$ (δ -16.59, $J_{\text{P-H}} = 9.3$ Hz) synthesized by Strickler.⁹¹ In the latter, the hydride resonances are chemically equivalent on the NMR time scale, and split equally by the four phosphines. In that same report, Strickler's neutron diffraction study of $(\text{PPhEt}_2)_4\text{Re}_2\text{H}_8$ showed the molecule to feature a Re-Re multiple bond with four bridging hydride ligands. We propose that the product of thermolysis of **205** is the analogous dimer $(\text{PCP}^{\text{iPr}})_2\text{Re}_2\text{H}_6$ (**209**), in which the aryl donors could be viewed as replacing two of the hydrides (most likely, terminal) in Strickler's dimer (Scheme II-7).



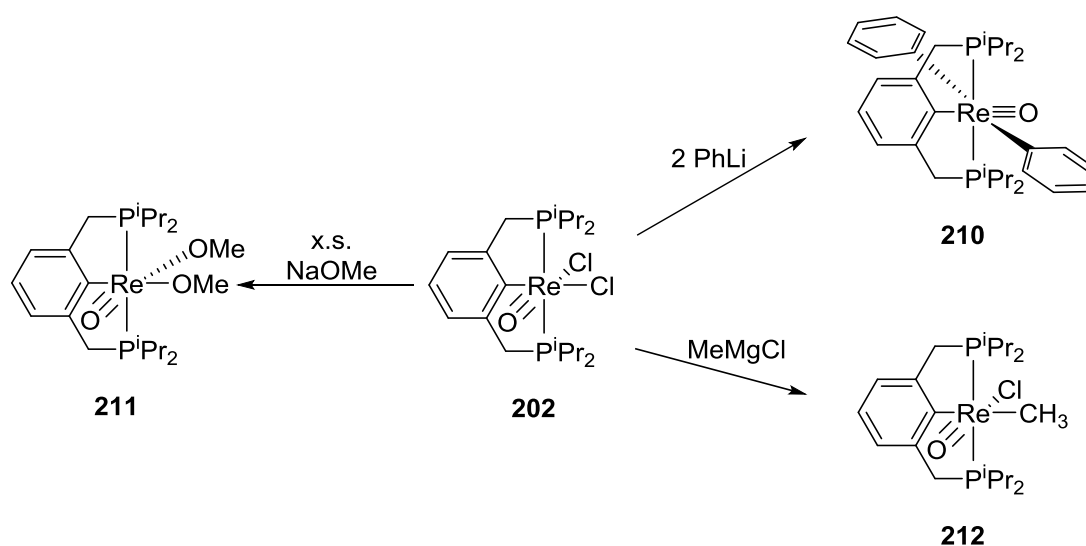
Scheme II-7. Dehydrogenative dimerization of **202** via loss of $3/2 \text{ H}_2$. Reprinted with permission from [107]

Seeking to further elucidate the binding modes of the hydrides, low temperature experiments conducted on the quintet hydride resonance of **209** (-6.3 ppm , $^1\text{H NMR}$, {500 MHz, Toluene- d_8 }) showed that even down to $-75 \text{ }^\circ\text{C}$, the chemical equivalence of the hydrides is maintained, providing a single broad resonance, and a T_1 minimum measurement of 410 ms, supportive of its formulation as containing only classically bound hydride ligands. Unfortunately, the high solubility of **209** precluded the growth of single crystals suitable for x-ray analysis and spectroscopic data alone do not allow for an unambiguous assignment of the connectivity and structure of **209**. It seems most likely that each PCP pincer is bound to a single Re center, however we cannot exclude that PCP is bridging in some fashion.⁹²

2.2.4 Metathesis Reactivity of $(\text{PCP}^{\text{iPr}})\text{ReOCl}_2$

Additional salt metathesis reactivity and cation generation reported here was performed following initial publication. **202** was found to undergo facile salt metathesis reactions with a variety of reagents, allowing access to $(\text{PCP}^{\text{iPr}})\text{ReOX}_2$ complexes of potential interest (Scheme II-8). Treatment with two equivalents of PhLi resulted in the clean formation of C_{2v} -symmetric ($^1\text{H NMR}$ evidence) $(\text{PCP}^{\text{iPr}})\text{ReO}(\text{Ph})_2$ (**210**) which exhibits a single resonance in its $^{31}\text{P}\{^1\text{H}\}$ NMR

spectrum at δ 44.7 ppm. The *isopropyl* methyl resonances appear as two doublet of virtual triplets (12H each) with a single benzylic methylene resonance (4H). Notably, the resonances corresponding to the *ortho* C-H protons on the two phenyl ligands are inequivalent (δ 8.08 and 6.03 ppm, 2H each) indicative of restricted rotation imposed by the sterically bulky *iPr* substituents on the flanking phosphine donors.



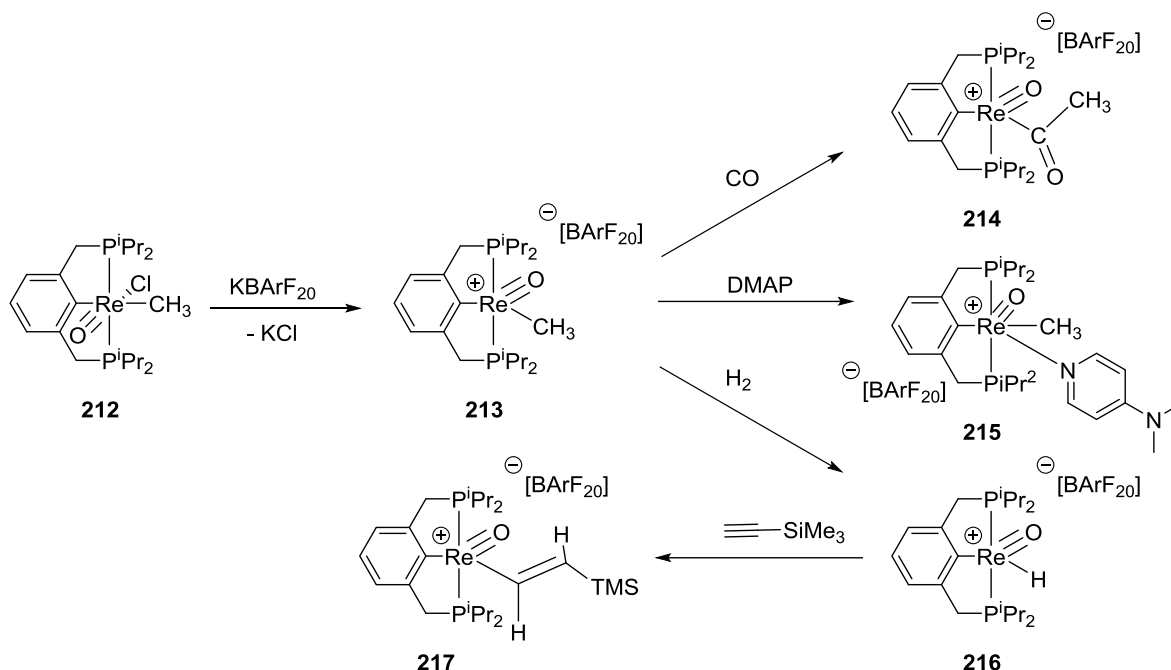
Scheme II-8. Salt metathesis reactivity of **202** with PhLi, NaOMe, and MeMgCl.

Reaction of **202** with an excess of NaOMe resulted in the clean formation of $(PCP^{iPr})ReO(OMe)_2$ (**211**) which presents a single resonance in its $^3P\{^1H\}$ NMR spectrum at δ 38.2 ppm. **211** exhibits C_s -symmetry in solution as evidenced by two separate Re-OMe resonance in the 1H NMR spectrum at δ 5.38 and 2.96 ppm (worth 3H each). The obvious more downfield

shifted Re-OMe resonance is likely attributed to the methoxide ligand *cis* to the rhenium-oxo experiencing significant deshielding effects. Finally, treatment of **202** with two equivalents of MeMgCl led to a mixture of products in which (PCP^{iPr})ReO(Me)(Cl) (**212**) was observed as the major product. From this it was inferred that while one methyl substitution should be easily accessed, a second methyl substitution may lead to a grievous *trans* influence conflict with the terminal oxo ligand in a C_s-symmetric form, or with another methyl in the putative C_{2v}-symmetric structure. Therefore, it was found that treatment with a single equivalent of MeMgCl led to clean formation and isolation of the monomethylated product, (PCP^{iPr})ReO(Me)(Cl) (**212**) in 80% yield as a brown solid of analytical purity. The complex features a singlet by ³¹P {¹H} NMR spectroscopy δ 45.2 ppm and its ¹H NMR spectrum evinces C_s-symmetry with a single Re-Me resonance at δ 4.40 (t, ³J_{P-H} = 2.7 Hz, 3H).

2.2.5. Generation and Reactivity of the (PCP^{iPr})ReOMe⁺ Cation

Five-coordinate, cationic rhenium oxo systems are relatively rare, but have shown use in the hydrofunctionalization of unsaturated substrates such as ketones.⁹³ Based on these observations, it seemed reasonable that removal of a chloride from **212** should be accessible, allowing the chemistry of a putative (PCP^{iPr})ReOMe⁺ fragment to be explored (Scheme II-9).



Scheme II-9. Generation and preliminary reactivity of the $(\text{PCP}^{\text{iPr}})\text{ReOMe}^+$ fragment

Gratifyingly mixing of **212** with KBarF_{20} in equimolar amounts in a 3:2 toluene- d_8 :1,2-difluorobenzene solution quantitatively produced $[(\text{PCP}^{\text{iPr}})\text{ReOMe}][\text{BarF}_{20}]$ (**213**) which exhibits a single, downfield shifted resonance by $^{31}\text{P}\{^1\text{H}\}$ NMR spectroscopy at δ 74.1 ppm and features a Re-Me resonance at δ 3.05 (t, $J_{\text{P-H}} = 5.0$ Hz, 3H).

Similar to the direct insertion chemistry observed by Ison and coworkers,⁹⁴ **213** appears to react with CO (^1H and $^{31}\text{P}\{^1\text{H}\}$ NMR evidence) to furnish the cationic acyl complex, $[(\text{PCP}^{\text{iPr}})\text{ReO}(\text{COMe})][\text{BarF}_{20}]$ (**214**). The CO insertion product has a single resonance by $^{31}\text{P}\{^1\text{H}\}$ NMR at δ 76.3 ppm and a new acyl methyl resonance as a singlet at δ 2.83 ppm from which no phosphine coupling is observed. Treatment of **213** with dmap appears to form the 1:1

dmap adduct, [(PCP^{iPr})ReOMe(DMAP)][BArF₂₀] (**215**) which reveals a new ³¹P{¹H} resonance at δ 73.1 ppm and contains all expected resonances in its ¹H NMR spectrum.

Looking to install a hydride directly, it was found that [(PCP^{iPr})ReOMe][BArF₂₀] reacts with H₂ at elevated temperatures to cleanly produce the cationic rhenium-oxo-hydride species, [(PCP^{iPr})ReO(H)][BArF₂₀] which has a downfield shifted resonance by ³¹P{¹H} NMR spectroscopy (δ 85.3 ppm) and features a diagnostically downfield shifted triplet hydride resonance at δ 10.07 ppm (t, *J* = 18.2 Hz, 1H), which is indicative of a hydride located *cis* to a terminal oxo ligand. Further evidencing the hydrogenolysis of the Re-Me bond is the observed formation of methane in the ¹H NMR spectrum. In testing the subsequent insertion chemistry of the cationic fragment, *in situ* generated [(PCP^{iPr})ReO(H)][BArF₂₀] was treated with two molar equivalents of trimethylsilylacetylene, resulting the spectroscopically observed formation of the insertion product, [(PCP^{iPr})ReO(-C(H)=C(H)(SiMe₃))][BArF₂₀] with a new ³¹P{¹H} NMR resonance at δ 75.4 ppm. Diagnostic resonances are observed for the *trans* rhenium vinyl product with the two vinylic protons appearing as doublets at δ 9.83 and 4.63 ppm with strong *trans* coupling (*J*_{H-H} = 20.0 Hz).

2.3 Conclusion

In summary, we have identified synthetic pathways for the installation of the PCP pincer ligand into the coordination sphere of rhenium. Rhenium(V) oxo complexes, as well as rhenium *polyhydride* complexes were characterized. (PCP^{iPr})ReH₆ undergoes dehydrogenative dimerization upon thermolysis to (PCP^{iPr})₂Re₂H₆. This is a potentially undesirable reaction for putative catalytic applications of pincer-supported Re complexes. Also, the metathesis reactivity

of (PCP^{iPr})ReOCl₂ was briefly expanded allowing for the generation and spectroscopic characterization of the putative, cationic (PCP^{iPr})ReO(Me)⁺ fragment.

2.4 Experimental

2.4.1 General Considerations.

Unless otherwise stated, all experiments were carried out using standard glovebox and Schlenk line techniques under a dry argon atmosphere. Triethylamine, cyclohexane, and C₆D₆ were dried over NaK, benzophenone, and 18-crown-6, distilled, and stored over molecular sieves in an argon glovebox prior to usage. Cyclooctane was distilled and stored over molecular sieves in an argon-filled glovebox. Diethyl ether, pentane, toluene, and tetrahydrofuran were dried and deoxygenated using a PureSolv MD-5 solvent purification system, and were stored over molecular sieves in an argon-filled glovebox. All other deuterated solvents were degassed and stored over molecular sieves in an argon-filled glovebox. (SMe₂)₂ReOCl₃,^{67a} and PC^HP^{iPr95} were synthesized using modified literature procedures. All other chemical reagents were purchased from commercial suppliers and were used as received. NMR spectra were recorded on Varian Inova 300 (¹H NMR, 299.952 MHz; ¹³C{¹H} NMR, 75.421 MHz; ³¹P{¹H} NMR, 121.42 MHz) and Varian iNova 500 (³¹P{¹H} NMR, 202.276 MHz; ¹³C{¹H} NMR, 125.670 MHz; ¹H NMR, 499.678 MHz) spectrometers in given solvents. Chemical shifts are reported in ppm (δ). ³¹P{¹H} NMR spectra were referenced externally to an 85% phosphoric acid standard at δ 0 ppm. ¹³C and ¹H NMR spectra were internally referenced to residual solvent resonances.⁹⁶ In reporting spectral data the following abbreviations were used: s=singlet; d=doublet; t=triplet; quint. = quintet; m=multiplet; dvt= doublet of virtual triplets; br. = broad. Infrared spectra were collected on a Shimadzu

IRAffinity-1 FTIR, as well as a Nicolet Nexus 470 FT-IR E.S.P. spectrophotometer using KBr plates and Nujol oil. Elemental analyses were performed by CALI, Inc. (Parsippany, NJ).

2.4.2 Synthesis and Characterization of Rhenium Complexes

(PC^HP^{iPr})ReOCl₃ (201): A 25 mL Schlenk flask equipped with magnetic stir bar was charged with a 3 mL acetonitrile solution of (SMe₂)₂ReOCl₃ (191 mg, 0.45 mmol) and stirred. To the stirring solution was added an oily suspension of PCP^{iPr} (156 mg, 0.46 mmol) in 2 mL of acetonitrile. Upon addition of the PCP^{iPr} suspension, a yellow-green solid immediately precipitates. The reaction was dried in vacuo to a dark, yellow-brown solid and washed three times with acetonitrile (ca. 3 mL) followed by drying in-vacuo. Next, over a frit, the product was washed with pentane (ca. 5 × 2 mL) and dried under reduced pressure to provide the product as a bright green powder in 85-90% purity, that could be used in subsequent steps without further purification. Crude isolated yield: 186 mg (64%). For characterization purposes, cleaner material could be recrystallized from dichloromethane and pentane at -35 °, over 12 h. Recrystallized yield: 30 mg (10%). ¹H NMR (300 MHz, CDCl₃): δ 7.12 - 7.6 (m, 4H), 3.96 (m, 4H), 2.94 (m, 4H), 1.38 (m, 12H), 1.21 (m, 12H). ³¹P{¹H} NMR (121 MHz, CDCl₃): δ -4.1 (s). IR (KBr) ν_{Re-O} = 978 cm⁻¹

(PCP^{iPr})ReOCl₂ (202): To a 20 mL, air-tight culture tube equipped with a magnetic stirbar was added (SMe₂)ReOCl₃ (906 mg, 2.12 mmol) and PCP^{iPr} (712 mg, 2.10 mmol) in 15 mL toluene.⁹⁷ The suspension was stirred for 12 h resulting in formation of a homogeneous, yellow-green solution of **201**(³¹P{¹H} NMR, toluene, δ -4.9). Triethylamine (300 μL, 2.15 mmol) was added and the solution was stirred at room temperature for 2 h, followed by heating at 140 °C for 48 h. Over this time, the solution became dark green in color, and colorless precipitate (presumed to be HNEt₃Cl) was observed to form on the side of the vial. The solution was cooled to room

temperature, filtered through Celite, and dried in vacuo to a glutinous, dark green solid. The solid was washed in two portions with 50 mL of a 2:1 pentane:diethyl ether mixture, and dried under reduced pressure to provide **202** as a pale green powder. Isolated Yield: 658 mg (51%). Dark green, single crystals suitable for X-ray analysis could be grown over 12 hours from a toluene solution layered with pentane (v:v = 1:5) at -35 °C. ^1H NMR (500 MHz, C_6D_6): δ 7.39 (d, $J_{\text{H-H}} = 7.5$ Hz, 2H), 7.18 (t, 1H, $J_{\text{H-H}} = 7.5$ Hz), 3.66 (dvt, $J = 16.1, 5.5$ Hz, 2H), 3.27 (dvt, $J = 16.1, 5.5$ Hz, 2H), 2.87 (m, 2H), 2.22 (m, 2H), 1.53 (dvt, $J = 15.8$ Hz, 7.6 Hz, 6H), 1.34 (dvt, $J = 15.8, 7.4$ Hz, 6H), 1.01 (dvt, $J = 14.1, 7.1$ Hz, 6H), 0.91 (dvt, $J = 13.6, 6.8$ Hz, 6H). $^{13}\text{C}\{^1\text{H}\}$ NMR (126 MHz, C_6D_6): δ 163.9 (s), 152.6 (s), 130.7 (s), 122.9 (t, $J_{\text{P-C}} = 7$ Hz), 41.9 (t, $J_{\text{P-C}} = 16$ Hz), 26.5 (t, $J_{\text{P-C}} = 15$ Hz), 25.2 (t, $J_{\text{P-C}} = 7.2$ Hz), 20.1 (s), 18.6 (s), 18.5 (s), 17.9 (s). $^{31}\text{P}\{^1\text{H}\}$ NMR (202 MHz, C_6D_6): δ 46.2 (s). IR (KBr) $\nu_{\text{Re-O}} = 978$ cm^{-1} Elem. An. Found (Calculated) for $\text{C}_{20}\text{H}_{35}\text{Cl}_2\text{OP}_2\text{Re}$: C, 39.43 (39.34); H, 5.78 (6.02)

(PCP^{iPr})ReOBr₂ (203): To a dark green, 3mL toluene solution of **202** (59 mg, 0.096 mmol) was added 177 μL (10 equiv.) of bromotrimethylsilane. After 12 h, an aliquot was analyzed by $^{31}\text{P}\{^1\text{H}\}$ NMR showing the presence of **202** (3%), and 64% of what is assumed to be a single preferred isomer of (PCP^{iPr})ReOBrCl ($^{31}\text{P}\{^1\text{H}\}$ NMR δ 45.07), the half brominated product, as well as **203** (33%). Another 177 μL was added to solution (20 equiv., 254 μL total, 1.92 mmol). The solution was allowed to stir at room temperature for 12 h more, over which time it became green in color as a small amount of unidentified grayish precipitate was noted. The solution was filtered through a plug of Celite, and volatiles were removed *in vacuo* to provide **203** as a dark sludge. Washing with a cold 2:1 pentane:diethyl ether mixture, and subsequent drying under reduced pressure provided the product as a dark green powder. Yield: 59 mg (88%). ^1H NMR (500 MHz, C_6D_6): δ 7.36 (d, $J_{\text{H-H}} = 7.5$ Hz, 2H), 7.17 (t, $J_{\text{H-H}} = 7.5$ Hz, 1H), 3.71 (dvt, $J = 16.2, 5.8$ Hz,

2H), 3.25 (dvt, $J = 16.2, 3.9$ Hz, 2H), 3.21 - 3.07 (m, 2H), 2.27 - 2.15 (m, 2H), 1.58 (dvt, $J = 9.2, 7.3$ Hz, 6H), 1.33 (dvt, $J = 9.5, 7.0$ Hz, 6H), 1.00 (dvt, $J = 7.3, 7.3$ Hz, 6H), 0.86 (dvt, $J = 7.0, 7.0$ Hz, 6H). $^{13}\text{C}\{^1\text{H}\}$ NMR (126 MHz, C_6D_6): δ 164.3 (s), 153.0 (t, $J_{\text{P-C}} = 5.3$ Hz), 131.5 (s), 123.3 (t, $J_{\text{P-C}} = 7.1$ Hz), 42.8 (t, $J_{\text{P-C}} = 16.3$ Hz), 28.2 (t, $J_{\text{P-C}} = 15.2$ Hz), 25.2 (t, $J_{\text{P-C}} = 7.9$ Hz), 20.6 (s), 19.0 (s, two overlapping signals), 18.6 (s). $^{31}\text{P}\{^1\text{H}\}$ NMR (202 MHz, C_6D_6): δ 38.9 (s). IR (KBr) $\nu_{\text{Re-O}} = 976$ cm^{-1} Elem. An. Found (Calculated) for $\text{C}_{20}\text{H}_{35}\text{Br}_2\text{OP}_2\text{Re}$: C, 34.44 (34.34); H, 4.93 (5.04)

(PCP^{iPr})ReOI₂ (204): To a dark green, 3 mL toluene solution of **202** (23 mg, 0.036 mmol) was added 5 equivalents of iodotrimethylsilane (27 μL , 0.19 mmol), resulting in an immediate color change to dark brown. The solution was allowed to stir at room temperature for 12 h, over which time a small amount of an unidentified grayish precipitate was noted. The solution was then filtered through Celite, dried under reduced pressure, and washed with pentane to provide **204** as a dark reddish-brown microcrystalline powder. Yield: 21 mg (70%). ^1H NMR (500 MHz, C_6D_6): δ 7.30 (d, $J_{\text{H-H}} = 7.5$ Hz, 2H), 7.12 (t, $J_{\text{H-H}} = 7.5$ Hz, 1H), 3.76 (dvt, $J = 16.5, 6.0$ Hz, 2H), 3.57 - 3.45 (m, 2H), 3.22 (dvt, $J = 16.5, 4$ Hz, 2H), 2.18 - 1.99 (m, 2H), 1.68 (dvt, $J = 16.9, 8.5$ Hz, 6H), 1.28 (dvt, $J = 18.8, 9.4$ Hz, 6H), 0.99 (dvt, $J = 14.4, 7.3$ Hz, 6H), 0.79 (dvt, $J = 14.0, 6.9$ Hz, 6H). $^{13}\text{C}\{^1\text{H}\}$ NMR (126 MHz, C_6D_6): δ 163.7 (s), 153.1 (m), 131.3 (s), 122.7 (t, $J_{\text{P-C}} = 7.5$ Hz), 43.4 (t, $J_{\text{P-C}} = 16.9$ Hz), 31.3 (m), 24.5 (t, $J_{\text{P-C}} = 8.0$ Hz), 20.6 (s), 19.5 (s), 18.7 (s), 18.6 (s). $^{31}\text{P}\{^1\text{H}\}$ NMR (202 MHz, C_6D_6): δ 23.9 (s). IR (KBr) $\nu_{\text{Re-O}} = 974$ cm^{-1} Elem. An. Found (Calculated) for $\text{C}_{20}\text{H}_{35}\text{I}_2\text{OP}_2\text{Re}$: C, 30.28 (30.27); H, 4.51 (4.45)

(PCP^{iPr})ReH₆ (205): **202** (125 mg, 0.21 mmol) was dissolved in 5 mL of THF and stirred, resulting in a homogeneous dark green solution. To this solution was added 5 equivalents of LiAlH_4 (525 μL , 2.0 M in THF, 1.05 mmol), resulting in an immediate color change to pale yellow. The solution was allowed to stir for 12 h, and degassed H_2O (74 μL , 4.1 mmol) was added,

resulting in vigorous bubbling as hydrogen evolved, as well as the precipitation of white solids. The tan-grey solution was then filtered through Celite, and dried under reduced pressure to provide a dark, viscous oil. The oil was allowed to sit for 12 h over which time it solidified to produce **205** as an ashy, dark gray, semi-crystalline solid. Yield: 77.2 mg (72%). ^1H NMR (500 MHz, C_6D_{12}): δ 6.82 (d, $J_{\text{H-H}} = 7.3$ Hz, 2H), 6.68 (t, $J_{\text{H-H}} = 7.3$ Hz, 1H), 3.37 (d, $J = 7.8$ Hz, 4H), 2.00 (m, 4H), 1.15 (dvt, $J = 14.5, 6.0$ Hz, 12H), 1.08 (dvt, $J = 13.7, 6.9$ Hz, 12H), -6.20 (t, $J_{\text{P-H}} = 16.9$ Hz, 6H). $^{13}\text{C}\{^1\text{H}\}$ NMR (126 MHz, C_6D_{12}): δ 147.5 (t, $J_{\text{P-C}} = 9.0$ Hz), 122.7 (s), 120.1 (t, $J_{\text{P-C}} = 7.8$ Hz), 43.8 (m, two overlapping signals), 27.33 (t, $J_{\text{P-C}} = 15.8$ Hz), 18.9 (s), 17.9 (s). $^{31}\text{P}\{^1\text{H}\}$ NMR (202 MHz, C_6D_{12}): δ 72.1 (s). T_1 min (-75 °C, 500 MHz, THF- d_8 , $\delta = -6.20$ ppm) = 225 ms. Elem. An. Found (Calculated) for $\text{C}_{20}\text{H}_{41}\text{P}_2\text{Re}$: C, 45.39 (45.35); H, 7.91 (7.80)

(PCP^{iPr})ReH₄(PMe₃) (206): To a 2 mL cyclohexane solution of **205** (10 mg, .019 mmol) was added 3 equivalents of PMe_3 (6 μL , .057 mmol). Addition of PMe_3 resulted in the observed evolution of H_2 , confirmed by ^1H NMR. The solution was then filtered through a plug of Celite, and volatiles were removed *in-vacuo*, resulting in the isolation of a pale, tan powder. The powder was quickly washed with a minimal amount of cold pentane, and dried under reduced pressure to provide **206** as an off-white solid. Yield: 8 mg (70%). ^1H NMR (500 MHz, C_6D_6): δ 7.20 (d, $J_{\text{H-H}} = 7.3$ Hz, 2H), 7.12 (t, $J_{\text{H-H}} = 7.3$ Hz, 1H), 3.25 - 3.21 (m, 4H), 1.90 - 1.76 (m, 4H), 1.43 (d, $J_{\text{H-P}} = 7.7$ Hz, 9H (PMe_3)), 1.12 - 1.04 (m, 12H), 0.90 - 0.97 (m, 12H), -5.48 (br, 4H). $^{13}\text{C}\{^1\text{H}\}$ NMR (126 MHz, C_6D_6): δ 148.9 (s), 122.6 (s), 119.7 (t, $J_{\text{P-C}} = 6.2$ Hz), 45.3 (m), 30.1 (d, $J_{\text{P-C}} = 32.4$ Hz, ($\text{P}(\text{CH}_3)_3$), 26.1 (m), 19.9 (s), 17.8 (s). $^{31}\text{P}\{^1\text{H}\}$ NMR (202 MHz, C_6D_6): δ 65.5 (br s), -40.9 (br s). Elem. An. Found (Calculated) for $\text{C}_{23}\text{H}_{48}\text{P}_3\text{Re}$: C, 45.76 (45.87); H, 8.01 (7.96).

(PCP^{iPr})ReH₄(DMAP) (207): To a tan 4 mL THF solution of **205** (14.2 mg, 0.027 mmol) was added dmap (4-dimethylaminopyridine) (3.1 mg, 0.025 mmol). Upon addition of dmap, the

tan solution became bright yellow as bubbling was observed (assumed to be the loss of H₂) and was allowed to stir for 3 h at room temperature. After 3 h, the volatiles were removed, furnishing a sticky, bright yellow residue. The residue was washed with cold pentane and dried under reduced pressure to provide **207** as a pale yellow powder. Yield: 8.7 mg (50%). Colorless crystalline platelets suitable for x-ray analysis could be grown over 5 h from a saturated pentane solution at -35 °C. ¹H NMR (500 MHz, C₆D₆): δ 8.35 (br, 2H), 7.46 (d, *J*_{H-H} = 7.4 Hz, 2H), 7.34 (7, *J*_{H-H} = 7.4 Hz, 1H), 5.43 (d, *J*_{H-H} = 6.3 Hz, 2H), 3.50 (m, 2H), 3.35 (m, 2H), 1.98 (m, 2H), 1.94 (s, 6H), 1.83 (m, 2H), 1.21 (m, 6H), 1.08 (m, 12H), 0.95 (m, 6H), -6.24 (br, 4H). ¹³C{¹H} NMR (126 MHz, C₆D₆): δ 152.1 (s), 150.2 (t, *J*_{P-C} = 12.9 Hz), 128.4 (s), 123.9 (s), 121.3 (t, *J*_{P-C} = 7.9 Hz), 106.9 (s), 43.5 (t, *J*_{P-C} = 11.9 Hz), 37.9 (s), 28.9 (t, *J*_{P-C} = 11.6 Hz), 20.6 (s), 19.9 (s), 19.6 (s), 18.9 (s). ³¹P{¹H} NMR (202 MHz, C₆D₆) δ 68.1 (s).

(PCPⁱPr)Re(CO)₃ (208): Method A. In a J. Young tube, a light yellow C₆D₆ solution of **205** (12.9 mg, 0.024 mmol) was frozen and degassed two times. 1 atm of CO was added, resulting in an immediate color change to dark pink. The solution was allowed to sit at room temperature for 24 hours, over which time it turned golden yellow, and ¹H NMR revealed the expulsion of free H₂ and H-D (result of H/D exchange of C₆D₆ with **205**), as **208** was formed quantitatively. The golden solution was then dried under reduced pressure, washed with cold pentane, and dried again to provide **208** as a light grey powder. Isolated Yield: 13.6 mg (93%). **Method B.** To a J. Young tube was added a C₆D₆ solution of **206**. The solution was frozen, degassed, refilled with 1 atm CO and heated in an oil bath at 80 °C. The reaction was monitored by ³¹P{¹H} NMR as well as ¹H NMR spectroscopy for observance of intermediates. An intermediate product (assumed to be (PCPⁱPr)Re(CO)₂(PMe₃)) was observed by ³¹P{¹H} NMR as two singlets in roughly 2:1 ratio at 48.2 and -53.1 ppm, respectively. Expulsion of H₂ was also observed by ¹H NMR. Over a period

of 96 h, and two subsequent CO refills (at 48 and 72 h), near quantitative conversion (>98%) to **208** was achieved, as well as the expulsion of free PMe_3 ($\delta = 62$ ppm, $^{31}\text{P}\{^1\text{H}\}$ NMR) and 4% free PCP^{iPr} ($\delta = 10.3$ ppm, $^{31}\text{P}\{^1\text{H}\}$ NMR), relative to **208**. The sample was then transferred to a scintillation vial, volatiles were removed under reduced pressure, the residue was washed with cold pentane (to remove PMe_3 and PCP^{iPr}) and dried again to provide **208** as a chalky powder. Isolated yield: 11 mg (81%). ^1H NMR (500 MHz, C_6D_6): δ 7.08 - 7.14 (m, 3H), 3.21 - 3.30 (m, 4H), 1.86 - 2.03 (m, 4H), 0.94 - 1.07 (m, 24H). $^{13}\text{C}\{^1\text{H}\}$ NMR (126 MHz, C_6D_6) δ 197.93 (s), 197.86 (s), 150.5 (t, $J_{\text{P-C}} = 8.0$ Hz), 124.0 (t, $J_{\text{P-C}} = 6.6$ Hz), 44.6 (t, $J_{\text{P-C}} = 15.7$ Hz), 27.8 (t, $J_{\text{P-C}} = 12.5$ Hz), 19.1 (d, $J_{\text{P-C}} = 8.6$ Hz). $^{31}\text{P}\{^1\text{H}\}$ NMR (202 MHz, C_6D_6) δ 53.2 (s). IR (KBr): 1901 (ms), 1911 (s), 2015 (m). Elem. An. Found (Calculated) for $\text{C}_{23}\text{H}_{35}\text{O}_3\text{P}_2\text{Re}$: C, 45.52 (45.46); H, 5.65 (5.81).

(PCP^{iPr})₂Re₂H₆ (209): To a J. Young tube was added a C_6H_{12} solution of **205** (17.8 mg, 0.034 mmol). The sample was frozen, degassed twice, and subsequently heated at 100 °C for 4 h, over which time conversion (> 99% by $^{31}\text{P}\{^1\text{H}\}$ NMR) of **205** to **209** was observed, along with concomitant darkening of the solution. The sample was then filtered through a plug of silica, and dried under reduced pressure to provide the product as a dark purple solid with broad spectroscopic signals. Yield: 7.7 mg (44%). ^1H NMR (500 MHz, C_6D_6): δ 7.18 (d, $J = 7.3$ Hz, 2H), 7.05 (t, $J = 7.3$ Hz, 1H), 3.80-3.40 (br, 4H), 1.80 - 1.45 (br, 4H), 1.30 - 0.75 (br, 24H), -6.95 (quint., $J_{\text{P-H}} = 7.2$ Hz, 3H). $^{13}\text{C}\{^1\text{H}\}$ NMR (126 MHz, C_6D_6): δ 149.4 (br), 122.7 (s), 120.1 (d, $J_{\text{P-C}} = 12$ Hz), 48.3 (br), 28.5 (br), 21.2 (br), 19.8 (br). $^{31}\text{P}\{^1\text{H}\}$ NMR (202 MHz, C_6D_6): δ 82.4 (br), 77.4 (br). T_1 min (-75 °C, 500 MHz, Toluene- d_8 , $\delta = -6.26$ ppm) = 410 ms. Elem. An. Found (Calculated) for $\text{C}_{40}\text{H}_{76}\text{P}_4\text{Re}_2$: C, 45.40 (45.61); H, 7.34 (7.27)

(PCP^{iPr})ReOPh₂ (210): To a scintillation vial was added **202** (18.9 mg, .03 mmol) and 3 mL THF resulting in a homogeneous, dark green solution. A 1.8 M dibutyl ether solution of PhLi (38 μ L, .06 mmol) was added resulting in a color change to dark brown. The solution was allowed to stir for 12 h after which time it had once again become dark green. A drop of degassed water was added and the solution was then dried *in vacuo* to a dark green residue. The residue was extracted with a 1:1 mixture of fluorobenzene and pentane, filtered through a plug of celite, and dried under reduced pressure to provide a bright green powder that was washed with a minimal amount of diethyl ether and pentane, and dried again to provide the product. Yield: 8 mg (37 %). ¹H NMR (500 MHz, C₆D₆): δ 8.08 (d, $J = 7.7$ Hz, 2H, *ortho Ph C-H*), 7.14 (m, 4H), 6.98 (m, 3H), 6.73 (t, $J = 7.2$ Hz, 2H), 6.03 (d, $J = 7.7$ Hz, 2H, *ortho Ph C-H*), 4.09 (br, 4H, *benzylic CH₂*), 2.37 (m, 4H), 1.05 (dvt, $J = 8.1, 7.3$ Hz, 12H), 0.95 (dvt, $J = 7.1, 6.4$ Hz). ³¹P{¹H} NMR (202 MHz, C₆D₆): δ 44.7.

(PCP^{iPr})ReO(OMe)₂ (211): To a scintillation vial equipped with a magnetic stir bar was added **202** (36.6 mg, 0.06 mmol), NaOMe (32.0 mg, 0.60 mmol), and 3 mL THF. The solution was stirred at room temperature for 36 hours, over which time it turned from dark green to bluish-purple. The solution was celite filtered, and dried under reduced pressure to form a purple residue. The residue was extracted with a 1:1 mixture of diethyl ether and pentane, filtered again, and dried *in vacuo* to provide the product as a purple, oily solid in over 98% purity by ¹H NMR. Yield 36.0 mg (94%). ¹H NMR (500 MHz, C₆D₆): δ 7.45 (d, $J = 7.5$ Hz, 2H), 7.24 (t, $J = 7.5$ Hz, 1H), 5.38 (s, 3H, *Re-OMe*), 3.48 (dvt, $J = 15.7, 4.6$ Hz, 2H), 3.41 (dvt, $J = 15.7, 4.2$ Hz, 2H), 2.96 (t, $J = 1.6$ Hz, 3H, *Re-OMe*), 2.03 (m, 4H), 1.22 (m, 12H), 1.12 (dvt, $J = 7.0, 6.5$ Hz, 6H), 0.99 (dvt, $J = 7.0, 6.3$ Hz, 6H). ³¹P{¹H} NMR (202 MHz, C₆D₆): δ 38.2

(PCP^{iPr})ReO(Me)(Cl) (212): To a scintillation vial equipped with a magnetic stir bar was added **202** (103 mg, 0.169 mmol) and 4 mL THF. To the stirring, dark green solution was added a 3.0 M THF solution of MeMgCl (68 μ L, 0.203 mmol) resulting in an immediate color change to dark brown. The solution was allowed to stir for 12 h, two drops of degassed H₂O were added, and the solution was dried *in vacuo* to provide a dark brown-yellow residue. The residue was then extracted in fluorobenzene, filtered through a plug of celite, and dried under reduced pressure to provide the product as a free-flowing, dark yellow-brown powder. Yield: 80 mg (80%) ¹H NMR (500 MHz, C₆D₆): δ 7.41 (d, $J = 7.4$ Hz, 2H), 7.07 (t, $J = 7.4$ Hz, 1H), 4.40 (t, $J = 2.7$ Hz, 3H, *Re-Me*), 4.12 (dvt, $J = 16.0, 5.6$ Hz, 2H), 3.70 (dvt, $J = 15.8, 4.0$ Hz, 2H), 2.89 (m, 2H), 2.45 (m, 2H), 1.49 (dvt, $J = 8.4, 7.4$ Hz, 6H), 1.44 (dvt, $J = 7.1, 6.9$ Hz, 6H), 1.33 (dvt, $J = 8.0, 7.4$ Hz, 6H), 1.16 (dvt, $J = 7.0, 6.6$ Hz, 6H). ³¹P{¹H} NMR (202 MHz, C₆D₆): δ 45.2 Elem. Anal Found (calc): C: 42.83 (42.74); H: 6.66 (6.49)

[(PCP^{iPr})ReOMe][BArF₂₀] (213): To a J. Young tube in a 3:2 d₈-toluene: 1,2-difluorobenzene mixture was added **212** (10 mg, 0.017 mmol) and KBarF²⁰ (13 mg, 0.017 mmol). The mixture was placed on an NMR rotator for twenty minutes (as the solution became golden brown in color) prior to observation by ¹H and ³¹P{¹H} NMR spectroscopy of an intermediate. After 12 hours, full conversion was observed to the spectroscopically characterized product. *Solvent mixture chosen for solubility precludes assignment of ligand aromatic resonances.* ¹H NMR (500 MHz, 3:2 d₈-toluene:1,2 difluorobenzene): δ 3.44 (dd, $J = 12.0, 5.6$ Hz, 2H), 3.19 (br d, $J = 17.6$ Hz, 2H), 3.05 (t, $J = 5.0$ Hz, 3H, *Re-Me*), 2.34 (br, 2H), 1.99 (br, 2H), 1.07 (m, 6H), 0.99 (m, 6H), 0.80 (m, 6H), -0.05 (m, 6H). ³¹P{¹H} NMR (202 MHz, 3:2 d₈-toluene: 1,2-difluorobenzene): δ 74.1.

[(PCP^{iPr})ReO(COMe)][BArF₂₀] (214): To a J. Young tube in a 3:2 d₈-toluene: 1,2-difluorobenzene was added **212** (10 mg, 0.017 mmol) and KBarF²⁰ (13 mg, 0.018mmol). The solution was then frozen, degassed, refilled with one atmosphere of carbon monoxide (CO), and placed on a rotator for 12 hours after which time a color change to dark yellow had occurred with concomitant conversion (ca. 87%) to the product, observed by ³¹P{¹H} NMR spectroscopy. ¹H NMR (500 MHz, 3:2 d₈-toluene:1,2 difluorobenzene): δ 3.03 (br d, *J* = 16.4 Hz, 2H), 2.89 (br d, *J* = 13.7 Hz, 2H), 2.83 (s, 3H, *C(O)Me*), 1.55 (m, 2H), 1.42 (m, 2H), 0.73 (dvt, *J* = 10.9, 6.9 Hz, 6H), 0.66 (dvt, *J* = 9.0, 7.5 Hz, 6H), 0.60 (dvt, *J* = 9.4, 7.1 Hz, 6H), 0.50 (dvt, *J* = 8.5, 7.3 Hz, 6H). ³¹P{¹H} NMR (202 MHz, 3:2 d₈-toluene: 1,2-difluorobenzene): δ 76.3.

[(PCP^{iPr})ReO(Me)(DMAP)][BArF₂₀] (215): To a J. Young tube in fluorobenzene was added **212** (18 mg, 0.03 mmol), DMAP(4 mg, 0.03 mmol), and KBarF²⁰ (23 mg, 0.03 mmol). The suspension was placed on a rotator for 12 hours after which time full conversion to the product was observed by ³¹P{¹H} NMR spectroscopy. ¹H NMR (500 MHz, 3:2 d₈-toluene:1,2 difluorobenzene): δ 8.14 (br, 2H, *dmap*), 7.28 (d, *J* = 7.4 Hz, 2H), 7.23 (t, *J* = 7.4 Hz, 1H), 6.15 (br, 2H, *dmap*), 3.46 (m, 2H), 3.22 (m, 2H), 3.11 (t, *J* = 4.8 Hz, 3H, *Re-Me*), 2.44 (s, 6H, *dmap-NMe₂*), 2.33 (m, 2H), 2.01 (m, 2H), 1.07 (dvt, *J* = 9.9, 7.1 Hz, 6H), 0.99 (dvt, *J* = 7.9, 6.8 Hz, 6H), 0.80 (dvt, *J* = 11.4, 6.9 Hz, 6H), -0.01 (dvt, *J* = 9.4, 6.9 Hz, 6H). ³¹P{¹H} NMR (202 MHz, 3:2 d₈-toluene: 1,2-difluorobenzene): δ 73.1.

[(PCP^{iPr})ReO(H)][BArF₂₀] (216): To a J. Young tube in a 3:2 d₈-toluene: 1,2-difluorobenzene was added **212** (8.2 mg, 0.014 mmol) and KBarF²⁰ (10 mg, 0.014 mmol). The solution was then frozen, degassed, refilled with one atmosphere of hydrogen(H₂), and placed on a rotator for 240 hours and observed by ³¹P{¹H} NMR spectroscopy. No evidence for coordination or hydrogenolysis was observed during this time. The mixture was then heated in a hot oil bath at

110 °C for 48 hours, over which time full conversion occurred to the product, with concomitant loss of methane (^1H NMR evidence). ^1H NMR (500 MHz, 3:2 d_8 -toluene:1,2 difluorobenzene): δ 10.07 (t, $J = 18.2$ Hz, 1H, *Re(O)-H*), 3.41 (dd, $J = 17.4, 9.2$ Hz, 2H), 3.32 (dd, $J = 17.5, 12.5$ Hz, 2H), 2.19 (m, 2H), 2.00 (m, 2H), 1.10 (dvt, $J = 11.3, 7.1$ Hz, 6H), 1.01 (dvt, $J = 10.1, 7.1$ Hz, 6H), 0.57 (dvt, $J = 10.5, 6.9$ Hz, 6H), 0.42 (dvt, $J = 9.5, 7.0$ Hz, 6H). $^{31}\text{P}\{^1\text{H}\}$ NMR (202 MHz, 3:2 d_8 -toluene: 1,2-difluorobenzene): δ 85.3.

[(PCP^{iPr})ReO(-C(H)=C(H)(SiMe₃))][BArF₂₀] (217): To **216**, previously generated *in situ*, was added two equivalents of trimethylsilylacetylene (2 μL , 0.03 mmol) upon which an immediate color change of solution to magenta occurred, and NMR spectroscopic evidence (^1H and $^{31}\text{P}\{^1\text{H}\}$) indicated clean conversion to the product. ^1H NMR (500 MHz, 3:2 d_8 -toluene:1,2 difluorobenzene): δ 9.83 (d, $J = 20.0$ Hz, 1H, *vinyl C-H*), 4.68 (d, $J = 20.0$ Hz, 1 H, *vinyl C-H*), 3.31 (br, 4H), 2.46 (m, 2H), 2.03 (m, 2H), 1.05 (m, 12H), 0.80 (dvt, $J = 9.2, 7.2$ Hz, 6H), 0.36 (dvt, $J = 7.4, 7.2$ Hz, 6H), 0.09 (9 H, *-SiMe₃*). $^{31}\text{P}\{^1\text{H}\}$ NMR (202 MHz, 3:2 d_8 -toluene: 1,2-difluorobenzene): δ 75.4.

X-ray Diffractometry Details for (PCP^{iPr})ReOCl₂ (202): Single crystals of C₂₇H₄₃Cl₂OP₂Re (**202**) were grown from a toluene solution layered in pentane. A dark green, multi-faceted block of suitable size (0.36 x 0.16 x 0.08 mm) was selected from a representative sample of crystals of the same habit using an optical microscope and mounted onto a nylon loop. Low temperature (110 K) X-ray data were obtained on a Bruker APEXII CCD based diffractometer (Mo sealed X-ray tube, $K_{\alpha} = 0.71073$ Å). Using Olex2⁹⁸, The structure was solved in the monoclinic P2₁/c space group using the ShelXT⁹⁹ structure solution program using Direct Methods and refined with the ShelXL¹⁰⁰ refinement package using Least Squares minimization. The structure was refined (weighted least squares refinement on F^2) and the final least-squares

refinement converged to $R_1 = 0.0356$ ($I \geq 2\sigma(I)$, 7368 data) and $wR_2 = 0.0606$ (F^2 , 12258 data, 372 parameters). Toluene, a crystallization solvent, was found in the asymmetric unit. (CSD Identifier/Number – MACXAS/1456066)

X-ray Diffractometry Details for (PCP^{iPr})ReH₄(dmap) (207): A colorless, multi-faceted block of suitable size (0.05 x 0.04 x 0.02 mm) was selected from a representative sample of crystals of the same habit using an optical microscope and mounted onto a nylon loop. Low temperature (150 K) X-ray data were obtained on a Bruker APEXII CCD based diffractometer (Mo sealed X-ray tube, $K_{\alpha} = 0.71073$ Å). All diffractometer manipulations, including data collection, integration and scaling were carried out using the Bruker APEXII software. An absorption correction was applied using SADABS. The space group was determined on the basis of systematic absences and intensity statistics and the structure was solved by direct methods and refined by full-matrix least squares on F^2 . The structure was solved in the monoclinic P 21/c space group using XS³ (incorporated in SHELXTL). No missed symmetry was reported by PLATON. All non-hydrogen atoms were refined with anisotropic thermal parameters. Hydrogen atoms were placed in idealized positions and refined using riding model. The structure was refined (weighted least squares refinement on F^2) (CSD Identifier/Number – MACXEW/1456067).

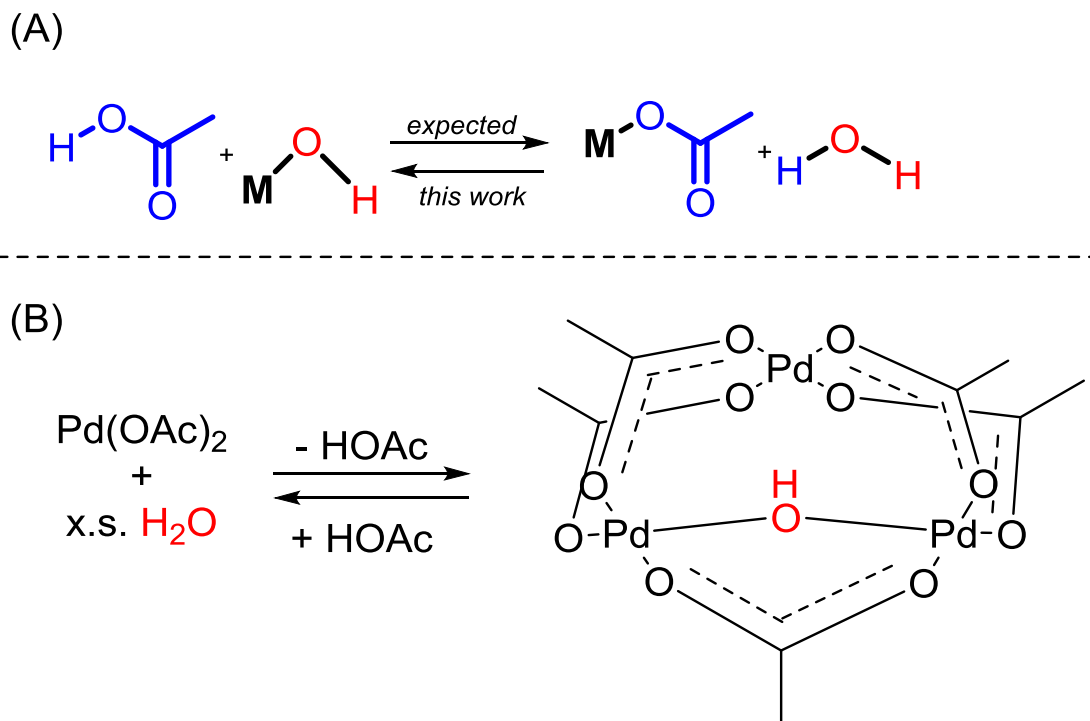
CHAPTER III

THE IRREVERSIBLE HYDROLYSIS OF PCP-SUPPORTED RHENIUM(V) ACETATES[†]

3.1 Introduction

Molecular metal carboxylates play a notable role in catalysis. Metal-carboxylate linkages are indispensable in the synthesis of metal-organic frameworks.^{101,102} Late metal acetates, pivalates, and other carboxylates have been shown to be important in homogeneous C-H activation.¹⁰³⁻¹⁰⁵ The reaction of a late metal carboxylate with a hydrocarbon may be favorable, in spite of the huge disparity in the Bronsted acidity of RC(O)O-H and C-H bonds. On the other hand, metathetic reactions between metal carboxylates and other O-H acids would generally be expected to follow pK_a values. In particular, hydrolysis of a terminal metal-acetate bond to a terminal hydroxide would be expected to be unfavorable (Scheme III-1A). Partial hydrolysis of metal acetates happen readily, but the equilibrium strongly favors water and metal acetate (or free acetate anion). Webster et al. have recently shown that [Pd(OAc)₂]₃ undergoes reversible hydrolysis with excess H₂O to form Pd-OH species (Scheme III-1B),¹⁰⁶ but this transformation involves a bridging acetate and a bridging hydroxide and it does not definitively favor Pd-OH. Thus we were surprised to come across an occurrence of complete and irreversible hydrolysis of a terminal metal acetate in the course of our investigations of pincer complexes of Re, which this report describes.

[†] Reprinted in part with permission from “Irreversible Hydrolysis of PCP-Supported Rhenium(V) Acetates” Kosanovich, A. J.; Shih, W. -C.; Ozerov, O. V. *Inorg. Chem.* **2018**, *57*, 545-547. Copyright 2018 by American Chemical Society. DOI: 10.1021/acs.inorgchem.7b02628



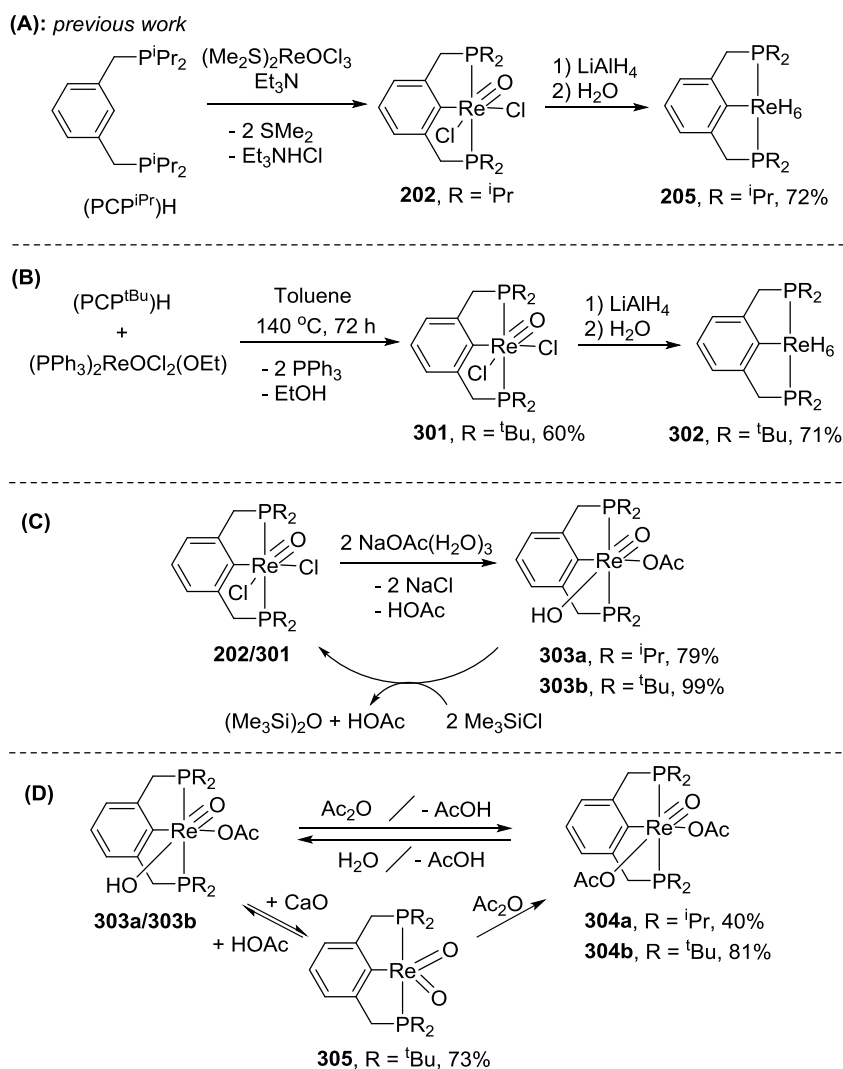
Scheme III-1. (A) Hydrolysis of a generic metal acetate (B) Equilibrium hydrolysis of a Pd-OAc bond in Pd(OAc)₂

3.2 Results and Discussion

3.2.1 Synthesis of (PCP^{tBu})ReOCl₂ and Formation of the Hexahydride

We previously reported¹⁰⁷ the synthesis of (PCP^{iPr})ReOCl₂ (**202**) in a reaction of (PCP^{iPr})H with (Me₂S)₂ReOCl₃ in the presence of Et₃N (Scheme III-2A), but this method was not suitable for the installation of the (PCP^{tBu})H analog. Instead, (PCP^{tBu})ReOCl₂ (**301**) was synthesized in 60% isolated yield via thermolysis of (PPh₃)₂ReOCl₂(OEt)¹⁰⁸ with (PCP^{tBu})H at 140 °C for 72 h (Scheme III-2B). Similarly to **202**, **301** presented C_s-symmetry on the NMR time scale and an IR band indicative of a single rhenium-oxo moiety ($\nu_{Re=O} = 975\text{ cm}^{-1}$). Treatment of **301** with LiAlH₄ followed by an aqueous workup afforded the hexahydride, (PCP^{tBu})ReH₆ (**302**) in good isolated

yields (Scheme III-2A). Analogously to the previously reported **205**, **302** is C_{2v} -symmetric on the NMR timescale, with all six (^1H NMR integration) hydrides presenting as an upfield triplet resonance in the ^1H NMR spectrum (δ -5.66, $^2J_{\text{P-H}} = 15.7$ Hz). In contrast to **205**, **302** was thermally stable, showing no sign of dehydrogenative dimerization after 24 h at 90 °C in C_6D_6 .



Scheme III-2. Synthesis and reactivity of PCP-supported rhenium complexes. Reprinted with permission from the American Chemical Society, Copyright 2018

3.2.2 Installation and Observed Hydrolysis of a Rhenium-Acetate Bond

We sought access to (PCP)ReO(OAc)₂ (**304a/b**), which we expected to possess C_s-symmetry by analogy with **202/301**. Surprisingly, treatment (Scheme III-2C) of emerald green, C₆D₆ solutions of **202** or **301** with excess NaOAc(H₂O)₃ led over 12 h to violet solutions which in each case showed full conversion to a single (PCP)Re product of apparent C_{2v} symmetry on the NMR timescale. The Re product of the reaction in the case of the PCP^{tBu} ligand was isolated in analytically pure form as dark purple, free-flowing solids in excellent yield and shown to possess the formulation (PCP^{tBu})ReO(OAc)(OH) (**303b**) based on structural (vide infra) and spectroscopic studies. Attempts at isolating pure (PCP^{iPr})ReO(OAc)(OH) (**303a**) inevitably led to partial degradation of the samples with only ca. 90% purity of isolated **303a** obtainable. Both **303a** and **303b** presented a single ³¹P{¹H} NMR resonance (**303a**, δ 39.4; **303b**, δ 48.6 ppm), a single ¹H NMR resonance for the benzylic protons, and one acetate resonance (**303a**, δ 2.42; **303b**, δ 2.25, 3H). **303a** featured a broad O-H resonance in its ¹H NMR spectrum (δ 12.03, 1H), whereas the corresponding resonance for **303b** was not observed. **303a** and **303b** proved sensitive to air, decomposing to brown mixtures of unidentified compounds. **303b** reacted cleanly with 2 equiv. of Me₃SiCl to produce **301**, (Me₃Si)₂O, and AcOH (Scheme III-2C).

3.2.3 Accessing (PCP)ReO(OAc)₂ and Mechanistic Inquiry

Access to the original target, (PCP^{tBu})ReO(OAc)₂ (**304b**) was possible via the reaction of **303b** with excess Ac₂O at 80 °C (Scheme III-2D).¹⁰⁹ *In situ* monitoring of the reaction of **303b** with excess Ac₂O, showed quantitative and clean conversion to **304b**, with an equivalent of free AcOH observed (¹H NMR evidence). **304b** gave rise to a singlet resonance by ³¹P{¹H} NMR spectroscopy (δ 59.1). The ¹H NMR spectra of **304b** revealed C_s-symmetry with two acetate resonances (δ 2.52 and 1.80). IR spectroscopy confirmed the presence of both acetate (1660 and

1630 cm^{-1}) and rhenium-oxo moieties (989 cm^{-1}). **304b** is highly sensitive to hydrolysis in solution. Treatment of **304b** with degassed H_2O led to quantitative, fast formation of **303b** and AcOH (Scheme III-2D). We propose that the lattice water of $\text{NaOAc}(\text{H}_2\text{O})_3$ is responsible for the hydrolysis of the unobserved **304a/b** in the reaction with **202/301** that led to the formation of **303a/b**. Usage of anhydrous NaOAc led to the formation of predominantly **304b** but no **303b**.¹¹⁰ Addition of 15 equiv of AcOH to **303b** did not lead to the reversion to **304b** and release of H_2O , while addition of AcOH to **304b** led to only <5% formation of **303b** after 24 h at ambient temperature. Thus, the equilibrium for the hydrolysis of the Re-OAc bond in **304b** lies far on the side of **303b** while the equilibrium for the reaction of **303b** with Ac_2O lies far on the side of **304b**.

3.2.4 Structural and Spectroscopic Study of $(\text{PCP})\text{ReO}(\text{OAc})(\text{OH})$

In contrast to its apparent C_{2v} -symmetry in solution, an XRD study on a suitable single crystal of **303a** revealed a C_s -symmetric structure with a rhenium oxo moiety, an acetate and a hydroxide ligand filling out the Re coordination sphere in addition to the PCP^{iPr} ligand (Figure III-1).

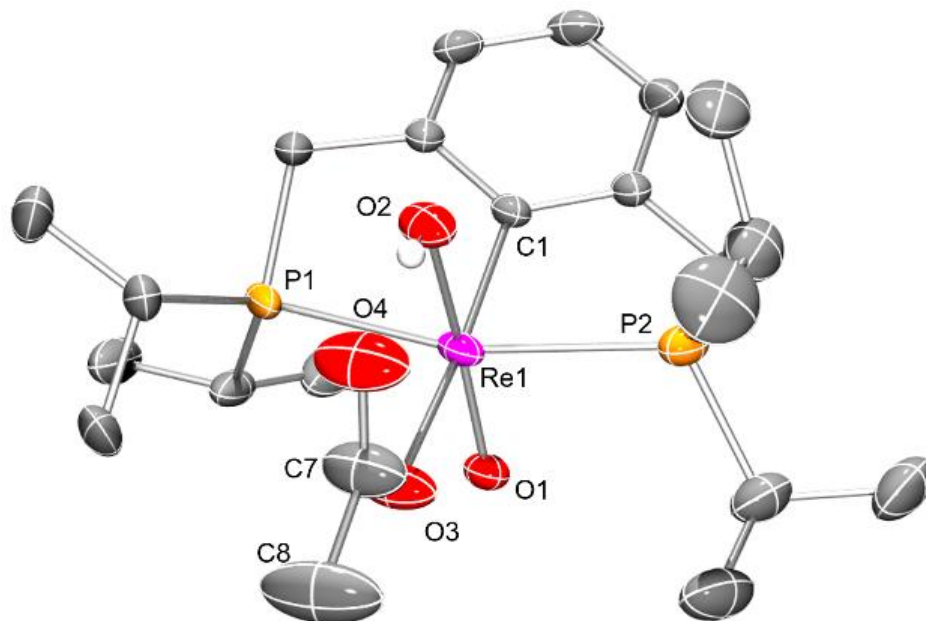
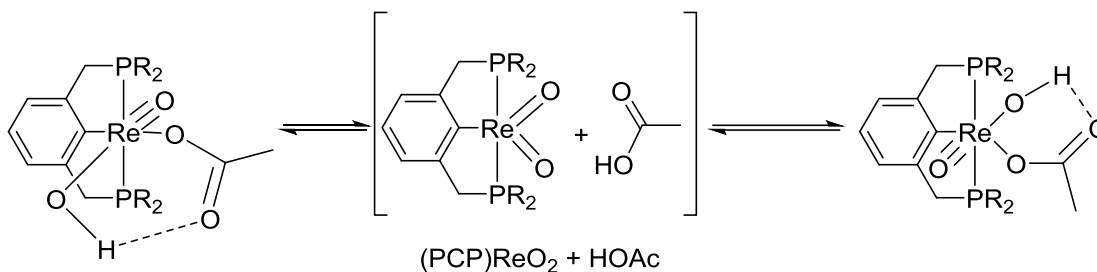


Figure III-1. ORTEP drawing (50% probability ellipsoids) of $(\text{PCP}^{\text{iPr}})\text{ReO}(\text{OAc})(\text{OH})$ (**303a**). Selected H atoms are omitted for clarity. Selected Distances (\AA) and angles (deg): Re1-O1, 1.719(2); Re1-O2, 1.908(3); Re1-O3, 2.241(3); O2-Re1-O3, 83.9(1); C7-O3, 1.258(5); C7-O4, 1.255(6); O1-Re1-O2, 171.4(1). Reprinted with permission from the American Chemical Society, Copyright 2018

The acetate ligand contains two similar C-O bond lengths (1.258(5) and 1.255(6) \AA), indicating a delocalization in the carboxylate unit. The O4 atom closely approaches (1.87(4) \AA) the hydrogen attached to the hydroxo O2, consistent with hydrogen bonding. Complex **303a** can be viewed as an adduct between $(\text{PCP}^{\text{iPr}})\text{ReO}_2$ (**5a**) and AcOH and this formulaic view may have a bearing on the fluxional behavior of **303a/b** in solution. Firstly, a low temperature ^1H NMR study of **303b** in CDCl_3 showed that even down to -60°C , C_{2v} -symmetry is retained. Secondly, solutions containing **303a** or **303b** and various amounts of AcOH display only a single acetate ^1H NMR resonance, suggesting rapid exchange between the acetate in **303a/b** and free AcOH. Both phenomena could be explained by unfavorable, but rapid and reversible loss of AcOH from **303a/b** in solution, serving to scramble the acetates and to provide for apparent C_{2v} symmetry. However,

we cannot exclude that the fluxionality of **303a/b** is an intramolecular process distinct from the exchange with external AcOH (Scheme III-3).



Scheme III-3. Possible interconversion between degenerate C_s-symmetric structures of **303**. H-bonding interaction is shown between OAc and OH ligands. Reprinted with permission from the American Chemical Society, Copyright 2018

3.2.5 Isolation and Reactivity of a Relevant (PCP)ReO₂ Species

Contemplation of the potential intermediacy of (PCP)ReO₂ in the fluxionality of **303a/b** led us to envisage a synthesis of it via reaction of **303a/b** with base to remove AcOH. CaO served suitably to dehydroacetoxylate **303b** in a C₆D₆ solution and allow isolation of (PCP^{tBu})ReO₂ (**305**) in 73% yield as an oily violet solid of ca. 95% purity. The highly lipophilic nature of **305** rendered further purification attempts fruitless, but its spectroscopic and reactivity characteristics are consistent with the dioxo formulation. Complex **305** gave rise to a singlet resonance by ³¹P{¹H} NMR spectroscopy (δ 48.4 ppm), and ¹H and ¹³C{¹H} NMR spectra indicative of C_{2v}-symmetry at ambient temperature. IR spectroscopy supports the presence of a rhenium-dioxo core with diagnostic¹¹¹ O=Re=O stretches at 812 and 832 cm⁻¹. No stretches attributable to O-H, rhenium mono-oxo, or acetate C=O were observed. The NMR resonances of **305** corresponding to the PCP^{tBu} ligand are close but distinguishable from those of **303b**. Furthermore, isolation of **303b** involves exposure to vacuum, indicating that AcOH is not easily lost from **303b** in the absence of

base, and thus **303b** is not a purely solid-state phenomenon. Consistent with these and other previous observations, treatment of **305** with AcOH or Ac₂O resulted in clean formation of **303b** and **304b**, respectively. It is possible that the reaction of **303b** with Ac₂O to give **304b** proceeds *via* intermediate, unfavorable release of **305**, which is then captured by Ac₂O.

3.3 Conclusion

The diacetate complexes **304a/b** presumably contain κ^1 -acetate ligands as that already lends an 18-electron character to the Re center. Hydrolysis of **304a/b** to **303a/b** results in an acetate that is also formally κ^1 (i.e., only bound to Re via one oxygen). However, the acetate in **303a/b** is stabilized by hydrogen bonding to the hydroxo ligand. Ostensibly, this may contribute to the unusual favorability of the hydrolysis of a metal acetate bond reported in this work.

3.4 Experimental

3.4.1 General Considerations

Unless otherwise stated, all experiments were carried out using standard glovebox and Schlenk line techniques under a dry argon atmosphere. C₆D₆ was dried over NaK, benzophenone, and 18-crown-6, distilled, and stored over molecular sieves in an argon glovebox prior to usage. Diethyl ether, pentane, toluene, and tetrahydrofuran (THF) were dried and deoxygenated using a PureSolv MD-5 solvent purification system and were stored over molecular sieves in an argon-filled glovebox. All other deuterated solvents were degassed and stored over molecular sieves in an argon-filled glovebox. (PCP^{iPr})ReOCl₂ (**202**)¹⁰⁷, PCP^{tBu}⁹⁵, and (PPh₃)₂ReOCl₂(OEt)¹⁰⁸ were synthesized using reported literature procedures. Ac₂O and AcOH were degassed and stored over mol sieves in an argon glovebox. Anhydrous NaOAc was obtained by twice melting NaOAc(H₂O)₃ over a flame, followed by drying under reduced pressure at 80 °C for 24 h, and storage under an inert atmosphere. All other chemical reagents were purchased from commercial

suppliers and were used as received. NMR spectra were recorded on a Varian iNova 500 ($^{31}\text{P}\{^1\text{H}\}$ NMR, 202.276 MHz; $^{13}\text{C}\{^1\text{H}\}$ NMR, 125.670 MHz; ^1H NMR, 499.678 MHz) spectrometer in given solvents. Chemical shifts are reported in ppm (δ). $^{31}\text{P}\{^1\text{H}\}$ NMR spectra were referenced externally to an 85% phosphoric acid standard at δ 0ppm. $^{13}\text{C}\{^1\text{H}\}$ and ^1H NMR spectra were internally referenced to residual solvent resonances.⁹⁶ In reporting spectral data, the following abbreviations were utilized: s = singlet; d = doublet; t = triplet; dd = doublet of doublets; vt = virtual triplet; dvt = doublet of virtual triplets; m = multiplet; br = broad; br s = broad singlet. Infrared spectra were collected on a Nicolet Nexus 470 FT-IR E.S.P. spectrometer using KBr plates and Nujol oil and an Agilent CARY FT-IR spectrometer. Elemental analyses were performed by CALI, Inc. (Highland Park, NJ, USA).

3.4.2 Synthesis and Characterization of Rhenium Complexes

(PCP^{tBu})ReOCl₂ (301): To a 50 mL culture tube equipped with a magnetic stir bar was added (PPh₃)₂ReOCl₂(OEt) (1.24 g, 1.47 mmol), PCP^{tBu} (589.0 mg, 1.47 mmol), and 15 mL toluene. The resultant brown suspension was heated at 140 °C for 72 h over which time it became a dark green, homogeneous solution. The solution was then cooled to room temperature, filtered through Celite, and dried under reduced pressure to form a glutinous, dark green residue. The residue was then washed first with pentane (2 x 20 mL), then with cold Et₂O (2 x 10 mL), and again with pentane until the washes were colorless. The resultant residue was then dissolved in a minimal amount of toluene, layered with pentane (v:v 1:5), and placed in a freezer at -35 °C for 48 h over which time analytically pure **301** precipitated as a light green, crystalline powder. Yield: 587 mg (60 %) ^1H NMR (500 MHz, C₆D₆): δ 7.43 (d, $J_{\text{H-H}} = 7.5$ Hz, 2H), 7.13 (t, $J_{\text{H-H}} = 7.5$ Hz, 1H), 3.93 (dvt, $J_{\text{H-H}} = 15.8$, $J_{\text{P-H}} = 4.9$, 2H), 3.33 (dvt, $J_{\text{H-H}} = 15.8$, $J_{\text{P-H}} = 3.8$ Hz, 2H), 1.42 (vt, $J_{\text{P-H}} = 6.7$ Hz, 18 H, (^tBu-CH₃)), 1.17 (vt, $J_{\text{P-H}} = 6.4$ Hz, 18H, (^tBu-CH₃)). $^{13}\text{C}\{^1\text{H}\}$ NMR (126 MHz,

C₆D₆): δ 161.2, 154.9(t, J_{P-C} = 4.7 Hz), 130.7, 122.6 (t, J_{P-C} = 6.3 Hz), 40.6 (t, J_{P-C} = 14.0 Hz), 40.1 (t, J_{P-C} = 8.5 Hz), 37.8 (t, J_{P-C} = 5.8 Hz), 30.1 (^tBu), 29.7 (^tBu). ³¹P{¹H} NMR (202 MHz, C₆D₆): δ 47.6. IR(KBr, cm⁻¹): 975(Re=O). Elem. Anal Found (calc): C: 43.28(43.24); H: 6.72 (6.50).

(PCP^tBu)ReH₆ (302): To a round bottom schlenk flask was added **301** (163.2 mg, 0.240 mmol) in 5 mL THF to form a homogeneous, green solution. To this solution was added a 2.0 M THF solution of LiAlH₄ (612 μ L, 1.20 mmol) resulting in a color change to a light orange solution. The solution was allowed to stir for 30 min, and then was treated with degassed H₂O until no more bubbling (evolved H₂) was observed. The resultant slurry was then filtered through a pad of silica and Celite on a fine frit and the solvent was removed under reduced pressure to provide **302** as a free-flowing tan powder. Yield: 102.5 mg (71%). ¹H NMR (500 MHz, C₆D₁₂): δ 6.83(d, J_{H-H} = 7.4 Hz, 2H), 6.68 (t, J_{H-H} = 7.4 Hz, 1H), 3.42 (m, 4H), 1.31 (m, 36H, (^tBu-CH₃)), -5.66 (t, J_{P-H} = 15.7 Hz, (Re-H)). ¹³C{¹H} NMR (126 MHz, C₆D₆): δ 160.6 (t, J_{P-C} = 5.5 Hz), 149.7 (t, J_{P-C} = 8.7 Hz), 123.4, 120.5 (t, J_{P-C} = 7.4 Hz), 42.4 (t, J_{P-C} = 12.0 Hz), 34.6 (t, J_{P-C} = 12.0 Hz), 29.5 ((^tBu-CH₃)). ³¹P{¹H} NMR (202 MHz, C₆D₁₂): δ 88.8 Elem. Anal Found (calc): C: 48.93(49.21); H: 8.13(8.43).

(PCPⁱPr)ReO(OAc)(OH) (303a): To a J. Young tube was added (PCPⁱPr)ReOCl₂ (**202**) (20.1 mg, 0.033 mmol), NaOAc(H₂O)₃ (10.0 mg, 0.07 mmol), and C₆D₆. The resultant suspension was placed on a rotator for 24 h over which time full conversion to **303a** was observed. The resultant, dark purple solution was then filtered through Celite and dried under reduced pressure producing a dark purple residue. This residue was then redissolved in pentane and placed in a freezer at -30 °C for 24 h, precipitating small, purple semicrystalline material. The supernatant was decanted and the solids dried under reduced pressure to **303a** as a free-flowing, dark purple powder of ca. 88% purity. A second, unidentified organometallic product of apparent C_s-symmetry (¹H NMR evidence) was observable after multiple recrystallizations by NMR spectroscopy with a

singlet resonance by $^{31}\text{P}\{^1\text{H}\}$ NMR (δ 52.3). Single crystals suitable for X-ray diffraction were grown from pentane at $-30\text{ }^\circ\text{C}$ over 24 h. Yield: 16.0 mg (79%). ^1H NMR (500 MHz, C_6D_6): δ 12.03 (br, 1H, OH), 7.42 (d, $J_{\text{H-H}} = 7.5$ Hz, 2H), 7.29 ($J_{\text{H-H}} = 7.4$ Hz, 1H), 3.49 (vt, $J_{\text{P-H}} = 4.2$ Hz, 4H), 2.42 (s, 3H), 2.17 (m, 4H), 1.20 (dvt, $J = 14.4, 7.3$ Hz, 12H, ($^i\text{Pr-CH}_3$)), 1.15 (dvt, $J = 14.0, 6.8$ Hz, 12H, ($^i\text{Pr-CH}_3$)). $^{13}\text{C}\{^1\text{H}\}$ (126 MHz, C_6D_6): δ 18.2, 22.6, 24.5 (t, $J_{\text{P-C}} = 10.5$ Hz), 40.3 (t, $J_{\text{P-C}} = 14.2$ Hz), 122.5, 130.1, 143.7, 152.2, 178.4. $^{31}\text{P}\{^1\text{H}\}$ NMR (202 MHz, C_6D_6): δ 39.5. ATR-IR (toluene, cm^{-1}): 3046_(\text{O-H}), 1660_(\text{C=O}), 1577_(\text{C=O}), 930

(PCP^{tBu})ReO(OAc)(OH) (303b): To a J. Young tube in C_6D_6 was added **301** (43.4 mg, 0.065 mmol) and $\text{NaOAc}(\text{H}_2\text{O})_3$ (18.0 mg, 0.13 mmol). The resultant light green suspension was heated at $70\text{ }^\circ\text{C}$ for 12 h over which time it changed in color from green, to blue, and eventually to dark purple, as full conversion to the product was observed by NMR ($^{31}\text{P}\{^1\text{H}\}$ and ^1H) evidence. From the resultant purple solution volatiles were removed under reduced pressure. The remaining dark purple residue was extracted in Et_2O , filtered through Celite, and dried under reduced pressure to provide **303b** as a light purple, free-flowing powder. Yield: 43.0 mg (99%). ^1H NMR (500 MHz, C_6D_6): δ 12.56 (br, 1H, OH), 7.30 (d, $J_{\text{H-H}} = 7.5$ Hz, 2H), 7.19 (t, $J_{\text{H-H}} = 7.5$ Hz, 1H), 3.54 (vt, $J_{\text{P-H}} = 4.0$ Hz, 4H), 2.25 (s, 3H, (OAc- CH_3)), 1.24 (vt, $J_{\text{P-H}} = 6.3$ Hz, 36 H, ($^t\text{Bu-CH}_3$)). $^{13}\text{C}\{^1\text{H}\}$ NMR (126 MHz, C_6D_6): δ 179.4 (OAc, C=O), 154.9, 130.7, 126.9, 122.5 (t, $J_{\text{P-C}} = 5.9$ Hz), 39.2 (t, $J_{\text{P-C}} = 10.9$ Hz), 36.1 (t, $J_{\text{P-C}} = 6.4$ Hz), 29.8, 23.1 (OAc- CH_3). $^{31}\text{P}\{^1\text{H}\}$ NMR (202 MHz, C_6D_6) δ 48.4. ATR-IR (cm^{-1}): 3042_(\text{O-H}), 1717_(\text{C=O}), 1572_(\text{COO}), 1556_(\text{COO}), 939_(\text{Re=O}), 834, 812. ATR-IR (toluene, cm^{-1}): 3044_(\text{O-H}), 935_(\text{Re=O}), 835, 820. Elem. Anal Found (calc): C: 46.17(46.48); H: 6.75(7.05)

(PCP^{iPr})ReO(OAc)₂ (304a): To a scintillation vial equipped with a magnetic stir bar was added (PCP^{iPr}) ReOCl_2 (**202**) (16.2 mg, 0.027 mmol), AgOAc (9.5 mg, 0.057 mmol), and 4 mL

CH₂Cl₂. The resultant solution was stirred, resulting in precipitation of gray solids (presumed to be AgCl) and a concomitant color change from emerald green to blue, then finally purple (ca. 30 min). The solution was then filtered through Celite and dried under reduced pressure, producing a purple oil. The resultant oil was then redissolved in 1 mL toluene, and Ac₂O (10 μL, 0.105 mmol) was added, causing the solution to take on a lighter hue. The solution was layered with 5 mL pentane and placed in a freezer set to -30 °C for 96 h, over which time **304a** precipitated as blue crystals. The supernatant was decanted and the product dried under reduced pressure to provide blue solids determined to be ca. 90% pure. Yield: 7 mg (40%). ¹H NMR (500 MHz, C₆D₆): δ 7.42 (d, *J* = 7.5 Hz, 2H), 7.22 (t, *J* = 7.5 Hz, 1H), 4.01 (dvt, *J* = 15.6, 5.2 Hz, 2H), 3.34 (dvt, *J* = 15.6, 3.7 Hz, 2H), 2.70 – 2.60 (m, 2H), 2.53 – 2.51 (m, 2H), 2.52 (s, 3H), 1.71 (s, 3H), 1.40 (dvt, *J* = 15.3, 7.4 Hz, 6H, (ⁱPr-CH₃)), 1.22 (dvt, *J* = 16.6, 7.2 Hz, 6H, (ⁱPr-CH₃)), 1.05 (dvt, *J* = 14.2, 7.2 Hz, 6H, (ⁱPr-CH₃)), 0.90 (dvt, *J* = 13.5, 7.0 Hz, 6H, (ⁱPr-CH₃)). ³¹P{¹H} (202 MHz, C₆D₆): δ 51.6. IR(KBr, cm⁻¹): 1653_(C=O), 1646_(C=O), 986_(Re=O) *Utilizing NaOAc(H₂O)₃ or anhydrous NaOAc instead of AgOAc led to an increase in more complicated, undesirable product mixtures.

(PCP^{uBu})ReO(OAc)₂(304b): Method A. To a 2 mL C₆D₆ solution of **301** (60.0 mg, 0.09 mmol) was added NaOAc(H₂O)₃ (27 mg, 0.20 mmol), and the resultant suspension was heated for 16 h at 70 °C, resulting in a color change from green to a dark purple. The solution was then brought back into a glovebox and filtered through Celite to remove excess NaOAc and resultant NaCl. Removal of volatiles provided a dark purple residue. This residue was then dissolved in C₆D₆ (2 mL) and to the resultant homogeneous, dark purple solution was added Ac₂O (85 μL, 0.90 mmol). The solution was allowed to stir for 16 h, resulting in a color change to lighter purple, and concomitant formation of the desired product as determined by ³¹P{¹H} NMR spectroscopy. After 32 h of reaction time, volatiles were removed under reduced pressure and the residue was washed

with pentane and dried, providing the product as a free-flowing, periwinkle powder. Recrystallization from a toluene:pentane mixture (v:v 1:5) at -35 °C yielded the product as air sensitive, bright blue-purple crystals of ca. 94% purity with an unidentified side product observed by ^1H and $^{31}\text{P}\{^1\text{H}\}$ NMR (δ 56.3) spectroscopies. Repeated recrystallization decreased yield and failed to improve purity. Yield: 38 mg (59%)

Method B. To a J. Young tube was added **303b** (23.7 mg, 0.035 mmol) and C_6D_6 , forming a homogeneous, violet solution. To this solution was added acetic anhydride (10 μL , 0.105 mmol) and the sample was then placed in an oil bath set to 80 °C for 16 h over which time the color changed to dark blue, and full, clean conversion was noted by $^{31}\text{P}\{^1\text{H}\}$ and ^1H NMR spectroscopy. The blue solution was then filtered through Celite and volatiles were removed under vacuum, providing a dark blue residue. The resultant residue was washed with pentane (2 x 2 mL) and dried under reduced pressure to provide the product as a free-flowing, periwinkle powder. Samples prepared in this way were found to be highly sensitive to hydrolysis both in solution and solid state, and even small amounts of adventitious water/moisture invariably could quickly lead to ca. 2% formation of **303b** often observable by ^1H NMR spectroscopy. Yield: 20.3 mg (81%). ^1H NMR (500 MHz, C_6D_6): δ 7.42 (d, $J_{\text{H-H}} = 7.6$ Hz, 2H), 7.19 (t, $J_{\text{H-H}} = 7.6$ Hz, 1H), 4.13 (dvt, $J_{\text{H-H}} = 16.1$ Hz, $J_{\text{P-H}} = 4.4$ Hz, 2H), 3.36 (dvt, $J_{\text{H-H}} = 16.1$ Hz, $J_{\text{P-H}} = 3.6$ Hz, 2H), 2.56 (s, 3H, (OAc- CH_3)), 1.80 (s, 3H, (OAc- CH_3)), 1.24 (vt, $J_{\text{P-H}} = 6.6$ Hz, 18H, ($^t\text{Bu-CH}_3$)), 1.19 (vt, $J_{\text{P-H}} = 6.4$ Hz, 18H, ($^t\text{Bu-CH}$)). $^{13}\text{C}\{^1\text{H}\}$ NMR (126 MHz, C_6D_6): δ 178.5 (C=O, OAc), 173.8 (C=O, OAc), 160.8, 154.7 (t, $J_{\text{P-C}} = 4.2$ Hz), 130.6, 122.2, 39.2 (br m), 37.1 (t, $J_{\text{P-C}} = 5.8$ Hz), 36.97 (t, $J_{\text{P-C}} = 8.6$ Hz), 29.3 (br s), 25.6, 23.3 (m). $^{31}\text{P}\{^1\text{H}\}$ NMR (202 MHz, C_6D_6): δ 59.1. ATR-IR (cm^{-1}): 1660 (C=O), 1630 (C=O), 989(Re=O). Elem. Anal Found (calc): C: 46.85(47.11); H: 6.59(6.92).

(PCP^{tBu})ReO₂ (305): To a J. Young tube was added **303b** (38.0 mg, 0.057 mmol), CaO (70.0 mg, 1.24 mmol), and C₆D₆, forming a violet-colored mixture. This mixture was placed on a rotator for 24 h and monitored by NMR spectroscopy. ³¹P{¹H} and ¹H NMR spectroscopy indicated formation (ca. 97%) of C_{2v}-symmetric **305**, in which no acetate resonance was present. The mixture was then filtered through Celite and solvent was removed under reduced pressure to provide a violet oil. This oil was washed quickly with cold pentane and dried *in vacuo* to provide the product as a dark purple, oily semi-solid of ca. 95% purity (¹H NMR evidence). Yield: 25.2 mg (73%). ¹H NMR (500 MHz, C₆D₆): δ 7.27 (d, *J* = 7.5 Hz, 2H), 7.18 (t, *J* = 7.5 Hz, 1H), 3.49 (vt, *J* = 4.1 Hz, 4H), 1.26 (vt, *J* = 6.3 Hz, 36H). ¹³C{¹H} NMR (126 MHz, C₆D₆): δ 159.6 (t, *J* = 5.0 Hz), 140.4 (br), 130.4, 122.0 (t, *J* = 5.7 Hz), 38.9 (t, *J* = 10.6 Hz), 35.7 (t, *J* = 5.9 Hz), 29.9. ³¹P{¹H} NMR (202 MHz, C₆D₆): δ 48.4. ATR-IR (cm⁻¹): 832_(Re=O), 812_(Re=O)

X-ray Diffractometry details for (PCP^{iPr})ReO(OAc)(OH) (303a): A dark purple, multi-faceted block of suitable size (0.34 x 0.28 x 0.11 mm) was selected from a representative sample of crystals of the same habit using an optical microscope and mounted onto a nylon loop. Low temperature (110 K) X-ray data were obtained on a Bruker APEXII CCD based diffractometer (Mo sealed X-ray tube, K_α = 0.71073 Å). All diffractometer manipulations, including data collection, integration and scaling were carried out using the Bruker APEXII software. An absorption correction was applied using SADABS. The space group was determined on the basis of systematic absences and intensity statistics and the structure was solved by direct methods and refined by full-matrix least squares on *F*². The structure was solved in the monoclinic P 2₁/c space group using XS (incorporated in SHELXLE). All non-hydrogen atoms were refined with anisotropic thermal parameters. All hydrogen atoms were placed in idealized positions and refined using riding model. The structure was refined (weighted least squares refinement on *F*²) and the

final least-squares refinement converged. No additional symmetry was found using ADDSYM incorporated in PLATON program. (CSD Identifier/Number – LEVPUA/ 1581039).

3.4.3 Reactivity of Rhenium Complexes

***In Situ* observation of Observation of (PCP^{iPr})ReO(OAc)(OH) in fast exchange with HOAc:** To a J. Young tube was added (PCP^{iPr})ReOCl₂ (**202**) (20.1 mg, 0.033 mmol), NaOAc(H₂O)₃ (10.0 mg, 0.07 mmol), and C₆D₆. The resultant suspension was placed on a rotator for 24 h over which time full conversion was observed by NMR spectroscopy. Some chemical shifts for (PCP^{iPr})ReO(OAc)(OH) (**303a**) generated in this manner were found to be different. This was particularly true for the acetate resonance which is shifted more towards free HOAc (δ 1.52 ppm) than in isolated **303a**. ¹H NMR (500 MHz, C₆D₆): δ 7.37 (d, $J_{H-H} = 7.5$ Hz, 2H), 7.23 (t, $J_{H-H} = 7.5$ Hz, 1H), 3.46 (vt, $J_{P-H} = 4.2$ Hz), 2.15 (m, 4H), 2.05 (s, 6H), 1.15 (dvt, $J = 14.9, 7.4$ Hz, 12H), 1.10 (dvt, $J = 14.6, 7.4$ Hz, 12H). ¹³C{¹H} (126 MHz, C₆D₆): δ 18.2, 22.6, 24.5 (t, $J_{P-C} = 10.5$ Hz), 40.3 (t, $J_{P-C} = 14.2$ Hz), 122.5, 130.1, 143.7, 152.2, 178.4. ³¹P{¹H} NMR (202 MHz, C₆D₆): δ 39.4.

***In Situ* observation of (PCP^{tBu})ReO(OAc)(OH) in fast exchange with HOAc:** To a J. Young tube in C₆D₆ was added (PCP^{tBu})ReOCl₂ (**301**) (43.4 mg, 0.065 mmol) and NaOAc(H₂O)₃ (16.0 mg, 0.12 mmol). The resultant light green suspension was heated at 70 °C for 12 h over which time it changed in color from green, to blue, and eventually to dark purple, as full conversion to the product was observed by NMR (³¹P{¹H} and ¹H) evidence. The solution is quite air sensitive, leading to fast decomposition to unknown, colorless products upon exposure. Repeated attempts to generate, isolate or crystallize this product only led to isolation and crystallization of (PCP^{tBu})ReO(OAc)(OH) (**303b**). Some chemical shifts for (PCP^{tBu})ReO(OAc)(OH) generated in

this manner were found to be different. This was particularly true for the acetate resonance which is shifted more towards free HOAc (δ 1.52 ppm) than in isolated (PCP^{tBu})ReO(OAc)(OH). ¹H NMR (500 MHz, C₆D₆): δ 7.30 (d, J_{H-H} = 7.5 Hz, 2H), 7.18 (t, J_{H-H} = 7.5 Hz, 1H), 3.55 (vt, J_{P-H} = 4.0 Hz, 4H), 2.06 (s, 6H), 1.23 (vt, J_{P-H} = 6.4 Hz, 36 H), *OH resonances were unable to be observed. ¹³C{¹H} NMR (126 MHz, C₆D₆): δ 179.4(OAc, C=O), 154.9, 130.7, 126.9, 122.5 (t, J_{P-C} = 5.9 Hz), 39.2 (t, J_{P-C} = 10.9 Hz), 36.1 (t, J_{P-C} = 6.4 Hz), 29.8, 23.1 (OAc, CH₃). ³¹P{¹H} NMR (202 MHz, C₆D₆) δ 48.7

Reaction of (PCP^{tBu})ReO(OAc)(OH) with Ac₂O: to a J. Young tube was added (PCP^{tBu})ReO(OAc)(OH) (**303b**) (7.0 mg, 0.01 mmol) and C₆D₆ forming a violet colored solution. To this solution was added Ac₂O (5 μ L, 0.05 mmol). No color change was observed and no reaction was observed by either ³¹P{¹H} or ¹H NMR spectroscopy after 10 min. at room temperature. The solution was heated in an oil bath set at 80 °C for 20 min, after which time it became light blue in color as full conversion to (PCP^{tBu})ReO(OAc)₂ (**304b**) was observed by ³¹P{¹H} and ¹H NMR spectroscopy.

Reaction of (PCP^{tBu})ReO(OAc)(OH) with 2 equivalents Me₃SiCl: To a J. Young tube was added (PCP^{tBu})ReO(OAc)(OH) (**303b**) (22.1 mg, 0.03 mmol) in CDCl₃. To the resultant purple solution was added Me₃SiCl (9 μ L, 0.071 mmol), resulting in an immediate color change to emerald green and the solution was placed on a rotator for 1.5 h to ensure reaction completion. Analysis by ³¹P{¹H} NMR spectroscopy revealed full, clean conversion to (PCP^{tBu})ReOCl₂ (**301**) (ca. δ 47 ppm). Analysis of the ¹H NMR spectrum confirmed the presence of **301** as the sole organometallic product, and showed a ca. 1:1:1 ratio of **301**, (Me₃Si)₂O, and HOAc.

Probing the Thermal Stability of (PCP^{tBu})ReH₆ (302) in C₆D₆: In a J. Young tube was added **302** (40.0 mg, 0.07 mmol) and C₆D₆, forming a tan solution. The solution was frozen,

degassed, and heated to 90 °C for 24 h. $^{31}\text{P}\{^1\text{H}\}$ NMR and ^1H NMR spectroscopy revealed no decomposition of **302** with no evidence of H_2 formation observed.

Probing the Stability of $(\text{PCP}^{\text{tBu}})\text{ReO}(\text{OAc})(\text{OH})$ in fast exchange with HOAc: A J. Young tube was charged with $\text{NaOAc}(\text{H}_2\text{O})_3$ (7.0 mg, 0.051 mmol), $(\text{PCP}^{\text{tBu}})\text{ReOCl}_2$ (14.5 mg, 0.022 mmol), and C_6D_6 . The resultant suspension was placed on a rotator for 24 h over which time full conversion was observed (NMR evidence) to $(\text{PCP}^{\text{tBu}})\text{ReO}(\text{OAc})(\text{OH})$ in fast exchange with HOAc. Following full conversion, the sample was then placed in a Rayonet Photochemical Reactor (cat no. RPR-100) and irradiated with broad spectrum UV light for 24 h, reaching a temperature of 35 °C. No reaction was observed by NMR spectroscopy. Following this, the sample was then frozen, degassed and heated at 90 °C for 24 h. No reaction was observed. The sample was then brought back into a glovebox and degassed H_2O was added (10 μL , 0.555 mmol). The sample was rotated for 24 h, showing no reaction by NMR spectroscopy. The sample was then heated at 90 °C for another 24 h and neither $^{31}\text{P}\{^1\text{H}\}$ or ^1H NMR spectroscopy showed any evidence of a decomposition or further reaction taking place.

Vacuum Transfer Experiment with $(\text{PCP}^{\text{tBu}})\text{ReO}(\text{OAc})(\text{OH})$ generated *in situ*: To a J. Young tube was added $\text{NaOAc}(\text{H}_2\text{O})_3$ (5.0mg, 0.036 mmol), $(\text{PCP}^{\text{tBu}})\text{ReOCl}_2$ (8.3 mg, 0.013 mmol), and C_6D_6 . The tube was placed on a rotator for 24 h over which time full conversion to $(\text{PCP}^{\text{tBu}})\text{ReO}(\text{OAc})(\text{OH})$ in fast exchange with HOAc (OAc signal worth 6H) was observed by $^{31}\text{P}\{^1\text{H}\}$ and ^1H NMR spectroscopy. The solution was then vacuum transferred to another J. Young tube using a vacuum transfer bridge, and analyzed spectroscopically. The ^1H NMR spectrum of the volatiles showed only a singlet corresponding to free AcOH (δ 1.52 ppm). The remaining solids were redissolved in C_6D_6 . $^{31}\text{P}\{^1\text{H}\}$ and ^1H NMR spectroscopy confirmed clean, quantitative conversion to $(\text{PCP}^{\text{tBu}})\text{ReO}(\text{OAc})(\text{OH})$.

Reaction of (PCP^{tBu})ReO(OAc)₂ with HOAc: To a J. Young tube was added a C₆D₆ solution of (PCP^{tBu})ReO(OAc)₂ (5.8 mg, 0.008 mmol). To this light blue solution was added five equiv. of a 0.5 M AcOH solution in C₆D₆ (80 μL, 0.04 mmol) and the solution was placed on a rotator for 24 h. ¹H NMR analysis reveals slight decomposition to (PCP^{tBu})ReO(OAc)(OH) (ca. 5%, likely from adventitious H₂O), and fast exchange of one of the acetate ligands in C_s-symmetric (PCP^{tBu})ReO(OAc)₂ resulting in a broadening of the OAc resonance at δ 1.8 ppm. No conversion to any other products was observed.

Reaction of *in situ* generated (PCP^{tBu})ReO(OAc)(OH) with 1.5 equiv. Me₃SiCl: To a J. Young tube was added (PCP^{tBu})ReOCl₂ (16.1 mg, 0.024 mmol), NaOAc(H₂O)₃ (7.0 mg, 0.051 mmol), and C₆D₆. The resultant suspension was heated overnight at 70 °C, resulting in full conversion to (PCP^{tBu})ReO(OAc)(OH) in fast exchange with HOAc (NMR evidence). Me₃SiCl (5 μL, 0.039 mmol) was added to the solution and the tube was placed on a rotator for 5 h to allow for reaction completion. ³¹P{¹H} NMR spectroscopy revealed the formation of two closely overlapping products in roughly 60:40 ratio (ca. δ 47.6 ppm). The ¹H NMR spectrum featured a 60:40 ratio of (PCP^{tBu})ReOCl₂ and one other, unidentified C_s-symmetric product likely of the formula (PCP^{tBu})ReOCl(OH)(HOAc)_x and may feature OAc exchange with Me₃SiOAc. Me₃SiOAc and (Me₃Si)₂O are observed in ca. 10:1 ratio.

Reaction of (PCP^{tBu})ReOCl₂ with excess anhydrous NaOAc: -To a J. Young tube was added (PCP^{tBu})ReOCl₂ (13.9 mg, 0.021 mmol), anhydrous NaOAc (9.0 mg, 0.110 mmol), and C₆D₆. The resultant suspension was heated at 100 °C in an oil bath and monitored by NMR spectroscopy. After 120 h the reaction had appeared to cease. Two products were observed in 70:30 ratio by ³¹P{¹H} NMR spectroscopy at δ 56.4 and 59.0 ppm, respectively. The resonance at δ 56.4 is likely the intermediate, (PCP^{tBu})ReO(OAc)(Cl), determined by ¹H NMR evidence. The

resonance at δ 59.0 ppm corresponds to formation of C_s -symmetric $(PCP^{tBu})ReO(OAc)_2$ which gains in intensity over time. **NMR Data for $(PCP^{tBu})ReO(OAc)(Cl)$ intermediate:** 1H NMR (500 MHz, C_6D_6): δ 7.42 (d, $J = 7.5$ Hz, 2H), 7.19 (d, $J = 7.5$ Hz, 1H), 4.10 (dvt, $J = 16.0, 4.3$ Hz, 2H), 3.33 (dvt, $J = 15.9, 3.6$ Hz, 2H), 1.81 (s, 3H), 1.24 (vt, $J = 6.6$ Hz, 18H), 1.18 (vt, $J = 6.3$ Hz, 18H). $^{31}P\{^1H\}$ NMR (202 MHz, C_6D_6): δ 56.4.

Addition of H_2O (5 μ L, 0.280 mmol) to the sample prepared above resulted in an immediate color change to purple. The $^{31}P\{^1H\}$ NMR spectrum revealed formation of $(PCP^{tBu})ReO(OAc)(OH)$ in fast exchange with HOAc (δ 48.7) and what is tentatively assigned as a hydrolyzed, C_s -symmetric (1H NMR evidence) $(PCP^{tBu})ReO(Cl)(OH)(HOAc)_x$ species (ca. δ 47.4 ppm). 1H NMR analysis confirms full conversion of $(PCP^{tBu})ReO(OAc)_2$ to $(PCP^{tBu})ReO(OAc)(OH)$ in fast exchange with HOAc.

Reaction of $(PCP^{tBu})ReO(OAc)(OH)$ with HOAc: To a J. Young tube was added $(PCP^{tBu})ReO(OAc)(OH)$ (19.4 mg, 0.029 mmol) and C_6D_6 , forming a purple solution. To this solution was added a 1.0 M C_6D_6 solution of AcOH (30 μ L, 0.030 mmol) causing no color change. After 10 min $^{31}P\{^1H\}$ NMR revealed full conversion to a single product with a singlet resonance at δ 48.8 ppm. The corresponding 1H NMR spectrum showed clean formation of a C_{2v} -symmetric $(PCP^{tBu})Re$ product containing a slightly upfield shifted, and broadened acetate singlet (δ 1.94 ppm, 6H), as well as a broad resonance at δ 12.1 ppm which integrated to 2H. This product was identified as $(PCP^{tBu})ReO(OAc)(OH)$ in fast exchange with an equivalent of HOAc. Removal of volatiles under reduced pressure allowed for the clean recovery of $(PCP^{tBu})ReO(OAc)(OH)$.

Reaction of $(PCP^{iPr})ReO(OAc)(OH)$ with NEt_3 : To a J. Young tube was added $(PCP^{iPr})ReO(OAc)(OH)$ (10.0 mg, 0.016 mmol) and C_6D_6 , forming a violet solution. To this

resultant solution was added NEt₃ (20 μL, 0.14 mmol). The solution was then placed on a rotator for 24 h and monitored by ³¹P{¹H} and ¹H NMR spectroscopy. No reaction was observed.

Reaction of (PCP^{tBu})ReO(OAc)(OH) with Na₂CO₃: To a J. Young tube was added (PCP^{tBu})ReO(OAc)(OH) (14.9 mg, 0.022 mmol), Na₂CO₃ (26.5 mg, 0.25 mmol), and C₆D₆ resulting in a violet-colored mixture. This mixture was placed on a rotator for 5 h and monitored by NMR spectroscopy. ³¹P{¹H} and ¹H NMR indicated no reaction. The mixture was then placed in an oil bath at 80 °C for 4 h. ³¹P{¹H} and ¹H NMR spectroscopy indicated that no reaction had occurred.

VT NMR study of (PCP^{tBu})ReO(OAc)(OH) with HOAc: To a J. Young tube was added (PCP^{tBu})ReO(OAc)(OH) (8.5 mg, 0.013 mmol) and CDCl₃ resulting in formation of a violet colored solution. To this solution was added a 1.0 M CDCl₃ solution of AcOH (13 μL, 0.013 mmol). After 10 min, ³¹P{¹H} and ¹H NMR spectroscopy revealed full conversion to (PCP^{tBu})ReO(OAc)(OH) in fast exchange with HOAc. ¹H NMR (500 MHz, CDCl₃): δ 12.06 (br, 1H), 7.39 (d, *J* = 7.5 Hz, 2H), 7.15 (t, *J* = 7.5 Hz, 1H), 3.80 (vt, *J* = 4.0 Hz, 4H), 2.16 (s, 6H), 1.35 (vt, *J* = 6.4 Hz, 36H). ³¹P{¹H} NMR (202 MHz, CDCl₃): 49.5.

A variable temperature NMR study was then undertaken showing that from 23 °C to -60 °C (within useful solvent-dependent temperature range), aside from minor broadening of ¹H NMR resonances, C_{2v}-symmetry was fully maintained as well as fast exchange of Re-OAc with HOAc giving rise to a singlet acetate resonance (ca. δ 2.16 ppm) worth 6H.

Reaction of (PCP^{tBu})ReO(OAc)₂ with H₂O: To a J. Young tube was added (PCP^{tBu})ReO(OAc)₂ (22.2 mg, 0.03 mmol) and C₆D₆, forming a deep blue solution. To this solution was added 1 drop degassed H₂O (ca. 20 ± 2 μL, ca. 1 mmol), causing a color change to violet at the interface. Upon inversion of the J. Young tube, the entire solution immediately became

violet in color. $^{31}\text{P}\{^1\text{H}\}$ and ^1H NMR spectroscopy revealed quantitative, clean conversion to $(\text{PCP}^{\text{tBu}})\text{ReO}(\text{OAc})(\text{OH})$ in fast exchange with 1 equiv. of HOAc.

Reaction of $(\text{PCP}^{\text{tBu}})\text{ReO}_2$ with HOAc: To a J. Young tube was added $(\text{PCP}^{\text{tBu}})\text{ReO}_2$ (12.6 mg, 0.021 mmol) as a C_6D_6 solution, and 1.0 M AcOH in C_6D_6 (21 μL , 0.021 mmol) was added via gas-tight syringe. $^{31}\text{P}\{^1\text{H}\}$ and ^1H NMR spectroscopy indicated full, clean conversion to $(\text{PCP}^{\text{tBu}})\text{ReO}(\text{OAc})(\text{OH})$.

Reaction of $(\text{PCP}^{\text{tBu}})\text{ReO}_2$ with Ac_2O : To a J. Young tube was added $(\text{PCP}^{\text{tBu}})\text{ReO}_2$ (12.6 mg, 0.021 mmol) as a C_6D_6 solution followed by addition of Ac_2O (4 μL , 0.04 mmol) added via gas-tight syringe. $^{31}\text{P}\{^1\text{H}\}$ and ^1H NMR spectroscopy indicated ca. 40% formation of $(\text{PCP}^{\text{tBu}})\text{ReO}(\text{OAc})_2$ after 30 minutes at r.t. The solution was then placed in an oil bath and heated at 70 $^\circ\text{C}$ for 1h. ^1H and $^{31}\text{P}\{^1\text{H}\}$ NMR spectroscopy indicated full, clean conversion to $(\text{PCP}^{\text{tBu}})\text{ReO}(\text{OAc})_2$.

Reaction of $(\text{PCP}^{\text{tBu}})\text{ReO}(\text{OAc})(\text{OH})$ with DOAc: To a J. Young tube was added $(\text{PCP}^{\text{tBu}})\text{ReO}(\text{OAc})(\text{OH})$ (24.3 mg, 0.036 mmol) and C_6D_6 , forming a violet solution. To this solution was added DOAc (4 μL , 0.07 mmol) and the reaction was monitored by NMR spectroscopy. $^{31}\text{P}\{^1\text{H}\}$ NMR showed a single resonance at δ 48.9 ppm (ca. 0.5 ppm shifted from pure $(\text{PCP}^{\text{tBu}})\text{ReO}(\text{OAc})(\text{OH})$) and ^1H NMR spectroscopy revealed a single acetate resonance, indicating fast exchange with DOAc. To this solution was then added an additional 16 μL DOAc ($V_{\text{TOT}} = 20$ μL , 0.34 mmol). The $^{31}\text{P}\{^1\text{H}\}$ NMR spectrum featured a single resonance at δ 49.4 ppm (ca. 1.0 ppm shifted from pure $(\text{PCP}^{\text{tBu}})\text{ReO}(\text{OAc})(\text{OH})$) and the ^1H NMR spectrum exhibited a single acetate resonance and no changes in solution-state symmetry, indicating continued fast exchange with DOAc. It was also noted that upon additions of DOAc the OH resonance begins to integrate much lower by ^1H NMR versus other proteo ligand resonances.

CHAPTER IV

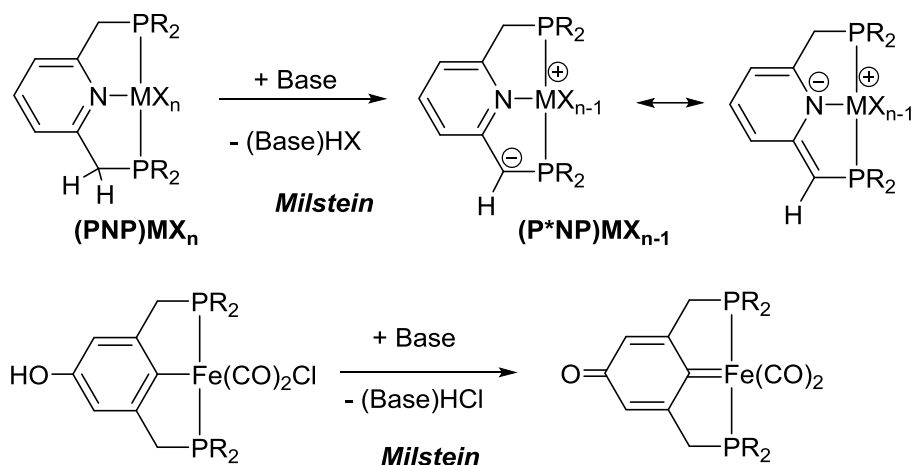
DEAROMATIZATION OF THE PCP PINCER LIGAND IN A RHENIUM(V) OXO COMPLEX[‡]

4.1 Introduction

Pincer ligands are a class of tridentate ligands that bind to the metal center in meridional fashion and they have attained special importance in organometallic chemistry and catalysis.^{112,113} Pincers based on the bis(phosphinomethyl)benzene (PCP) or bis(phosphinomethyl)pyridine (PNP, Scheme IV-1)¹¹⁴ core are among the most common. They have arguably served as the historical and intellectual progenitors of the many other types of anionic and neutral pincers, which are often derived from and compared against the parent PCP and PNP. Pincer ligands are more commonly used as spectator supporting ligands, defining the coordination sphere of the metal complex, but not themselves participating in the bond-breaking and bond-making events. On the other hand, pioneering work by the Milstein group identified PNP as a ligand capable of metal-ligand cooperation by virtue of proton loss and recovery (Scheme IV-1).¹¹⁵ This spurred the development of (de)hydrogenation catalysis by many related systems based on pincers with the central nitrogen donor.¹¹⁶ Deprotonation of the PNP ligand (normally accomplished as an HX loss from the PNP complex) leads to a new anionic P*NP ligand, which has been described as “dearomatized”. One of the main resonance forms is an amido/bis(phosphine) (Scheme IV-1). However, unlike a number of other amido/bis(phosphine)

[‡] Reprinted in part with permission from “Dearomatization of the PCP Pincer Ligand in a Re(V) Oxo Complex” Kosanovich, A. J.; Komatsu, C. H.; Bhuvanesh, N.; Perez, L. M.; Ozerov, O. V. *Chem. Eur. J.* **2018** Copyright 2018. Wiley-VCH. DOI: 10.1002/chem.201802589

pincer ligands, re-protonation of the P*NP ligand occurs at the carbon and not at the nitrogen. This minimizes structural differences between the protonated and deprotonated forms via preservation of planarity at the central nitrogen.



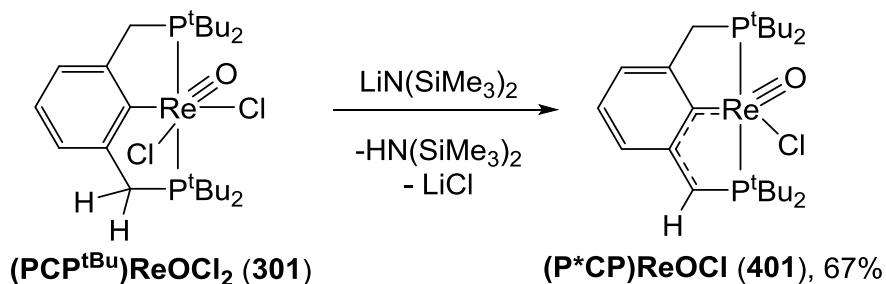
Scheme IV-1. Generic depiction of HX loss from pyridine-based PNP complexes and an example of dearomatization of a hydroxyl-substituted PCP complex. Reprinted with permission from Wiley-VCH, Copyright 2018

Milstein previously explored dearomatization of modified PCP ligands via deprotonation of a *para*-hydroxy group (Scheme IV-1),^{117,118} but “dearomatization” of PCP ligands via loss of a proton from a benzylic CH₂ position has not been reported up to this point. This absence is noteworthy given the prominence of PCP in organometallic explorations of bond-breaking.¹¹⁹ In the course of our investigations of pincer complexes of high-valent rhenium, we serendipitously came across an example of just such reactivity with PCP, which we disclose in the present report.¹²⁰

4.2 Results and Discussion

4.2.1 Initial Observations of PCP Ligand Dearomatization

Treatment of an emerald green C_6D_6 solution of C_3 -symmetric $(PCP^{tBu})ReOCl_2$ (**301**) with $(Me_3Si)_2NLi$ resulted in the immediate formation of a dark blue solution with a colorless precipitate (presumed to be $LiCl$). 1H NMR analysis revealed the formation of $(Me_3Si)_2NH$ along with an equimolar amount of a new “dearomatized” complex $(P^*CP)ReOCl$ (**401**) possessing C_1 symmetry (Scheme IV-2).¹²¹ **401** was isolated in 67% yield upon workup. $(PCP^{tBu})ReOCl_2$ (**301**) was also converted to **401** by the action of sodium *tert*-pentoxide in C_6D_6 , but not triethylamine. $NaOAc$ also does not convert **301** to **401**. These observations roughly delineate the range of basicity necessary for this dehydrochlorination.



Scheme IV-2. Dearomatization of **301** *via* base mediated dehydrochlorination

4.2.2 Spectroscopic Study of a Dearomatized P^*CP -Re Complex

The two inequivalent phosphorus nuclei in **401** ($^{31}P\{^1H\}$ NMR: δ 77.6 and 72.8 ppm) are strongly coupled to each other ($^2J_{P-P} = 112$ Hz). Signals at δ 6.98, 6.64, and 5.51 ppm in the 1H NMR spectrum correspond to the central six-membered ring and their chemical shifts are

consistent with the disruption of aromaticity. The two hydrogens of the surviving benzylic CH₂ are inequivalent (δ 3.14 and 2.67 ppm) and are each coupled to one phosphorus nucleus and to each other ($^2J_{H-H} = 16.3$ Hz). The deprotonated benzylic position gave rise to a single doublet resonance (δ 3.84, $^2J_{P-H} = 10.3$ Hz). Four distinct *tert*-butyl methyl resonances (9H each) further confirmed the C₁ symmetry of **401**. The ¹³C{¹H} NMR spectrum notably featured a resonance for the benzylic methine at δ 92.0 ppm which exhibits strong C-P coupling ($^1J_{P-C} = 62.2$ Hz) as well as a downfield shifted resonance corresponding to the *ipso*-carbon of the P*CP pincer at δ 180.5 ppm. The rhenium-oxo stretch in the IR spectrum of **401** was found at a lower frequency (925 cm⁻¹) than that of **301** ($\nu_{Re-O} = 975$ cm⁻¹), indicating the greater donicity of the dianionic P*CP-pincer in **401**, versus PCP in **301**.

4.2.3 Structural Study of (P*CP)ReOCl

An X-ray crystallographic study of **401** revealed a five-coordinate geometry about Re ($\tau = 0.24$) with a typical rhenium-oxo triple bond (1.686(5)Å).¹²² The asymmetric nature of the P*CP ligand (Figure IV-1) is manifested in the difference between the C2-C7 bond length (1.472(13) Å) compared to that of C6-C8 (1.399(13) Å), although the Re-P bond distances remain very similar. The Re1-C1 bond in **401** (2.026(5) Å) is shortened by ca. 0.1 Å versus that in (PCP^{iPr})ReOCl₂, (2.116(3)Å), potentially indicating multiple bond character. Despite this shortening, the bond length in **401** is ca. 0.1-0.15 Å longer than in the Re^V and Re^{VII} un-conjugated alkylidene complexes^{123,124} but is ca. 0.2 Å shorter than in the Re^V NHC complexes.¹²⁵

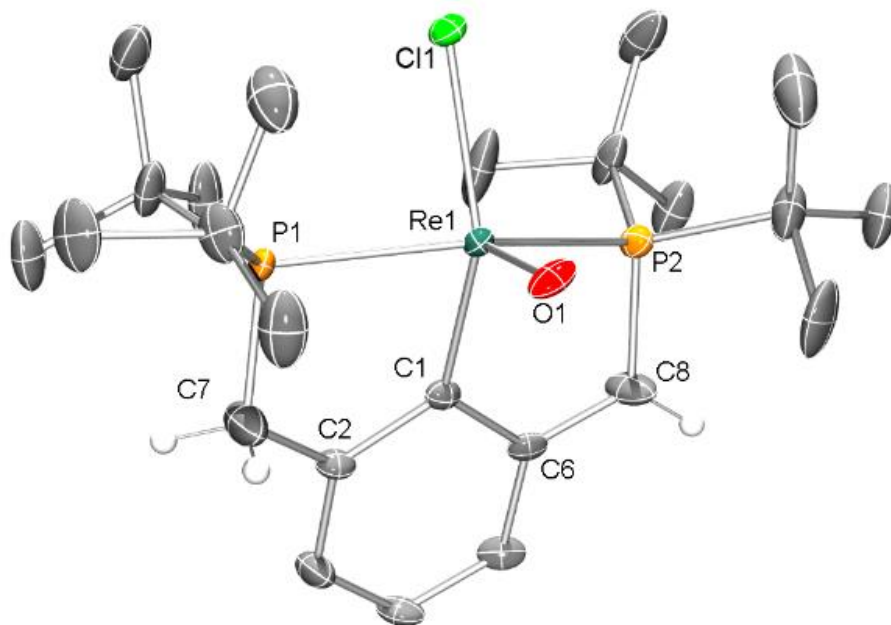


Figure IV-1. ORTEP drawing (50% probability ellipsoids) of $(P^*CP)ReOCl$ (**401**). Select H atoms and a second molecule in the unit cell are omitted for clarity. Selected distance (\AA) and angles ($^\circ$): Re1-C1, 2.026(5); C2-C7, 1.472(13); C6-C8, 1.399(13); Re1-O1, 1.686(5); P1-Re1, 2.445(3); P2-Re1, 2.460(3); P1-Re1-P2, 149.87(15); P1-Re1-C1, 80.5(4); P2-Re1-C1, 79.1(3). Reprinted with permission from Wiley-VCH, Copyright 2018

4.2.4 Computational Analysis of $(P^*CP)ReOCl$

DFT calculations¹²⁶ allowed for greater insight into the bonding in **401**. The calculated Re-C_{ipso} bond lengths in **301** (2.128 \AA) and **401** (2.039 \AA) match the experimental data reasonably well. The Re-C Wiberg¹²⁷ index values and the Re-C delocalization index¹²⁸ values for **301** and **401** differ by about 0.3, supporting partial multiple bond character in **401** (Figure IV-2). The transformation from **301** to **401** can be analyzed in a thought experiment as a two-step process with a loss of H⁺ and of Cl⁻.

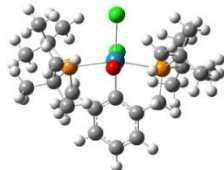
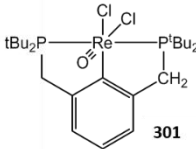

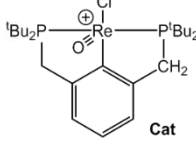
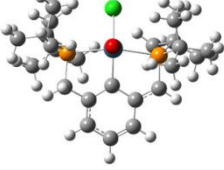
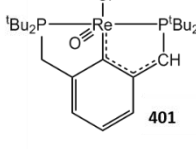

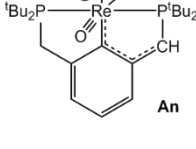
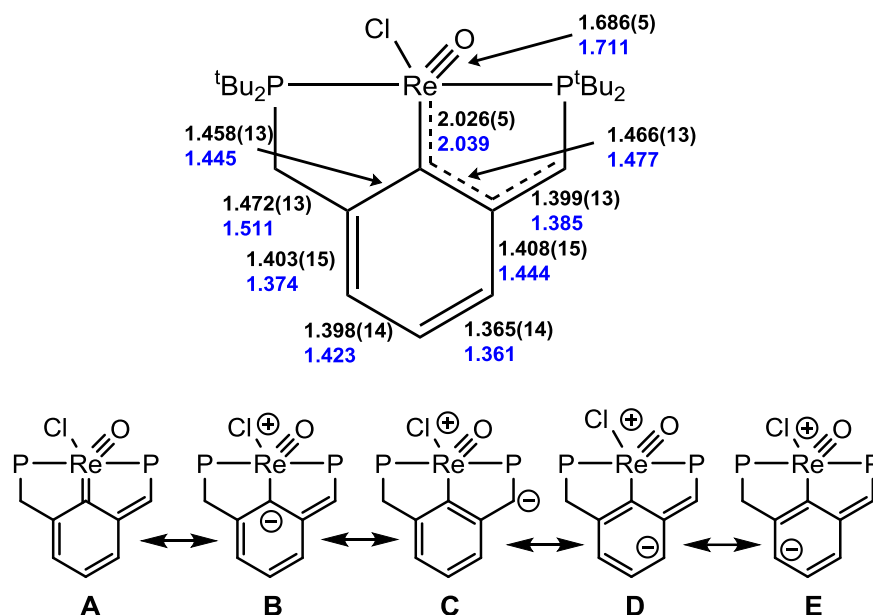
Calculated Structure	Compound	Re-C Wiberg Index (NBO)	Re-C Delocalization Index (AIM)
	 301	0.79	0.88
	 Cat	0.87	0.96
	 401	1.10	1.18
	 An	0.99	1.09

Figure IV-2. Calculated Wiberg Bond Index and Delocalization Index values. Reprinted with permission from Wiley-VCH, Copyright 2018

Figure IV-2 illustrates how each of these steps was calculated to affect the Re-C Wiberg index and the delocalization index through the comparison of **301** and **401**, along with $[(PCP)ReOCl]^+$ (**Cat**) and $[(P^*CP)ReOCl_2]^-$ (**An**). Loss of chloride alone (**301**→**Cat**, or **An**→**401**) does lead to higher values, but only by approximately 0.1, or a third of the difference between **301** and **401**. Loss of a proton (**301**→**An** or **Cat**→**401**) leads to a greater change in index values, on the order of 0.2. Thus, we can conclude that the increase in the Re-C bond order in the **301**→**401** transformation is not owing simply to a lower coordination number and higher unsaturation at Re, but is mostly a consequence of the P*CP ligand being capable of greater π -donation to Re compared with the parent PCP.



Scheme IV-3. Graphical representation of (P*CP)ReOCl (**401**) showing experimentally (black) and computationally (blue) determined bond distances. Reprinted with permission from Wiley-VCH, Copyright 2018

Considering the C-C distances within the P*CP ligand, the X-ray data and the DFT calculations (Scheme IV-3) agree on the presence of a substantial alternation of C-C bond lengths within the six-membered ring, consistent with the “dearomatization” terminology. Several resonance structures can be drawn for **401** (Scheme IV-3), of which **A** and **C** appear to be the greater contributors. This view is illustrated by the graphical representation of the calculated HOMO of **401** in Figure IV-3, showing both the Re-C π -overlap and the presence of electron density on the benzylic CH.

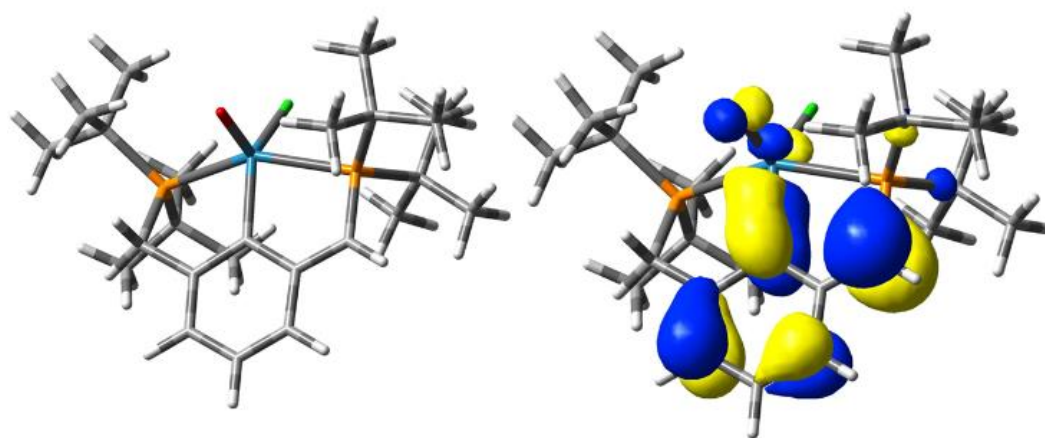
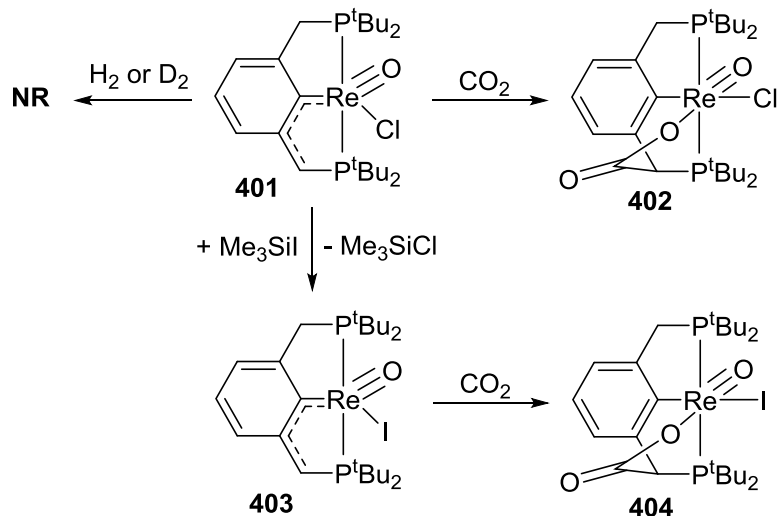


Figure IV-3. (left) DFT (B3LYP/BSI) optimized structure of **401** (right) Highest Occupied Molecular Orbital (HOMO) of **401** (isovalue = 0.04). Reprinted with permission from Wiley-VCH, Copyright 2018

4.2.5 Cycloaddition Reactivity of $(P^*CP)ReOCl$ with CO_2

The great success of complexes of PNP ligands capable of metal-ligand cooperation relies on their ability to reversibly add and lose H_2 , as well as polar H-X and C=X bonds. Inspired by this analogy, we wished to explore the reactivity of **401** with small molecules. Exposure of C_6D_6 solution of **401** to 1 atm H_2 for 24 h or to 1 atm of D_2 for 48 h resulted in no discernible changes in the NMR spectra. It is possible that H_2 activation does not occur because the putative product would place a hydride on Re *trans* to the oxo ligand, bringing about a grave *trans*-influence conflict. It is also possible that the Re center in **401** is not capable of forming a dihydrogen complex that may be required as an intermediate *en route* to splitting H_2 .



Scheme IV-4. Reactions of **401** with H₂ and CO₂ and the synthesis of iodo derivatives **403** and **404**. Reprinted with permission from Wiley-VCH, Copyright 2018

We reasoned that **401** may be much more suited for addition of polar X-Y bonds which would result in a less *trans*-influencing new ligand *trans* to the oxo. Indeed, reaction with CO₂ at ambient temperature rapidly furnished a new, light-green product **402** (Scheme IV-4). The NMR data for **402** were consistent with C₁ symmetry and restoration of aromaticity in the six-membered ring (δ 7.35, 7.24, and 7.02 ppm for the ¹H NMR resonances). The benzylic methine resonance was identified at δ 4.83 ppm (d, ²J_{P-H} = 4.83 Hz). The resultant carboxylate moiety produced the expected resonance in the ¹³C{¹H} NMR spectrum at δ 174.3 ppm, and diagnostic C=O and Re=O stretches were observed by IR spectroscopy at 1676 and 983 cm⁻¹, respectively. The reaction of **401/403** with CO₂ can be viewed as activation of CO₂ by a frustrated C/Re Lewis pair if resonance form **C** is considered for **401**, or as a formal *hetero*-Diels-Alder [4+2] cycloaddition, if resonance form **A** is considered instead. In contrast to **401**, Milstein's Re^I complex (P*NP)Re(CO)₂ adds

both H₂ and CO₂. Addition of CO₂ via metal-ligand cooperation with a dearomatized PNP or PNN ligand has been reported for Ru, as well.^{129,130}

4.2.6 Halide Metathesis and Structural Study of CO₂ Cycloaddition Product

We succeeded in obtaining single crystals of **402** (Figure IV-5-*left*), but the structure solutions, despite multiple diffraction attempts, showed significant disorder in the Re-bound carboxylate oxygen. Because of this, we synthesized the iodo analogue **404** via *in situ* conversion of **401** to **403** with Me₃SiI and subsequent reaction of **403** with CO₂. The NMR data for **403** and **404** matched those of **401** and **402** very closely and we were able to acquire a single crystal of **404**. **404** crystallized in a different space group than **402** and the structure of **404** (Figure IV-5-*right*) was solved without the disorder in the oxygen position. The solution revealed a distorted octahedral geometry about Re and confirmed C-C bond formation at the benzylic position, furnishing a new rhenium carboxylate (Re1-O2; 2.109(4)). A lengthened Re1-C8_{ipso} bond (2.094(5) Å) as well as similar C_{aryl}-C_{benzyl} bonds (C2-C3: 1.515(7) Å; C7-C9 1.509(8) Å) further confirmed the "rearomatization" of the ligand backbone.

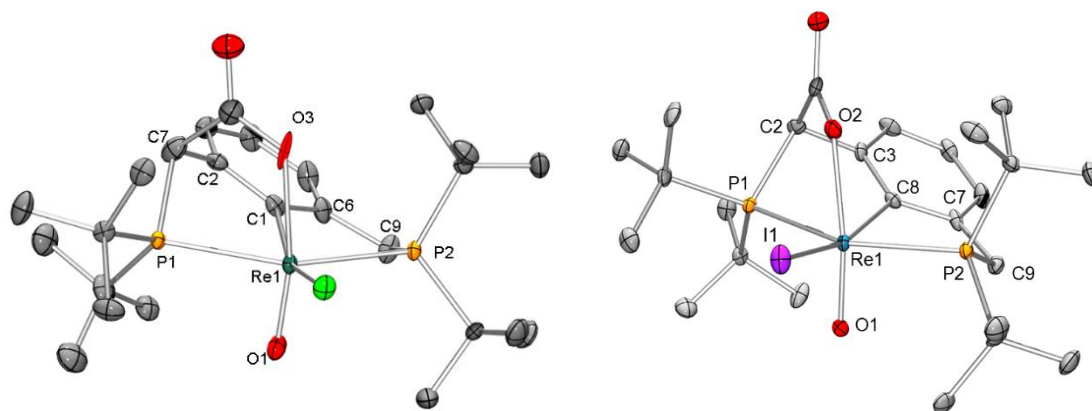


Figure IV-4. ORTEP structures of CO₂ cycloaddition products (left) **402** and (right) **404**

4.3 Conclusion

In summary, we report characterization for the first example of a complex featuring a “dearomatized” parent PCP pincer ligand. It is difficult to ascertain why this type of transformation has not been previously observed. Certainly, PCP ligands have been used in conjunction with a great variety of transition metals and in situations similar to those in which PNP undergoes “dearomatization”. PCP complexes have been exposed to action of strong bases, including in complexes carrying halogens on the metal. As well, PCP complexes carrying ligands (hydrides, alkyls, amidos, alkoxides) that could potentially serve as intramolecular bases are many. However, stable products similar to the one we report here have not been characterized. One reason is likely that PCP analogues possess lower acidity for the benzylic C-H bonds compared to the PNP complexes. However, it is also likely that the stability of the deprotonated PCP may require a greater “assist” from the metal center compared to the case of PNP ligands where the negative charge can be localized on an electronegative nitrogen atom. Thus, it is possible that the

presently described system benefits from both the electron-withdrawing power of the Re^V oxo center, as well as from the propensity of Re for formation of multiple metal-element bonds, thereby stabilizing the deprotonated PCP via a carbene-like structure.

4.4 Experimental

4.4.1 General Considerations

Unless otherwise stated, all experiments were carried out using standard glovebox and Schlenk line techniques under a dry argon atmosphere. C₆D₆ was dried over NaK, benzophenone, and 18-crown-6, distilled, and stored over molecular sieves in an argon glovebox prior to usage. Diethyl ether, pentane and toluene were dried and deoxygenated using a PureSolv MD-5 solvent purification system and were stored over molecular sieves in an argon-filled glovebox. (PCP^{tBu})ReOCl₂ was synthesized using reported literature procedures. All other chemicals were used as received from commercial suppliers. NMR spectra were recorded on a Varian iNova 500 (³¹P{¹H} NMR, 202.276 MHz; ¹³C{¹H} NMR, 125.670 MHz; ¹H NMR, 499.678 MHz) spectrometer in given solvents. Chemical shifts are reported in ppm (δ). ³¹P{¹H} NMR spectra were referenced externally to an 85% phosphoric acid standard at δ 0 ppm. ¹³C{¹H} and ¹H NMR spectra were internally referenced to residual solvent resonances. In reporting spectral data, the following abbreviations were utilized: s = singlet; d = doublet; t = triplet; dd = doublet of doublets; m = multiplet. Infrared spectra were collected on an Agilent CARY FT-IR spectrometer. Elemental analyses were performed by CALI, Inc. (Highland Park, NJ, USA).

4.4.2 Computational Details and Optimization

The parent starting material (**301**), de-aromatized (**401**), **Cat** and **An** PCP-pincer compounds were optimized at the B3LYP level of theory using the SDD basis set¹³¹ with a small-core effective core potential (ECP) for the rhenium atom and the 6-311G(d)¹³² basis set for

all other atoms (B3LYP/BSI) using the *Gaussian 09* software package.¹³³ The B3LYP/BSI optimized structures are displayed in Figures S10-S13. Wiberg¹²⁷ indices were calculated from the Natural Bond Orbital¹³⁴ (NBO) analysis at the B3LYP/BSI optimized geometries of **301**, **401**, **Cat**, and **An**.

4.4.3 Synthesis and Characterization of the (P*CP)Re Complexes

(P*CP)ReOCl (401): To a J. Young tube was added (PCP^{tBu})ReOCl₂ (**301**) (41.2 mg, 0.062 mmol), LiN(SiMe₃)₂ (11.7 mg, 0.07 mmol), and C₆D₆ forming a deep blue solution. ³¹P{¹H} and ¹H NMR spectroscopy revealed full conversion to (P*CP)ReOCl (**401**) within minutes. The solution was then brought into the glovebox, filtered through Celite, and dried *in vacuo* to a dark blue solid. The solid was washed with pentane (2 x 5mL), then dried under reduced pressure to provide the product as a dark blue residue. The residue was then dissolved in a minimal amount of a Et₂O:PhF (v:v 3:1) solution, filtered through a plug of Celite, and crystallized at -38 °C over 48 h. Washing the resultant dark crystals with pentane and subsequent drying under reduced pressure provided the product as a dark blue solid. Yield: 26.0 mg (67%). Single crystals suitable for X-ray diffraction were grown from a Et₂O:PhF (v:v 3:1) solution at -38 °C. ¹H NMR (500 MHz, C₆D₆): δ 6.98 (d, *J* = 8.8 Hz, 1H), 6.64 (m, 1H), 5.51 (d, *J* = 6.3 Hz, 1H), 3.84 (d, *J* = 10.3 Hz, 1H), 3.14 (dd, *J* = 16.3, 11.2 Hz, 1H), 2.67 (dd, *J* = 16.3, 8.4 Hz, 1H), 1.44 (d, *J* = 13.9 Hz, 9H), 1.41 (d, *J* = 14.1 Hz, 9H), 1.22 (d, *J* = 13.7 Hz, 9H), 1.07 (d, *J* = 13.5 Hz, 9H). ¹³C{¹H} NMR (126 MHz, C₆D₆): δ 180.5 (dd, *J* = 22.9, 5.7 Hz), 180.0, 161.7 (dd, *J* = 11.1, 4.3 Hz), 134.21 (d, *J* = 19.8 Hz), 130.3, 126.6 (d, *J* = 24.2 Hz), 107.5 (d, *J* = 15.2 Hz), 92.0 (d, *J* = 62.2 Hz), 43.6 (d, *J* = 16.9 Hz), 38.7 (t, *J* = 23.5 Hz), 36.2 (d, *J* = 15.4 Hz), 35.3 (d, *J* = 30.0 Hz), 30.6, 30.3, 29.6, 29.4. ³¹P{¹H} NMR (202 MHz, C₆D₆): δ 77.6 (d, *J*_{P-P} = 112 Hz), 72.8 (d, *J*_{P-P} = 112 Hz). ATR-IR: ν_{Re=O} - 925 cm⁻¹. Elem. Anal Found (calc): C: 45.67 (45.74); H: 6.99 (6.72).

Generation and Spectroscopic Characterization of (P*CP)ReOI (403): To a J. Young tube was added (P*CP)ReOCl (9.8 mg, 0.015 mmol) and C₆D₆, forming a dark blue solution. To the resultant solution was added Me₃SiI (7 μL, 0.049 mmol) and the sample was placed on an NMR rotator. After 12 h, full conversion to (P*CP)ReOI was observed by ³¹P{¹H} and ¹H NMR as the major organometallic product (ca. 95%), with a slight darkening of solution. ¹H NMR revealed 70% formation of Me₃SiCl and 30% formation of (Me₃Si)₂O. ¹H NMR (500 MHz, C₆D₆): δ 6.92 (d, *J* = 8.8 Hz, 1H), 6.66 (ddd, *J* = 8.8, 6.3, 2.3 Hz, 1H), 5.46 (d, *J* = 6.3 Hz, 1H), 3.81 (d, *J* = 10.5 Hz, 1H), 3.31 (dd, *J* = 16.1, 11.7 Hz, 1H), 2.66 (dd, *J* = 16.0, 7.9 Hz, 1H), 1.48 (d, *J* = 14.1 Hz, 9H), 1.44 (d, *J* = 14.1 Hz, 9H), 1.32 (d, *J* = 14.0 Hz, 9H), 1.03 (d, *J* = 13.5 Hz, 9H). ³¹P{¹H} NMR (202 MHz, C₆D₆): δ 79.8 (d, *J*_{P-P} = 96.8 Hz), 72.9 (d, *J*_{P-P} = 96.8 Hz).

(PCP)ReOCl(CO₂) (402): To a J. Young tube was added (P*CP)ReOCl (18.0 mg, 0.029 mmol) and Et₂O. The resultant, dark blue solution was then frozen, degassed, and thawed (repeated twice). The degassed solution was filled with 1 atm CO₂ and placed on a rotator for 12 h. Over this time a color change was observed to a light green solution. Upon standing, a green solid was observed to form. The solution was decanted and the solid was washed with pentane (2 x 1mL) and dried under reduced pressure to provide the product as an emerald green solid of ca. 95% purity (¹H NMR evidence). Single crystals suitable for X-ray diffraction were grown at room temperature from a concentrated C₆H₆ solution layered with pentane. Yield: 11.4 mg (59%). ¹H NMR (500 MHz, C₆D₆): δ 7.35 (d, *J* = 7.4 Hz, 1H), 7.24 (d, *J* = 7.7 Hz, 1H), 7.02 (dd, *J* = 7.4, 7.7 Hz, 1H), 4.83 (d, *J* = 4.8 Hz, 1H), 3.65 (dd, *J* = 15.7, 12.5 Hz, 1H), 3.22 (dd, *J* = 15.2, 4.9 Hz, 1H), 1.68 (d, *J* = 13.4 Hz, 9H), 1.33 (d, *J* = 13.9 Hz, 9H), 0.88 (d, *J* = 13.7 Hz, 9H), 0.87 (d, *J* = 12.4 Hz, 9H). ¹³C{¹H} NMR (126 MHz, C₆D₆): δ 174.3(m, C=O), 162.1, 153.1 (dd, *J* = 4.8, 2.2 Hz), 150.1 (d, *J* = 6.8 Hz), 131.6, 123.3 (d, *J* = 10.5 Hz), 122.7 (d, *J* = 7.6 Hz), 64.2 (dd, *J* = 21.1, 5.5

Hz), 43.5 (t, $J = 3.5$ Hz), 39.7 (d, $J = 24.6$ Hz), 37.7 (m), 36.7 (d, $J = 10.0$ Hz), 36.5 (d, $J = 11.4$ Hz), 30.6, 30.4, 29.9, 29.2. $^{31}\text{P}\{^1\text{H}\}$ NMR (202 MHz, C_6D_6): δ 87.3 (d, $J_{P-P} = 240.0$ Hz), 73.5 (d, $J_{P-P} = 240.0$ Hz). ATR-IR: $\nu_{\text{C=O}}$ - 1676 cm^{-1} ; $\nu_{\text{Re=O}}$ - 983 cm^{-1} . Elem. Anal Found (calc): C: 44.37 (44.54); H: 6.29 (6.28).

Continuous synthesis and *in situ* Characterization of (PCP)ReOI(CO₂) (404): To a J. Young tube was added (P*CP)ReOCl (22.8 mg, 0.036 mmol) and C_6D_6 , forming a blue solution. To this blue solution was added Me_3SiI (18 μL , 0.126 mmol), and the sample was placed on an NMR rotator for 12 h, allowing conversion to (P*CP)ReOI. The solution was then transferred to a 20 mL scintillation vial and dried under reduced pressure, giving a dark blue-green residue which was washed with pentane and dried *in-vacuo*. The resultant solid was then redissolved in C_6D_6 , forming a dark blue solution which was then transferred to a J. Young tube. The solution was frozen, degassed, and thawed twice, then refilled with 1 atm CO_2 . Upon inversion the sample changed color to a brownish-green and $^{31}\text{P}\{^1\text{H}\}$ and ^1H NMR indicated ca. 92% purity of the desired product, (PCP)ReOI(CO₂). The sample was then filtered through Celite into a small vial and single crystals suitable for X-ray analysis were grown from vapor diffusion of pentane into the C_6D_6 solution, at room temperature. ^1H NMR (500 MHz, C_6D_6): δ 7.29 (br, 1H), 7.22 (br, 1H), 7.03 (t, $J = 7.7$ Hz, 1H), 4.70 (s, 1H), 3.73 (t, $J = 13.7$ Hz, 1H), 3.18 (d, $J = 14.9$ Hz, 1H), 1.71 (d, $J = 13.0$ Hz, 9H), 1.39 (d, $J = 13.4$ Hz, 9H), 0.87 (d, $J = 14.3$ Hz, 9H), 0.85 (d, $J = 13.8$ Hz, 9H). $^{31}\text{P}\{^1\text{H}\}$ NMR (202 MHz, C_6D_6): δ 79.5 (d, $J_{P-P} = 233.0$ Hz), 72.9 (d, $J_{P-P} = 233.0$ Hz).

Reaction of (P*CP)ReOCl with H₂: To a J. Young tube was added (P*CP)ReOCl (401) (11.5 mg, 0.018 mmol) and C_6D_6 , forming a dark blue solution. The solution was frozen, degassed, and thawed twice, then refilled with 1 atm H_2 and monitored by $^{31}\text{P}\{^1\text{H}\}$ and ^1H NMR spectroscopy

after 30 min and 24 h. Though the resonance for H₂ was readily observed by ¹H NMR at both times, no reaction was observed spectroscopically.

X-ray Diffractometry Details for (P*CP)ReOCl (401): A Leica MZ 75 microscope was used to identify a suitable dark blue, multi-faceted block with dimensions (max, intermediate, and min) 0.548 x 0.304 x 0.08 mm³ from a representative sample of crystals of the same habit. The crystal mounted on a nylon loop was then placed in a cold nitrogen stream (Oxford) maintained at 110K. A BRUKER APEX 2 Duo X-ray (three-circle) diffractometer was employed for crystal screening, unit cell determination, and data collection. The goniometer was controlled using the APEX2 software suite, v2008-6.0. The sample was optically centered with the aid of a video camera such that no translations were observed as the crystal was rotated through all positions. The detector was set at 6.0 cm from the crystal sample (APEX2, 512x512 pixel). The X-ray radiation employed was generated from a Mo sealed X-ray tube ($K_{\alpha} = 0.70173 \text{ \AA}$ with a potential of 40 kV and a current of 40 mA). 45 data frames were taken at widths of 1.0°. These reflections were used in the auto-indexing procedure to determine the unit cell. A suitable cell was found and refined by nonlinear least squares and Bravais lattice procedures. The unit cell was verified by examination of the *h k l* overlays on several frames of data. No super-cell or erroneous reflections were observed. After careful examination of the unit cell, an extended data collection procedure (4 sets) was initiated using omega scans. Integrated intensity information for each reflection was obtained by reduction of the data frames with the program APEX2. The integration method employed a three dimensional profiling algorithm and all data were corrected for Lorentz and polarization factors, as well as for crystal decay effects. Finally the data was merged and scaled to produce a suitable data set. The absorption correction program SADABS was employed to correct the data for absorption effects. Systematic reflection conditions and statistical tests of the data

suggested the space group $Pna2_1$. A solution was obtained readily using XT/XS in APEX2. Hydrogen atoms were placed in idealized positions and were set riding on the respective parent atoms. All non-hydrogen atoms were refined with anisotropic thermal parameters. Absence of additional symmetry and voids were confirmed using PLATON (ADDSYM). The structure was refined (weighted least squares refinement on F^2) to convergence. Olex2 was employed for the final data presentation and structure plots. (CSD Identifier/Number – QJGOI/1826253)

X-ray Diffractometry Details for $(PCP^{tBu})ReOCl(CO_2)$ (402): A Leica MZ 75 microscope was used to identify a suitable green plate with very well defined faces with dimensions (max, intermediate, and min) $0.152 \times 0.137 \times 0.035 \text{ mm}^3$ from a representative sample of crystals of the same habit. The crystal mounted on a nylon loop was then placed in a cold nitrogen stream (Oxford) maintained at 100 K. A BRUKER Venture X-ray (kappa geometry) diffractometer was employed for crystal screening, unit cell determination, and data collection. The goniometer was controlled using the APEX3 software suite. The sample was optically centered with the aid of a video camera such that no translations were observed as the crystal was rotated through all positions. The X-ray radiation employed was generated from a Cu- $I\mu s$ X-ray tube ($K\alpha = 1.5418\text{\AA}$ with a potential of 50 kV and a current of 1.0mA). 45 data frames were taken at widths of 1° . These reflections were used to determine the unit cell. The unit cell was verified by examination of the $h k l$ overlays on several frames of data. No super-cell or erroneous reflections were observed. After careful examination of the unit cell, an extended data collection procedure (15 sets) was initiated using omega and phi scans. Integrated intensity information for each reflection was obtained by reduction of the data frames with the program APEX3. The integration method employed a three dimensional profiling algorithm and all data were corrected for Lorentz and polarization factors, as well as for crystal decay effects. Finally, the data was merged and scaled

to produce a suitable data set. The absorption correction program SADABS was employed to correct the data for absorption effects. Systematic reflection conditions and statistical tests of the data suggested the space group *Pn*. A solution was obtained readily using XT/XS in APEX3. Hydrogen atoms were placed in idealized positions and were set riding on the respective parent atoms. All non-hydrogen atoms were refined with anisotropic thermal parameters. O3 shows elongated ellipsoid suggesting possible disorder. Our efforts to model the $-\text{[O-C(=O)-Re]}$ as disordered $-\text{[O-C(=O)-Re]}$ and $-\text{[O-C(=O) Re]}$ did not improve the results. Other possible models to disorder O3 did not yield any meaningful options. Absence of additional symmetry or void were confirmed using PLATON (ADDSYM). The structure was refined (weighted least squares refinement on F^2) to convergence. Olex2 was employed for the final data presentation and structure plots. (CSD Identifier/Number – QIHVUB/1826254)

X-ray Diffractometry Details for (PCP^{tBu})ReOI(CO₂) (404): A Leica MZ 75 microscope was used to identify a suitable green block with very well defined faces with dimensions (max, intermediate, and min) 0.152 x 0.034 x 0.025 mm³ from a representative sample of crystals of the same habit. The crystal mounted on a nylon loop was then placed in a cold nitrogen stream (Oxford) maintained at 100 K. A BRUKER Quest X-ray (fixed-Chi geometry) diffractometer was employed for crystal screening, unit cell determination, and data collection. The goniometer was controlled using the APEX3 software suite. The sample was optically centered with the aid of a video camera such that no translations were observed as the crystal was rotated through all positions. The detector was set at 3.4 cm from the crystal sample. The X-ray radiation employed was generated from a Mo- $\text{I}\mu\text{s}$ X-ray tube ($K_{\alpha} = 0.71073\text{\AA}$). 45 data frames were taken at widths of 1°. These reflections were used to determine the unit cell. The unit cell

was verified by examination of the $h k l$ overlays on several frames of data. No super-cell or erroneous reflections were observed. After careful examination of the unit cell, an extended data collection procedure (4 sets) was initiated using omega scans. Integrated intensity information for each reflection was obtained by reduction of the data frames with the program APEX3. The integration method employed a three dimensional profiling algorithm and all data were corrected for Lorentz and polarization factors, as well as for crystal decay effects. Finally, the data was merged and scaled to produce a suitable data set. The absorption correction program SADABS was employed to correct the data for absorption effects. Systematic reflection conditions and statistical tests of the data suggested the space group $P2_12_12_1$. A solution was obtained readily using XT/XS in APEX3. Hydrogen atoms were placed in idealized positions and were set riding on the respective parent atoms. All non-hydrogen atoms were refined with anisotropic thermal parameters. Absence of additional symmetry and voids were confirmed using PLATON (ADDSYM). The structure was refined (weighted least squares refinement on F^2) to convergence. Olex2 was employed for the final data representation and structure plots. (CSD Identifier/Number – QIHWAI/1826255)

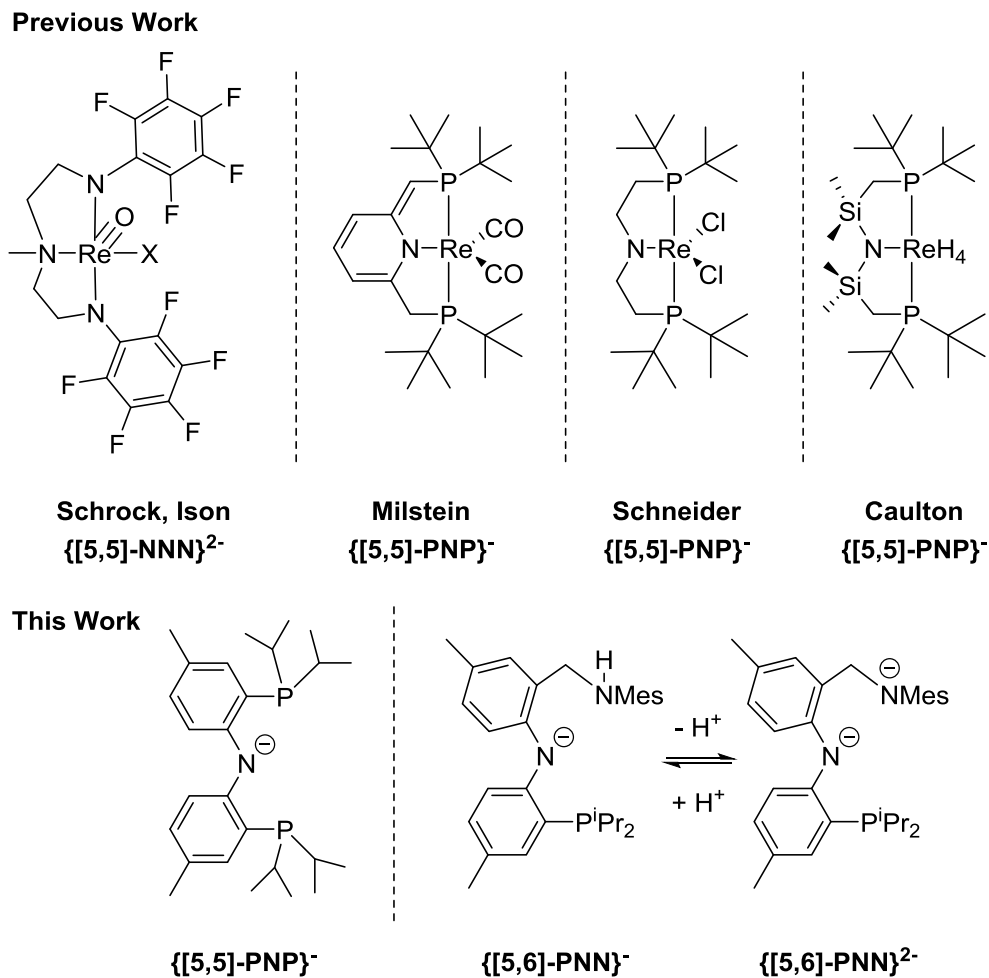
CHAPTER V

N-H CLEAVAGE AS A ROUTE TO NEW PINCER COMPLEXES OF HIGH-VALENT RHENIUM[§]

5.1 Introduction

Pincer ligands are tridentate and tend to coordinate to transition metals in meridional fashion, engendering significant thermal stability and geometric rigidity. As a result of these attractive features, they have been utilized in the study of multiple, challenging reactions of both catalytic and stoichiometric interest. We became interested in the chemistry of high-valent rhenium supported by pincers, and recently reported a Re system accessed via C-H activation at Re(V) of a pincer ligand that can be referred to as a {[5,5]-PCP}⁻ using the Fryzuk notation.⁷⁴ Given the wide variety of available tridentate ligands, Fryzuk's notation can be used to conveniently describe pincer frameworks based on the size of the two chelate rings, the donor atoms involved, as well as the overall charge (as used in Scheme 1). Much of the previous chemistry done with pincer-supported Re(V) has involved either neutral, mono-, or dianionic pincers with nitrogenous donors (Scheme V-1 *top*).¹³⁵

[§] Adapted from “N-H Cleavage as a Route to New Pincer Complexes of High-Valent Rhenium” Kosanovich, A. J.; Shih, W. -C.; Ramirez-Contreras, R.; Ozerov, O. V. *Dalton Trans.* **2016**, 45, 18532-18540 with permission from The Royal Society of Chemistry, Copyright 2016. DOI: 10.1039/C5DT03640F



Scheme V-1. (top) Examples of pincer-supported rhenium with central amido-, amino-, or pyridyl-type donors (bottom) ligands utilized in this study. Reprinted with permission from The Royal Society of Chemistry, Copyright 2016

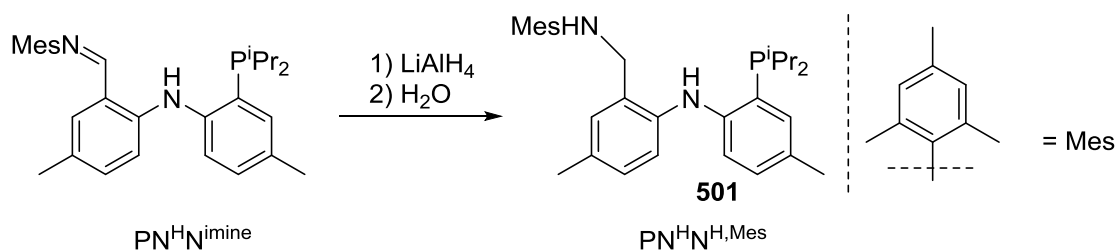
The Caulton group explored reactivity of Re in C-H activation and formation of metal-carbon multiple bonds using the Fryzuk-type amido/bis(phosphine) PNP ligand.⁸¹ Schneider and co-workers reported dinitrogen splitting in a Re system supported with a dialkylamido/bis(phosphine) PNP ligand. Milstein et al. explored reversible activation of unsaturated organic molecules by low-valent Re complexes supported by a dearomatized pyridine/bis(phosphine) PNP ligand.⁶³ The work of the Ison group examined¹³⁶ the

insertion reactivity of CO using a dianionic amine/bis(amido) NNN pincer first introduced into Re chemistry by Schrock.¹³⁷ Re complexes of {[5,5]-NNO}⁻, of {(5,6)-PNN}⁻, and of {(6,6)-NNN}⁻ pincers have also been reported.¹³⁸⁻¹⁴⁰ Most of these examples include Re-oxo complexes in the +5 oxidation state where a low-spin d² configuration is ensured in part by the strong triple bond between Re and oxygen engaging the two formally vacant d_π orbitals. Looking to expand upon the chemistry of pincer-supported, high-valent rhenium, we targeted a pincer framework with access to variable modes of protonation. To this end, we report the synthesis of Re(V) oxo complexes of {5,6-(PNN)}⁻²⁻ ligands (Scheme V-1 *bottom*). For comparison, we also report a complex of the {5,5-(PNP)}⁻ ligand.

5.2 Results and Discussion

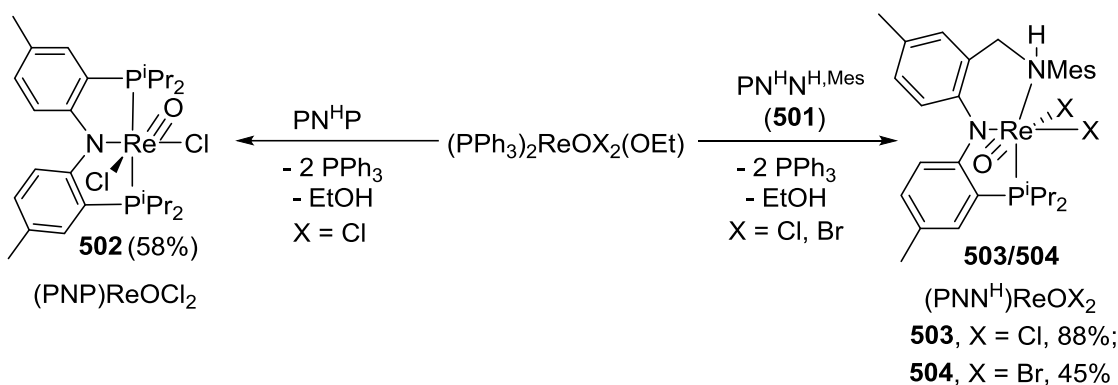
5.2.1 Synthesis and Metalation of Diarylamido Ligands

Imine reduction of PN^HN^{imine} with LiAlH₄ produced the PN^HN^H proligand, **501**, as a free-flowing white powder in 65% yield upon workup (Scheme V-2). **501** gave rise to a single resonance by ³¹P{¹H} NMR spectroscopy (δ -14.5 ppm) and to C_s-symmetric ¹H and ¹³C{¹H} NMR spectra in solution at ambient temperature.



Scheme V-2. Synthesis of PNN^H proligand **501**. Reprinted with permission from The Royal Society of Chemistry, Copyright 2016

It was envisaged that a Re(V) alkoxide might serve as a convenient precursor for metalation of an N-H containing pincer ligand *via* aminolysis of the Re-OR bond. Gratifyingly, treatment of **501** with $(\text{PPh}_3)_2\text{ReOX}_2(\text{OEt})$ ($\text{X} = \text{Cl}, \text{Br}$)¹⁴¹ in toluene for 12 h led to quantitative expulsion of free PPh_3 and EtOH (^1H and $^{31}\text{P}\{^1\text{H}\}$ NMR evidence observed in toluene- d_8) with clean formation of the metallated products, $(\text{PNN}^{\text{H}})\text{ReOX}_2$ isolated in moderate to excellent yields (**503**, $\text{X} = \text{Cl}$, 88%; **504**, $\text{X} = \text{Br}$, 45%) (Scheme V-3 *right*). In a similar fashion, $(\text{PNP})\text{ReOCl}_2$ (**502**) was synthesized and isolated in 58% yield via reaction of $\text{PN}^{\text{H}}\text{P}$ with $(\text{PPh}_3)_2\text{ReOCl}_2(\text{OEt})$ in toluene, albeit at 110 °C. (Scheme V-3 *left*).



Scheme V-3 Synthesis of PNP and PNN complexes of rhenium. Reprinted with permission from The Royal Society of Chemistry, Copyright 2016

5.2.2 Structural and Spectroscopic Study of PNP and PNN Complexes

X-ray diffractometry studies on dark green, single crystals established the molecular structures of $(\text{PNP})\text{ReOCl}_2$ (**502**) and $(\text{PNN}^{\text{H}})\text{ReOCl}_2$ (**503**) in the solid state (Figures V-1 and V-2). Both structures feature *cis*-chlorides, meridionally disposed pincer ligands, and

short Re-O distances consistent with triply bonded, terminal Re-oxo moieties. IR spectroscopy corroborated the presence of Re-oxo moieties in **502** ($\nu_{\text{Re}=\text{O}} = 940 \text{ cm}^{-1}$) and **503** ($\nu_{\text{Re}=\text{O}} = 963 \text{ cm}^{-1}$) and **504** ($\nu_{\text{Re}=\text{O}} = 962 \text{ cm}^{-1}$). The Re-N1_{amido} distances in both structures are comparable, while the Re-N2 distance in the structure of (PNN^H)ReOCl₂ (**503**) is over 0.2 Å longer. Together with the pyramidalization at N2, these indicate a neutral amine bound to Re. This notion is supported by the observation of the N-H stretch by IR spectroscopy in **503** (3214 cm⁻¹) and **504** (3189 cm⁻¹). The X-ray structure solution for (PNP)ReOCl₂ (**502**) contains a crystallographic two-fold axis of symmetry, however, this is owing to disorder along the O1/Re1/Cl1 axis. Each individual molecule of **502**, as well as of **503** is C₁-symmetric in the solid state.

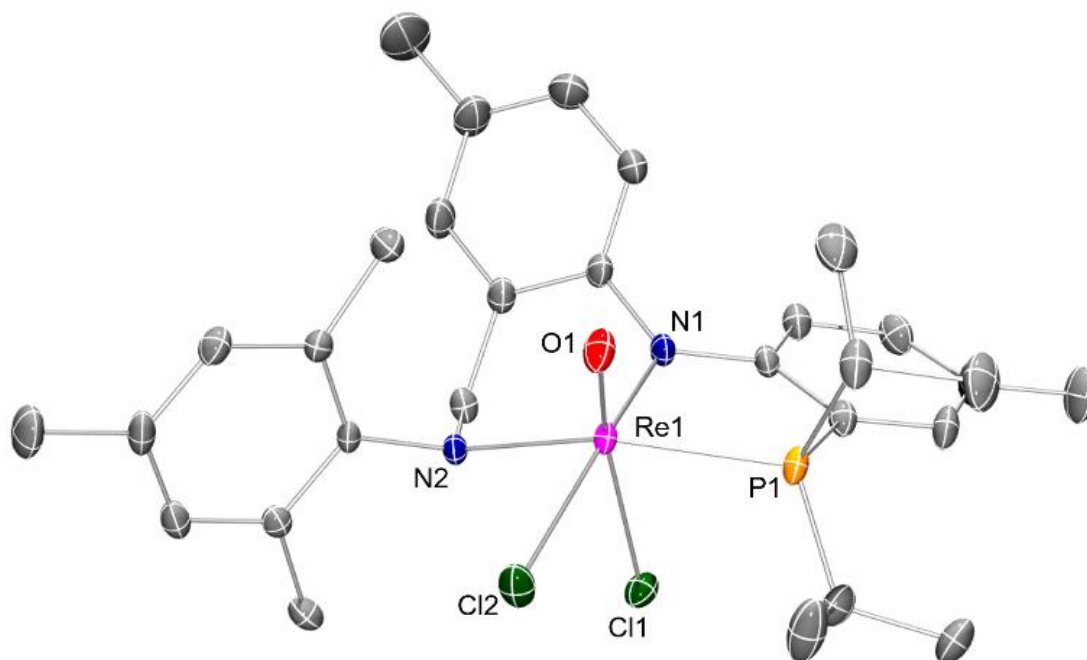


Figure V-1. ORTEP drawing (50% probability ellipsoids) of (PNN^H)ReOCl₂ (**503**). H atoms are omitted for clarity. Selected distance (Å) and angles (deg): Re1-N1, 1.984(2); Re1-N2, 2.2126(2); Re1-O1, 1.684(2); P1-Re1-N2, 155.62(6). Reprinted with permission from The Royal Society of Chemistry, Copyright 2016

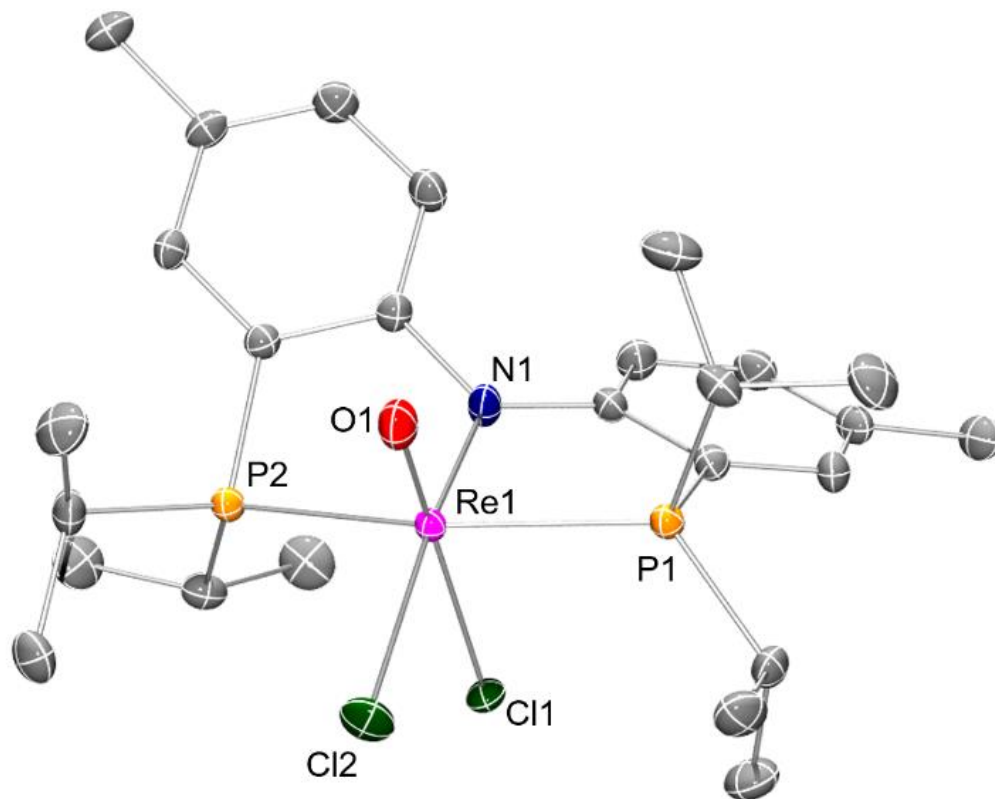
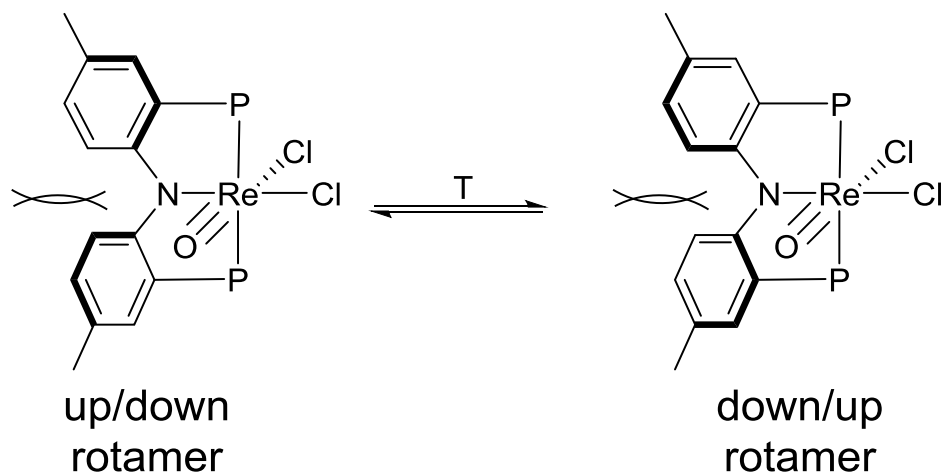


Figure V-2. ORTEP drawing (50% probability ellipsoids) of (PNP)ReOCl₂ (**502**). O1/Re1/Cl1 disorder and H atoms are omitted for clarity. Selected distance (Å) and angles (deg): Re1-N1, 2.028(4); Re1-O1, 1.67(2); P1-Re1-P2, 155.79(3). Reprinted with permission from The Royal Society of Chemistry, Copyright 2016

Ambient temperature ³¹P{¹H} NMR spectra of (PNP)ReOCl₂ (**502**) feature two broad resonances at δ 34.1 (br d, ²J_{P-P} = 174 Hz) and 27.2 ppm (br d, ²J_{P-P} = 174 Hz), consistent with the inequivalent phosphorus environments indicated by the X-ray structure.¹⁴² A ³¹P{¹H} NMR spectrum collected at 80 °C revealed coalescence to a single resonance. These observations are consistent with rapid interconversion of two degenerate C₁-symmetric structures, resulting in time-averaged C_s symmetry at 80 °C.¹⁴³ We propose that the nature of the interconversion lies in the “flipping” of the two aromatic rings of the diarylamido backbone past each other (Scheme V-4). We have previously described such

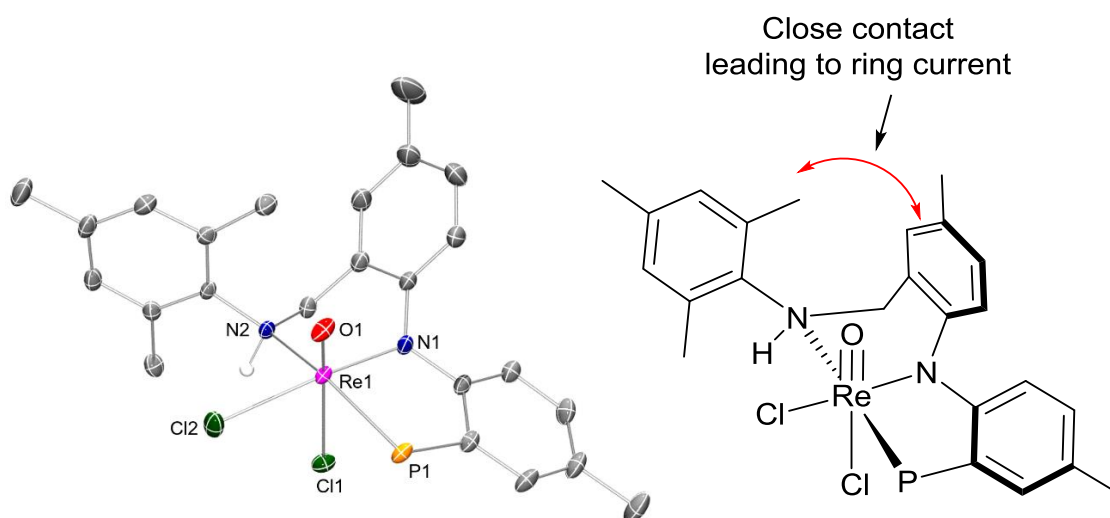
“flipping” being slow on the NMR time scale for certain complexes of the diarylamido-based $\text{PNN}^{\text{imine}}$ pincer.¹⁴⁴ In PNP complexes, this “flipping” is typically fast, although $(\text{PNP})\text{AlCl}_2$ displayed lowered symmetry presumably for this reason.¹⁴⁵



Scheme V-4. Two different rotamers/enantiomers possible for $(\text{PNP})\text{ReOCl}_2$ (**502**). Reprinted with permission from The Royal Society of Chemistry, Copyright 2016

The two interconverting rotamers in $(\text{PNP})\text{ReOCl}_2$ (**502**) are enantiomers, i.e., species of degenerate energy that give rise to identical NMR spectra. Similar rotamerism in $(\text{PNN}^{\text{H}})\text{ReOCl}_2$ (**503**) would give rise to diastereomers distinguishable by NMR spectroscopy. The molecule of **503** possesses chiral centers at N2 and at Re itself, with multiple theoretically possible diastereomers. Yet, only one diastereomer¹⁴⁶ of C_1 -symmetry is observed by NMR spectroscopy, with a specific feature in accord with the solid-state structure. One of the singlet methyl ^1H NMR resonances is shifted considerably upfield (**503**, δ 1.27 ppm; **504**, δ 1.23 ppm). We ascribe this to one of the *ortho*-methyl

groups of the mesityl ring being affected by the ring current of one of the other aromatic rings, based on the positioning of an *ortho*-methyl directly above an aromatic ring in the solid-state structure of **503** (Scheme V-5). Observation of separate *ortho*-methyl resonances by NMR spectroscopy also indicates that rotation about the N-C_{Mes} bond is slow on the NMR time scale.

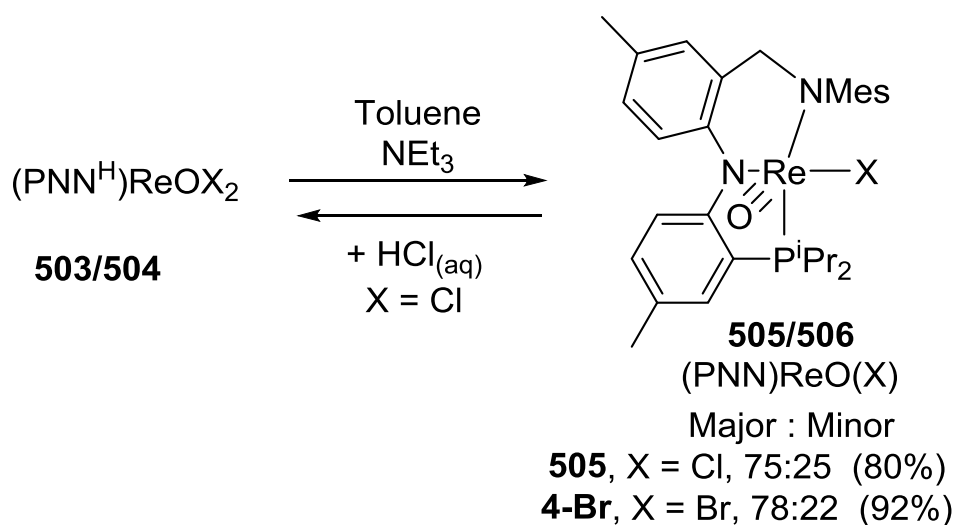


Scheme V-5. Alternate view of (PNN^H)ReOCl₂ (**503**) and representative schematic of observed proximity of benzylic methyl protons with PNN^H ligand's aromatic backbone, leading to ring current effects. Reprinted with permission from The Royal Society of Chemistry, Copyright 2016

5.2.3 Dehydrohalogenation of (PNN^H)ReOX₂ Complexes

Reaction of (PNN^H)ReOX₂ with triethylamine in toluene at 70 °C for 10 min led to precipitation of [HNEt₃][X] and quantitative conversion to (PNN)ReOX (**505/506**) (¹H and ³¹P{¹H} NMR evidence), isolated as dark green powders (Scheme V-6). These materials consist of a mixture of C₁-symmetric diastereomers in a roughly 3:1 ratio, as evidenced by solution NMR studies. IR spectra confirm the terminal rhenium-oxo (**505**, X = Cl, 962,

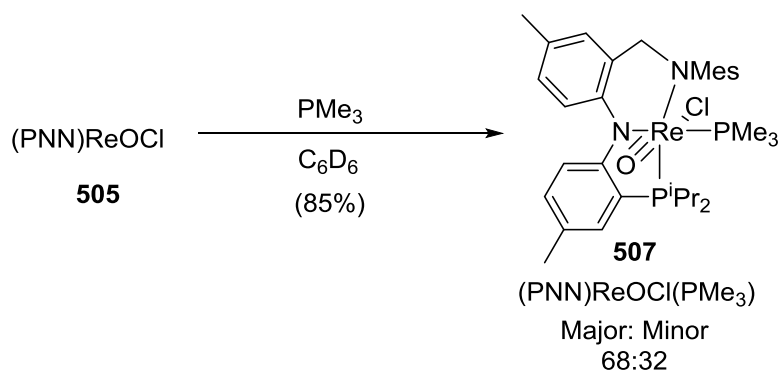
970 cm^{-1} ; **506**, X = Br, 968 cm^{-1}) and show no N-H stretching modes. All PNN-supported chloride and bromide complexes were determined to be air-stable. Dehydrohalogenation of $(\text{PNN}^{\text{H}})\text{ReOCl}_2$ (**503**) was reversed by treatment of a sample of $(\text{PNN})\text{ReOCl}$ (**505**) in C_6D_6 with concentrated $\text{HCl}_{(\text{aq})}$ (Scheme V-6).



Scheme V-6. Reversible deprotonation of $(\text{PNN}^{\text{H}})\text{ReOX}_2$ (**503/504**) to give $(\text{PNN})\text{ReOX}$ (**505/506**). Reprinted with permission from The Royal Society of Chemistry, Copyright 2016

5.2.4 Reaction with Trimethylphosphine

Illustrating the unsaturated nature of $(\text{PNN})\text{ReOCl}$ (**505**), addition of PMe_3 in C_6D_6 led to a color change from dark green to purple, as C_1 -symmetric $(\text{PNN})\text{ReOCl}(\text{PMe}_3)$ (**507**) was formed in a 68:32 isomeric ratio (Scheme V-7). **507** was isolated in 85% yield as a dark purple powder. Two rhenium-oxo stretches were evident in its IR spectrum (957 and 945 cm^{-1}).

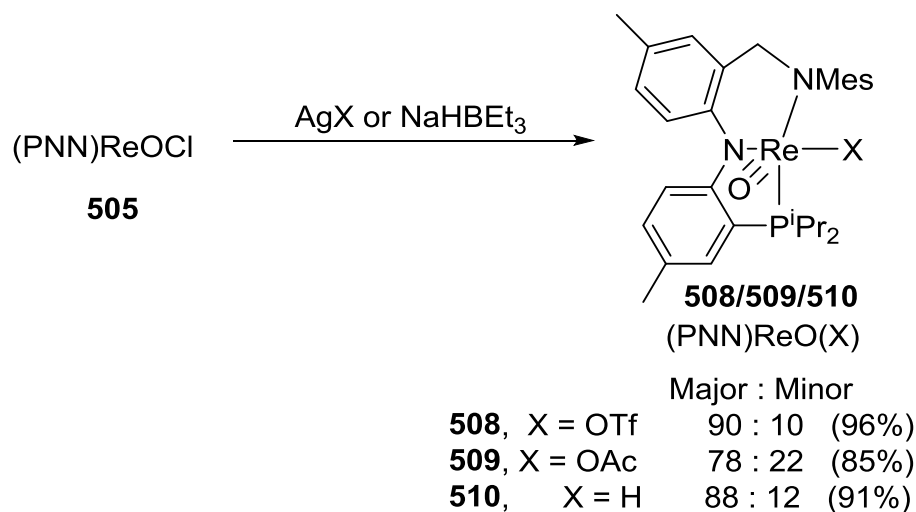


Scheme V-7. Reaction of $(\text{PNN})\text{ReOCl}$ (**505**) with PMe_3 to form $(\text{PNN})\text{ReOCl}(\text{PMe}_3)$ (**507**) in isomeric ratios. One possible isomer is shown. Reprinted with permission from The Royal Society of Chemistry, Copyright 2016

Each isomer displays two resonances in its $^{31}\text{P}\{^1\text{H}\}$ NMR spectrum (major: δ 4.4 (PNN) and -50.2 (PMe_3) ppm; minor: δ 0.3 (PNN) and -49.2 (PMe_3) ppm). The lack of perceptible P-P coupling points to *cis*-disposition of the two phosphorus donors in both isomers. We cannot be certain of which ligand is *trans* to the oxo in **507**, but favour it being the chloride for thermodynamic reasons as the weakest *trans*-influence ligand in the molecule. The close similarity of the ^{31}P NMR chemical shifts for the PMe_3 group suggests that PMe_3 is *trans* to the same donor atom in both isomers and thus the isomerism is not due to changes in the mutual disposition of ligands about Re.

5.2.5 Chloride Metathesis Reactivity of (PNN)ReOCl

Treatment of (PNN)ReOCl (**505**) with AgOTf, AgOAc, or NaHBEt₃ allowed isolation of the respective (PNN)ReOX chloride metathesis products (X = OTf, OAc, H) in excellent yield upon workup (Scheme V-8).



Scheme V-8. Chloride metathesis reactions with (PNN)ReOCl (**505**). Reprinted with permission from The Royal Society of Chemistry, Copyright 2016

Each of these new products was isolated as a mixture of two diastereomers distinct by NMR spectroscopy. In each case, two singlets were present in the ³¹P{¹H} spectrum and two different resonances were detected for the corresponding X groups: two different ¹⁹F NMR resonances for (PNN)ReO(OTf) (**508**) (δ -73.1 and -73.6 ppm), two different ¹H NMR singlets for the acetate groups in (PNN)ReO(OAc) (**509**) (δ 2.84 and 1.53 ppm), and two different doublets for the hydrides in (PNN)ReO(H) (**510**) (δ 8.22, ²J_{P-H} = 17.4 Hz, and

δ 3.94, $^2J_{\text{P-H}} = 14.5$ Hz). The downfield chemical shift of these Re hydrides is unusual, but appears to be typical for hydrides *cis* to a triply bound oxo ligand.¹⁴⁷ Re(V) oxo/hydride complexes have been implicated in schemes of catalytic reduction.¹⁴⁸ Additional support for these formulations comes from IR spectroscopy where bands corresponding to the various element-oxygen stretches were observed for each compound, a band corresponding to triflate (1154 cm^{-1}) in (PNN)ReO(OTf) (**508**), and a band corresponding to acetate (1653 cm^{-1}) in (PNN)ReO(OAc) (**509**). Separate bands for each isomer could not be observed presumably because of close overlap.

5.2.6 Structural and Isomerism Analysis

We were able to obtain single crystals of (PNN)ReOCl (**505**) (dark-green) and (PNN)ReO(OTf) (**508**) (dark-red) that were suitable for an X-ray diffraction study. Both structures feature short $\text{Re}\equiv\text{O}$ bonds. All the Re-N distances in the two structures fall into the ca. 1.95-2.00 Å range, consistent with two amide donors on Re. The mutual disposition of donor atoms (accounting for the Cl/OTf change) is approximately the same in both structures. The resulting five-coordinate environment about Re cannot be accurately described by idealized square pyramidal or trigonal bipyramidal geometries (the τ parameter¹⁴⁹ is 0.33 for (PNN)ReOCl (**505**) and 0.66 for (PNN)ReO(OTf) (**508**). The triflate O of **508** is at a ca. 90° angle to the Re-oxo bond, but all other donor atoms in both molecules bend away from the oxo to a greater degree (Element-Re-O angles of ca. 103-130°). The largest of these are the angles between the Re-oxo and the Re-N(Mes) bonds (ca. 131° in **508** and ca. 117° in **505**). Such bending away of a π -donating amido ligand may be reflective of maximizing π -donation to the otherwise unsaturated Re center. An analogy could be drawn to the Y-shaped distortions in five-coordinate complexes of d^6

metal centers.¹⁵⁰ Although Re here is d^2 , the formally empty d_π orbitals are effectively unavailable because of strong π -bonding in the $\text{Re}\equiv\text{O}$ fragment.

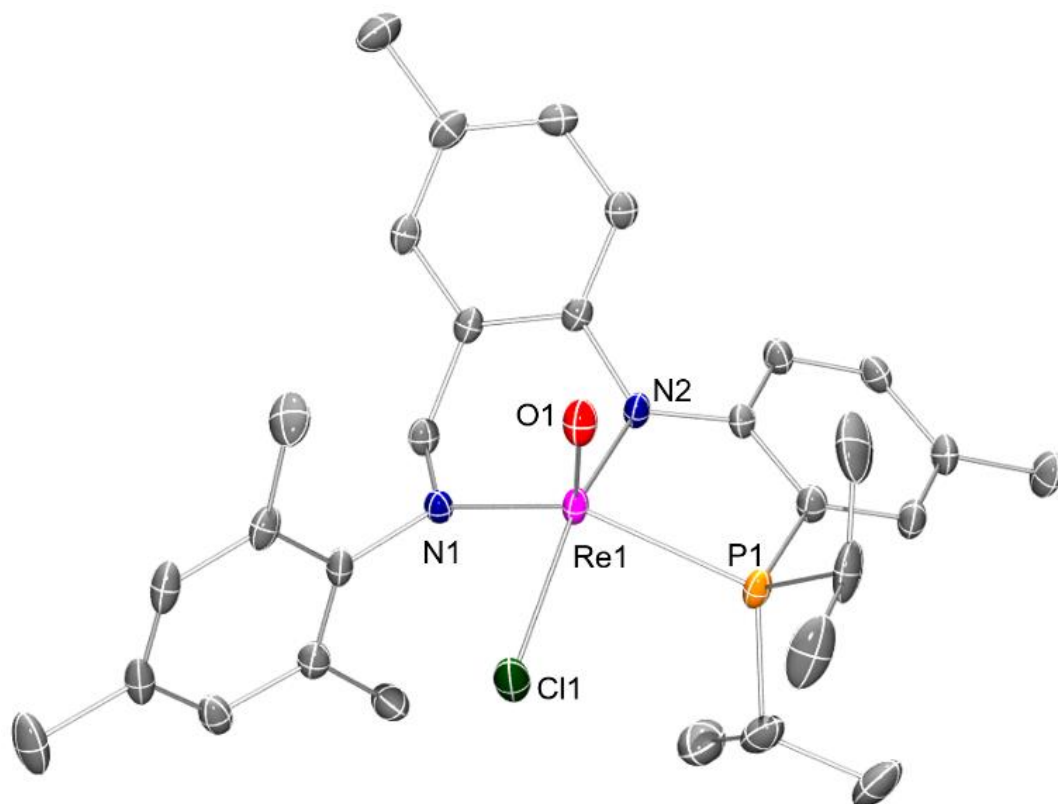


Figure V-3. ORTEP drawing (50% probability ellipsoids) of $(\text{PNN})\text{ReOCl}$ (**505**). H atoms are omitted for clarity. Selected distance (\AA) and angles (deg): Re1-N1, 1.955(3); Re1-N2, 1.997(4); Re1-O1, 1.684(3); P1-Re1-N2, 80.3(1); N1-Re1-N2, 87.1(1); O1-Re1-N1, 117.1(1); O1-Re1-N2, 103.4(1); P1-Re1-O1, 106.6(1); P1-Re1-N1, 136.2(1); Cl1-Re1-N2, 154.1(1). Reprinted with permission from The Royal Society of Chemistry, Copyright 2016

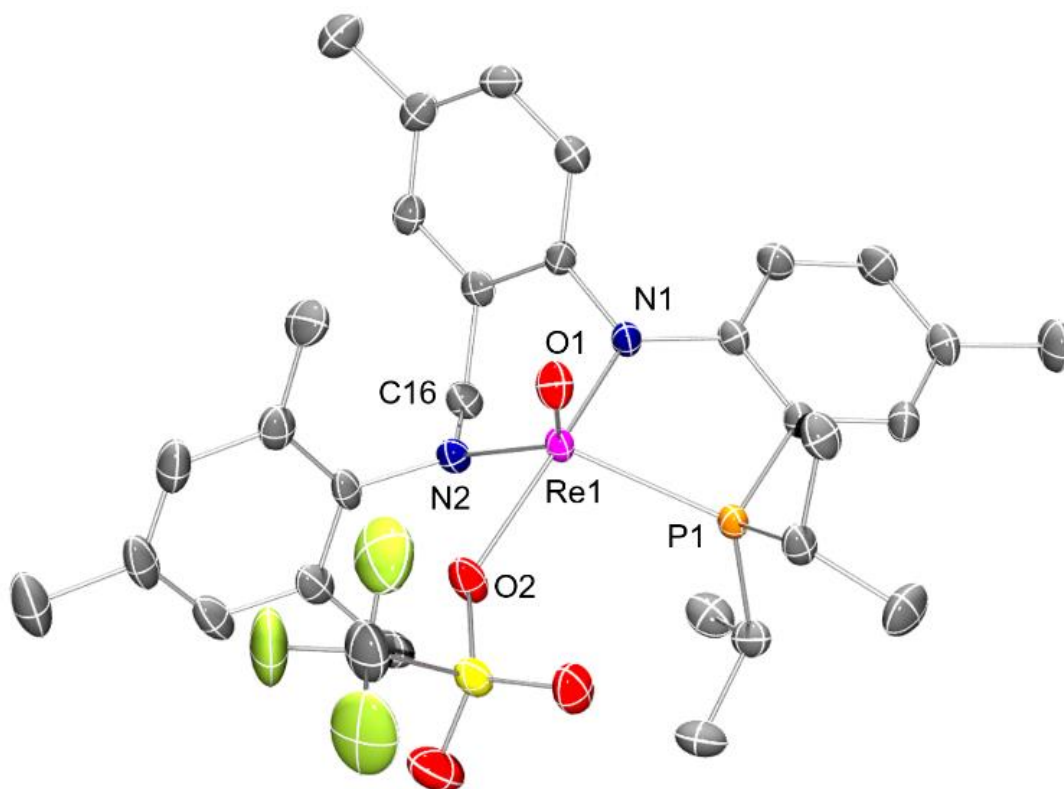
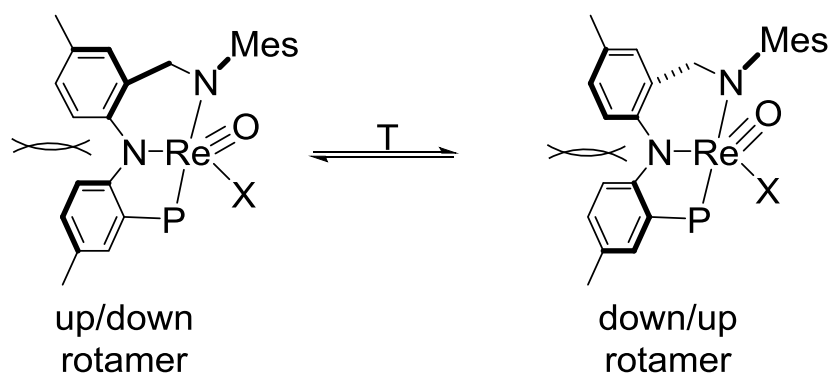


Figure V-4. ORTEP drawing (50% probability ellipsoids) of (PNN)ReO(OTf) (**508**). H atoms are omitted, and mirror image of original structure is shown for clarity and ease of comparison. Selected distance (Å) and angles (deg): Re1-N1, 1.958(3); Re1-N2, 1.949(3); Re1-O1, 1.698(3); P1-Re1-N2, 123.73(8); P1-Re1-O1, 105.68(9); O1-Re1-N2, 130.6(1); N1-Re1-O2, 164.5(1); P1-Re1-N1, 80.89(8); N1-Re1-N2, 86.70(1); Re1-N2-C16, 122.0(2). Reprinted with permission from The Royal Society of Chemistry, Copyright 2016

505 and **508** possess analogous PNN conformations with regard to the discussion of rotamers in (PNN^H)ReOCl₂ (**503**) (*vide supra*). The aromatic ring attached to P is approximately coplanar with the P1-Re1-N2 plane, while the other ring of the diarylamido backbone is tilted towards the oxo ligand. This conformation is also analogous to that observed in **503**. As in the latter, one of the *ortho*-methyl groups of the mesityl is positioned over one of the diarylamido rings, although that positioning is more pronounced in **508**. This is consistent with the NMR observations for the pairs of isomers of (PNN)ReOX (X = Cl, OTf, OAc, H), as well as of (PNN)ReOCl(PMe₃) (**507**) – in each case, one of the

isomers displays an anomalously upfield shifted (to δ 1.1-1.5 ppm) ^1H NMR resonance for a benzylic methyl group. Thus, we propose that the observed pairs of isomers correspond to the two rotameric diastereomers (Scheme V-9) arising from slow “flipping” of the rings of the diarylamido backbone and that the isomers displaying upfield shifted benzylic methyl resonances correspond to the conformation observed in the solid-state structures of **505** and **508**.



Scheme V-9. Representation of different possible rotameric diastereomers envisioned for the PNN-type framework. Reprinted with permission from The Royal Society of Chemistry, Copyright 2016

Interestingly, these isomers are the minor isomers for all (PNN)Re(O)(X) except X = OAc. Unfortunately, all of our attempts to obtain an X-ray quality crystal of the other type of isomer have been unsuccessful.

We have considered diastereomerism arising from different arrangements of donor atoms about Re. However, given the very strong *trans*-influence of the oxo ligand disfavoring the positioning of a ligand strictly *trans* to it in five-coordinate structures and the inherent constraints of the PNN ligand, that seems unlikely.

5.3 Conclusion

In conclusion, we have presented a series of new synthetic methods for the metalation of a PNP and PNN-type pincer ligand via N-H aminolysis of a rhenium-alkoxide bond. The newly synthesized PNN ligand allows for variable modes of reversible protonation, and the formation and stabilization of unsaturated, high-valent Re(V). Complexes of the dianionic PNN ligand exist as pairs of diastereomers which are thought to arise from the restricted motion of the diarylamido backbone. Solid-state structural studies support this notion. Future studies should focus on the reversible protonation of the amido sites and its potential role in new reactivity which may feature significant potential for metal-ligand cooperativity.

5.4 Experimental

5.4.1 General Considerations

Unless otherwise stated, all experiments were carried out using standard glovebox and Schlenk line techniques under a dry argon atmosphere. Triethylamine and C₆D₆ were dried over NaK, benzophenone, and 18-crown-6, distilled, and stored over molecular sieves in an argon glovebox prior to usage. Diethyl ether, pentane, toluene, and tetrahydrofuran (THF) were dried and deoxygenated using a PureSolv MD-5 solvent purification system and were stored over molecular sieves in an argon-filled glovebox. All other deuterated solvents were degassed and stored over molecular sieves in an argon-filled glovebox. PN^HP, PN^HN^{imine}, (PPh₃)₂ReOCl₂(OEt) and (PPh₃)₂ReOBr₂(OEt)¹⁰⁸ were synthesized using reported literature procedures. All other chemical reagents were purchased from

commercial suppliers and were used as received. NMR spectra were recorded on a Varian iNova 500 ($^{31}\text{P}\{^1\text{H}\}$ NMR, 202.276 MHz; $^{13}\text{C}\{^1\text{H}\}$ NMR, 125.670 MHz; ^{19}F NMR, 470.385 MHz, ^1H NMR, 499.678 MHz) spectrometer in given solvents. Chemical shifts are reported in ppm (δ). $^{31}\text{P}\{^1\text{H}\}$ NMR spectra were referenced externally to an 85% phosphoric acid standard at δ 0 ppm. ^{19}F NMR spectra were referenced externally to 1,2-difluorobenzene at δ -139 ppm. $^{13}\text{C}\{^1\text{H}\}$ and ^1H NMR spectra were internally referenced to residual solvent resonances. In reporting spectral data, the following abbreviations were utilized: s = singlet; d = doublet; t = triplet; dd = doublet of doublets; m = multiplet; br = broad. Infrared spectra were collected on a Nicolet Nexus 470 FT-IR E.S.P. spectrometer using KBr plates and Nujol oil. Elemental analyses were performed by CALI, Inc. (Parsippany, NJ, USA).

SAFETY NOTE: *Although the following procedure for LiAlH_4 reduction was quenched in open air, and no incidents occurred in our hands, on larger scales, an inert atmosphere quenching and workup is highly recommended. Screened reaction conditions with THF as solvent and excess (≥ 2 equiv.) of LiAlH_4 led only to partial reduction of the imine moiety. Therefore, it was found that thermolysis in toluene was necessary for this transformation to proceed efficiently.*

5.4.2 Synthesis and Characterization of PNP and PNN Complexes

$\text{PN}^{\text{H}}\text{N}^{\text{H}}$ (501) $\text{PN}^{\text{H}}\text{N}^{\text{imine}}$ (0.2 g, 0.436 mol), lithium aluminum hydride (0.017 g, 0.436 mol) and 10 mL of dry toluene were charged in a 50 mL Teflon taped culture tube equipped with a PTFE-coated stir bar. The sealed culture tube was placed in an oil bath and heated overnight to 120 °C with vigorous stirring. Within 1 h the yellow color of the suspension had turned into an intense neon orange color. The next morning it was observed

that the suspension had turned white. The cap was removed and reaction was quenched with 1 mL of a 1.74 M solution of water in THF. The resulting suspension was filtered through a short path of silica gel and the filtrate dried in vacuo to obtain a white solid. The product was dissolved in the minimum amount of hexanes and the solution placed overnight in a freezer set to $-30\text{ }^{\circ}\text{C}$ to obtain a white, crystalline solid that was pure by NMR. Yield: 130.5 mg (65%) ^1H NMR (500 MHz, C_6D_6) δ 0.97 (dd, 6H, $^3\text{J}_{\text{P-H}} = 11.6\text{ Hz}$, $^3\text{J}_{\text{H-H}} = 6.9\text{ Hz}$), 1.06 (dd, 6H, $^3\text{J}_{\text{P-H}} = 15.3\text{ Hz}$, $^3\text{J}_{\text{P-H}} = 7.0\text{ Hz}$), 1.95 (hd, 2H, $^3\text{J}_{\text{P-H}} = 7.0\text{ Hz}$, $^3\text{J}_{\text{P-H}} = 1.8\text{ Hz}$), 2.14 (s, 3H), 2.15 (s, 3H), 2.20 (s, 3H), 2.24 (s, 6H), 3.07 (t, 1H, $^3\text{J}_{\text{H-H}} = 6.7\text{ Hz}$, benzylic NH), 4.06 (d, 2H, $^3\text{J}_{\text{H-H}} = 6.7\text{ Hz}$), 6.76 (s, 2H), 6.92 (ddd, 2H, $J = 6.9, 6.1, 1.8\text{ Hz}$), 7.05 (d, 1H, $J = 1.5\text{ Hz}$), 7.19 (t, 1H, $J = 2.3\text{ Hz}$), 7.28 (dd, 1H, $J = 8.3, 4.7\text{ Hz}$), 7.38 (d, 1H, $J = 8.1$), 8.16 (d, 1H, $J = 9.5\text{ Hz}$, aromatic NH). $^{13}\text{C}\{^1\text{H}\}$ NMR (126 MHz, C_6D_6) δ 148.51, 148.35, 144.09, 141.85, 133.69, 131.95, 131.47, 131.00, 130.86, 130.51, 129.91, 129.32, 128.90, 128.06, 122.55, 122.42, 118.94, 118.38, 51.81, 23.32, 20.97, 20.85, 20.82, 20.46, 20.31, 19.06, 18.99. $^{31}\text{P}\{^1\text{H}\}$ NMR (202 MHz, C_6D_6) δ -14.5 . Elem. Anal. Found (Calc): C: 78.21 (78.22); H: 8.98 (8.97)

(PNP)ReOCl₂ (502): To a Teflon taped culture tube equipped with a magnetic stir bar was added $(\text{PPh}_3)_2\text{ReOCl}_2(\text{OEt})$ (1.56 g, 1.85 mmol), $\text{PN}^{\text{H}}\text{P}$ (885 mg, 2.06 mmol), and 10 mL of toluene resulting in a tan suspension. After ten minutes at room temperature, the mixture took on a dark purple color and became homogeneous. The solution was then stirred in an oil bath at $110\text{ }^{\circ}\text{C}$ for 12 h over which time the solution became dark green and solids were noted to precipitate. Cooling of the solution to room temperature resulted in the precipitation of dark solids that were collected by filtration, washed with diethyl ether (10 mL) and dried *in vacuo* to provide the product as an analytically pure, dark, semicrystalline

powder. Yield: 750 mg (58%). Single crystals suitable for X-ray diffraction were grown over 72 h from slow evaporation of a concentrated CDCl_3 solution at room temperature. ^1H NMR (500 MHz, CDCl_3 , 22 °C): δ 1.09 (br, 6H), 1.64 (br, 18H), 2.49 (s, 6H), 3.20 (br, 2H), 7.19 (br, 4H), 7.34 (br, 2H). ^1H NMR (500 MHz, toluene- d_8 , 80 °C): δ 0.93 (dvt, $J = 14.6$, 7.2 Hz, 6H), 1.47 (m, 12H), 1.60 (dvt, $J = 8.0$ Hz, 6H), 2.27 (s, 6H), 2.44 (m, 2H), 3.10 (m, 2H), 6.82 (d, $J = 8.4$ Hz, 2H), 7.16 (br s, 2H), 7.22 (d, $J = 8.4$ Hz, 2H). $^{13}\text{C}\{^1\text{H}\}$ NMR (126 MHz, CDCl_3 , 22 °C): δ 18.4 (br), 19.0 (br), 20.2, 27.6 (br), 117.9 (br), 130.9, 131.4, 133.4 (d, $J_{\text{P-C}} = 5.9$ Hz), 165.1. $^{31}\text{P}\{^1\text{H}\}$ NMR (202 MHz, CDCl_3 , 22 °C) δ 34.1 (br d, $^2J_{\text{P-P}} = 174$ Hz), 27.2 (br d, $^2J_{\text{P-P}} = 174$ Hz). $^{31}\text{P}\{^1\text{H}\}$ NMR (202 MHz, toluene- d_8 , 80 °C): δ 33.4 (br s). IR(KBr) = 940 cm^{-1} . Elem. Anal Found (Calc): C: 44.59 (44.51); H: 5.63 (5.75).

(PNN^H)ReOCl₂ (503) To a 20 mL scintillation vial equipped with magnetic stir bar was added $(\text{PPh}_3)_2\text{ReOCl}_2(\text{OEt})$ (1.06 g, 1.26 mmol), $\text{PN}^{\text{H}}\text{N}^{\text{H}}$ (**501**) (0.58 g, 1.26 mmol), and 3 mL toluene. The resultant suspension was stirred for 12 h, layered with ca. 15 mL pentane, and placed in a freezer at -35 °C. After 4 h, a dark precipitate had formed and was isolated on a fine frit, washed with 10 mL of a 2:1 pentane: Et_2O mixture, then again with 5 mL pentane, and dried under reduced pressure to provide the product as a dark brown powder. Yield: 0.81 g (88%). Single crystals suitable for X-ray diffraction were grown by slow evaporation of a concentrated toluene solution. ^1H NMR (500 MHz, CDCl_3): δ 1.10 (dd, $J = 15.4$, 6.9 Hz, 3H), 1.27 (s, 3H), 1.33 (dd, $J = 16.5$, 6.8 Hz, 3H), 1.80 (dd, $J = 18.2$, 7.4 Hz, 3H), 1.87 (dd, $J = 15.7$, 7.1 Hz, 3H), 2.25 (s, 3H), 2.41 (m, 1H), 2.45 (s, 3H), 2.46 (s, 3H), 2.64 (s, 3H), 3.26 (m, 1H), 3.98 (dd, $J = 12.4$ Hz, 2.9 Hz, 1H), 5.09 (dd, $J = 12.4$, 5.9 Hz, 1H), 6.70 (s, 1H), 6.78 (d, $J = 8.1$ Hz, 1H), 6.92 (m, 1H), 7.03 (m, 2H), 7.10 (d, J

= 8.5 Hz, 1H), 7.24 (dd, $J = 8.2, 1.9$ Hz, 1H), 7.50 (m, 1H), 8.29 (br d, $J = 5.9$ Hz, 1H). $^{13}\text{C}\{^1\text{H}\}$ NMR (126 MHz, CDCl_3) : δ 18.79, 19.58, 19.80, 19.99, 20.27, 20.33, 20.38, 20.64, 21.16, 29.83 (d, $J_{\text{P-C}} = 36$ Hz) 31.26 (d, $J_{\text{P-C}} = 25$ Hz), 56.96, 118.19, 122.66, 129.76, 130.03, 131.66, 131.83, 131.97, 132.47, 133.05, 133.55, 134.48, 136.59, 141.75, 154.36. $^{31}\text{P}\{^1\text{H}\}$ NMR (202 MHz, CDCl_3): δ 37.4 (s). IR (KBr): 963 ($\nu_{\text{Re=O}}$), 3214 ($\nu_{\text{N-H}}$) cm^{-1} . Elem. Anal. Found (Calc): C: 48.73 (49.18); H: 5.22 (5.50); N: 3.46 (3.82).

(PNN^H)ReOBr₂ (504) To a 20 mL scintillation vial equipped with magnetic stir bar was added $(\text{PPh}_3)_2\text{ReOBr}_2(\text{OEt})$ (364 mg, 0.391 mmol), $\text{PN}^{\text{H}}\text{N}^{\text{H}}$ (**501**) (181 mg, 0.394 mmol), and 3 mL toluene. The resultant suspension was stirred for 12 h, layered with ca. 15 mL pentane, and placed in a freezer at -35 °C. After 4 h, a dark precipitate had formed and was isolated on a fine frit, washed with 10 mL of a 2:1 pentane: Et_2O mixture, then again with 5 mL pentane, and dried under reduced pressure to provide the product as a dark brown powder. Yield: 145 mg (45%). ^1H NMR (500 MHz, CDCl_3): δ 1.08 (dd, $J = 15.5, 6.9$ Hz, 3H), 1.23 (s, 3H), 1.33 (dd, $J = 16.6, 6.8$ Hz, 3H), 1.91 (m 6H), 2.26 (s, 3H), 2.43 (m, 1H), 2.46 (s, 3H), 2.47 (s, 3H), 2.66 (s, 3H), 3.37 (m, 1H), 4.00 (dd, $J = 12.4, 2.8$ Hz, 1H), 5.21 (dd, $J = 12.4, 6.2$ Hz), 6.71 (s, 1H), 6.75 (d, $J = 8.1$ Hz, 1H), 6.90 (dd, $J = 8.5, 4.4$ Hz, 1H), 7.04 (d, $J = 1.0$ Hz, 2H), 7.11 (d, $J = 8.5$ Hz, 1H), 7.24 (d, $J = 1.7$ Hz, 1H), 7.55 (dd, $J = 8.7, 1.0$ Hz, 1H), 8.60 (d, $J = 5.9$ Hz). $^{13}\text{C}\{^1\text{H}\}$ NMR (126 MHz, CDCl_3) : δ 18.96, 19.67, 20.01, 20.39, 20.62, 20.66, 22.32, 31.36 (d, $J_{\text{P-C}} = 24.8$ Hz), 31.69 (d, $J_{\text{P-C}} = 36.5$ Hz), 56.99, 115.39, 118.43, 122.55, 128.21, 129.02, 129.60, 129.81, 130.12, 131.63, 132.00, 132.31, 133.58, 134.80, 136.68, 142.06, 152.25, 154.05, 157.19. $^{31}\text{P}\{^1\text{H}\}$ NMR (202 MHz, CDCl_3): δ 35.2 (s). 962 ($\nu_{\text{Re=O}}$), 3189 ($\nu_{\text{N-H}}$) cm^{-1}

(PNN)ReOCl (505) To a Teflon taped culture tube in toluene was added **(PNN^H)ReOCl₂ (503)** (238 mg, 0.325 mmol) and triethylamine (0.060 mL, 0.43 mmol). The solution was then heated at 80 °C for 1 h over which time full conversion to a 75:25 mixture of products was observed by ¹H and ³¹P{¹H} NMR spectroscopy corresponding to deprotonated isomers of (PNN)ReOCl, and concomitant formation of colorless solids (assumed to be HNEt₃Cl) was observed. The solution was then filtered through a pad of Celite and dried under reduced pressure to provide a glutinous, dark green residue. The residue was washed with 2 mL of pentane and dried to give the desired product in analytically pure form as a dark green, free-flowing powder. Yield: 180 mg (80%). Single crystals suitable for X-ray diffraction were grown from a concentrated toluene solution layered with pentane. **Major Isomer (75%)** - ¹H NMR (500 MHz, CDCl₃): δ 0.72 (dd, *J* = 19.0, 7.0 Hz, 3H), 1.24 (dd, *J* = 19.1, 6.9 Hz, 3H), 1.39 (dd, 14.1, 7.2 Hz, 3H), 1.58 (dd, *J* = 17.8, 6.9 Hz, 3H), 1.91 (s, 3H), 1.99 (s, 3H), 2.34 (s, 3H), 2.40 (s, 3H), 2.45 (s, 3H), 2.86 (m, 1H), 3.06 (m, 1H), 4.27 (dd, *J*_{H-H} = 12.4, *J*_{H-P} = 4.1 Hz, 1H), 4.35 (d, *J* = 12.4 Hz, 1H), 6.95 (m, 4H), 7.17 (m, 2H), 7.27 (m, 1H), 7.49 (dd, *J* = 8.5, 4.5 Hz, 1H). ³¹P{¹H} NMR (CDCl₃, 202 MHz): δ 60.2 (s) **Minor Isomer (25%)** - ¹H NMR (500 MHz, CDCl₃): δ 0.66 (m, 3H), 1.01 (dd, *J* = 18.2, 6.8 Hz, 3H), 1.18 (s, 3H), 1.50 (dd, *J* = 16.9, 7.0 Hz, 3H), 2.30 (s, 3H), 2.31 (s, 3H), 2.36 (s, 3H), 2.43 (s, 3H), 2.52 (m, 1H), 2.72 (m, 1H), 4.89 (d, *J* = 12.8 Hz, 1H), 5.42 (dd, *J* = 12.8, 8.9 Hz, 1H), 6.78 (s, 1H). *The fourth isopropyl CH₃ and remaining 7 aromatic resonances cannot be resolved due to presumed overlap with resonances corresponding to the minor isomer.* ³¹P{¹H} NMR (202 MHz, CDCl₃): δ 39.1 (s) ¹³C{¹H} NMR (126 MHz, CDCl₃): δ 16.62, 17.56, 17.96, 18.35, 18.68, 19.79, 20.31, 20.61 (d, *J*_{P-C} = 19.6 Hz), 20.90 (d, *J*_{P-C} = 29.8 Hz), 21.30 (d, *J*_{P-C} = 23.7 Hz), 23.05 (d, *J*_{P-}

c = 29.2 Hz), 23.79 (d, $J_{P-C} = 23.6$ Hz), 26.60 (d, $J_{P-C} = 26.5$ Hz), 64.72, 69.01, 114.58, 114.97, 116.17 (d, $J_{P-C} = 10.3$ Hz), 119.78, 120.12, 122.73 (d $J_{P-C} = 8.6$ Hz), 125.42, 127.72, 127.87, 128.09, 128.19, 129.10, 129.16, 129.43, 130.56, 130.80, 130.89, 130.94, 131.42, 132.69, 133.14, 133.28, 133.44, 134.00, 134.05, 134.42, 137.55, 146.69 (m), 149.82, 160.78, 170.44 (d, $J_{P-C} = 15.4$ Hz). IR (KBr): 962 ($\nu_{Re=O}$), 970 ($\nu_{Re=O}$) cm^{-1} . Elem. Anal. Found (Calc): C: 51.60 (51.75); H: 5.64 (5.65); N: 3.81 (4.02).

(PNN)ReOBr(506) To a J. Young tube in toluene was added (PNN^H)ReOBr₂ (**504**) (41 mg, 0.049 mmol) and triethylamine (0.014 mL, 0.10 mmol). The solution was then heated at 80 °C for 1 h over which time full conversion to a 75:25 mixture of products was observed by ¹H and ³¹P{¹H} NMR spectroscopy corresponding to deprotonated isomers of **506**, and concomitant formation of colorless solids (assumed to be HNEt₃Br) was observed. The solution was then filtered through a pad of Celite and dried under reduced pressure to provide a glutinous, dark green residue. The residue was washed with 5 mL of pentane and dried to give the desired product as a dark green, free-flowing powder. Yield: 34 mg (92%).

Major Isomer (78%) ¹H NMR (500 MHz, CDCl₃): δ 0.69 (dd, $J = 19.3, 7.0$ Hz, 3H), 1.23 (dd, $J = 19.3, 6.9$ Hz, 3H), 1.43 (dd, $J = 14.0, 7.1$ Hz, 3H), 1.63 (dd, $J = 17.6, 6.9$ Hz, 3H), 1.89 (s, 3H), 1.98 (s, 3H), 2.35 (s, 3H), 2.40 (s, 3H), 2.44 (s, 3H), 2.87 (m, 1H), 3.21 (m, 1H), 4.19 (dd, $J_{H-H} = 12.3, J_{H-P} = 3.8$ Hz, 1H), 4.32 (d, $J = 12.3$ Hz, 1H), 6.94 (m, 3H), 7.08 (m, 1H), 7.16 (m, 2H), 7.28 (m, 1H), 7.46 (dd, $J = 8.6, 4.5$ Hz, 1H). ³¹P{¹H} NMR (202 MHz, CDCl₃): δ 60.7 (s).

Minor Isomer (22%) – ¹H NMR (500 MHz, CDCl₃): δ 0.67 (dd, $J = 18.0, 7.0$ Hz, 3H), 0.99 (dd, $J = 18.2, 6.8$ Hz, 3H), 1.14 (s, 3H), 1.43 (m, 3H), 1.57 (dd, $J = 16.7, 7.0$ Hz, 3H), 2.31 (s, 3H), 2.32 (s, 3H), 2.41 (s, 3H), 2.42 (s, 3H), 2.73 (m, 1H), 3.13 (m, 1H), 4.86 (d, $J = 12.6$ Hz, 1H), 5.39 (dd, $J = 12.6, 9.1$ Hz), *The expected remaining*

7 aromatic resonances cannot be resolved due to presumed overlap with resonances corresponding to the major isomer. $^{31}\text{P}\{^1\text{H}\}$ NMR (202 MHz, CDCl_3): δ 37.4 (s). $^{13}\text{C}\{^1\text{H}\}$ NMR (126 MHz, CDCl_3): δ 16.55 ($J_{\text{P-C}} = 5.3$ Hz), 18.23, 18.49, 19.06, 19.76, 19.82, 20.18, 20.39, 20.55, 20.76, 23.45 (d, $J = 29.6$ Hz), 26.72 (d, $J = 27.0$ Hz), 64.92, 114.76, 115.67, 115.76, 120.01, 120.16, 127.67, 127.98, 128.16, 128.19, 128.94, 129.01, 130.65, 130.87, 130.93, 132.58, 133.22, 133.92, 134.28, 137.65, 149.31, 162.37, 169.93. IR (KBr): 968 ($\nu_{\text{Re=O}}$) cm^{-1} .

(PNN)ReOCl(PMe₃) (507): To a J. Young tube in C_6D_6 was added (PNN)ReOCl (**505**) (15 mg, 0.022 mmol) and PMe_3 (0.003 mL, 0.03 mmol). Upon addition of PMe_3 the dark green solution immediately became purple, as full conversion to the adduct was noted by $^{31}\text{P}\{^1\text{H}\}$ NMR and ^1H NMR spectroscopy. The solution was then filtered through Celite, dried under reduced pressure to provide a dark purple residue. The residue was then redissolved in pentane and filtered again. Subsequent removal of solvent under reduced pressure provided the product as a free-flowing, dark purple powder in >97% purity (NMR evidence). Yield: 14 mg (85%). **Major Isomer (68%):** ^1H NMR (500 MHz, C_6D_6): δ 1.05 (d, $^2J_{\text{P-H}} = 9.2$ Hz, 9H), 1.20 (dd, $J = 11.7, 5.6$ Hz, 3H), 1.24 (dd, $J = 13.7, 5.5$ Hz, 3H), 1.36 (dd, $J = 11.6, 7.3$ Hz, 3H), 1.51 (dd, $J = 13.7, 7.2$ Hz, 3H), 2.01 (s, 3H), 2.14 (m, 1H), 2.25 (s, 3H), 2.27 (s, 3H), 2.31 (s, 3H), 2.84 (m, 1H), 2.85 (s, 3H), 4.67 (dd, $J = 12.3, 3.3$ Hz, 1H), 6.00 (dd, $J = 12.3, 3.0$ Hz, 1H), 6.74 (m, 1H), 6.84 (d, $J = 1.8$ Hz, 1H), 6.88 (br, 1H), 6.91 (br, 1H), 7.0 (d, $J = 8.1$ Hz, 1H), 7.07 (td, $J = 8.5, 2.0$ Hz, 1H), 7.29 (dd, $J = 8.4, 4.4$ Hz, 1H), 7.33 (dd, $J = 7.3, 2.0$ Hz, 1H). $^{31}\text{P}\{^1\text{H}\}$ NMR (202 MHz, C_6D_6): δ 4.38 (s, P^iPr_2), -50.2 (s, PMe_3). **Minor Isomer (32%):** ^1H NMR (500 MHz, C_6D_6): δ 1.10 (d, $J = 9.5$ Hz, 9H), 1.08 (dd, $J = 14.0, 5.7$ Hz, 3H), 1.16 (dd, $J = 10, 7.2$ Hz, 3H), 1.22 (s, 3H),

1.25 (dd, $J = 16.7, 7.8$ Hz, 3H), 1.38 (dd, $J = 15, 6.8$ Hz, 3H), 2.18 (s, 3H), 2.23 (s, 3H), 2.34 (s, 3H), 2.41 (m, 1H), 2.50 (m, 1H), 2.57 (s, 3H), 4.78 (dd, $J = 12.3, 4.0$ Hz, 1H), 5.75 (dd, $J = 12.3, 7.1$ Hz, 1H), 6.80 (s, H), 6.94 (d, $J = 1.9$ Hz, 1H), 7.13 (m, 1H), 7.22 (dd, $J = 8.6, 4.5$ Hz, 1H), 7.39 (d, $J = 8.1$ Hz, 1H). *The expected remaining 3 aromatic resonances were unable to be found and resolved due to presumed overlap with resonances corresponding to the major isomer.* $^{31}\text{P}\{^1\text{H}\}$ NMR (202 MHz, C_6D_6): δ 0.3 (s, P^iPr_2), -49.2 (s, PMe_3) $^{13}\text{C}\{^1\text{H}\}$ NMR (126 MHz, C_6D_6): δ 18.89, 18.94, 19.14, 19.22 (d, $J = 3.6$ Hz), 19.43, 19.86 (m), 19.96(m), 20.17, 20.24, 20.34, 20.41, 20.59, 20.66, 22.29, 25.50 (d, $J = 14.0$ Hz), 30.20 (d, $J = 16.4$ Hz), 67.66, 119.94, 128.78, 129.33, 129.85, 130.19, 130.82, 131.27, 134.06, 136.02, 151.03. IR (KBr): 957 ($\text{Re}=\text{O}$), 945 ($\text{Re}=\text{O}$).

(PNN)ReO(OTf) (508): To a scintillation vial equipped with a magnetic stir bar was added (PNN)ReOCl (**505**) (19.0 mg, 0.027 mmol) in 3 mL of a 2:1 CH_2Cl_2 : Et_2O solution. To the stirring, dark green solution was added AgOTf (6.9 mg, 0.027 mmol) resulting in an immediate color change to dark red-brown. The solution was allowed to stir for 12 h over which time a suspension had formed as AgCl precipitated out of solution. The solution was then filtered through a pad of Celite and dried under reduced pressure to give a dark red-brown residue. The residue was then washed with pentane, and dried under reduced pressure to provide **508** as a 90:10 mixture of isomers in ca. 97% purity (^1H NMR evidence). Yield: 21 mg (96%). Single crystals suitable for X-ray diffraction were grown from a concentrated THF solution layered with pentane. **Major Isomer (90%)** – ^1H NMR (500 MHz, C_6D_6): δ 0.62 ($J = 17.8, 7.0$ Hz, 3H), 1.01 (dd, $J = 16.2, 7.1$ Hz, 3H), 1.12 (dd, $J = 18.1, 7.7$ Hz, 3H), 1.33 (dd, $J = 20.3, 7.0$ Hz, 3H), 1.95 (s, 3H), 2.09 (s, 3H), 2.15 (s, 3H), 2.19 (s, 3H), 2.22 (s, 3H), 2.49 (m, 1H), 3.09 (m, 1H), 3.86 (d, $J = 12.4$ Hz, 1H), 3.90

(d, $J = 12.4$ Hz, 1H), 6.66 (s, 1H), 6.86 (m, 4H), 7.01 (m, 2H), 7.29 (dd, $J = 8.5, 4.3$ Hz). ^{19}F NMR (407 MHz, C_6D_6): δ -73.06 (s). $^{31}\text{P}\{^1\text{H}\}$ NMR (202 MHz, C_6D_6): δ 64.5 (s). **Minor Isomer (10%)**- ^1H NMR (500 MHz, C_6D_6): δ 0.73 (dd, $J = 16.6, 6.8$ Hz, 3H), 1.11 (s, 3H), 1.59 (dd, $J = 18.4, 7.4$ Hz, 3H), 1.97 (s, 3H), 2.13 (s, 3H), 3.71 (d, $J = 13.3$ Hz, 1H), 5.30 (dd, $J = 13.3, 6.3$ Hz, 1H). Other expected resonances were unable to be located and resolved due to presumed overlap with resonances corresponding to the major isomer. ^{19}F NMR (407 MHz, C_6D_6): δ -73.57. $^{31}\text{P}\{^1\text{H}\}$ NMR (202 MHz, C_6D_6): δ 42.2 (s). $^{13}\text{C}\{^1\text{H}\}$ NMR (126 MHz, C_6D_6): δ 17.29, 19.68, 20.24, 20.39, 26.30, 26.50, 26.54, 26.71, 62.98, 114.60, 117.96, 122.51, 128.56, 128.85, 129.03, 129.57, 130.37, 131.14, 131.29, 132.02, 134.19, 134.31, 134.89, 139.71, 151.07, 156.57, 169.82. IR (KBr): 1195 (V_{OTf}), 1154 (V_{OTf}), 966 ($\text{V}_{\text{Re=O}}$) cm^{-1} .

(PNN)ReO(OAc) (509): To a scintillation vial equipped with a magnetic stir bar was added (PNN)ReOCl (**505**) (32.8 mg, 0.047 mmol) in 4 mL of a 1:1 CH_2Cl_2 : Et_2O solution. To the stirring, dark green solution was added AgOAc (8.0 mg, 0.047 mmol) resulting in immediate precipitation of white solids, presumed to be AgCl. After being allowed to stir for 16 h, another 1 mL of Et_2O was added resulting in further precipitation of solids. The resultant suspension was filtered through a pad of Celite and dried under reduced pressure to provide the product as a light, yellow-green powder in >95% purity, determined to be a mixture of isomers by ^1H and $^{31}\text{P}\{^1\text{H}\}$ NMR spectroscopy. Yield: 28.8 mg (85%). **Major Isomer (78%)** ^1H NMR (500 MHz, C_6D_6): δ 1.03 (dd, $J = 16.2, 6.9$ Hz, 3H), 1.11 (m, 6H), 1.17 (dd, $J = 17.5, 6.9$ Hz, 3H), 1.30 (s, 3H), 1.79 (s, 3H), 1.82 (m, 1H), 2.09 (m, 1H), 2.15 (s, 3H), 2.22 (s, 3H), 2.27 (s, 3H), 2.84 (s, 3H), 4.99 (dd, $J = 13.2, 2.5$ Hz), 5.83 (dd, $J = 13.2, 9.7$ Hz), 6.77 (d, $J = 12.0$ Hz, 2H), 6.86 (m, 1H), 6.99 (m, 3H), 7.08

(dd, $J = 8.3, 4.2$ Hz, 1H), 7.42 (d, $J = 8.3$ Hz) $^{31}\text{P}\{^1\text{H}\}$ NMR (202 MHz, C_6D_6): δ 27.9 (s). **Minor Isomer (22%)** ^1H NMR (500 MHz, C_6D_6): δ 0.53 (dd, $J = 18.8, 7.0$ Hz, 3H), 0.82 (dd, $J = 13.9, 7.1$ Hz), 1.12 (s, 3H) 1.53 (s, 3H), 2.16 (s, 3H), 2.31 (s, 3H), 2.43 (s, 3H), 2.49 (s, 3H), 4.75 (d, $J = 13.9$ Hz, 1H), 5.33 (dd, $J = 13.9, 6.1$ Hz, 1H). Two expected resonances for the isopropyl methyl (CH_3) protons, and all eight aromatic protons were unable to be found and resolved presumably due to overlap with signals corresponding to the major isomer in solution. $^{31}\text{P}\{^1\text{H}\}$ NMR (202 MHz, C_6D_6): δ 33.3 (s). $^{13}\text{C}\{^1\text{H}\}$ NMR (126 MHz, C_6D_6): δ 16.90, 17.10, 17.51, 17.88, 18.89, 19.16, 19.79, 20.37, 20.53, 20.57, 20.78, 24.06 (d, $J = 20.6$ Hz), 69.23, 120.52, 126.91, 128.19, 129.49, 129.69, 129.92, 130.72, 131.84, 133.54, 134.87, 135.85, 136.56, 139.73, 147.13, 154.91, 175.03, 175.21, 178.28. IR (KBr): 939 ($\nu_{\text{Re=O}}$), 1653 ($\nu_{\text{C=O}}$) cm^{-1} .

(PNN)ReO(H) (510): To a J. Young tube in C_6D_6 was added (PNN)ReOCl (**505**) (24 mg, 0.035 mmol) and a 1.0 M toluene solution of NaHBET_3 (0.035 mL, 0.035 mmol). The solution was then rotated for ten minutes allowing formation of an emerald green, homogeneous solution. The solution was allowed to react for 16 h, then filtered through Celite, and dried under reduced pressure. The resultant residue was washed with a minimum of cold pentane and dried to provide the product as a lime green solid determined to be >95% pure by ^1H NMR spectroscopy. Yield: 21 mg, (91%). **Major Isomer (88%)** ^1H NMR (500 MHz, C_6D_6): δ 0.54 (dd, $J = 17.5, 7.0$ Hz, 3H), 0.90 (dd, $J = 17.5, 6.9$ Hz, 3H), 0.98 (dd, $J = 15.0, 7.0$ Hz, 3H), 1.24 (dd, $J = 17.8, 6.8$ Hz, 3H), 2.01 (s, 3H), 2.07 (m, 2H), 2.13 (s, 3H), 2.31 (s, 3H), 2.32 (s, 3H), 2.50 (s, 3H), 4.36 (dd, $J = 13.0, 4.4$ Hz, 1H), 4.57 (d, $J = 13.0$ Hz, 1H), 6.85 (m, 2H), 6.99 (br, 3H), 7.06 (m, 2H), 7.54 (dd, $J = 8.9, 4.4$ Hz, 1H), 8.22 (d, $J_{\text{P-H}} = 17.4$ Hz, 1H, Re-H). $^{31}\text{P}\{^1\text{H}\}$ NMR (202 MHz, C_6D_6): δ 74.4 (s).

Minor Isomer (12%) - ^1H NMR (500 MHz, C_6D_6): δ 0.57 (dd, $J = 17.2, 7.1$ Hz, 3H), 0.85 (dd, $J = 12.6, 6.9$ Hz, 3H), 1.51 (s, 3H), 2.14 (s, 3H), 2.15 (s, 3H), 2.28 (s, 3H), 2.75 (s, 3H), 3.94 (d, $J = 14.5$ Hz, 1H, Re-H), 4.82 (d, $J = 13.0$ Hz, 1H), 5.13 (dd, $J = 13.0, 8.3$ Hz, 1H), 7.51 (d, $J = 8.1$ Hz, 3H). *Two isopropyl methyl signals were observed but unable to be resolved due to significant overlap with major isomer. No isopropyl methine signals were found for the minor isomer, and no other aromatic signals were able to be resolved due to significant overlap with the resonances of the major isomer.* $^{31}\text{P}\{^1\text{H}\}$ NMR (202 MHz, C_6D_6): δ 49.9 (s). $^{13}\text{C}\{^1\text{H}\}$ (126 MHz, C_6D_6): δ 19.58, 20.53, 23.62, 27.82, 61.86, 112.57, 112.94, 116.48, 119.75, 128.33, 128.54, 128.80, 129.19, 129.30, 129.54, 129.74, 130.23, 130.47, 131.16, 133.08, 134.29, 134.73, 135.30, 146.75, 166.12, 168.77. Anal. Found(Calcd): C: 54.18(54.44); H: 5.98 (6.09); N: 3.77 (4.23).

X-ray Diffractometry Details for (PNP)ReOCl₂ (502): A dark green, multi-faceted block of suitable size (0.35 x 0.29 x 0.05 mm) was selected from a representative sample of crystals of the same habit using an optical microscope and mounted onto a nylon loop. Low temperature (150 K) X-ray data were obtained on a Bruker APEXII CCD based diffractometer (Mo sealed X-ray tube, $K_{\alpha} = 0.71073 \text{ \AA}$). All diffractometer manipulations, including data collection, integration and scaling were carried out using the Bruker APEXII software. An absorption correction was applied using SADABS. The space group was determined on the basis of systematic absences and intensity statistics and the structure was solved by direct methods and refined by full-matrix least squares on F^2 . The structure was solved in the monoclinic P 2/n space group using XS (incorporated in SHELXL). All non-hydrogen atoms were refined with anisotropic thermal parameters. All hydrogen atoms were placed in idealized positions and refined using riding model. Elongated/unusual thermal ellipsoid on Re1, Cl1, and O1 indicated that these atoms are disordered

and was modeled successfully with half occupancies. The structure was refined (weighted least squares refinement on F^2) and the final least-squares refinement converged. No additional symmetry was found using ADDSYM incorporated in PLATON program. (CSD Identifier/Number – EYUNOD/1504712)

X-ray Diffractometry Details for (PNN^H)ReOCl₂ (503): A dark green, multi-faceted block of suitable size (0.33 x 0.25 x 0.15 mm) was selected from a representative sample of crystals of the same habit using an optical microscope and mounted onto a nylon loop. Low temperature (150 K) X-ray data were obtained on a Bruker APEXII CCD based diffractometer (Mo sealed X-ray tube, $K_{\alpha} = 0.71073 \text{ \AA}$). All diffractometer manipulations, including data collection, integration and scaling were carried out using the Bruker APEXII software. An absorption correction was applied using SADABS. The space group was determined on the basis of systematic absences and intensity statistics and the structure was solved by direct methods and refined by full-matrix least squares on F^2 . The structure was solved in the triclinic P-1 space group using XS (incorporated in SHELXLE). All non-hydrogen atoms were refined with anisotropic thermal parameters. All hydrogen atoms were placed in idealized positions and refined using riding model. The structure was refined (weighted least squares refinement on F^2) and the final least-squares refinement converged. No additional symmetry was found using ADDSYM incorporated in PLATON program. (CSD Identifier/Number – EYUNUJ/1504713)

X-ray Diffractometry Details for (PNN)ReOCl (505): A green, multi-faceted block of suitable size (0.90 x 0.62 x 0.10 mm) was selected from a representative sample of crystals of the same habit using an optical microscope and mounted onto a nylon loop. Low temperature (110 K) X-ray data were obtained on a Bruker APEXII CCD based diffractometer (Mo sealed X-ray tube, $K_{\alpha} = 0.71073 \text{ \AA}$). All diffractometer manipulations, including data collection, integration and

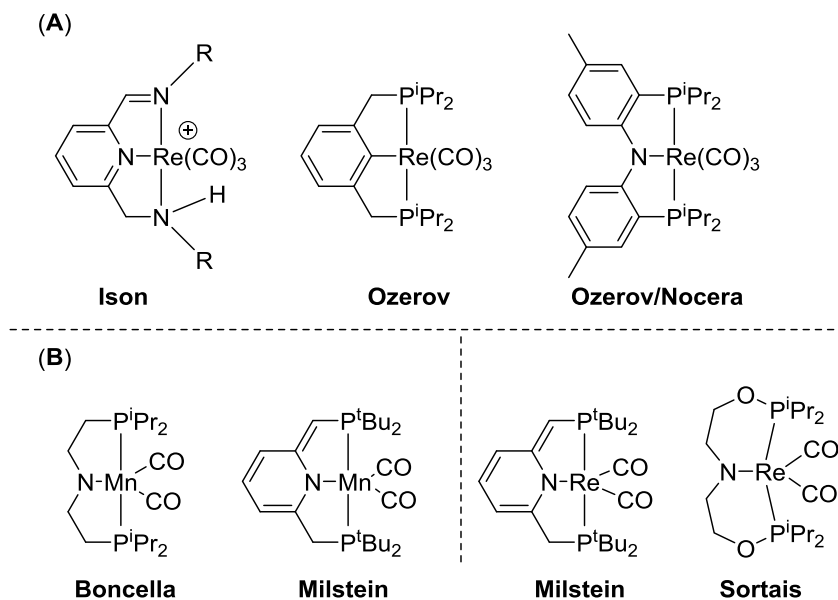
scaling were carried out using the Bruker APEXII software. An absorption correction was applied using SADABS. The space group was determined on the basis of systematic absences and intensity statistics and the structure was solved by direct methods and refined by full-matrix least squares on F^2 . The structure was solved in the triclinic $C 2/c$ space group using XS (incorporated in SHELXLE). All non-hydrogen atoms were refined with anisotropic thermal parameters. All hydrogen atoms were placed in idealized positions and refined using riding model. The structure was refined (weighted least squares refinement on F^2) and the final least-squares refinement converged. No additional symmetry was found using ADDSYM incorporated in PLATON program. (CSD Identifier/Number – EYUPAR/1504714)

X-ray Diffractometry Details for (PNN)ReO(OTf) (508): A dark red, multi-faceted block of suitable size (0.15 x 0.12 x 0.08 mm) was selected from a representative sample of crystals of the same habit using an optical microscope and mounted onto a nylon loop. Low temperature (150 K) X-ray data were obtained on a Bruker APEXII CCD based diffractometer (Mo sealed X-ray tube, $K_{\alpha} = 0.71073 \text{ \AA}$). All diffractometer manipulations, including data collection, integration and scaling were carried out using the Bruker APEXII software. An absorption correction was applied using SADABS. The space group was determined on the basis of systematic absences and intensity statistics and the structure was solved by direct methods and refined by full-matrix least squares on F^2 . The structure was solved in the triclinic $P-1$ space group using XS (incorporated in SHELXLE). All non-hydrogen atoms were refined with anisotropic thermal parameters. All hydrogen atoms were placed in idealized positions and refined using riding model. The structure was refined (weighted least squares refinement on F^2) and the final least-squares refinement converged. No additional symmetry was found using ADDSYM incorporated in PLATON program. (CSD Identifier/Number – EYUPEV/1504715)

CHAPTER VI
SYNTHESIS AND REACTIVITY OF UNSATURATED CARBONYL COMPLEXES OF
RHENIUM AND MANGANESE SUPPORTED BY THE PNP PINCER

6.1 Introduction

Group VII *polycarbonyls* of manganese (Mn) and rhenium (Re) have found broad utility in a range of reactions stretching from C-H activation¹⁵¹ to the electrocatalytic reduction of CO₂ into synthetically useful C1 building blocks.¹⁵² Often, a fully saturated *polycarbonyl* is utilized as the pre-catalyst. However, it has long been supposed and recently studied computationally that the active catalyst is a transient, unsaturated complex which has undergone either electrochemical or photolytic loss of at least one carbonyl (CO) ligand.¹⁵³ We have recently become interested in the chemistry of rhenium in a pincer ligand context, and in that vein have sought to examine the chemistry of pincer-supported Re and Mn *poly-carbonyls*.



Scheme VI-1. (A) Examples of saturated pincer-supported rhenium *polycarbonyls* (B) unsaturated PNP-supported Mn *dicarbonyls* and (C) PNP-supported Re *di-carbonyls*

Pincers are tridentate ligands which bind most typically in meridional fashion and have ostensibly allowed for the stabilization and observation of what would normally be considered highly reactive intermediates.¹⁵⁴ Saturated, pincer-rhenium *tri-carbonyls* have been reported (Scheme VI-1 A)^{68,155} and recently, pincer-supported *di-carbonyls* of manganese have exhibited powerful modes of reactivity (Scheme VI-1 B)¹⁵⁶ Despite this, the chemistry of five-coordinate rhenium *dicarbonyls* is comparatively underdeveloped¹⁵⁷ with the only previous example of an isolated, unsaturated rhenium *di-carbonyl* reported by Milstein *et al*, featuring cooperative reactivity at a non-innocent PNP-ligand capable of undergoing reversible dearomatization (Scheme VI-1 C).⁶³ Sortais and coworkers generated and spectroscopically characterized a PONOP-Re dicarbonyl, though it was not isolated. Thus, study of the at-metal chemistry of a discrete, unsaturated pincer-rhenium *di-carbonyl* remains an attractive target. Herein we report the

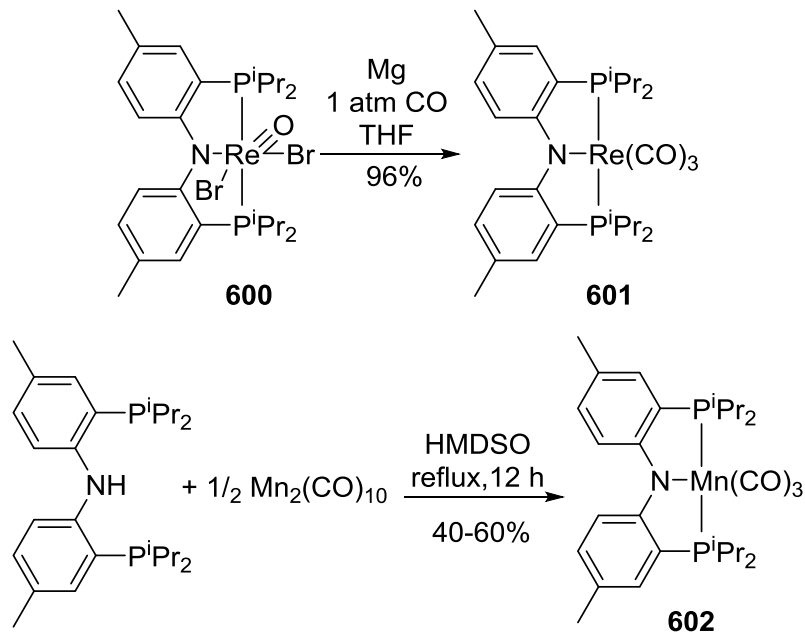
first examples of direct acid-assisted chemical decarbonylation of saturated tri-carbonyls, and their subsequent dehydrohalogenation giving access to well-defined, PNP-supported *di*-carbonyls of manganese and rhenium.

6.2 Results and Discussion

6.2.1 Synthesis of (PNP)*M*(CO)₃ (*M* = Mn, Re)

(PNP^{iPr})ReOBr₂ (**600**) was synthesized and isolated as a dark, semi-crystalline powder in 88% yield *via* reaction of PN^HP with (PPh₃)₂ReOBr₂(OEt), which led to expulsion of free PPh₃ and EtOH (¹H and ³¹P{¹H} NMR evidence). (PNP^{iPr})ReOBr₂ features a terminal rhenium-oxo stretch in its IR spectrum at 940 cm⁻¹. Two broad doublet ³¹P{¹H} resonances at δ 27.4 and 21.9 (d, *J*_{P-P} = 186 Hz), and broad ligand resonances in the ¹H NMR spectrum arise from rotameric isomerism in the diarylamido backbone similar to that seen for **502**.

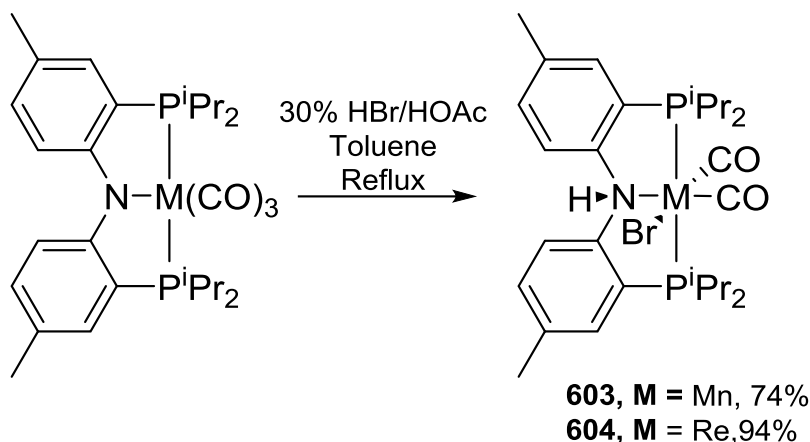
Reduction of (PNP^{iPr})ReOBr₂ with excess magnesium powder in THF under an atmosphere of CO results in clean formation and isolation of the previously reported complex, (PNP^{iPr})Re(CO)₃ (**601**), in 96% yield. (PNP^{iPr})Mn(CO)₃ (**602**) was obtained in moderate yields by direct metalation of Mn₂(CO)₁₀ with PN^HP (Scheme VI-2).



Scheme VI-2. Synthesis of saturated PNP-supported Mn and Re *poly*-carbonyls

6.2.2 Hydrobrominative Decarbonylation of (PNP)*M*(CO)₃ (*M* = Mn, Re)

Reaction of the strong acid, HOTf with (PNP^{iPr})*M*(CO)₃ (*M*=Re, Mn) protonates the central nitrogen and furnishes the ionic species, [(PN^HP^{iPr})*M*(CO)₃][OTf], in which the *tricarbonyl* motif is retained. In light of this result, we surmised that addition of an acid with a more coordinating anion might work to displace a carbonyl ligand. Reaction of a 30:70 HBr/AcOH solution with refluxing toluene solutions of **601** or **602** results in a noteworthy increase in solution turbidity (presumed to be CO evolution) and an immediate color change to yellow (Mn) or violet (Re) with formation of an orange precipitate. After workup, the decarbonylated products of HBr addition, (PN^HP^{iPr})MnBr(CO)₂ (**603**) and (PN^HP^{iPr})ReBr(CO)₂ (**604**), are obtained as yellow (Mn) and blue-green (Re) powders in high yield (**Scheme VI-3**).



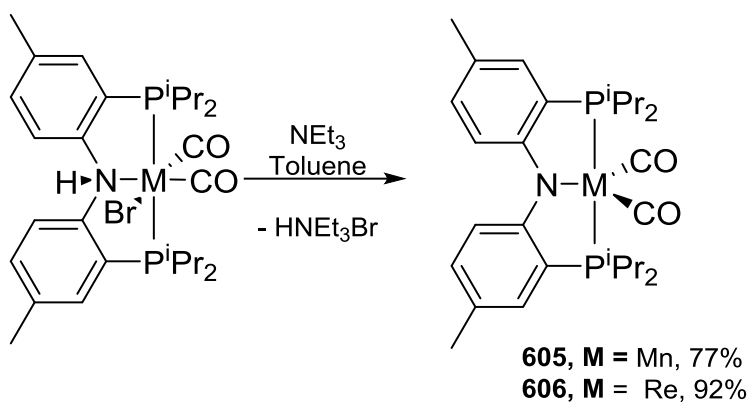
Scheme VI-3. Hydrobrominative decarbonylation of *tricarbonyls*

The $^{31}\text{P}\{^1\text{H}\}$ NMR spectra of **603** and **604** exhibit a single, broad resonance (Mn, δ 73.3; Re, δ 40.9 ppm). The ^1H NMR spectra for **603** and **604** each feature broad aromatic resonances (6H total) and four separate isopropyl methyl resonances (6H each) which indicate C_s -symmetry and show doublet of virtual triplet splitting, typical of *trans* disposed phosphines. Each exhibit two carbonyl CO stretches in their IR spectra (**603**, Mn, 1916 and 1836 cm^{-1} ; **604**, Re, 1910 and 1830 cm^{-1}) with intensities in a ca. 1:1 ratio, supportive of a *cis* dicarbonyl formulation.

6.2.3 Synthesis of Unsaturated (PNP) $M(\text{CO})_2$ ($M = \text{Mn}, \text{Re}$)

(PNP^{iPr})Mn(CO)₂ (**605**) has previously been reported and spectroscopically characterized as part of a 70:30 mix with (PNP^{iPr})Mn(CO)₃ *via* direct decarbonylation under forcing conditions. Though generated **605** was unable to be isolated in that report, analogous chemistry with (PNP^{iPr})Re(CO)₃ (**601**) was shown to remain entirely elusive.

Treatment of **603** or **604** with NEt₃ in toluene led to an immediate color change to blue (Mn) or red (Re) solutions with formation of a colorless precipitate (presumed to be HNEt₃Br). ³¹P{¹H} NMR analysis indicated clean formation of (PNPⁱPr)Mn(CO)₂ (**605**) (δ 83.7 ppm) and (PNPⁱPr)Re(CO)₂ (**606**) (δ 63.9 ppm). **605** and **606** were isolated as dark blue (Mn) and dark red (Re) powders in good to excellent yields (**Scheme VI-4**).



Scheme VI-4. Facile dehydrohalogenation to access unstaturated, *dicarbonyl* species

605 and **606** exhibit C_{2v}-symmetry in their ¹H NMR spectra with two doublet of virtual triplet resonances for the isopropyl methyls (Mn, δ 1.27 and 1.07 ppm; Re, δ 1.23 and 0.98 ppm, 12H each), a singular methine resonance (worth 4H), and three aromatic resonances (6H total). **605** has a triplet (*J_{P-C}* = 19.6 Hz) carbonyl CO resonance in its ¹³C{¹H} NMR spectrum at δ 239.5 ppm (worth 2 CO), and two rather low frequency CO stretches via IR spectroscopy at 1898 and

1824 cm⁻¹. The ¹³C{¹H} NMR spectrum of **606** similarly reveals a triplet resonance ($J_{P-C} = 6.0$ Hz) at δ 210.1 ppm (worth 2 CO), and two low frequency stretches in its IR spectrum at 1896 and 1820 cm⁻¹. The carbonyl stretching frequencies of **605** and **606** evidence increased electron richness at the metal centers as compared to the previously reported, dearomatized (PNP*)Mn(CO)₂ (1833, 1904 cm⁻¹) and (PNP*)Re(CO)₂ (1826, 1905 cm⁻¹) complexes.

6.2.4 Structural Study of (PNP)Re(CO)₂

An X-ray diffraction study of a ruby-red, single crystal grown from CH₂Cl₂ and pentane confirmed the connectivity and revealed the C₂-symmetry of (PNP^{iPr})Re(CO)₂ (**606**) in the solid state (**Figure VI-1**). Similar to the previously reported structure of **605**, **606** takes on a five-coordinate, Y-shaped geometry ($\tau = 0.33$) in which the pincer PNP is bound meridionally (P1-Re1-P2 = 158.65), and the two carbonyl ligands are of an expected cis-disposition to one another (C1-Re1-C2 = 82.6). Notably, the Y-shaped geometry should allow for an optimization of amido π -donation into the Re $d\pi$ -orbital. This, in concert with the lower coordinate Re center, without a CO trans to N, ostensibly contributes to the shortening of the Re1-N1 bond (2.078 Å) versus that observed in the corresponding *tri*-carbonyl (PNP)Re(CO)₃ (2.191 Å). The removal of one CO ligand also allows for an increased back-donation into the remaining CO π^* orbitals insofar as the Re-CO bonds (1.874 Å) in (PNP)Re(CO)₂ are ca. 0.06 Å shorter than the shortest Re-CO bonds in the *tricarbonyl*, **601** (1.930 and 1.972 Å).

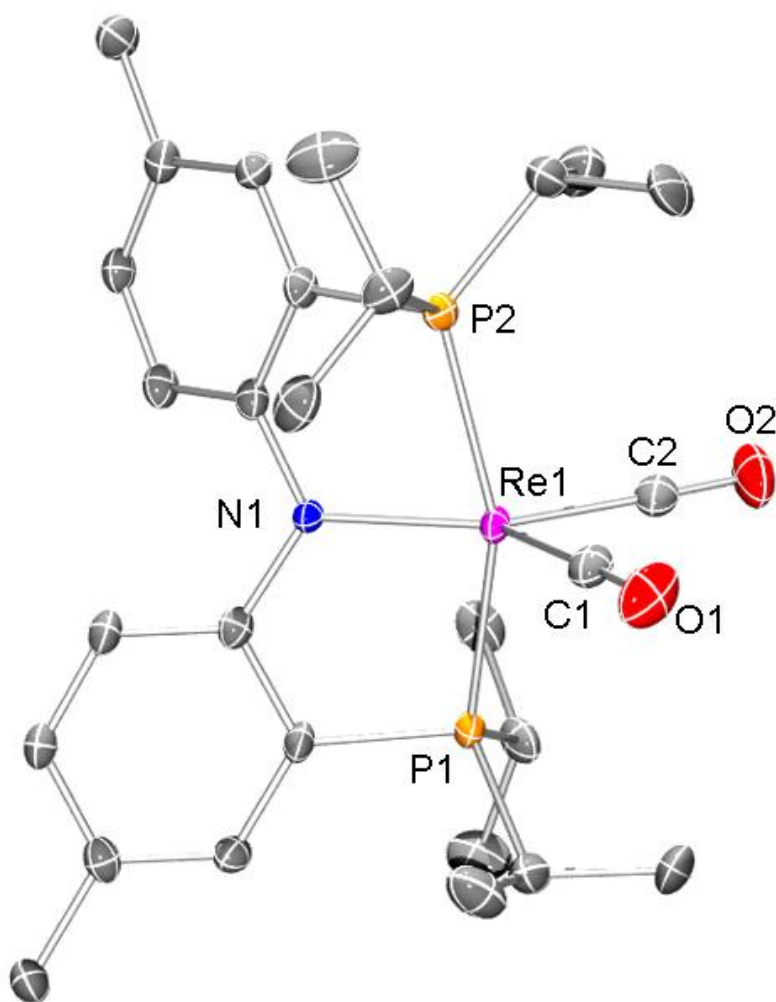
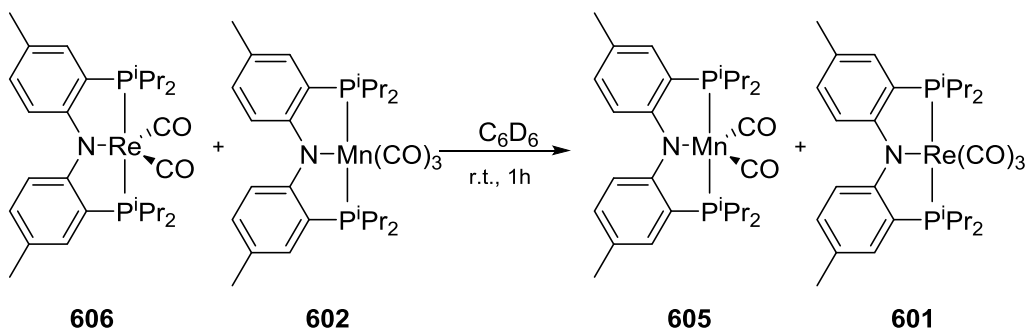


Figure VI-1. ORTEP drawing (50% probability ellipsoids) of $(\text{PNP}^{\text{iPr}})\text{Re}(\text{CO})_2$ (**606**). H atoms are omitted for clarity. Selected distance (Å) and angles (deg): N1-Re1, 2.078(6); Re1-P1, 2.388(17); Re1-C1, 1.874(6); C1-Re1-C2, 82.6(4), P1-Re1-P2, 158.65(7); C1-Re1-N1.

6.2.5 Carbonyl Reactivity of $(\text{PNP})\text{M}(\text{CO})_2$ ($M = \text{Mn}, \text{Re}$)

Reaction of either **605** or **606** with 1 atm of CO in C_6D_6 results in immediate formation of the *tri*-carbonyl species, **602** and **601**, respectively. Despite similar IR stretching frequencies, as a 5d transition metal, and stronger π -base, **606** would be expected to have a greater carbonyl affinity

than **605**. Supporting this hypothesis, reaction of equimolar **602** with **606** in C_6D_6 at room temperature for 1 h resulted in quantitative, clean conversion ($^{31}P\{^1H\}$ and 1H NMR evidence) to **605** and **601** (Scheme VI-5). Applying heat up to 80 °C for 24 h does not result in any further observable changes. It has been shown that various late transition metal complexes supported by the PNP ligand can chemically abstract a carbonyl from organic substrates such as aldehydes *via* bond-making and breaking steps.¹⁵⁸ Given the carbonyl affinity of **606**, we attempted to test whether it might also be capable of abstracting CO from an organic substrate, however, no reaction was observed with benzaldehyde, even upon prolonged heating. **606** was also determined to be incapable of displacing a second CO from **605**, as no additional reactivity was observed between **605** and **606**.

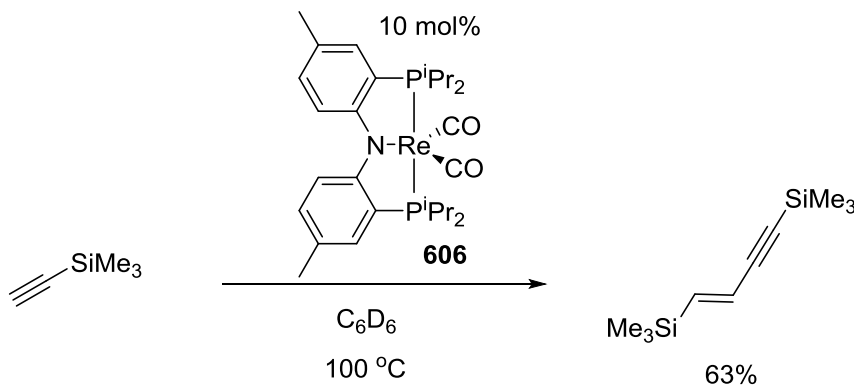


Scheme VI-5. Reaction to gauge preliminary carbonyl affinity of $(PNP)Re(CO)_2$

6.2.6 Further Reactivity of $(PNP)Re(CO)_2$ (**606**)

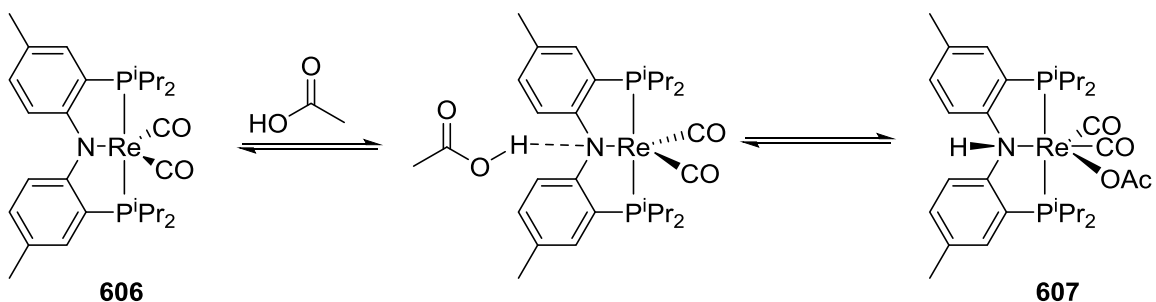
Looking to test the reactivity of **606** further, it has been determined that the complex is surprisingly unreactive. **606** shows high thermal stability with a lack of notable degradation ($^{31}P\{^1H\}$ NMR evidence) in cyclooctane solutions heated up to 150 °C for multiple hours.

(PNP)Re(CO)₂ showed no reactivity in the high temperature dehydrogenation of cyclooctane, or in the addition of H-B or B-B bonds in pinacolborane or dipinacoldiboron (B₂pin₂), respectively, either at room temperature, or under thermolysis conditions. Though highly air-sensitive, decomposing to a mixture of tan products upon exposure, no reactivity was observed upon treatment with degassed H₂O. Dissolution in acetonitrile causes an immediate color change from red to green with a new, broad resonance observed by ³¹P{¹H} NMR spectroscopy around δ 46 ppm which is generally diagnostic of a six-coordinate product, expected to be (PNP)Re(CO)₂(NCMe), arising simply from acetonitrile coordination. **606** was also determined to react as a rather incompetent catalyst for alkyne dimerization, dimerizing Me₃SiCCH with ca. 63% formation of the *trans* enyne, alkyne dimerization product at 10 mol% catalyst loading (Scheme VI-6).



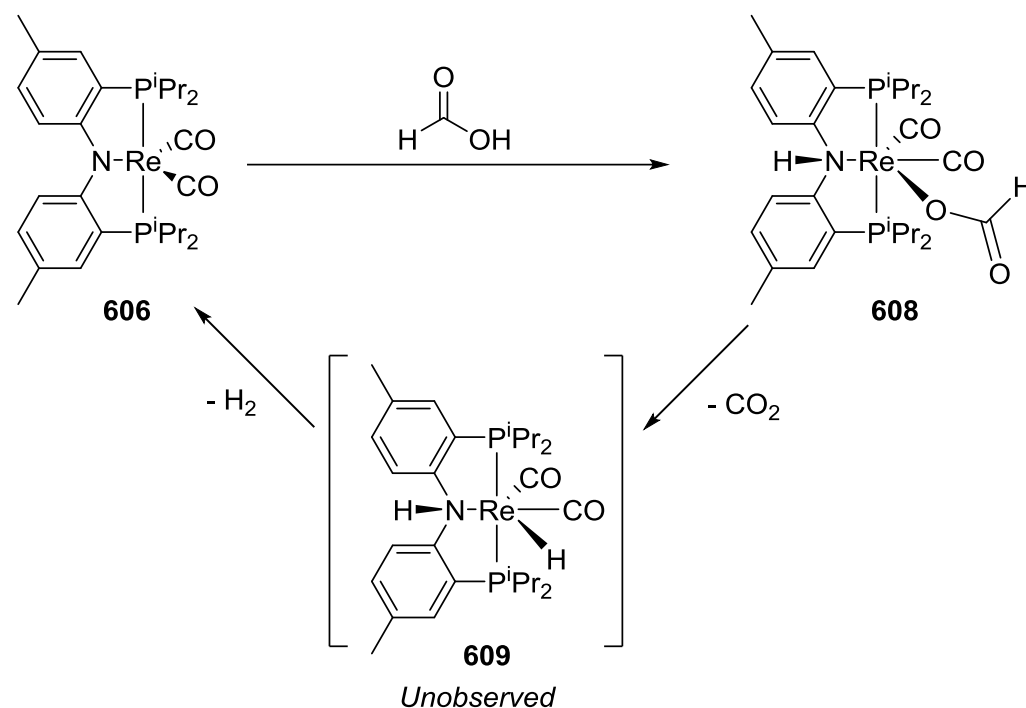
Scheme VI-6. Catalytic alkyne dimerization of trimethylsilylacetylene

While **606** did not undergo a reaction upon treatment with Me_3SiBr , addition of ethanol generated HBr which immediately added across the N-Re bond to furnish **604**. Furthermore, reaction with acetic acid gives full conversion to the spectroscopically characterized H-OAc addition product, $(\text{PN}^{\text{H}}\text{P})\text{Re}(\text{OAc})(\text{CO})_2$ (**607**). **607** features a single resonance by $^{31}\text{P}\{^1\text{H}\}$ NMR at δ 47.4 ppm, and based on its ^1H NMR spectrum appears to exhibit high fluxionality and exchangeability of the N(H)-Re(OAc) moiety with excess HOAc as the N-H resonance (while found by $\text{IR } \nu_{\text{N-H}} = 3172 \text{ cm}^{-1}$) is not observed, and there is a single OAc resonance (δ 1.72 ppm) which is significantly broadened and overintegrates in the presence of excess HOAc. Though not further investigated, the ^1H NMR spectrum counterintuitively exhibits either C_2 or C_{2v} -symmetry. This could arise from an equilibrium at room temperature in which HOAc is either coming on and off of the Re center at a fast rate, or HOAc is associated but not fully added across the N-Re bond (Scheme VI-7). Supportive of this, attempts to isolate **607** using low pressure removal of solvent resulted in significant degradation (as observed spectroscopically).



Scheme VI-7. Possible origins of the fluxionality observed in reaction of HOAc addition to **606**

Inspired by the ability of **606** to undergo H-X addition with acidic reagents, its reactivity with neat formic acid was tested. Treatment of **606** with H₂CO₂ in CH₂Cl₂ causes an immediate color change from red to purple with concomitant formation of the isolable rhenium formate, (PN^HP)Re(CO₂H)(CO)₂ (**608**) which has a single resonance in its ³¹P{¹H} NMR spectrum at δ 48.4 ppm. ¹H NMR spectroscopy reveals the presence of a broad N-H resonance (δ 8.53 ppm) as well as a formate C-H resonance at δ 13.62 as a broad hump.



Scheme VI-8. Formation and presumed, selective thermal decomposition of rhenium-formate

Interestingly, thermolysis of **608** results in a loss of H₂ (¹H NMR evidence) and reformation of **606** (Scheme VI-8). No intermediates are observed in the transformation, though it would be reasonable to presume the intermediacy of a Re-hydride, such as would be found in the

species (PN^HP)Re(H)(CO₂) (**609**). Attempts to isolate such a species *via* alternative synthetic routes have not yet been fruitful, and **606** reveals no reactivity under an atmosphere of H₂. In preliminary support of selective decomposition of formic acid to CO₂ and H₂, no **601** is observed to form in a J. Young tube reaction with 20 mol% Re, and H₂ is observed by ¹H NMR spectroscopy.

6.3 Conclusion

The synthesis of **601** *via* magnesium reduction of **600** under a CO atmosphere has been disclosed. A new method of hydrobrominative decarbonylation has been reported allowing access to the six-coordinate Mn(I) and Re(I) complexes, **603** and **604**. These complexes undergo facile dehydrohalogenation upon treatment with triethylamine to furnish the PNP-supported Mn and Re-dicarbonyls, **605** and **606**. A structural study of **606** revealed a highly symmetric, five-coordinate, Y-shaped geometry with increased N-Re π -donation, as compared to **601**. Despite similar IR stretching frequencies, **606** more strongly binds CO, allowing the direct, clean transfer of a CO ligand from the saturated **602**. Given that **606** shows promising, preliminary reactivity for the irreversible sequestration of a strongly bound organometallic carbonyl, we believe it may find future use as an activator for other, saturated *polycarbonyl* fragments giving access to reactivity paths which may have been previously inaccessible. Finally, the preliminary reactivity of **606** in various H-X splitting reactions was explored, and its initial reactivity as a potential catalyst for the dehydrogenation of formic acid, shown.

6.4 Experimental

6.4.1 General Considerations

Unless otherwise stated, all experiments were carried out using standard glovebox and Schlenk line techniques under a dry argon atmosphere. C₆D₆ was dried over NaK, benzophenone, and 18-crown-6, distilled, and stored over molecular sieves in an argon glovebox prior to usage. Diethyl ether, pentane, toluene, and tetrahydrofuran (THF) were dried and deoxygenated using a PureSolv MD-5 solvent purification system and were stored over molecular sieves in an argon-filled glovebox. All other deuterated solvents were degassed and stored over molecular sieves in an argon-filled glovebox. PNP-H and (PPh₃)₂ReOBr₂(OEt)¹⁰⁸ were synthesized using reported literature procedures. All other chemical reagents were purchased from commercial suppliers and were used as received. NMR spectra were recorded on a Varian iNova 500 (³¹P{¹H} NMR, 202.276 MHz; ¹³C{¹H} NMR, 125.670 MHz; ¹H NMR, 499.678 MHz) spectrometer in given solvents. Chemical shifts are reported in ppm (δ). ³¹P{¹H} NMR spectra were referenced externally to an 85% phosphoric acid standard at δ 0ppm. ¹³C{¹H} and ¹H NMR spectra were internally referenced to residual solvent resonances. In reporting spectral data, the following abbreviations were utilized: s = singlet; d = doublet; t = triplet; dd = doublet of doublets; vt = virtual triplet; dvt = doublet of virtual triplets; m = multiplet; br = broad; br s = broad singlet; v br = very broad. ATR-IR spectra were collected on an Agilent CARY 630 FT-IR spectrometer. Elemental analyses were performed by CALI, Inc. (Highland Park, NJ, USA).

6.4.2 Synthesis and Reactivity of Manganese and Rhenium Complexes

(PNPⁱPr)ReOBr₂ (600). This compound was synthesized using a modified literature procedure.⁸ To a 50 mL Teflon taped culture tube equipped with magnetic stir bar was added

(PPh₃)₂ReOBr₂(OEt) (1.08 g, 1.16 mmol), PN^HP^{iPr} (525 mg, 1.22 mmol), and 15 mL toluene, forming a tan suspension which quickly turns dark violet. The violet suspension was then heated in an oil bath set to 100 °C for 2 h, over which time it became dark green and solids began to precipitate. The culture tube was cooled to room temperature, brought back into the glovebox, and 35 mL pentane was added, causing additional precipitation. The resultant mixture was then shaken briefly and placed in a freezer set to -38 °C for 1 h, allowing precipitation of the product. The solids were isolated on a fine frit, washed with pentane (2 x 5mL) and dried *in vacuo*, to provide (PNP)ReOBr₂ as a dark, microcrystalline powder. Yield: 805 mg (88%). ¹H NMR (500 MHz, CDCl₃): δ 7.40 (br, 2H, Ar CH), 7.15 (br m, 4H, Ar CH), 3.38 (br, 2H, ⁱPr methine), 3.03 (v br, 2H, ⁱPr methine), 2.51 (s, 6H, benzylic CH₃), 1.54 (br, 18H, three overlapping ⁱPr CH₃), 0.94 (br, 6H, ⁱPr CH₃). ¹³C{¹H} NMR (126 MHz, CDCl₃): δ 165.5, 133.9, 131.2, 128.9, 128.2, 125.3, 28.2 (br), 21.4 (br), 20.2, 19.1, 18.4. ³¹P{¹H} NMR (202 MHz, CDCl₃): δ 27.4 (d, *J*_{P-P} = 186 Hz), 21.9 (d, *J*_{P-P} = 186 Hz). IR: ν_{Re=O} - 940 cm⁻¹ Elem Anal Found(calc): C: 39.19(39.50); H: 4.98(5.10)

(PNP^{iPr})Re(CO)₃ (601). To a 200 mL Teflon stoppered bomb flask equipped with a magnetic stir bar was added (PNP)ReOBr₂ (540 mg, 0.68 mmol), magnesium powder (332 mg, 13.7 mmol), and 10 mL THF, forming a dark green suspension. The resultant suspension was then frozen, degassed, and allowed to thaw (2x) prior to being refilled with 1 atm carbon monoxide. The vessel was then allowed to stir at room temperature for 24 h, over which time the solution became homogeneous and dark yellow. To this solution was added degassed H₂O, resulting in bubbling, and the precipitation of white solids. The resultant opaque, yellow solution was then filtered through silica and Celite on a fine frit, and solvent was removed *in vacuo* to provide the product as a bright yellow, free-flowing powder in >98% purity (¹H NMR evidence). Yield: 459 mg (96%). Spectroscopic data matches that previously reported by Ozerov and Nocera *et al.*^{5c}

(PN^HPⁱPr)ReBr(CO)₂ (603). In a 50 mL Schlenk flask equipped with a magnetic stir bar was added (PNP)Re(CO)₃ (735 mg, 1.05 mmol) and 20 mL toluene, forming a yellow suspension. The flask was then placed under argon and a 30% HBr in AcOH (1.50 mL, 7.54 mmol HBr) solution was added via syringe, resulting in a darkening of solution. The resultant mixture was then fitted with a reflux condenser and brought to reflux for 2 h under argon. Solvent was removed under reduced pressure, giving a light blue solid. The solid was extracted with 5 mL dichloromethane, filtered through a plug of Celite removing orange-brown solids, and then layered with 15 mL of pentane and stored at -37 °C for 12 h over which time additional orange-brown residue precipitated. The solvent was filtered cold through Celite, dried under reduced pressure, washed with pentane and dried once more to provide the product as a blue-green solid. Yield: 585 mg (74%). ¹H NMR (500 MHz, CDCl₃): δ 7.39 (br, 2H, Ar CH), 7.21 (br 1H, N-H), 7.13 (br m, 4H, Ar CH), 2.97 (m, 2H, ⁱPr methine), 2.89 (m, 2H, ⁱPr methine), 2.42 (s, 6H, benzylic CH₃), 1.47 (m, 18H, three ⁱPr CH₃), 1.10 (dvt, *J* = 8.5, 7.1 Hz, 6H, ⁱPr CH₃). ¹³C{¹H} NMR (126 MHz, CDCl₃): δ 205.9 (CO), 195.7 (CO), 136.5, 133.2 (*multiple overlapping signals*), 130.5 (*multiple overlapping signals*), 27.3 (m), 26.2 (d, *J* = 26.4 Hz), 21.6 (br), 20.9, 20.3, 20.2 (*three closely overlapping signals*), 19.0. ³¹P{¹H} NMR (202 MHz, CDCl₃): δ 40.9 (br). ATR-IR: 3346($\nu_{\text{N-H}}$), 1910(ν_{CO}), 1830(ν_{CO}) cm⁻¹. Elem Anal Found(calc): C: 44.41(44.74); H: 5.13(5.50)

(PN^HPⁱPr)MnBr(CO)₂ (603). In a 25 mL schlenk flask equipped with a magnetic stir bar was added (PNP)Mn(CO)₃ (215 mg, 0.38 mmol) and 10 mL toluene, forming an orange suspension. The flask was fitted with a reflux condenser and brought to reflux. Upon achieving reflux a 30% HBr in AcOH (300 μ L, 1.50 mmol HBr) solution was added via syringe, resulting in an immediate color change to yellow as some dark solids were observed to form. Upon HBr addition, an observable increase in solution turbidity was noted, indicating evolution of gaseous

CO. The solution was allowed to reflux an additional 30 min and then solvent was removed under reduced pressure to give a yellow residue. The residue was dissolved in CH₂Cl₂, filtered through Celite twice, and dried under reduced pressure to a yellow, oily solid. This was washed with pentane (2x3mL) and dried again to provide the product as a bright yellow, free-flowing powder. Yield: 220 mg (94%). ¹H NMR (500 MHz, CDCl₃): δ 7.38 (br, 2H, Ar CH), 7.20 (s, 1H, N-H), 7.11 (m, 4H, Ar CH), 2.93 (m, 2H, ⁱPr methine), 2.86 (m, 2H, ⁱPr methine), 2.40 (s, 6H, benzylic CH₃), 1.49 (m, 18H, three ⁱPr CH₃), 1.20 (dvt, *J* = 7.3, 6.8 Hz, 6H, ⁱPr CH₃). ¹³C{¹H} NMR (126 MHz, CDCl₃): δ 135.9, 135.0, 132.3, 130.5, 122.7, 27.8 (m), 26.1 (m), 21.4, 21.2, 20.4, 19.7, 19.6. ³¹P{¹H} NMR (202 MHz, CDCl₃): δ 73.3. ATR-IR: 1916(_νCO), 1836(_νCO) cm⁻¹ Elem Anal Found(calc): C: 54.69(54.21); H: 6.71(6.66)

(PNP^{*i*}Pr)Mn(CO)₂ (605). To a 20 mL scintillation vial equipped with a magnetic stir bar was added (PN^{*H*}P^{*i*}Pr)MnBr(CO)₂ (127 mg, 0.21 mmol) and 3 mL toluene, forming a yellow suspension. To this suspension was added triethylamine (34 μL, 0.23 mmol) causing an immediate color change to dark blue, with concomitant formation of solids (presumed to be HNEt₃Br). The resultant suspension was allowed to stir for 10 min then filtered through a plug of Celite and silica, providing a homogeneous, dark blue solution. Volatiles were removed under reduced pressure and the dark blue residue was washed with pentane (3 x 2 mL) and dried again, giving the product as a dark blue, free-flowing powder. Yield: 85 mg (77%). ¹H NMR (500 MHz, C₆D₆): δ 7.41 (d, *J* = 8.2 Hz, 2H, Ar CH), 6.89 (s, 2H, Ar CH), 6.72 (d, *J* = 8.2 Hz, 2H, Ar CH), 2.56 (m, 4H, ⁱPr methine), 2.11 (s, 6H, benzylic CH₃), 1.27 (dvt, *J* = 9.0, 7.0 Hz, 12H, ⁱPr CH₃), 1.07 (dvt, *J* = 6.6, 6.8 Hz, 12H, ⁱPr CH₃). ¹³C{¹H} NMR (126 MHz, CDCl₃): δ 239.5 (t, *J* = 19.6 Hz, two CO), 162.7 (t, *J* = 16.0Hz), 132.1, 132.0, 122.2 (t, *J* = 14.5 Hz), 115.7 (m), 24.7 (br), 20.5, 18.3, 17.5. ³¹P{¹H}

NMR (202 MHz, C₆D₆): δ 83.7. ATR-IR: 1898(ν_{CO}), 1824(ν_{CO}) Elem Anal Found(calc): C: 62.15(62.33); H: 7.63(7.47)

(PNP^{iPr})Re(CO)₂. (606) To a 20 mL scintillation vial equipped with a magnetic stir bar was added (PN^HP)ReBr(CO)₂ (111 mg, 0.15 mmol) and 3 mL toluene forming a bluish green suspension. To this suspension was added triethylamine (27 μ L, 0.19 mmol) resulting in an immediate color change to dark red as colorless solids (presumed to be HNEt₃Br) were observed to precipitate. The solution was allowed to stir at room temperature for 30 min, then filtered through Celite and silica, and dried *in vacuo*, giving a dark red residue. The resultant residue was washed with pentane (2 x 2 mL) and dried under reduced pressure to give (PNP)Re(CO)₂ as a free-flowing red solid of ca. 97% purity (¹H NMR evidence. Yield: 91 mg (92%). Red, single crystals suitable for X-ray diffraction were grown from CH₂Cl₂ and pentane at -38 °C over 96 h. ¹H NMR (500 MHz, C₆D₆): δ 7.49 (d, J = 8.4 Hz, 2H, Ar CH), 6.91 (br, 2H, Ar CH), 6.80 (d, J = 8.1 Hz, 2H, Ar CH), 2.41 (m, 4H, ⁱPr CH₃), 2.12 (s, 6H, benzylic CH₃), 1.23 (dvt, J = 9.2, 7.3 Hz, 12H, ⁱPr CH₃), 0.98 (dvt, J = 7.4, 7.0 Hz, 12H, ⁱPr CH₃). ¹³C{¹H} NMR (126 MHz, C₆D₆): δ 210.1 (t, $J_{\text{P-C}}$ = 6.0 Hz, two CO), 164.1, 132.9, 131.9, 130.8, 123.4, 116.8, 20.4, 18.8, 17.8. ³¹P{¹H} NMR (202 MHz, C₆D₆): δ 63.9. ATR-IR: 1896(ν_{CO}), 1820(ν_{CO}) cm⁻¹ Elem Anal Found(calc): C: 49.68(50.14); H: 5.86(6.01)

X-ray Diffractometry Details for (PNP^{iPr})Re(CO)₂ (606): A red, multi-faceted block of suitable size (0.26 x 0.24 x 0.09 mm) was selected from a representative sample of crystals of the same habit using an optical microscope and mounted onto a nylon loop. Low temperature (110 K) X-ray data were obtained on a Bruker APEXII CCD based diffractometer (Mo sealed X-ray tube, K_{α} = 0.71073 Å). All diffractometer manipulations, including data collection, integration and scaling were carried out using the Bruker APEXII software. An absorption correction was applied

using SADABS. The space group was determined on the basis of systematic absences and intensity statistics and the structure was solved by direct methods and refined by full-matrix least squares on F^2 . The structure was solved in the orthorhombic $Fdd2$ space group using XS (incorporated in SHELXL). All non-hydrogen atoms were refined with anisotropic thermal parameters. All hydrogen atoms were placed in idealized positions and refined using riding model. The structure was refined (weighted least squares refinement on F^2) and the final least-squares refinement converged. No additional symmetry was found using ADDSYM incorporated in PLATON program.

(PN^HPⁱPr)Re(OAc)(CO)₂ (607): To a J. Young tube was added (PNP)Re(CO)₂ (18 mg, 0.03 mmol), AcOH (2 μ L, 0.03 mmol), and C₆D₆ immediately forming a light green solution. ¹H and ³¹P{¹H} NMR revealed full, clean conversion to the presumed product, (PN^HP)Re(OAc)(CO)₂. ¹H NMR (500 MHz, C₆D₆): δ 7.23 (d, J = 8.0 Hz, 2H), 7.15 (br, 2H), 6.70 (d, J = 8.1 Hz, 2H), 2.63 (br, 4H), 2.08 (s, 6H), 1.72 (br, 3H, *acetate resonance which is in exchange with excess HOAc*), 1.37 (dvt, J = 8.1, 7.2 Hz, 12H), 1.22 (dvt, J = 7.7, 7.2 Hz, 12H). *N-H resonance not located, likely due to exchange with HOAc in solution.* ³¹P{¹H} NMR (202 MHz, C₆D₆): δ 47.4 (v br)

(PN^HPⁱPr)Re(CO₂H)(CO)₂ (608): To a 20 mL scintillation vial was added (PNP)Re(CO)₂ (16.8 mg, 0.025 mmol) and CH₂Cl₂ resulting in a dark red solution. To this solution was added formic acid (5 μ L, 0.1 mmol) resulting in an immediate color change to dark blue. The solvent was then removed under reduced pressure and the residue washed once with 2 mL pentane, and dried *in vacuo* to a green solid. Heating of the isolated samples results in reformation of (PNP)Re(CO)₂ and evolution of H₂ as observed by ¹H NMR evidence. Yield: 18 mg. ¹H NMR (500 MHz, C₆D₆):

δ 13.6 (br, 1H, $-CO_2H$), 8.53 (br, 1H, $N-H$), 7.14 (br, 4H), 6.69 (d, $J = 7.6$ Hz, 2H), 2.61 (br, 4H), 2.08 (s, 6H), 1.31 (br, 12H), 1.20 (br, 12H). $^{31}P\{^1H\}$ NMR (202 MHz, C_6D_6): δ 48.4 (v br)

Reaction of $(PNP^{iPr})Re(CO)_2$ with $(PNP^{iPr})Mn(CO)_3$: To a J. Young tube was added $(PNP^{iPr})Re(CO)_2$ (10.5 mg, 0.016 mmol), $(PNP^{iPr})Mn(CO)_3$ (8.8 mg, 0.016 mmol), and C_6D_6 . The resultant brown-orange suspension was placed on an NMR rotator for 1 h, over which time it became a dark green, homogeneous solution. Analysis by 1H and $^{31}P\{^1H\}$ NMR spectroscopy indicated full, clean conversion to $(PNP^{iPr})Re(CO)_3$ and $(PNP^{iPr})Mn(CO)_2$ in a 1:1 ratio.

Reaction of $(PNP^{iPr})Re(CO)_2$ with $(PNP^{iPr})Mn(CO)_2$: To a J. Young tube was added $(PNP^{iPr})Re(CO)_2$ (13.3 mg, 0.02 mmol), $(PNP^{iPr})Mn(CO)_2$ (10.7 mg, 0.02 mmol) and C_6D_6 , forming a purple solution. This solution was heated at 80 °C and monitored spectroscopically. After 24 h $^{31}P\{^1H\}$ and 1H NMR spectroscopy revealed a 1:1 ratio of $(PNP^{iPr})Re(CO)_2$ and $(PNP^{iPr})Mn(CO)_2$, indicating no reaction have occurred.

Reaction of $(PNP^{iPr})Re(CO)_2$ with CO: To a J. Young tube was added $(PNP)Re(CO)_2$ (17.9 mg, 0.03 mmol) and C_6D_6 , forming a red solution. The solution was then frozen, degassed, and refilled with 1 atm of CO. Upon thawing of the solution and inverting the sample once, it immediately became bright yellow, and full, clean formation of $(PNP)Re(CO)_3$ was observed by 1H and $^{31}P\{^1H\}$ NMR spectroscopy.

Reaction of $(PNP^{iPr})Mn(CO)_2$ with CO: To a J. Young tube was added $(PNP)Mn(CO)_2$ (15.0 mg, 0.03 mmol) and C_6D_6 , forming a dark blue solution. The solution was then frozen, degassed, and refilled with 1 atm of CO. Upon thawing of the solution and inverting the sample, it immediately became a dull orange, and full, clean formation of $(PNP)Mn(CO)_3$ was observed by 1H and $^{31}P\{^1H\}$ NMR spectroscopy.

Reaction of (PNP^{iPr})Re(CO)₂ with benzaldehyde: To a J. Young tube was added (PNP^{iPr})Re(CO)₂ (14.7 mg, 0.022 mmol) and C₆D₆, forming a red solution. To this solution was added benzaldehyde (5 μL, 0.05 mmol) resulting in no color change or immediate observable reaction. The solution was then placed in an oil bath set to 100 °C for 24 h and monitored by NMR spectroscopy. After 24 h, the solution remained scarlet red in color and ¹H NMR and ³¹P{¹H} NMR spectroscopy revealed that no reaction had occurred.

Observation of (PNP)Re(CO)₂(NCMe): To a J. Young tube was added (PNP)Re(CO)₂ (18 mg, 0.027 mmol), acetonitrile (3 μL, 0.05 mmol), and CDCl₃, forming a green solution. ³¹P{¹H} NMR indicated a reaction with a new, broad resonance at ca. δ 46 ppm diagnostic of a six-coordinate species. ¹H NMR spectroscopy revealed very broad signals from which no further structural information was able to be gleaned.

(PNP)Re(CO)₂ Catalyzed Dimerization of Me₃SiCCH: To a J. Young tube was added (PNP)Re(CO)₂ (21.9 mg, 0.033 mmol), C₆D₆, and Me₃SiCCH (46 μL, 0.3 mmol) forming a red solution. The solution was then heated to 100 °C for 24 h and monitored by ¹H NMR spectroscopy. After 24 h, it was found that ca. 63% of the *trans* enyne had formed. Of the remaining organometallic products, ³¹P{¹H} NMR spectroscopy revealed a clean mixture consisting of 40% of (PNP)Re(CO)₂ and 60% of a potential six-coordinate species at δ 45.4 ppm which was not further identified.

Reaction of (PNP)Re(CO)₂ with H₂: to a J. Young tube was added (PNP)Re(CO)₂ (14.5 mg, 0.021 mmol) and C₆D₆, forming a dark red solution. The resultant solution was froze, degassed, and allowed to thaw, three times, and was then refilled with 1 atm of H₂ and monitored by NMR spectroscopy over 24 h. No reaction was observed by either ¹H or ³¹P{¹H} NMR spectroscopy.

Reaction with *in situ* generated HBr: To a J. Young tube was added (PNP)Re(CO)₂ (17 mg, 0.03 mmol), EtOH (3 μL, 0.05 mmol), and C₆D₆ forming a red solution and no observed initial reactivity by ¹H NMR spectroscopy. To the solution was added Me₃SiBr resulting in an immediate color change to light yellow and quantitative formation of (PN^HP)ReBr(CO)₂ as observed by ¹H and ³¹P{¹H} NMR evidence.

Reaction with B₂pin₂: To a J. young tube was added (PNP)Re(CO)₂ (12 mg, 0.02 mmol), B₂pin₂ (10 mg, 0.04 mmol), and C₆D₆, forming a red solution. The sample was then heated at 80 °C for 24 h over which time no reaction was observed by ¹H or ³¹P{¹H} NMR spectroscopy.

Thermolysis in Cyclooctane: To a 10 mL Teflon stoppered tube was added (PNP)Re(CO)₂ (12 mg, 0.02 mmol) and cyclooctane (1 mL), the solution was then heated at 150 °C in an oil bath for 24 h. An aliquot was taken and dissolved in C₆D₆ and no degradation or reaction of (PNP)Re(CO)₂ was observable by NMR spectroscopy.

Reaction with Methyl Iodide: To a J. Young tube was added (PNP)Re(CO)₂ (30 mg, 0.045 mmol), C₆D₆, and MeI (3 μL, 0.05 mmol). The resultant red solution was then heated at 100 °C for 48 h and monitored periodically. After 48 h, no reaction was observed to have occurred.

Reaction with Pinacolborane: To a J. Young tube was added (PNP)Re(CO)₂ (20.6 mg, 0.03 mol), C₆D₆, and HBpin (9 μL, 0.06 mmol). The resultant red solution was heated at 100 °C for 24 h and monitored by ³¹P{¹H} and ¹H NMR spectroscopy. After 24 h, no reaction was observed to have occurred.

Dehydrogenation of Formic Acid: To a J. Young tube was added (PNP)Re(CO)₂ (26.2 mg, 0.04 mmol), C₆D₆, and H₂CO₂ (8 μL, 0.2 mmol). The resultant blue solution was then heated

to 70 °C for 1h over which time it became red. Analysis by ^1H NMR spectroscopy revealed the presence of H_2 with no remaining formic acid resonances.

CHAPTER VII

PINCER LIGANDS CONTAINING ANCILLARY ANTIMONY DONORS**

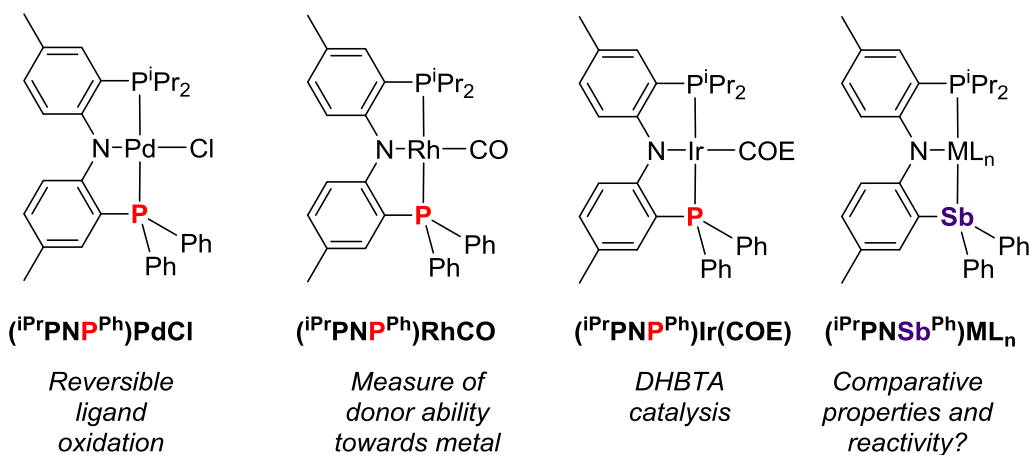
7.1 Introduction

Pincer ligands are widely used in the studies of stoichiometric and catalytic reactions taking place at transition metal centers.¹⁵⁹ The design in which the central pincer donor is connected to the flanking donor sites via an *ortho*-arylene linker is among the most common. A large number of various elements have been employed in the central donor position, including B,¹⁶⁰ C,¹⁶¹ Si,¹⁶² Ge,¹⁶³ N, P,¹⁶⁴ Sb,¹⁶⁵ O,¹⁶⁶ S.¹⁶⁷ Variations of the outer donors have been explored to some extent,^{168,169,170,171} but the overwhelming majority of such pincers utilize either phosphine or nitrogenous donors in the flanking sites. We became interested in examining the potential of stibines in the flanking position of a diarylamido-based pincer and report our efforts in the synthesis and characterization of representative complexes of a new ⁱPrPNSb^{Ph} ligand (Scheme VII-1). Stibines (SbR₃) have occasionally been utilized in coordination chemistry, and their use and properties have been reviewed.^{172,173} However, stibines have not found widespread use as components of multidentate ligands. To the best of our knowledge, the only prior example of the use of an organostibine as a flanking donor in any pincer ligand is in a recent PhD thesis.¹⁷⁴ The role of Sb as a central atom in pincer and tripodal ligand designs has been extensively

** Adapted from “Synthesis and Characterization of Rhodium, Iridium, and Palladium complexes of a Diarylamido-Based PNSb Pincer Ligand” Kosanovich, A. J.; Jordan, A. M.; Bhuvanesh, N.; Ozerov, O. V. *Dalton Trans.* **2018** with permission from The Royal Society of Chemistry, Copyright 2016. DOI: 10.1039/C8DT02207K

explored by the Gabbai group, with the focus on the non-innocence of the coordination and redox behaviour of Sb ligands.^{175,176}

Our previous work on dissymmetric PNP' and PNN pincers targeted (pincer)PdCl complexes for the evaluation of the ease of oxidation of the diarylamido-based ligand and (pincer)RhCO complexes for the comparison of the overall donor ability towards the metal. Various (PNP)Ir complexes proved to be excellent catalysts for the dehydrogenative borylation of terminal alkynes (DHBTA).¹⁷⁷ Here, initially, we focused on the analogous $i\text{PrPN}^{\text{Ph}}\text{Sb}^{\text{Ph}}$ derivatives for convenient comparison with the $i\text{PrPNP}^{\text{Ph}}$ counterparts (Figure VII-1).



Scheme VII-1. Comparison of $i\text{PrPNP}^{\text{Ph}}$ and $i\text{PrPNSb}^{\text{Ph}}$ complexes. Reprinted with permission from The Royal Society of Chemistry, Copyright 2016

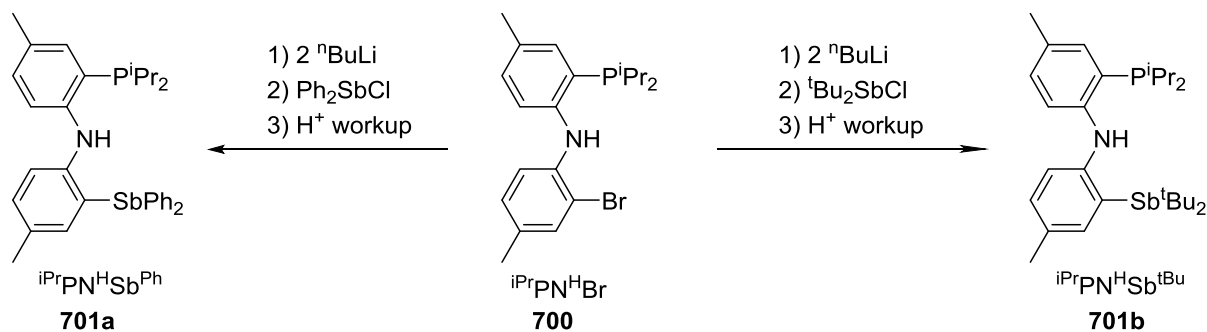
Further, we herein present an asymmetric ligand featuring a di-*tert*butylstibine donor, $i\text{PrPNSb}^{\text{tBu}}$ along with its complexes of iridium, rhodium, and palladium. Studies

were also done on the symmetric $^{\text{Ph}}\text{SbNSb}^{\text{Ph}}$ proligand and its oxidation to bis-stiboranyl amine and bis-stibonium amine complexes.

7.2 Results and Discussion

7.2.1 Synthesis and Spectroscopic Characterization of PNSb Ligands

Similar to the syntheses of $i^{\text{Pr}}\text{PNP}'$ ligands, $i^{\text{Pr}}\text{PN}^{\text{H}}\text{Br}$ (**700**) served as a convenient precursor in the synthesis of $i^{\text{Pr}}\text{PN}^{\text{H}}\text{Sb}^{\text{Ph}}$ (**701a**) and $i^{\text{Pr}}\text{PN}^{\text{H}}\text{Sb}^{\text{tBu}}$ (**701b**) (Scheme VII-2). Lithiation of **700** with 2 equiv. of $^n\text{BuLi}$ followed by reaction with one equiv. of Ph_2SbCl or $^t\text{Bu}_2\text{SbCl}$ produced **701a** and **701b**, respectively, which were isolated in moderate yields. **701a** and **701b** present the expected C_s symmetry in their NMR spectra. Single ^{31}P NMR resonances are present at -15.4 ppm and -15.6 ppm, and the ^1H NMR N-H resonances (**701a**, δ 7.27 (d, $J_{\text{H-P}} = 6$ Hz); **701b**, δ 7.80 (d, $J_{\text{H-P}} = 11.1$ Hz)) appear at chemical shifts similar to the corresponding $\text{PN}^{\text{H}}\text{P}'$ ligands.

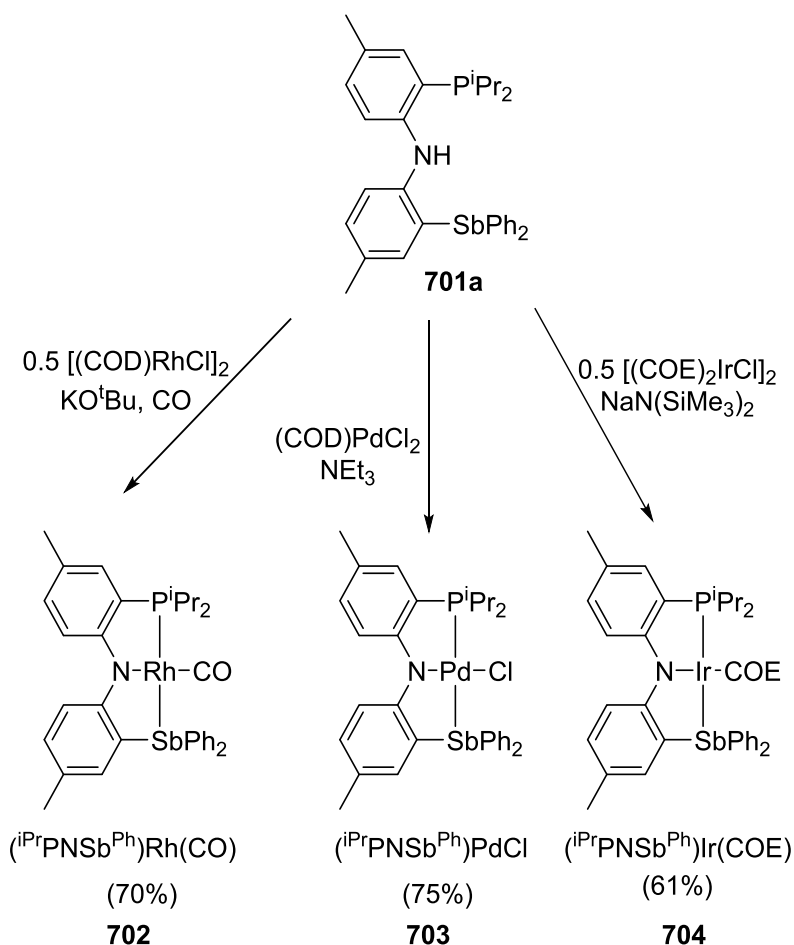


Scheme VII-2. Synthesis of PNSb pincer ligands

7.2.2 Metalation of the PNSb Ligand to Rhodium, Palladium, and Iridium

The synthesis of $(iPrPNSb^{Ph})RhCO$ (**702**) was accomplished by treatment of **701a** with $[(COD)RhCl]_2$, potassium *t*-butoxide, and CO, with a 70% isolated yield. Reaction of **701a** with $(COD)PdCl_2$ in the presence of Et_3N permitted isolation of $(iPrPNSb^{Ph})PdCl$ (**703**). **703** was obtained in ca. 95% purity and ca. 75% yield. Recrystallization yielded analytically pure samples of **703** at the expense of yield (26%). Interestingly, **703** appears in two solid forms of different color (purple and bright green). Dissolution of either results in a turquoise solution of identical spectral properties.

To prepare an Ir derivative, **701a** was reacted with one equiv of $NaN(SiMe_3)_2$, followed by 0.5 equiv of $[(COE)_2IrCl]_2$, providing upon workup a 61% yield of $(iPrPNSb^{Ph})Ir(COE)$ (**704**). C_6D_6 solutions of **704** were observed to undergo decomposition to unidentified compounds upon standing for 24 h (Scheme VII-3).



Scheme VII-3. Metalation of the $\text{iPrPNSb}^{\text{Ph}}$ proligand. Reprinted with permission from The Royal Society of Chemistry, Copyright 2016

7.2.3 Spectroscopic Analysis of PNSb^{Ph} Complexes

Similarly to **701a**, the Rh and Pd complexes possess an apparent C_s symmetry in their NMR spectra at ambient temperature. The six aromatic resonances of the diarylamine backbone exhibit closely similar patterns in the three metal complexes, consistent with the structural similarity of the meridionally disposed diarylamido-PNSb ligand. Some of the Sb-C₆H₅ and the P-CHMe₂ resonances of **703** are significantly broadened in the ¹H NMR spectrum. It is possible that this reflects the slowed “flipping” motion of the two aromatic

rings of the diarylamido backbone past each other. In **704** this motion is apparently even slower, resulting in the observed C_1 symmetry by NMR spectroscopy at ambient temperature. We previously analyzed this in (PNN)PdCl complexes, coming to the conclusion that the enlarged ring size associated with the imine vs phosphine side donor pushes the two diarylamido rings closer together. Although PNSb forms the same {5,5}-pincer rings (in the Fryzuk notation)⁷⁴ as PNP, Sb is a considerably larger atom that may result in an effect similar to that caused by ring expansion. VT-NMR studies of **703** evince C_1 symmetry at -40 °C (inequivalent Ph groups and inequivalent ⁱPr groups) and C_s symmetry with sharp lines at +60 °C, consistent with the “flipping” proposal.

7.2.4 Infrared and Electrochemical Analysis of $PNSb^{Ph}$ Complexes

The $^1J_{P-Rh} = 167$ Hz in **702** is greater than the analogous value for the $-P^iPr_2$ phosphine (133 Hz) in the (ⁱPrPNP^{Ph})RhCO analog. Considering the IR spectra, the ν_{CO} value in **702** is higher than that in (ⁱPrPNP^{Ph})RhCO (1951 vs 1941 cm^{-1}) (Figure VII-1). Cyclic voltammetry studies indicated that the redox potential for **703** ($E_{1/2} = 0.00$ V vs Fc/Fc⁺) does not differ significantly from that of (ⁱPrPNP^{Ph})PdCl ($E_{1/2} = -0.02$ V vs Fc/Fc⁺) (Figure VII-2). The range of redox potential values among the various (PNP)PdCl complexes with different organic substituents on the P donors exceeded 0.02 V. Our data suggest that the $-SbPh_2$ donor is less donating towards the metal and possesses weaker *trans*-influence than $-PPh_2$, but has a similar influence on the ease of oxidation of the diarylamido π -system. The conclusion concerning the donor strength and the *trans*-influence of a stibine vs phosphine agrees with the discussion by Levason and Reid in their 2006 review.¹⁷²

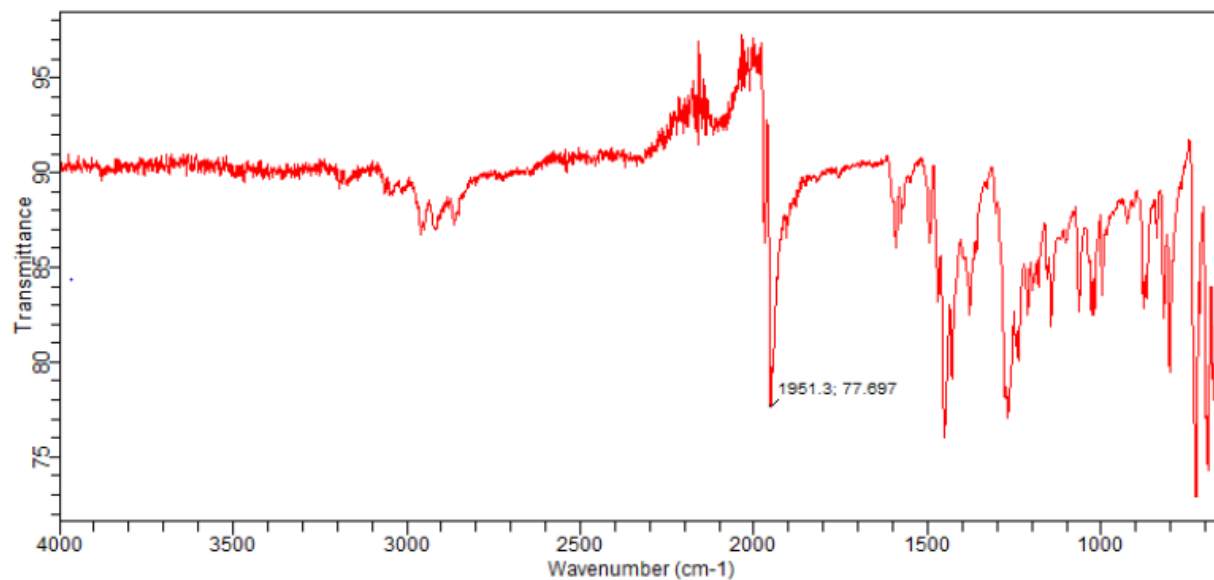


Figure VII-1. ATR-IR spectrum of $(i\text{Pr})\text{PNSb}^{\text{Ph}}\text{Rh}(\text{CO})$ (**702**) featuring a diagnostic CO stretch at 1951 cm^{-1} . Reprinted with permission from The Royal Society of Chemistry, Copyright 2016

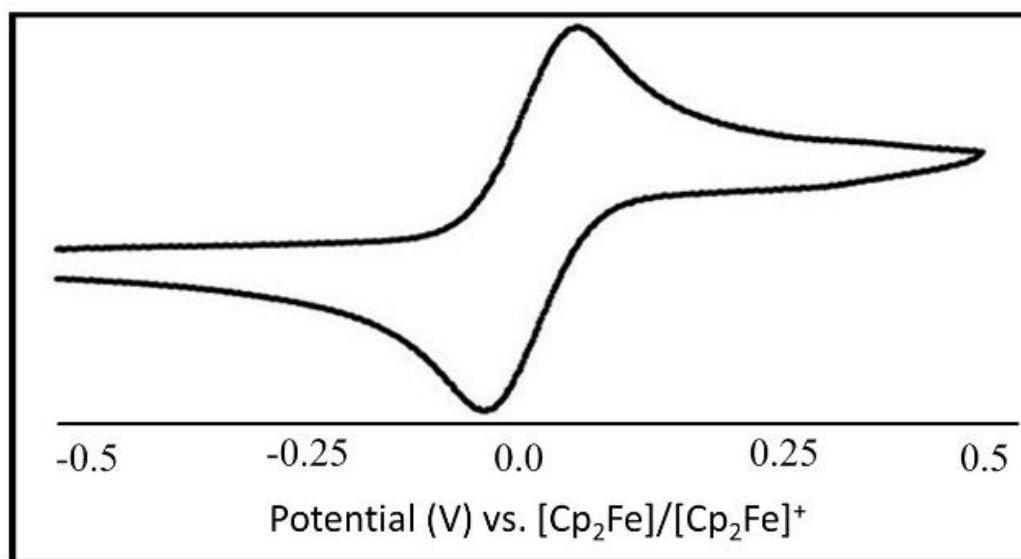


Figure VII-2. Cyclic voltammogram of $(i\text{Pr})\text{PNSb}^{\text{Ph}}\text{PdCl}$ (**703**) in CH_2Cl_2 at $25\text{ }^\circ\text{C}$. The scan rate was 100 mV/s in the positive direction. The cyclic voltammogram was obtained with $0.1\text{ M } [\text{Bu}_4\text{N}][\text{PF}_6]$ as the supporting electrolyte and resulted in a measured potential ($E_{1/2}$) equal to $0.0\text{ V vs. } [\text{Cp}_2\text{Fe}]/[\text{Cp}_2\text{Fe}]^+$. Reprinted with permission from The Royal Society of Chemistry, Copyright 2016

7.2.5 Structural Characterization and Analysis of the PNSb^{Ph} Ligand

An X-ray diffraction study on a single crystal of **702** allowed the determination of the solid-state structure of this complex (Figure VII-3). As expected, an approximately square-planar environment was determined about the Rh center. The Rh-P distance (2.2626(14) Å) is slightly shorter than the Rh-PⁱPr₂ distance in (ⁱPrPNP^{Ph})RhCO (2.2861(4) Å), consistent with the notion of -SbPh₂ exerting weaker *trans*-influence than -PPh₂. The Rh-Sb distance of 2.5539(5) Å appears to be unremarkable. For comparison, Rh-Sb distances determined for the structures of (Ph₃Sb)₃Rh(COMe)(CO),¹⁷⁸ (Ph₃Sb)₃Rh(Cl)(CO), and *trans*-(Ph₃Sb)₂Rh(Cl)(CO) fall into the 2.55-2.63 Å range.

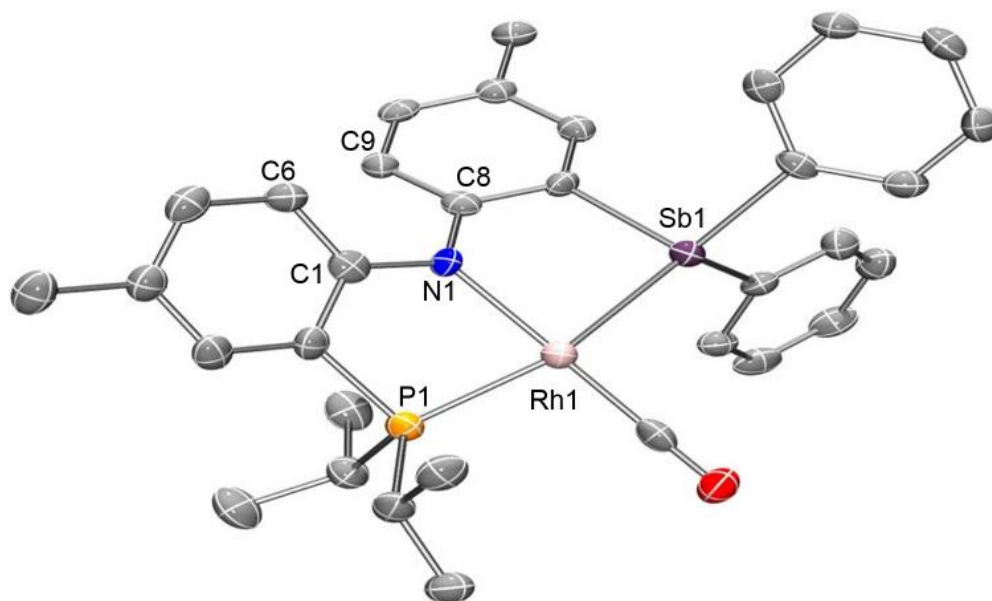
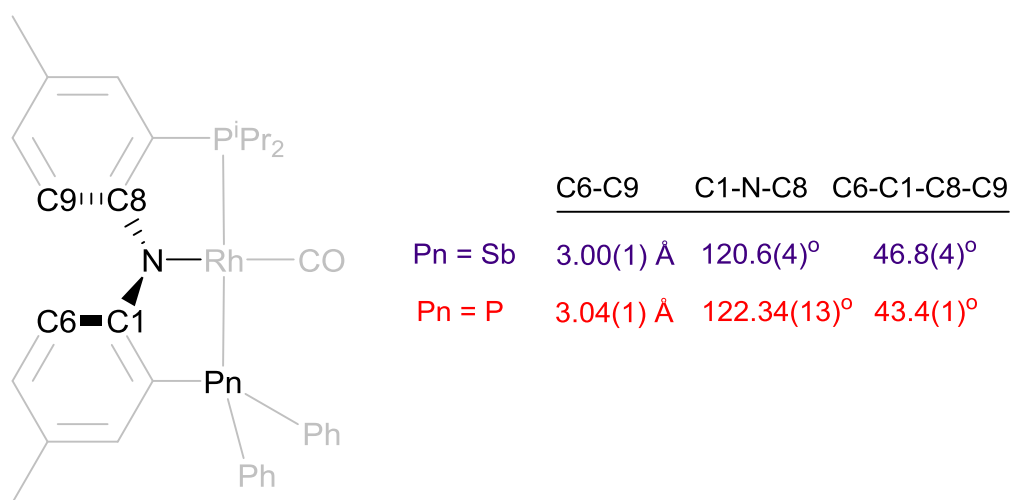


Figure VII-3. ORTEP drawing (50% probability ellipsoids) of $(i\text{PrPNSb}^{\text{Ph}})\text{Rh}(\text{CO})$ (**702**). H atoms are omitted for clarity. Selected distance (Å) and angles (deg): Rh1-N1, 2.105(4); Rh1-P1, 2.263(1); Rh1-Sb1, 2.5539(5); P1-Rh1-Sb1, 161.30(4). Reprinted with permission from The Royal Society of Chemistry, Copyright 2016



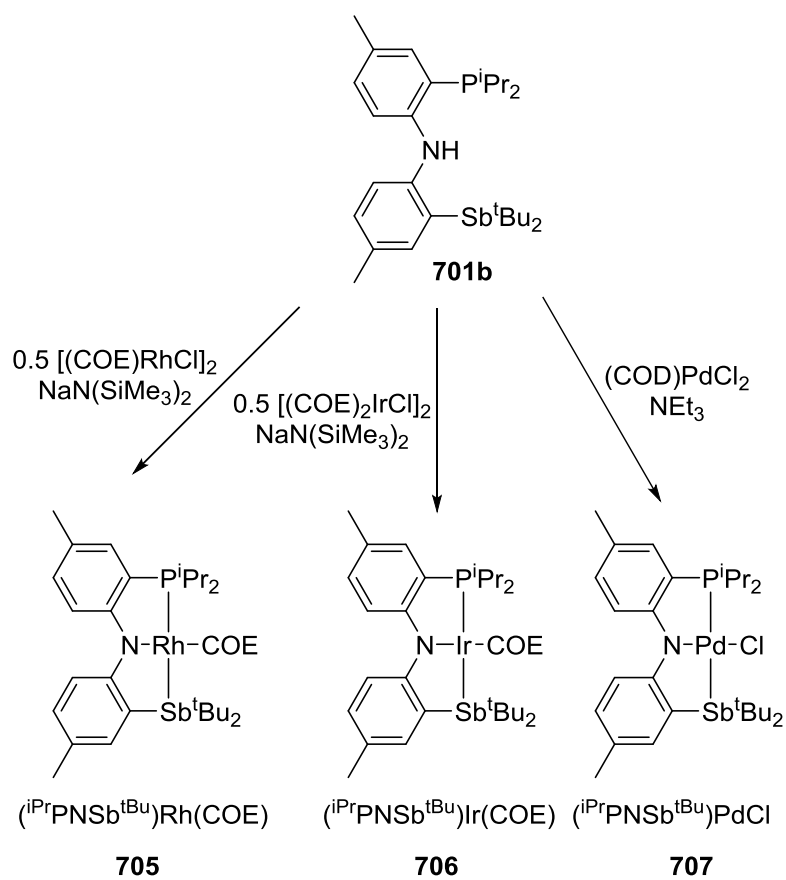
Scheme VII-4. Selected metrics from the X-ray structures of $(i\text{PrPNSb}^{\text{Ph}})\text{Rh}(\text{CO})$ (**702**) and $(i\text{PrPNP}^{\text{Ph}})\text{Rh}(\text{CO})$. Reprinted with permission from The Royal Society of Chemistry, Copyright 2016

The larger size of Sb vs P does have an influence on the exact geometry of the diarylamido backbone. As illustrated in Scheme VII-4, the dihedral angle (C6-C1-C8-C9) between the two diarylamido rings is greater, the C1-N-C8 angle is smaller, and the distance between the two *ortho*-CH carbons (C6-C9) is smaller in **702** than in (ⁱPrPNP^{Ph})RhCO. These differences, albeit modest, are consistent with the greater difficulty of the “flipping” of the two rings past each other in PNSb complexes because of the extra hindrance arising from the closer disposition of the C-H bonds from C6 and C9.

7.2.6 Metalation of PNSb^{tBu} to Rhodium, Iridium, and Palladium

The synthesis of **701b** and its subsequent metalations were performed following the publication of **701a** and its complexes. The metalation of the **701b** was achieved in similar fashion as **701a** was installed (Scheme VII-5). Reaction of the *in situ* generated sodium salt using NaN(SiMe₃)₂ followed by reaction with [(COE)₂RhCl]₂ or [(COE)₂IrCl]₂ smoothly furnished (ⁱPrPNSb^{tBu})Rh(COE) (**705**) and (ⁱPrPNSb^{tBu})Ir(COE) (**706**) in good yields. Both **705** and **706** exhibit a single resonance by ³¹P{¹H} NMR spectroscopy (**705**, δ 56.6 ppm (d, *J*_{Rh-P} = 182.6 Hz); **706**, δ 31.1 ppm). ¹H NMR spectroscopy revealed all expected resonances as well as C₁-symmetry in solution for **705** and **706**. (ⁱPrPNSb^{tBu})PdCl (**707**) was synthesized *via* reaction of **701b** with (COD)PdCl₂ and NEt₃ and was isolated as a blue powder in moderate yields. **707** features a single resonance by ³¹P{¹H} NMR spectroscopy at 55.6 ppm. Similar to **703**, **707** features some broadness of the *isopropyl* resonance in its ¹H NMR spectrum, likely due to rotational motion of the diarylamido backbone on the NMR timescale. **707** otherwise has sharp resonances corresponding to six separate aromatic

C-H protons, two methyl resonances (6H each) for the diastereotopic methyl substituents on the *isopropyl* phosphine, and a single *tert*-butyl resonance (δ 1.47 ppm, 18H).

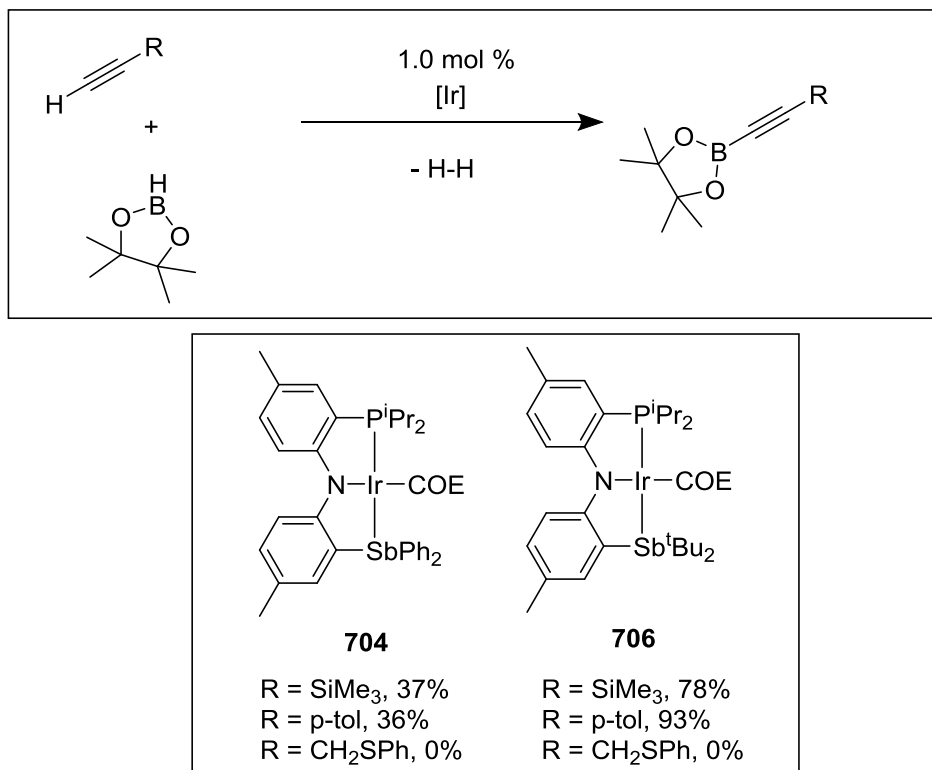


Scheme VII-5. Metalation of the $iPrPNSb^tBu$ proligand

7.2.7 Catalytic Activity of PNSb-Iridium Complexes in DHBTA

Iridium complexes supported by the $iPrPNP^{Ph}$ and other tested PNP ligands proved to be excellent catalysts for DHBTA.¹⁷⁷ For example, with 0.25% loading of **704** as the precatalyst, DHBTA of *p*-MeC₆H₄CCH was observed to be complete within 10 min at

ambient temperature. In contrast, the reactivity of **704** as a DHBTA catalyst turned out to be poor and unselective (Scheme VII-6).



Scheme VII-6. Catalytic dehydrogenative borylation of terminal alkynes by PNSb complexes of iridium

A negligible amount of the DHBTA product of *p*-MeC₆H₄CCH was detected after 40 min at ambient temperature with 1% of **704** as the precatalyst. Heating of the mixture at 80 °C for 15 min did result in the consumption of *p*-MeC₆H₄CCH, however, only 36% of the alkyne was converted into the DHBTA product, with hydroboration products

accounting for another 38% (25% trans, 13% cis). The remaining organic products in the mixture were not identified. Thus, $i\text{PrPNSb}^{\text{Ph}}$ as the supporting ligand results in a much lower DHBTA reaction rate and much poorer chemoselectivity when compared with $i\text{PrPNP}^{\text{Ph}}$. Similar conversion was also observed with trimethylsilylacetylene as well. Switching to 1.0 mol% ($i\text{PrPNSb}^{\text{tBu}}$)Ir(COE) (**706**) as precatalyst resulted in a marked increase in catalytic activity with 93% conversion of p-MeC₆H₄CCH to the corresponding alkynylboronate in 3 h at room temperature. **706** also performed well with trimethylsilylacetylene, providing 78% formation of the alkynylboronate. Unfortunately, similarly to the PNP variants, neither **704** or **706** showed any DHBTA activity for propargyl phenylsulfide.

7.3 Conclusion

In conclusion, we have synthesized –PdCl, -RhCO, Rh(COE), and -Ir(COE) complexes of new diarylamido-based $i\text{PrPNSb}^{\text{Ph}}$ and $i\text{PrPNSb}^{\text{tBu}}$ ligands with a flanking stibine donor site. Comparison of $i\text{PrPNSb}^{\text{Ph}}$ complexes with the $i\text{PrPNP}^{\text{Ph}}$ analogs indicated that a) –SbPh₂ acts as donor of lesser trans influence and lesser donor ability than –PPh₂; 2) –SbPh₂ vs –PPh₂ substitution does not significantly affect the ease of oxidation of the diarylamido ligand system; 3) $i\text{PrPNSb}^{\text{Ph}}$ and $i\text{PrPNSb}^{\text{tBu}}$ are not nearly as effective in supporting Ir for the catalysis of DHBTA, in contrast to $i\text{PrPNP}^{\text{Ph}}$ and other PNP ligands.

7.4 Experimental

7.4.1 General Considerations

Unless otherwise stated, all experiments were carried out using standard glovebox and Schlenk line techniques under a dry argon atmosphere. C₆D₆ was dried over NaK, benzophenone, and 18-crown-6, distilled, and stored over molecular sieves in an argon glovebox prior to usage. Diethyl ether, pentane and toluene were dried and deoxygenated using a PureSolv MD-5 solvent purification system and were stored over molecular sieves in an argon-filled glovebox. PNB_r was synthesized using previously reported procedures. Ph₂SbCl was synthesized by a neat 2:1 reaction of SbPh₃ and SbCl₃, used as received from commercial suppliers. NMR spectra were recorded on a Varian iNova 500 (³¹P{¹H} NMR, 202.276 MHz; ¹³C{¹H} NMR, 125.670 MHz; ¹H NMR, 499.678 MHz) spectrometer in given solvents. Chemical shifts are reported in ppm (δ). ³¹P{¹H} NMR spectra were referenced externally to an 85% phosphoric acid standard at δ 0ppm. ¹³C{¹H} and ¹H NMR spectra were internally referenced to residual solvent resonances. In reporting spectral data, the following abbreviations were utilized: s = singlet; d = doublet; t = triplet; dd = doublet of doublets; dm = doublet of multiplets; sept. d. = septet of doublets; m = multiplet. NMR resonances assigned to either the “*aromatic backbone C-H*” or annotated as “*Sb-ring C-H*” or “*P-ring C-H*” refer to those arising from the general ditolylamine ligand motif, or those specific rings containing the respective stibine or phosphine donor. Infrared spectra were collected on an Agilent CARY FT-IR spectrometer. Elemental analyses were performed by CALI, Inc. (Highland Park, NJ, USA). Electrochemical studies were carried out using a GAMRY Ref600 potentiostat under argon with a three electrode setup: A glassy carbon disk (BasInc) working electrode, a non-aqueous reference electrode (Ag/Ag⁺ CH₂Cl₂; BasInc) separated from solution by a fine porosity frit, and graphite counter electrode (Alfa Aesar). Solutions were 1.0 mM in analyte and 0.1 M in supporting electrolyte (NBu₄PF₆) and spectra were referenced to the ferrocene/ferrocenium redox couple.

7.4.2 Synthetic Details for Antimony-Containing Complexes

$iPrPN^H Sb^Ph(701a)$: To a 50 mL Schlenk flask equipped with magnetic stir bar was added **700** (530 mg, 1.35 mmol) and 30 mL diethyl ether. To this stirring solution was added a 2.5 M solution of *n*-butyllithium in hexanes (1.08 mL, 2.7 mmol) causing the solution to become yellow and slightly cloudy. The mixture was allowed to stir for 3 h, and then Ph_2SbCl (441 mg, 1.42 mmol) was added in one portion, resulting in an immediate darkening of solution and formation of a colorless precipitate. The resultant mixture was allowed to stir for 24 h, then 1 mL degassed H_2O was added, and the solvent was removed under reduced pressure, providing a yellow, sticky solid. This residue was then dissolved in diethyl ether, filtered through Celite and silica, and dried under reduced pressure to give a yellow powder. The powder was washed with *isooctane* and dried *in vacuo* to provide the product as a white, free-flowing solid. Yield: 387 mg (49%). 1H NMR (500 MHz, C_6D_6): δ 7.55 (dd, $J = 7.5, 1.8$ Hz, 4H, *-SbPh₂*), 7.34 (d, $J = 12.2$ Hz, 1H, *N-H*), 7.29 (s, 1H, *Sb-ring C-H*), 7.28 (d, $J = 8.1$ Hz, 1H, *P-ring C-H*), 7.10 (m, 7H, *-SbPh₂* and overlapping aromatic backbone *C-H*), 6.95 (m, 2H, two overlapping aromatic backbone *C-H*), 6.86 (dd, $J = 8.3, 1.6$ Hz, 1H, *P-ring C-H*), 2.16 (s, 3H, *benzylic CH₃*), 1.97 (s, 3H, *benzylic CH₃*), 1.87 (sept. d., $J = 6.9, 2.9$ Hz, 2H, *iPr-methine*), 1.01 (dd, $J = 15.6, 7.0$ Hz, 6H, *iPr-CH₃*), 0.91 (dd, $J = 12.1, 6.9$ Hz, 6H, *iPr-CH₃*). $^{13}C\{^1H\}$ NMR (126 MHz, C_6D_6): δ 150.2 (d, $J = 19.5$ Hz), 146.5 (d, $J = 1.4$ Hz), 139.1, 137.9, 137.3, 137.0, 135.0, 134.2 (m), 133.3, 131.3, 131.0, 129.3, 128.7, 124.2, 120.2 (d, $J = 14.7$ Hz), 116.0 (d, $J = 2.8$ Hz), 23.7 (d, $J = 10.5$ Hz), 20.9 (d, $J = 8.0$ Hz), 20.6, 20.4, 19.3 (d, $J = 9.3$ Hz). $^{31}P\{^1H\}$ NMR (202 MHz, C_6D_6): δ -15.4. ATR-IR = $\nu_{N-H} - 3255$ cm^{-1} . Elem Anal Found (calc): C: 65.16 (65.32) H: 6.41 (6.34)

$i\text{PrPN}^{\text{H}}\text{Sb}^{\text{tBu}}$ (701b): To a 50 mL Schlenk flask equipped with magnetic stir bar was added **700** (310 mg, 0.79 mmol) and 20 mL diethyl ether. To this stirring solution was added a 2.5 M solution of *n*-butyllithium in hexanes (0.63 mL, 1.6 mmol) causing the solution to become yellow and slightly cloudy. The mixture was allowed to stir for 3 h, and then ${}^{\text{tBu}}_2\text{SbCl}$ (236 mg, 0.87 mmol) was added in one portion, resulting in an immediate darkening of solution and formation of a colorless precipitate. The resultant mixture was allowed to stir for 36 h, then 1 mL degassed H_2O was added, and the solvent was removed under reduced pressure, providing a yellow, sticky solid. This residue was then dissolved in diethyl ether, filtered through Celite and silica, and dried under reduced pressure to give the product as a yellow paste of ca. 93% purity, which further solidified upon standing. Yield: 397 mg (92%). ${}^1\text{H}$ NMR (500 MHz, C_6D_6): δ 7.80 (d, $J_{\text{P-H}} = 11.1$ Hz, 1H, N-H), 7.64 (dd, $J = 1.8, 0.4$ Hz, 1H), 7.37 (d, $J = 8.2$ Hz, 1H), 7.13 (dd, $J = 8.3, 4.8$ Hz, 1H), 6.94 (m, 2H), 6.90 (ddd, $J = 8.3, 1.6, 0.5$ Hz, 2H), 2.20 (s, 3H), 2.17 (s, 3H), 2.01, (sept d, $J = 7.0, 2.7$ Hz, 2H), 1.36 (s, 18 H, Sb^{tBu}_2), 1.15 (dd, $J = 15.4, 7.0$ Hz, 6H), 1.01 (dd, $J = 12.0, 7.0$ Hz, 6H). ${}^{31}\text{P}\{^1\text{H}\}$ NMR (202 MHz, C_6D_6): δ -15.6.

$(i\text{PrPNSb}^{\text{Ph}})\text{Rh}(\text{CO})$ (702): To a 10 mL Teflon stoppered flask equipped with a magnetic stir bar was added **701a** (50 mg, 0.085 mmol), $[(\text{COD})\text{Rh}(\mu\text{-Cl})]_2$ (21 mg, 0.042 mmol), KO^{tBu} (14 mg, 0.13 mmol), and 4 mL PhF as solvent, forming a yellow-orange suspension. The suspension was frozen, degassed, and refilled with 1 atm CO, then placed in an oil bath set to 60 °C for 24 h. Over this time, the solution darkened in color. The resultant solution was filtered through a plug of Celite and silica, and solvent was removed *in vacuo* to give a dark residue. The residue was washed with cold pentane and dried to provide the product as a red-orange solid. Single crystals suitable for X-ray diffraction were grown over 48 h from a concentrated diethyl ether solution at -38 °C. Yield: 42 mg (70%). ${}^1\text{H}$ NMR (500 MHz, C_6D_6) δ 7.75 (d, $J = 8.5$ Hz,

1H, *Sb*-ring C-H), 7.69-7.63(m, 5H, -*SbPh*₂ and overlapping *P*-ring C-H), 7.29 (d, *J* = 1.9 Hz, 1H, *Sb*-ring C-H), 7.04 – 6.97 (m, 6H, -*SbPh*₂), 6.89 (dd, *J* = 8.3, 1.8 Hz, 1H, aromatic backbone C-H), 6.82 (dd, *J* = 8.5, 2.2 Hz, 1H, aromatic backbone C-H), 6.77 (d, *J* = 8.6 Hz, 1H, *P*-ring C-H), 2.19 (sept., *J* = 7.5 Hz, 2H, *iPr*-methine), 2.17 (s, 3H, benzylic CH₃), 1.99 (s, 3H, benzylic CH₃), 1.30 (dd, *J* = 17.2, 6.9 Hz, 6H, *iPr*-CH₃), 1.05 (dd, *J* = 15.5, 6.9 Hz, 6H, *iPr*-CH₃). ¹³C NMR (126 MHz, C₆D₆): δ 196.1 (dd, *J*_{Rh-C} = 63.6, ²*J*_{Pj-C} = 13.7 Hz, *Rh*-CO), 164.3 (dd, *J* = 21.5, 2.1 Hz), 160.6, 136.2, 132.6, 132.0, 131.5, 130.0, 129.6 (two overlapping singlets), 127.5 (d, *J* = 20.3 Hz), 126.7, 125.3 (d, *J* = 6.5 Hz), 121.3 (d, *J* = 40.4 Hz), 118.5 (d, *J* = 12.3 Hz), 117.7, 26.2-25.4 (m), 20.5, 20.3, 19.5, 18.4. ³¹P{¹H} NMR (202 MHz, C₆D₆): δ 71.1 (d, *J*_{Rh-P} = 167 Hz). ATR-IR: ν_{Rh-CO} - 1951 cm⁻¹ Elem Anal Found (calc): C: 55.30(55.18) H: 4.99(5.05)

(*iPr*PNSb^{Ph})PdCl (703): To a J. Young tube was added **701a** (48 mg, 0.082 mmol), (COD)PdCl₂ (23 mg, 0.081 mmol), triethylamine (14 μL, 0.10 mmol), and PhF, forming a dark yellow-green suspension. The suspension was heated in an oil bath at 60 °C for 1 h, and then placed on a rotator for 18 h over which time a dark turquoise solution had formed with a colorless precipitate (presumed to be HNEt₃Cl) observed. Filtration through a plug of Celite and silica, followed by solvent removal under reduced pressure provide a dark turquoise solid determined to be ca. 95% pure (¹H and ³¹P{¹H} NMR evidence). Crude yield: 44 mg (75%). This solid could be recrystallized from a concentrated Et₂O solution at -38 °C to give separate polymorphic crops of bright green and purple solids. Recrystallized yield: 15 mg (26%). Upon dissolving, both form a turquoise solution, and share identical spectroscopic characteristics. ¹H NMR (500 MHz, C₆D₆) δ 7.96-7.37 (v br, 4H, -*SbPh*₂) 7.64 (d, *J* = 8.5 Hz, 1H, *Sb*-ring C-H), 7.55 (dd, *J* = 8.6, 4.3 Hz, 1H, *P*-ring C-H), 7.26 (s, 1H, *Sb*-ring C-H), 6.97 (br, 6H, -*SbPh*₂), 6.80 (d, *J* = 10.0 Hz, 1H, aromatic backbone C-H), 6.78 (dd, *J* = 8.6, 2.2 Hz, 1H, aromatic backbone C-H), 6.71 (d, *J* = 8.6 Hz, 1H,

aromatic backbone C-H), 2.31 (v br, 2H, *iPr-methine*), 2.11 (s, 3H, *benzylic CH₃*), 1.93 (s, 3H, *benzylic CH₃*), 1.46 (dd, $J = 17.5, 6.5$ Hz, 6H, *iPr-CH₃*), 1.12 (br, 6H, *iPr-CH₃*). $^{13}\text{C}\{^1\text{H}\}$ NMR (126 MHz, C_6D_6): δ 163.8 (d, $J = 20$ Hz), 160.4, 136.5 (br), 136.3, 133.1, 132.0, 131.4, 130.1, 129.6, 128.8, 126.7 (d, $J = 6.7$ Hz), 124.1 (d, $J = 3.9$ Hz), 120.3 (d, $J = 14.3$ Hz), 119.8 (d, $J = 42.8$ Hz), 118.8, 115.5 (d, $J = 21.0$ Hz), 28.4, 20.4, 20.3, 18.7 (br), 17.8 (br). ^{31}P NMR (202 MHz, C_6D_6) δ 69.6. Elem. Anal. Found (calc). C: 52.89 (52.71); H: 5.10 (4.98)

(*iPr*PNSb^{Ph})Ir(COE) (**704**): To a 20 mL scintillation vial was added **701a** (60 mg, 0.10 mmol), $\text{NaN}(\text{SiMe}_3)_2$ (18 mg, 0.10 mmol), and 2 mL PhF, resulting in a bright yellow solution. The resultant solution was then transferred to a stirring PhF solution of $[(\text{COE})_2\text{IrCl}]_2$ (45 mg, 0.050 mmol) causing a color change to dark red with immediate formation of colorless solids (presumed to be NaCl). The suspension was allowed to stir for 1.5 h after which time it was filtered through a plug of Celite and silica, and solvent was removed under reduced pressure to give a scarlet red residue. The residue was washed with diethyl ether (2 x 2 mL) and dried under vacuum for 24 h which removes residual diethyl ether, cyclooctene, and $\text{HN}(\text{SiMe}_3)_2$ to provide the product as a scarlet red powder of analytical purity. Yield: 55 mg (61%). In C_6D_6 solutions over 24 h at room temperature, **704** can be observed (NMR evidence) to decompose to an unidentified mixture of products. ^1H NMR (500 MHz, C_6D_6): δ 8.01 (br s, 2H, *-SbPh₂*), 7.69 (d, $J = 8.5$ Hz, 1H, *aromatic backbone C-H*), 7.54 (br s, 3H, *-SbPh₂* and overlapping *aromatic backbone C-H*), 7.24 (s, 1H, *Sb-ring C-H*), 7.03 (br s, 6H, *-SbPh₂*), 6.88 (d, $J = 8.0$ Hz, 1H, *aromatic backbone C-H*), 6.84 (d, $J = 8.6$ Hz, 1H, *aromatic backbone C-H*), 6.73 (d, $J = 8.5$ Hz, 1H, *P-ring C-H*), 3.26 (br s, 1H, *COE vinylic C-H*), 3.18 (br s, 1H, *COE vinylic C-H*), 2.89 (br s 1H), 2.43 – 2.28 (br m, 3H), 2.17 (s, 3H, *benzylic CH₃*), 2.04 (s, 3H, *benzylic CH₃*), 1.72 – 1.63 (m, 3H), 1.63 – 1.54 (m, 4H), 1.54 – 1.37

(m, 5H), 1.37-1.25 (m, 1H), 1.08 – 0.96 (m, 9H, *overlapping iPr-CH₃ and COE resonances*). ³¹P NMR (202 MHz, C₆D₆): δ 32.5. Elem. Anal. Found (calc). C: 53.87 (53.99); H: 5.50 (5.66)

(ⁱPrPNSb^tBu)Rh(COE) (705): To a 20 mL scintillation vial equipped with a magnetic stir bar was added [(COE)₂RhCl]₂ (10 mg, 0.014 mmol) and PhF, resulting in an orange suspension. To the stirring suspension was added an orange PhF solution of **701b** (16.1 mg, 0.028 mmol) and NaN(SiMe₃)₂ (5.4 mg, 0.028 mmol) causing an immediate color change to dark red with the noted precipitation of colorless solids (presumed to be NaCl). The mixture was allowed to stir for 1 h, then was filtered through a plug of Celite and silica, and volatiles were removed *in vacuo* to furnish an orange solid. The solid was washed with cold pentane and dried under reduced pressure to provide the product as a free-flowing red solid. Yield: 15 mg (71%). ¹H NMR (500 MHz, C₆D₆): δ 7.45 (d, *J* = 8.4 Hz, 1H), 7.40 (d, *J* = 8.5, 4.0 Hz, 1H), 7.38 (d, *J* = 1.7 Hz, 1H), 6.82 (ddd, *J* = , 8.4, 2.2, 0.7 Hz, 1H), 6.79 (d, *J* = 7.9 Hz, 1H), 6.76 (d, *J* = 8.5 Hz, 1H), 3.61 (m, 1H), 3.40 (m, 1H), 2.61 (m, 1H), 2.22 (s, 3H), 2.17 (s, 3H), 2.08 (m, 3H), 1.74 (m, 7H), 1.62 (s, 9H), 1.59 (dd, *J* = 17.0, 7.1 Hz, 3H), 1.45 (s, 9H), 1.43 (m, 3H), 1.13 (dd, *J* = 15.5, 7.0 Hz, 3H), 1.03 (dd, *J* = 11.4, 6.9 Hz, 3H), 0.95 (dd, *J* = 13.6, 7.3 Hz, 3H). ³¹P NMR (202 MHz, C₆D₆): δ 56.6 (d, *J*_{Rh-P} = 182.6 Hz)

(ⁱPrPNSb^tBu)Ir(COE) (706): To a 20 mL scintillation vial equipped with a magnetic stir bar was added [(COE)₂IrCl]₂ (33 mg, 0.037 mmol) and PhF, resulting in an orange suspension. To the stirring suspension was added an orange PhF solution of **701b** (41.4 mg, 0.08 mmol) and NaN(SiMe₃)₂ (14 mg, 0.08 mmol) causing an immediate color change to dark red with the noted precipitation of colorless solids (presumed to be NaCl). The mixture was allowed to stir for 1 h, then was filtered through a plug of Celite and silica, and volatiles were removed *in vacuo* to furnish a sticky, red solid. The solid was washed with cold pentane and dried under reduced pressure to

provide the product as a free-flowing red solid. Yield: 20 mg (32%). ^1H NMR (500 MHz, C_6D_6): δ 7.51 (d, $J = 8.4$ Hz, 1H), 7.45 (dd, $J = 8.9, 4.0$ Hz, 1H), 7.43 (s, 1H), 6.87 (dd, $J = 8.0, 1.7$ Hz, 1H), 6.83 (dd, $J = 8.3, 1.5$ Hz, 1H), 6.78 (d, $J = 8.5$ Hz, 1H), 3.06 (m, 1H, *alkenyl C-H*), 2.80 (m, 1H, *alkenyl C-H*), 2.70 (m, 1H), 2.54 (m, 1H), 2.36 (m, 2H), 2.25 (s, 3H), 2.20 (s, 3H), 2.19 (m, 1H), 1.81 (m, 4H), 1.64 (br, 4H), 1.58 (s, 9H, *Sb^tBu*), 1.47 (dd, $J = 16.6, 7.1$ Hz, 6H, *ⁱPr-CH₃*), 1.44 (s, 9H, *Sb^tBu*), 1.11 – 0.98 (m, 9H, *overlapping COE and ⁱPr-CH₃ resonances*). ^{31}P NMR (202 MHz, C_6D_6): δ 31.1

(ⁱPrPNSb^tBu)PdCl (707): To a J. Young tube was added **701b** (41.8 mg, 0.076 mmol), (COD)PdCl₂ (21.0 mg, 0.073 mmol), and C_6D_6 , forming a yellow-green suspension. To this suspension was added NEt₃ (11 μL , 0.08 mmol) and the resulting mixture was heated in an oil bath at 70 °C for 1 h, resulting in a color change to turquoise, with concomitant precipitation of colorless solids (presumed to be HNEt₃Cl). The mixture was then filtered through a plug of silica and Celite and the solvent was removed *in vacuo* to provide a blue-green residue. The residue was then dissolved in pentane and cooled to -38 °C for 48 h over which time the product precipitated as a blue powder. Yield: 22 mg (43%). ^1H NMR (500 MHz, C_6D_6): δ 7.63 (d, $J = 8.5$ Hz, 1H), 7.51 (dd, $J = 8.6, 4.3$ Hz, 1H), 7.21 (d, $J = 1.8$ Hz, 1H), 6.82 (dd, $J = 8.5, 2.1$ Hz, 1H), 6.78 (ddd, $J = 8.5, 2.2, 0.6$ Hz, 1H), 6.70 (d, $J = 8.6$ Hz, 1H), 2.38 – 2.21 (m, 2H), 2.15 (s, 3H), 2.11 (s, 3H), 1.47 (s, 18H, *Sb^tBu₂*), 1.44 (dd, $J = 16.8, 7.1$ Hz, 6H, *ⁱPr-CH₃*), 1.22 – 1.08 (m, 6H, *ⁱPr-CH₃*). $^{31}\text{P}\{^1\text{H}\}$ NMR (202 MHz, C_6D_6): δ 55.6. Elem. Anal. Found (calc). C: 49.19 (48.79); H: 6.47 (6.43)

General Procedure for Ir-catalyzed DHBTA. To a J. Young tube in specific order was added a 0.162 M HBpin solution in C_6D_6 (430 μL , 0.07 mmol) followed by 35 μL of a 0.1 M C_6D_6 solution of either **704** or **706**, then 0.035 mmol of terminal alkyne (trimethylsilylacetylene/*p*-MeC₆H₄CCH/phenylpropargylsulfide) in C_6D_6 solution ($V_{\text{TOT}} = 0.5$ mL) was added and the J.

Young tube was closed, inverted and monitored by ^1H NMR spectroscopy. Upon reaction completion 1,4-dioxane was added as an internal standard and percent conversion to the corresponding alkynylboronate was determined.

X-ray Diffractometry Details for ($i^{\text{Pr}}\text{PNSb}^{\text{Ph}}\text{Rh}(\text{CO})$) (702): A Leica MZ 75 microscope was used to identify a suitable colorless block with very well defined faces with dimensions (max, intermediate, and min) $0.021 \times 0.015 \times 0.013 \text{ mm}^3$ from a representative sample of crystals of the same habit. The crystal mounted on a nylon loop was then placed in a cold nitrogen stream (Oxford) maintained at 110 K. A BRUKER APEX 2 Duo X-ray (three-circle) diffractometer was employed for crystal screening, unit cell determination, and data collection. The goniometer was controlled using the APEX2 software suite, v2008-6.0. The sample was optically centered with the aid of a video camera such that no translations were observed as the crystal was rotated through all positions. The detector was set at 6.0 cm from the crystal sample (APEX2, 512x512 pixel). The X-ray radiation employed was generated from a IuS Cu X-ray tube ($K_{\alpha} = 1.5418 \text{ \AA}$ with a potential of 45 kV and a current of 0.65 mA). 45 data frames were taken at widths of 1.0° . These reflections were used in the auto-indexing procedure to determine the unit cell. A suitable cell was found and refined by nonlinear least squares and Bravais lattice procedures. The unit cell was verified by examination of the hkl overlays on several frames of data. No super-cell or erroneous reflections were observed. After careful examination of the unit cell, an extended data collection procedure (33 sets) was initiated using omega and phi scans. Integrated intensity information for each reflection was obtained by reduction of the data frames with the program APEX2. The integration method employed a three dimensional profiling algorithm and all data were corrected for Lorentz and polarization factors, as well as for crystal decay effects. Finally, the data was merged and scaled to produce a suitable data set. The absorption correction program SADABS was employed

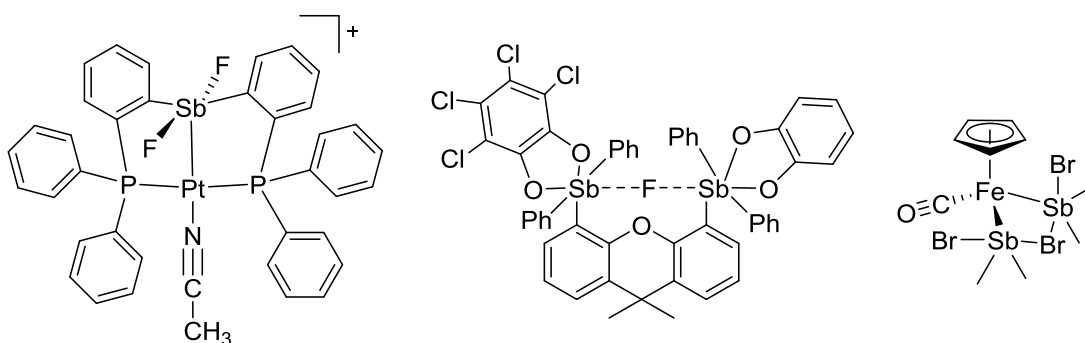
to correct the data for absorption effects. Systematic reflection conditions and statistical tests of the data suggested the space group $P2_1/n$. A solution was obtained readily using XT/XS in APEX2. Hydrogen atoms were placed in idealized positions and were set riding on the respective parent atoms. All non-hydrogen atoms were refined with anisotropic thermal parameters. Absence of additional symmetry and voids were confirmed using PLATON (ADDSYM). The structure was refined (weighted least squares refinement on F^2) to convergence. Olex2 was employed for the final data presentation and structure plots. (CSD Identifier/Number – IFIRUN/1843710).

CHAPTER VIII

OXIDATION OF A BIS-STIBINO AMINE AND SPONTANEOUS FORMATION OF A STIBAACRIDINIUM

8.1 Introduction

Antimony (Sb) has recently received increased attention and development as a ligand for transition metals,¹⁷⁹ and a species useful in catalysis¹⁸⁰ and anion sensing.¹⁸¹ Stibines (SbR_3) behave not only as heavier analogues of phosphorous, but also feature redox non-innocence which allows greater access to highly Lewis acidic stiboranes (SbR_5) that have a variety of potential functions. Though certain Sb(III) species are capable of acting as Lewis acids, Sb(V) is a typically more reactive species¹⁸² and has garnered greater interest as a result. Work by Gabbai and others has shown that the redox non-innocence and Lewis acidity of Sb can be leveraged to affect catalysis¹⁸³ and anion sensing¹⁸⁴ utilizing multidentate ligands (Scheme VIII-1).



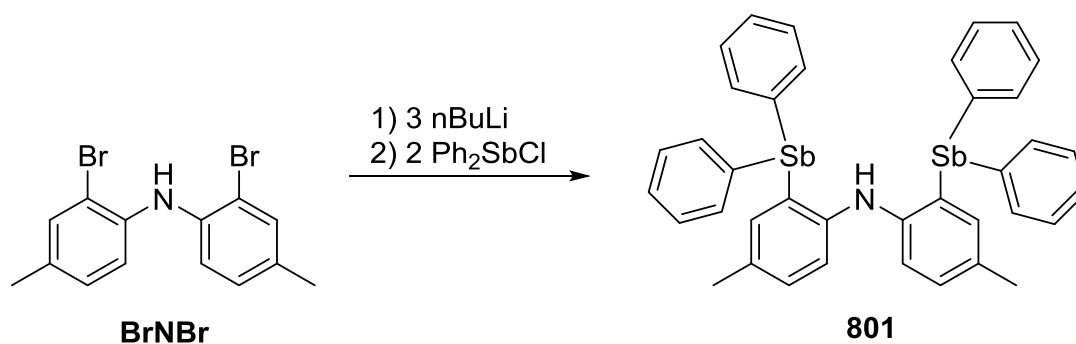
Scheme VIII-1. Examples of multidentate, Sb-containing ligands

We recently began studying the effects of replacing phosphorous with a heavier pnictogen in tridentate pincer-ligated systems based on a diarylamine core.¹⁸⁵ In the course of these studies, we also became interested in the possibility of leveraging similar diarylamine-based Sb-containing systems which featured a preserved N-H moiety as a possible ambiphilic central donor for small molecule activation. This report describes the synthesis of a *bis*-stibino amine and the chemistry it undergoes upon oxidation to Sb(V).

8.2 Results and Discussion

8.2.1 Synthesis of *SbNSb*

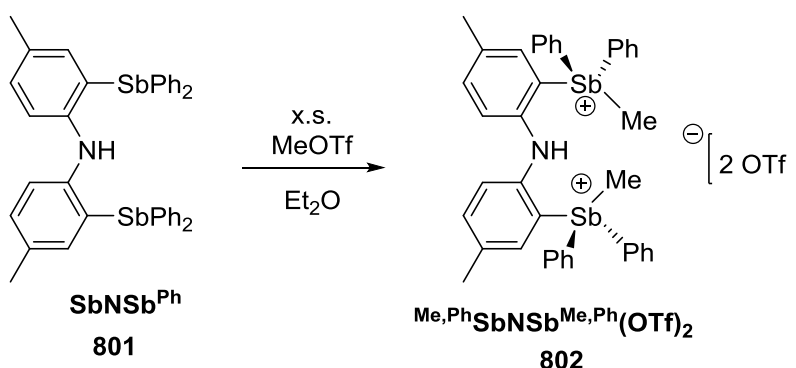
Treatment of BrNBr with three equivalents of butyllithium, followed by addition of two equivalents Ph₂SbCl and an aqueous workup led to isolation of SbN^HSb^{Ph} in 31% yield as a free-flowing, white solid (Scheme VIII-2). ¹H and ¹³C{¹H} NMR spectroscopy revealed the presence of all expected resonances with the *bis*-SbPh₂ substituents giving rise to broad signals at δ 7.46 and 7.07 ppm with 8H and 12H, respectively. The N-H is observed by ¹H NMR at δ 5.68 ppm and exhibits a stretch by IR spectroscopy at 3338 cm⁻¹.



Scheme VIII-2. Synthesis of SbNSb (**801**)

8.2.2 Oxidation of *SbNSb* with *MeOTf*

Seeking to access a highly electrophilic, bidentate, Lewis acidic antimony complex. We initially targeted oxidation to a bis-stibonium moiety. Gratifyingly, it was found that treatment of **801** with an excess of *MeOTf* allowed clean formation and isolation of the *bis*-triarylmethylstibonium amine, **802** in good yield (Scheme VIII-3).



Scheme VIII-3. Oxidation of **801** to **802** using an excess of *MeOTf*

The ^1H NMR spectrum of **802** features a broad multiplet δ 7.67 – 7.48 ppm (worth 20H) which corresponds to all the SbPh_2 aromatic protons. Three separate aromatic resonances are observed (2H each) for the diarylamino backbone, as well as a single N-H resonance (δ 6.96 ppm). Two singlet resonances (worth 6H) each at δ 2.26 and 2.24 ppm correspond to the benzylic CH_3 and Sb-CH_3 protons. Finally, in the $^{13}\text{C}\{^1\text{H}\}$ NMR spectrum, there are 14 separate aromatic resonances, which are indicative of C_2 -symmetry in solution, likely due to the inability of the Sb-Me bonds to rotate past one another. This is in full accordance with the solid-state structure, determined by X-ray diffractometry (Figure VIII-1).

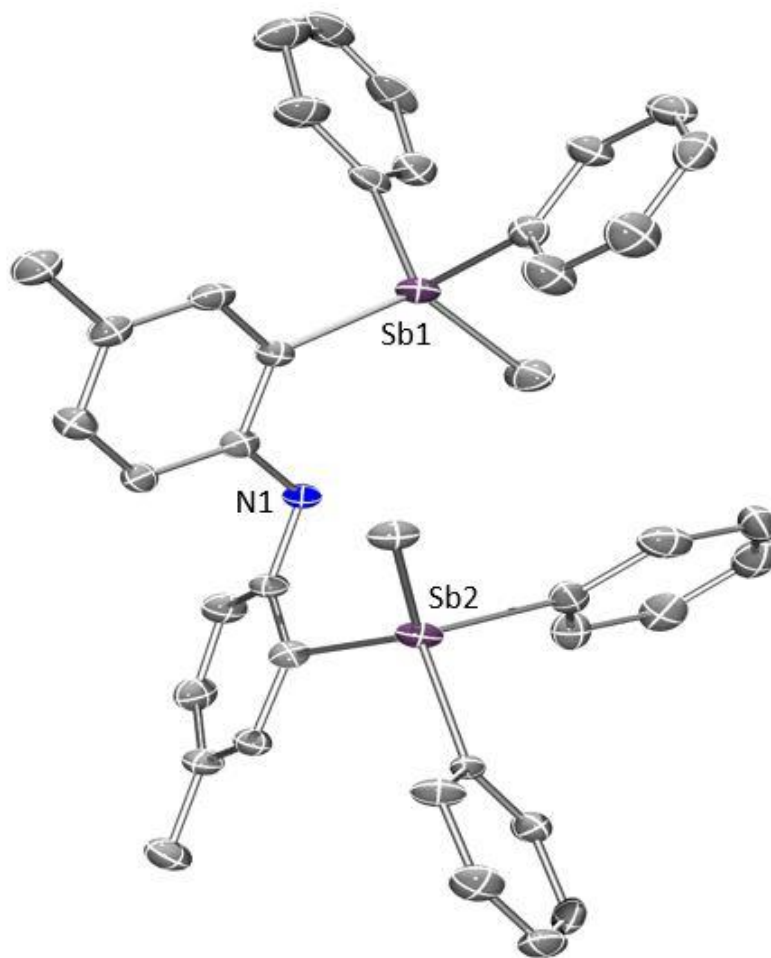
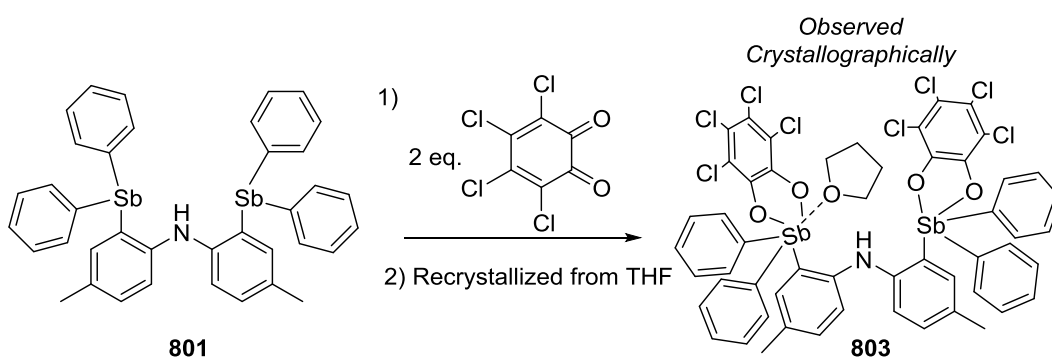


Figure VIII-1. ORTEP drawing (50% probability ellipsoids) of $\text{Me,PhSbN}^{\text{H}}\text{Sb}^{\text{Me,Ph}}(\text{OTf})_2$ (**802**). H atoms are omitted for clarity.

8.2.3 Oxidation of *SbNSb* with Chloranil

Treatment of $\text{SbN}^{\text{H}}\text{Sb}^{\text{Ph}}$ with chloranil (3,4,5,6-tetrachloro-*o*-quinone) in CH_2Cl_2 caused an initial color change of the colorless solution to yellow, then finally to dark green (Scheme VIII-4). After 12 h, a gray precipitate forms which is able to be recrystallized from THF to provide the product in 41% yield. Initially, X-ray diffractometry revealed formation of $\text{SbN}^{\text{H}}\text{Sb}^{[\text{O}]}$ in which oxidation of both stibine arms had occurred to furnish the *bis*-stiboranyl amine (Figure VIII-2). The Lewis acidic nature of the *bis*-stiboranyl moieties

can be observed as one equivalent of THF is coordinated to a stiborane at a distance of 2.522(3) Å, and the other stiborane appears to feature a N→Sb interaction with a distance of 2.970 Å. The aryl-stiborane bond distances appear to be typical with Sb1-C19 (2.161(5)) and Sb2-C48 (2.130(4)) showing little difference. The aryl nitrogen distances, C24-N1 (1.438(7)) and C49-N1 (1.442(6)) are also typical of aryl C-N single bonds.



Scheme VIII-4. Oxidation of **801** with chloranil leading to crystallographic observation of *bis*-stiboranyl amine-THF adduct **803**.

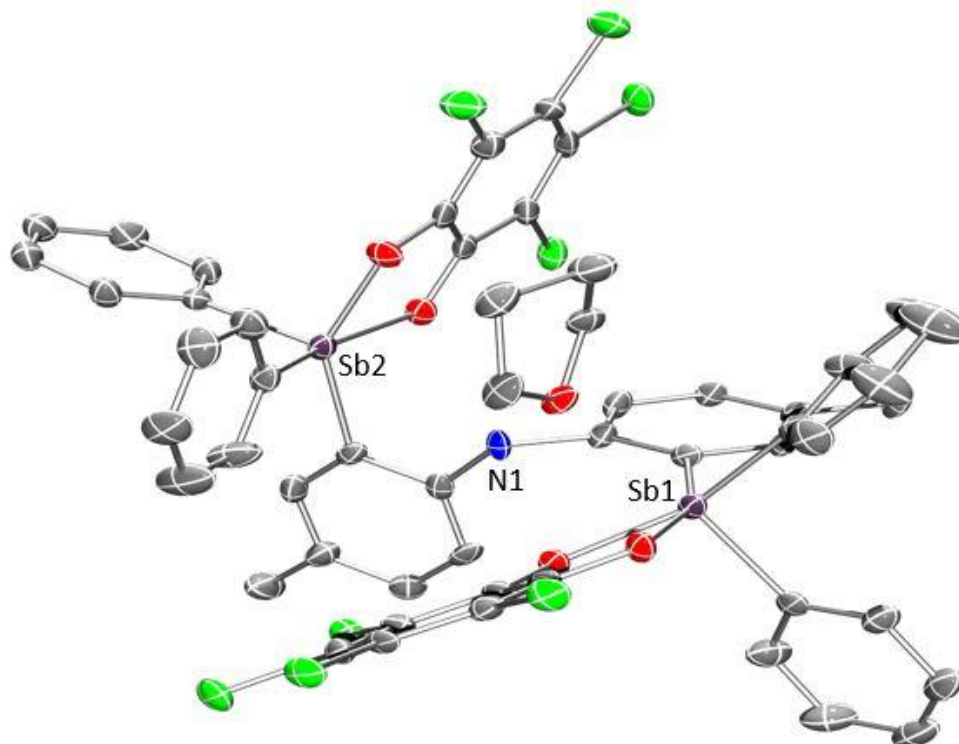
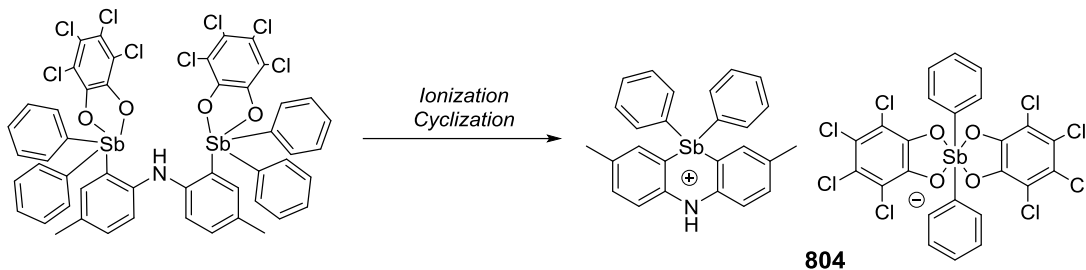


Figure VIII-2. ORTEP drawing (50% probability ellipsoids) of **803**. Selected H atoms are omitted for clarity. Selected Distances (Å): C19-Sb1, 2.161(5); C48-Sb2, 2.130(4); C24-N1, 1.438(7); C49-N1, 1.442(6).

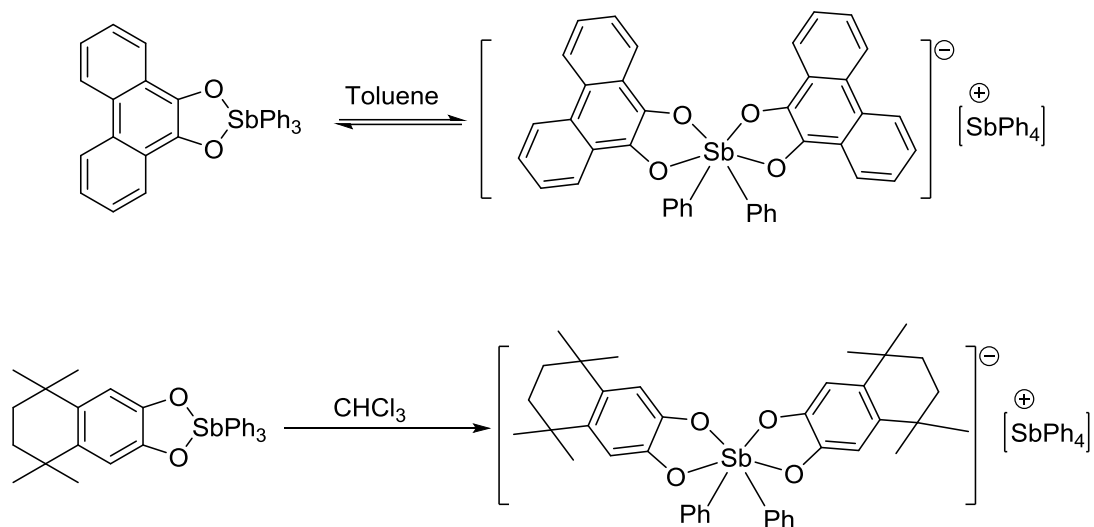
Despite being observed crystallographically, **803** is not the product that is ultimately formed, but rather, an intermediate. Upon solvation or recrystallization of the structurally confirmed **803** a selective and complete cyclization and ionizing rearrangement to a stibaacridinium antimonate salt occurs (Scheme VIII-5). In subsequent syntheses, the stibaacridinium antimonate was the only observable product to form either by NMR spectroscopy or X-ray diffractometry.



Scheme VIII-5. Rearrangement of *bis*-stiboranyl amine to ionic isomer **804**.

804 features limited solubility which necessitated its spectroscopic characterization in either THF- d_8 or $dms\text{-}d_6$. Following the dissociation of THF and subsequent rearrangement to the stibaacridine, a free molecule of THF is still observed to co-crystallize. A significantly downfield shifted N-H resonance is observed by ^1H NMR spectroscopy at δ 9.79 ($dms\text{-}d_6$) or 9.24 ppm (THF- d_8). The presence of the N-H is also confirmed by IR spectroscopy with a stretch at 3334 cm^{-1} . Multiple SbPh resonances are observed between δ 7.81 – 7.43 ppm (20H total) which correspond to either the stibaacridinium or antimonate species, and all the expected resonances by $^{13}\text{C}\{^1\text{H}\}$ NMR spectroscopy are able to be resolved. A singlet resonance is observed at δ 2.24 ($dms\text{-}d_6$) or 2.23 ppm (THF- d_8) which corresponds to symmetric, benzylic CH_3 substituents.

To test whether the isomerization was fluxional, a variable temperature NMR study was performed in THF- d_8 . It was found that at either 25, 0, -20, or -40 $^\circ\text{C}$, no changes were observed by ^1H NMR spectroscopy. Rearrangements such as this at Sb(V) catecholates have been previously observed to occur semi-reversibly in toluene and irreversibly in polar solvents such as CHCl_3 or acetone (Scheme VIII-6).¹⁸⁶ As both stiboranes are attached to the same, flexible backbone, the rearrangement to the ionic isomer causes a cyclization to occur, forming a six-membered, formally Hückel aromatic ring.



Scheme VIII-6. Previous examples of ionizing rearrangements of stiborane catecholates to stibonium antimonate salts.

8.2.4 Structural Consideration of **804**

Compared to the *bis*-stiboranyl amine isomer, the Sb-Ph bond length in the antimonate anion is typical (2.131(3)). The structure of the stibaacridinium, however, reveals features which appear to evidence some level of conjugation (Figure VIII-3). Notably, the six membered ring is completely planar and the intraring C-N and Sb-C bond lengths are shortened. The C-N bond lengths (C30-N1 and C33-N1) being 1.386(3) and 1.389(3) Å, are shortened by ca. 0.6 Å *versus* that of the *bis*-stiboranyl amine (1.438(7) and 1.442(6) Å). These values are ca. 0.03 Å longer than the C-N bond distances in the parent acridine (1.353 Å).¹⁸⁷ More significantly, however, is the observed shortening of the intraring Sb-C bond lengths. Whereas the *exocyclic* Sb-Ph bond length

is unremarkable (Sb2-C45, 2.091(2) Å) the endocyclic distances (Sb2-C25, 2.063(2); Sb2-C32, 2.067(2) Å) are shortened by ca. 0.06 Å.

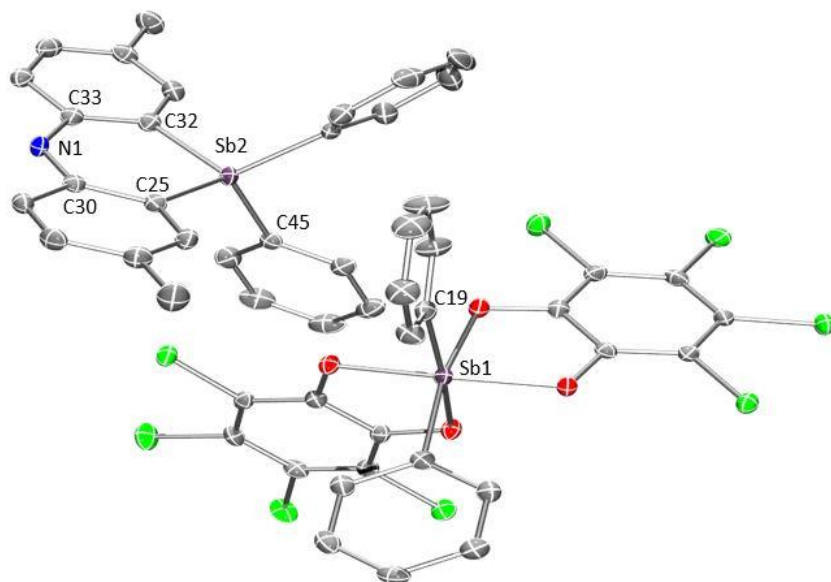
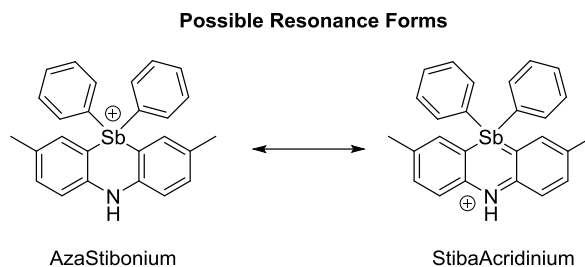


Figure VIII-3. ORTEP drawing (50% probability ellipsoids) of **804**. All H atoms and one molecule of THF are omitted for clarity. Selected Distances (Å): Sb1-C19, 2.131(3); Sb2-C45, 2.091(2); Sb2-C25, 2.063(2); Sb2-C32, 2.067(2); C30-N1, 1.386(3); C33-N1, 1.389(3).

Looking simply at the cationic cyclization product, there are two resonance forms which could be expected to contribute to the observed structure (Scheme VIII-7).



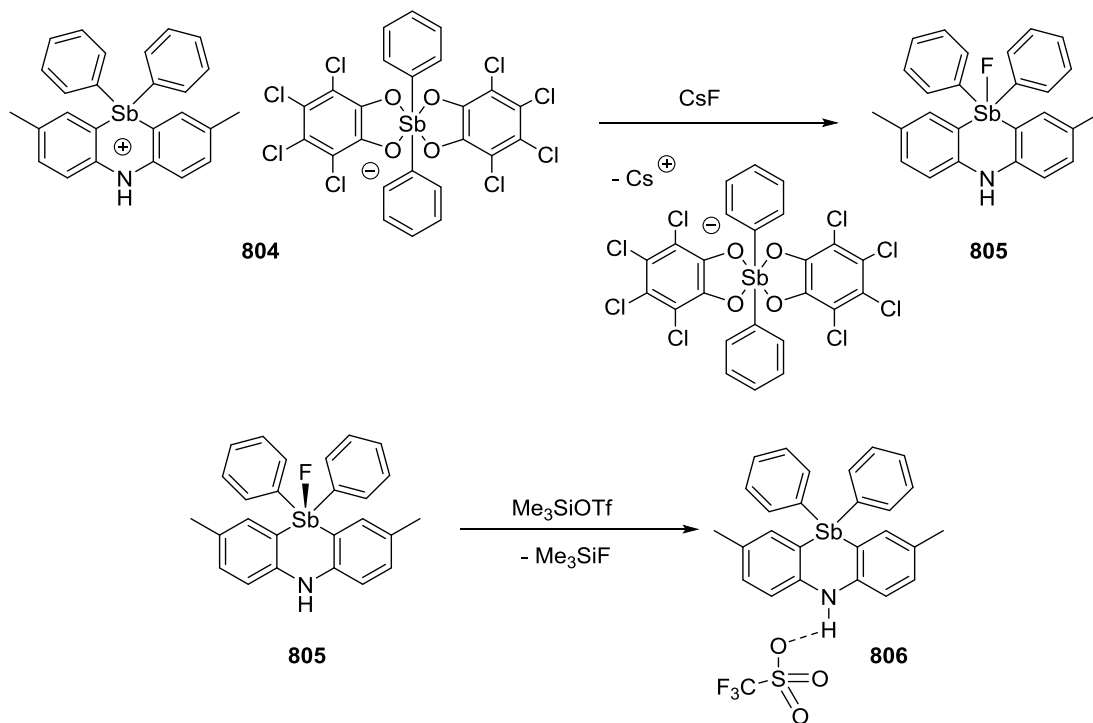
Scheme VIII-7. Possible resonance contributors for **804** cation

The first carries a positive charge entirely at antimony, giving rise to an azastibonium formulation, and the second involves conjugation of the amine π -electrons into the ring to stabilize the stibonium, providing the stibaacridinium form. Given the concomitant shortening of the Sb-C and N-C bond lengths in the cyclized product, it appears reasonable that amine π -electrons are in some level of conjugation with an empty Sb(V) orbital, allowing for putative assignment as a stibaacridinium. The extent of this conjugation is likely small in magnitude as cyclic Sb-C multiple bonding has been shown to be largely disfavored and can lead to thermally unstable species.¹⁸⁸

8.2.5 Reaction with Fluoride and Reformation of Stibaacridinium Cation

Seeking to probe whether the Lewis acidity of the stibonium is retained, a stirred suspension of **804** was treated with one equivalent of CsF in THF causing an immediate change to a clear, homogeneous solution. After removal of volatiles, and extraction with PhF, **805** was isolated in 84% yield as a free-flowing white powder (Scheme VIII-8). The ^{19}F NMR spectrum features a single resonance at δ -100.4 ppm confirming the presence of the Sb-F bond. **805** exhibits broad resonances by ^1H NMR spectroscopy with a single resonance corresponding to the N-H at

δ 8.25 ppm, two resonances for the SbPh₂ substituents at δ 7.88 and δ 7.41 ppm (4H and 6 H, respectively), and a single benzylic CH₃ resonance at δ 2.20 ppm (6H).



Scheme VIII-8. Synthesis of neutral fluorostiborane and net anion metathesis with TMSOTf.

Reaction of **805** with Me₃SiOSO₂CF₃ (TMSOTf) led to release of an equivalent of free Me₃SiF and formation of **806** which was characterized by ¹H and ¹⁹F NMR spectroscopy as well as X-ray diffractometry. Resonances by ¹H NMR support the identity of the cation with a downfield N-H resonance at δ 9.18 ppm, along with all expected aromatic and benzylic (δ 1.85

ppm, 6H) resonances. **806** exhibits a singlet in the ^{19}F NMR spectrum at δ -76.91 ppm, corresponding to the triflate anion. Structural analysis reveals an H-bonding interaction between the N-H and an oxygen atom of the triflate anion (2.039 Å) (Figure VIII-4). Such H-bonding interactions of a parent acridinium N-H with the oxygen of a triflate anion (2.743(2) Å) have been documented by Catty and coworkers.¹⁸⁹ Intraring C-N (1.392(7) Å) and Sb-C (2.093(5) Å) bond distances appeared to increase slightly, but insignificantly from those of the stibaacridinium antimonate.

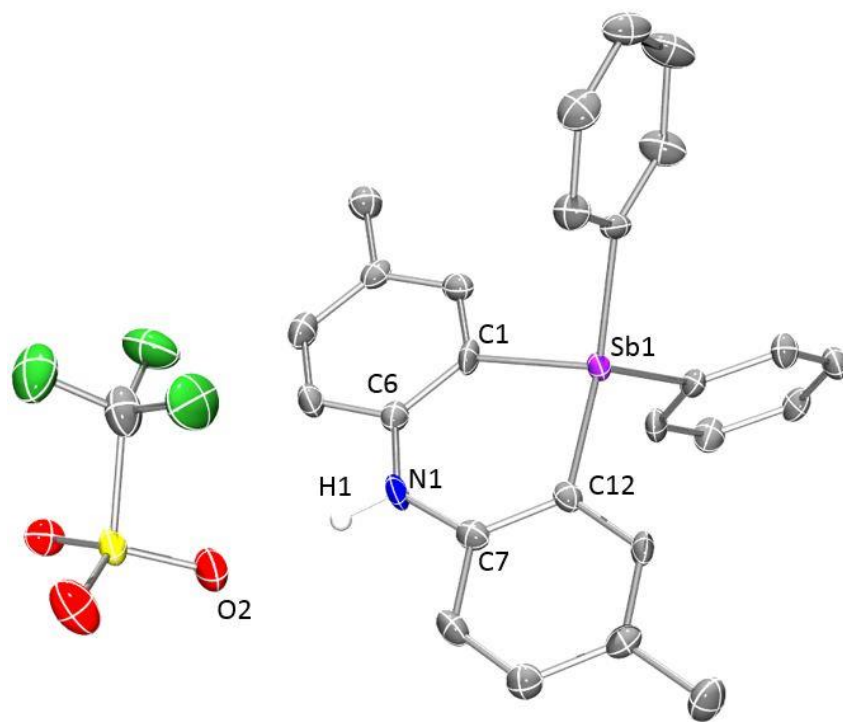


Figure VIII-4. ORTEP drawing (50% probability ellipsoids) of **806**. Selected H atoms are omitted for clarity. Selected Distances (Å): Sb1-C1, 2.093(5); Sb1-C12, 2.094(5); N1-C6, 1.376(7); N1-C7, 1.392(7); O2-H1, 2.039(14).

8.3 Conclusion

In summary, oxidation of a *bis*-stibino amine with chloranil led first to a crystallographically observed *bis*-stiboranyl amine with inter- and intramolecular Lewis acid/base interactions. The *bis*-stiboranyl amine then undergoes a selective and irreversible cyclizing rearrangement to the formally aromatic Sb^+NH with an antimonate anion. Structural analysis led to its putative assignment as a stibaacridinium antimonate, and further reaction with fluoride showed a retention of Lewis acidity in the clean formation of a fluorostiborane. Triflate for fluoride metathesis with the fluorostiborane refurnished the stibaacridinium core. Future studies are ongoing regarding deprotonation of the stibaacridinium to provide access to neutral species with potentially higher orders of Sb-C bond character.

8.4 Experimental

8.4.1 General Considerations

Unless otherwise stated, all experiments were carried out using standard glovebox and Schlenk line techniques under a dry argon atmosphere. C_6D_6 was dried over NaK, benzophenone, and 18-crown-6, distilled, and stored over molecular sieves in an argon glovebox prior to usage. All other deuterated solvents were degassed and stored over molecular sieves. Diethyl ether, tetrahydrofuran, and pentane were dried and deoxygenated using a PureSolv MD-5 solvent purification system and were stored over molecular sieves in an argon-filled glovebox. BrNBr^{190} was synthesized using previously reported procedures. Ph_2SbCl was prepared *via* neat reaction of SbPh_3 and SbCl_3 in a 2:1 ratio. NMR spectra were recorded on a Varian iNova 500 ($^{31}\text{P}\{^1\text{H}\}$ NMR, 202.276 MHz; $^{13}\text{C}\{^1\text{H}\}$ NMR, 125.670 MHz; ^1H NMR, 499.678 MHz, ^{19}F NMR, 470.385 MHz) spectrometer in

given solvents. Chemical shifts are reported in ppm (δ). $^{13}\text{C}\{^1\text{H}\}$ and ^1H NMR spectra were internally referenced to residual solvent resonances.¹⁹¹ In reporting spectral data, the following abbreviations were utilized: s = singlet; d = doublet; t = triplet; dd = doublet of doublets; m = multiplet. Infrared spectra were collected on an Agilent CARY FT-IR spectrometer. Elemental analyses were performed by CALI, Inc. (Highland Park, NJ, USA). Mass spectrometry was performed by the Laboratory for Biological Mass Spectrometry at Texas A&M University.

8.4.2 Synthesis of *Sb*-complexes

***SbNSb^{Ph}* (801):** To a 200 mL Schlenk flask equipped with a magnetic stir bar was added BrNBr (2.18 g, 6.13 mmol) and 50 mL diethyl ether. To this stirring solution was slowly added a 2.5 M solution of *n*-butyllithium in hexanes (7.44 mL, 18.6 mmol) causing the solution to become slightly yellow. The solution was allowed to stir for 3 h, and then Ph₂SbCl (3.83 g, 12.3 mmol) was added as a suspension in 3 mL of THF, causing the solution to become a cloudy, bright yellow. After the addition was completed, the suspension was allowed to stir for 16 h. To the suspension was then added 1 mL of degassed H₂O, causing the mixture to become a light yellow, homogeneous solution, which was then allowed to stir for 1 h. Solvent was then removed under reduced pressure to yield a waxy yellow residue which was dissolved in a minimal amount of fluorobenzene and filtered through a frit containing Celite and silica. The fluorobenzene was removed *in vacuo* to give a waxy yellow solid which was washed with 20 mL of *isooctane* and dried. The resultant solid was dissolved in a minimal of diethyl ether, layered with *isooctane*, and recrystallized at -37 °C over 12 h. The solvent was decanted and the solids were washed with *isooctane*

then pentane and dried, providing the product as an off-white, free-flowing solid of ca. 95% (NMR evidence) purity. Yield: 1.407 g (31%). ^1H NMR (500 MHz, C_6D_6): δ 7.46 (m, 8H, Sb-Ph), 7.25 (s, 2H, Ar CH), 7.07 (m, 12 H, Sb-Ph), 6.90 (d, $J_{\text{HH}} = 8.0$ Hz, 2H, Ar CH), 6.85 (d, $J_{\text{HH}} = 8.0$ Hz, 2H, Ar CH), 5.68 (s, 1H, N-H) 1.95 (s, 6H, benzylic CH_3). $^{13}\text{C}\{^1\text{H}\}$ NMR (126 MHz, C_6D_6): δ 147.7, 138.4, 138.0, 136.8, 133.0, 132.5, 131.3, 129.3, 128.8, 121.1, 20.7 (benzylic CH_3). ATR-IR (cm^{-1}): $\nu_{\text{N-H}}$ 3338 cm^{-1} HRMS (ESI $^+$) m/z $[\text{M}+\text{H}]^+$: calc'd for $\text{C}_{38}\text{H}_{33}\text{NSb}_2$: 748.0766, found 748.0719.

$\text{Me,PhSbN}^{\text{H}}\text{Sb}^{\text{Me,Ph}}(2 \text{ OTf})$ (802): To a 20 mL scintillation vial equipped with a magnetic stir bar was added **801** (142 mg, 0.19 mmol) and 4 mL diethyl ether, forming a clear solution. To this solution was then added a large excess of methyl trifluoromethanesulfonate (415 μL , 3.79 mmol) and the solution was allowed to stir for 48 h over which time the product precipitated as a fluffy white solid. The solvent was decanted and the solid was washed with diethyl ether (2 x 20 mL) and dried *in vacuo* to a free-flowing white solid. Yield: 122 mg (60%). ^1H NMR (500 MHz, CDCl_3): 7.67-7.48 (m, 20H, Sb-Ph), 7.19 (dd, $J = 8.3, 1.4$ Hz, 2H, Ar CH), 7.08 (d, $J = 1.2$ Hz, 2H, Ar CH), 6.96 (s, 1H, N-H), 6.67 (d, 8.3 Hz, 2H, Ar CH), 2.26 (s, 6H), 2.24 (s, 6H). $^{13}\text{C}\{^1\text{H}\}$ NMR (126 MHz, CDCl_3): 146.3, 136.1, 135.7 (Sb-Ph), 135.6 (Sb-Ph), 135.3 (Sb-Ph), 135.2 (Sb-Ph), 133.1 (Sb-Ph), 133.0 (Sb-Ph), 130.9 (Sb-Ph), 130.6 (Sb-Ph), 124.6, 124.5, 124.1, 120.3, 120.3 (q, $J_{\text{C-F}} = 320.8$ Hz, OTf- CF_3), 20.9 (Ar- CH_3), 5.29 (Sb- CH_3). ^{19}F NMR (470 MHz, CDCl_3): -79.27 (OTf). Elem Anal Found (calc): C: 46.91 (46.91) H: 3.73 (3.66).

Crystallographic Observation of *bis*-stiboranyl amine (803): To a 20 mL scintillation vial equipped with a magnetic stir bar was added **801** (358.7 mg, 0.48 mmol) and 2 mL CH_2Cl_2 forming a light yellow solution. To this stirring solution was slowly added

chloranil (238.6 mg, 0.97 mmol) in 1 mL CH₂Cl₂ which produces a gradual color change to a dark purple solution that was allowed to stir for 12 h, resulting in formation of a dark precipitate. The precipitate was isolated on a fine frit and washed with CH₂Cl₂ and Et₂O until most of the purple coloration had disappeared. The solid was then suspended in THF and filtered through a plug of Celite, giving a pale yellow solution. To the filtrate was then added pentane until precipitation was observed to begin, and the mixture was placed in a freezer at -38 °C for 48 h over which time the product crystallized as a pale yellow solid. White, single crystals suitable for X-ray diffraction were grown from a THF/pentane mixture at -38 °C over 24 h. These crystals provided the structure of the neutral isomer. Yield: 255.9 mg (41%). *This result was unable to be reproduced such that the neutral isomer was observable crystallographically, and upon dissolution in either dmsO-d₆ or THF-d₈ only the ionic isomer is observed.*

[^{Ph}Sb^{N^H}][Sb(O[^]O)₂Ph₂] (**804**): Crystallographically confirmed **803** (26.5 mg, 0.02 mmol) was dissolved in 2 mL THF and filtered through a plug of Celite into a small vial. To this vial was added pentane until precipitation was observed to begin. The mixture was then allowed to sit at r.t. for 24 h over which time single crystals (both platelets and needles) suitable for X-ray diffraction had formed. Both polymorphic crystals were determined *via* x-ray diffractometry to exhibit the same unit cell and solely provided the structure of the ionic isomer. Washing with pentane and subsequent drying under reduced pressure gave the product as pale yellow crystals. Yield: 19.7 mg (74%). ¹H NMR (500 MHz, dmsO-d₆): δ 9.79 (s, 1H, *N-H*), 7.81 (d, *J* = 7.3 Hz, 4H), 7.65 (br, 8 H), 7.55 (m, 4H), 7.43 (m, 6H), 7.36 (d, *J* = 8.4 Hz, 2H), 7.29 (d, *J* = 8.4 Hz, 2H), 2.24 (s, 6H). *One equivalent of free THF is also observed.* ¹H NMR (500 MHz, THF-d₈): δ 9.24 (s, 1H, *N-H*), 7.76. (m,

4H), 7.61(m, 10H), 7.50 (br, 2H), 7.21 (s, 6H), 7.15 (m, 2H), 7.00 (m, 2H), 2.23 (s, 6H, benzylic CH₃), 1.66 (br, 4H, THF-CH₂). ¹³C{¹H} NMR (126 MHz, dms_o-d₆): 147.5, 146.0, 144.7, 144.2, 134.8, 134.8, 134.3, 132.5, 132.2, 130.4, 130.3, 130.1, 129.0, 119.0, 118.2, 117.2, 116.0, 115.2, 105.3, 20.1. ATR-IR (cm⁻¹): ν_{N-H}- 3334 cm⁻¹. Elem Anal Found (calc): C: 49.46 (49.47) H: 3.12 (3.15).

Variable Temperature NMR Study of 804 To a J. Young tube was added **804** (17.0 mg, 0.013 mmol) and THF-d₈ resulting in a clear, colorless solution. ¹H NMR spectra taken at variable temperatures (25, 0, -20, and -40 °C) revealed no changes in solution symmetry on the NMR timescale.

Ph₂(F)Sb⁺NH⁻ (805): To a 20 mL scintillation vial equipped with a magnetic stir bar was added **804** (625 mg, 0.50 mmol) and 3 mL THF. To this stirring suspension was then added CsF (77 mg, 0.50 mmol), causing the suspension to form a homogeneous solution. The resultant solution was then stirred for 16 h, and then volatiles were removed under reduced pressure, forming an off-white residue. The residue was then extracted with 5 mL PhF and filtered through a plug of Celite to give a clear, colorless solution. Volatiles were removed *in vacuo* to provide the product as a free-flowing, white powder. Yield: 247 mg (84 %). ¹H NMR (500 MHz, CDCl₃): δ 8.25 (br s, 1H, *N-H*), 7.88 (br, 4H, SbPh₂), 7.41 (br, 6H, SbPh₂), 7.13 (br, 2H), 6.82 (br, 3H), 6.56 (br, 1H), 2.20 (s, 6H, Ar-CH₃). ¹⁹F{¹H} NMR (470 MHz, CDCl₃): δ -100.4. HRMS (ESI⁺) m/z [M+H]⁺: calc'd for C₂₆H₂₃FNSb: 491.0851, found 491.0847.

[^{Ph}Sb⁺N^H][OTf] (806): To a J. Young tube was added **805** (23 mg, 0.05mmol) and CDCl₃, forming a clear, colorless solution. To this solution was added Me₃SiOTf (17 μL, 0.09 mmol) resulting in a slight color change to yellow. ¹H and ¹⁹F NMR spectroscopy evidenced a full, clean conversion to the product, along with formation of one equivalent of Me₃SiF. Colorless crystals

suitable for X-ray diffraction were grown from a toluene/pentane vapor diffusion at room temperature. ^1H NMR (500 MHz, CDCl_3): δ 9.18 (s, 1H, N-H), 7.29 (m, 2 H), 7.23 (br m, 9 H), 6.91 (d, $J = 8.7$ Hz, 2H), 6.83 (m, 1H), 6.81 (br, 2H), 1.85 (s, 6H, benzylic CH_3). $^{19}\text{F}\{^1\text{H}\}$ NMR (470 MHz, CDCl_3): δ -76.91.

X-ray Diffractometry Details for 802: A Leica MZ 75 microscope was used to identify a suitable yellow plate with very well defined faces with dimensions (max, intermediate, and min) $0.42 \times 0.373 \times 0.344 \text{ mm}^3$ from a representative sample of crystals of the same habit. The crystal mounted on a nylon loop was then placed in a cold nitrogen stream (Oxford) maintained at 100 K. A BRUKER Quest X-ray (fixed-Chi geometry) diffractometer was employed for crystal screening, unit cell determination, and data collection. The goniometer was controlled using the APEX3 software suite. The sample was optically centered with the aid of a video camera such that no translations were observed as the crystal was rotated through all positions. The X-ray radiation employed was generated from a Mo- $\text{I}\mu\text{s}$ X-ray tube ($K_\alpha = 0.71073\text{\AA}$). 45 data frames were taken at widths of 1° . These reflections were used to determine the unit cell. The unit cell was verified by examination of the $h k l$ overlays on several frames of data. No super-cell or erroneous reflections were observed. After careful examination of the unit cell, an extended data collection procedure (8 sets) was initiated using omega scans. Integrated intensity information for each reflection was obtained by reduction of the data frames with the program APEX3. The integration method employed a three dimensional profiling algorithm and all data were corrected for Lorentz and polarization factors, as well as for crystal decay effects. Finally, the data was merged and scaled to produce a suitable data set. The absorption correction program SADABS was employed to correct the data for absorption effects. Systematic reflection conditions and statistical tests of

the data suggested the space group $P2_1/c$. A solution was obtained readily ($Z=16$; $Z'=4$) using XT/XS in APEX3. Hydrogen atoms were placed in idealized positions and were set riding on the respective parent atoms. All non-hydrogen atoms were refined with anisotropic thermal parameters. Absence of additional symmetry and voids were confirmed using PLATON (ADDSYM). The structure was refined (weighted least squares refinement on F^2) to convergence. Olex2 was employed for the final data presentation and structure plots.

X-ray Diffractometry Details for 803: A Leica MZ 75 microscope was used to identify a suitable colorless block with very well defined faces with dimensions (max, intermediate, and min) $0.286 \times 0.099 \times 0.048 \text{ mm}^3$ from a representative sample of crystals of the same habit. The crystal mounted on a nylon loop was then placed in a cold nitrogen stream (Oxford) maintained at 110 K. A BRUKER APEX 2 Duo X-ray (three-circle) diffractometer was employed for crystal screening, unit cell determination, and data collection. The goniometer was controlled using the APEX2 software suite, v2008-6.0. The sample was optically centered with the aid of a video camera such that no translations were observed as the crystal was rotated through all positions. The detector was set at 6.0 cm from the crystal sample (APEX2, 512x512 pixel). The X-ray radiation employed was generated from a Mo sealed X-ray tube ($K_\alpha = 0.70173\text{\AA}$ with a potential of 40 kV and a current of 40 mA). 45 data frames were taken at widths of 1.0° . These reflections were used in the auto-indexing procedure to determine the unit cell. A suitable cell was found and refined by nonlinear least squares and Bravais lattice procedures. The unit cell was verified by examination of the hkl overlays on several frames of data. No super-cell or erroneous reflections were observed. After careful examination of the unit cell, an extended data collection procedure (6 sets) was initiated using omega and phi scans. Integrated intensity information for each reflection was obtained by reduction of the data frames with the program APEX2. The integration

method employed a three dimensional profiling algorithm and all data were corrected for Lorentz and polarization factors, as well as for crystal decay effects. Finally, the data was merged and scaled to produce a suitable data set. The absorption correction program SADABS was employed to correct the data for absorption effects. Systematic reflection conditions and statistical tests of the data suggested the space group $P-1$. A solution was obtained readily using XT/XS in APEX2. Hydrogen atoms were placed in idealized positions and were set riding on the respective parent atoms. All non-hydrogen atoms were refined with anisotropic thermal parameters. Absence of additional symmetry and voids were confirmed using PLATON (ADDSYM). The structure was refined (weighted least squares refinement on F^2) to convergence. Olex2 was employed for the final data presentation and structure plots. CCDC 1901508.

X-ray Diffractometry Details for 804: A Leica MZ 75 microscope was used to identify a suitable colorless plate with very well defined faces with dimensions (max, intermediate, and min) $0.324 \times 0.224 \times 0.042 \text{ mm}^3$ from a representative sample of crystals of the same habit. The crystal mounted on a nylon loop was then placed in a cold nitrogen stream (Oxford) maintained at 110 K. A BRUKER APEX 2 Duo X-ray (three-circle) diffractometer was employed for crystal screening, unit cell determination, and data collection. The goniometer was controlled using the APEX2 software suite, v2008-6.0. The sample was optically centered with the aid of a video camera such that no translations were observed as the crystal was rotated through all positions. The detector was set at 6.0 cm from the crystal sample (APEX2, 512x512 pixel). The X-ray radiation employed was generated from a Mo sealed X-ray tube ($K\alpha = 0.70173\text{\AA}$ with a potential of 40 kV and a current of 40 mA). 45 data frames were taken at widths of 1.0° . These reflections were used in the auto-indexing procedure to determine the unit cell. A suitable cell was found and refined by nonlinear least squares and Bravais lattice procedures. The unit cell was verified by

examination of the hkl overlays on several frames of data. No super-cell or erroneous reflections were observed. After careful examination of the unit cell, an extended data collection procedure (4 sets) was initiated using omega scans. Integrated intensity information for each reflection was obtained by reduction of the data frames with the program APEX2. The integration method employed a three dimensional profiling algorithm and all data were corrected for Lorentz and polarization factors, as well as for crystal decay effects. Finally, the data was merged and scaled to produce a suitable data set. The absorption correction program SADABS² was employed to correct the data for absorption effects. Systematic reflection conditions and statistical tests of the data suggested the space group $P-1$. A solution was obtained readily using XT/XS in APEX2. A molecule of THF was found solvated. Hydrogen atoms were placed in idealized positions and were set riding on the respective parent atoms. All non-hydrogen atoms were refined with anisotropic thermal parameters. Absence of additional symmetry and voids were confirmed using PLATON (ADDSYM). The structure was refined (weighted least squares refinement on F^2) to convergence. Olex2 was employed for the final data presentation and structure plots. CCDC1901509.

X-ray data collection, solution, and refinement for 806: A Leica MZ 75 microscope was used to identify a suitable colorless plate with very well defined faces with dimensions (max, intermediate, and min) 0.146 x 0.094 x 0.053 mm³ from a representative sample of crystals of the same habit. The crystal mounted on a nylon loop was then placed in a cold nitrogen stream (Oxford) maintained at 110 K. A BRUKER Quest X-ray (fixed-Chi geometry) diffractometer was employed for crystal screening, unit cell determination, and data collection. The goniometer was controlled using the APEX3 software suite. The sample was optically centered with the aid of a video camera such that no translations were observed as the crystal was rotated through all positions. The X-ray radiation employed was generated from a Mo-I μ s X-ray tube ($K\alpha =$

0.71073 Å). 45 data frames were taken at widths of 1°. These reflections were used to determine the unit cell. The unit cell was verified by examination of the $h k l$ overlays on several frames of data. No super-cell or erroneous reflections were observed. After careful examination of the unit cell, an extended data collection procedure (5 sets) was initiated using omega scans. Integrated intensity information for each reflection was obtained by reduction of the data frames with the program APEX3. The integration method employed a three dimensional profiling algorithm and all data were corrected for Lorentz and polarization factors, as well as for crystal decay effects. Finally, the data was merged and scaled to produce a suitable data set. The absorption correction program SADABS was employed to correct the data for absorption effects. Systematic reflection conditions and statistical tests of the data suggested the space group $Fdd2$. A solution was obtained readily using XT/XS in APEX3. Hydrogen atoms were placed in idealized positions and were set riding on the respective parent atoms. All non-hydrogen atoms were refined with anisotropic thermal parameters. Absence of additional symmetry and voids were confirmed using PLATON (ADDSYM). The structure was refined (weighted least squares refinement on F^2) to convergence. Olex2 was employed for the final data presentation and structure plots. CCDC 1901510.

CHAPTER IX

CONCLUSIONS

The chemistry of rhenium and other transition metals supported by various pincer-type ligands was disclosed. In all cases, the chemistry was supported by a central aryl or amido, anionic ligand with flanking group XV donors (amines, phosphines, amides, stibines). The variety of donors led to a diverse array of new reactivity primarily at rhenium and antimony centers.

The first well-defined example of C-H activation at a high-valent rhenium center was developed to furnish a PCP-supported complex of rhenium. The presence of a terminal oxo ligand allowed for heightened thermal stability and relatively predictable substitution chemistry at the rhenium center. These predictable substitutions provided access to putative, five-coordinate rhenium cations which showed both well-precedented and novel reactivity in the activation of small molecules. Further, reduction of the (PCP)ReOCl₂-type species generated the classical hexhydride, (PCP)ReH₆, which underwent substitution chemistry with various neutral donors, displacing dihydrogen, and furnishing eight-coordinate, *tetrahydride* species. In the case where a less sterically encumbering PCP-ligand was utilized, a thermally induced, dehydrogenative dimerization occurred giving a species of the general formula, (PCP)₂Re₂H₆.

Though substitution chemistry remained relatively predictable, a notable exception was found in the attempted installation of acetate (OAc) ligands at (PCP)Re. The *bis*-OAc product was found to undergo an irreversible hydrolysis which resulted in loss of HOAc and formation of a “masked” dioxo species which bound an equivalent of acetic acid in highly fluxional fashion. The independent syntheses of each of the individual species allowed for an elucidation of a possible

mechanistic pathway which shows an unusual, inverse thermodynamic preference for hydrolysis which seems to bend traditional organic pKa rules.

Through these studies it was also discovered that *via* the action of a strong, bulky base such as LiHMDS, the (PCP)ReOCl₂ fragment could undergo a clean dehydrohalogenation involving the benzylic methylene to form a dearomatized complex which was formulated as a dianionic, “pseudo-carbene.” The dearomatized product was studied computationally and spectroscopically and was shown to behave chemically as a charge separated species involving a benzylic anion and a rhenium cation. This reactivity allowed for the clean [4+2] cycloaddition of CO₂ in a *hetero* Diels Alder reaction, creating a *tetradentate* dianionic ligand scaffold with both aryl and carboxylate donors.

Pincer complexes of rhenium were made which featured a central amido-type donor with either two phosphines or one phosphine and one amine side donors. The PNN ligands showed slow rotational diastereomerism on the NMR timescale allowing for well-defined studies of rotational isomerism at variable temperatures. In addition, the side-donor amine was able to be reversibly deprotonated showing fully reversible switching between amino- and amido-type donorities. PNP ligands were also introduced which showed rotational isomerism on the NMR timescale due to the aromatic backbone rings flipping past one another. These PNP complexes of rhenium were then able to be reduced down to their *poly*-carbonyls which, along with their manganese analogues, exhibited reactivity befitting five-coordinate unsaturates.

Finally, antimony-type donors were incorporated into the diarylamino backbone and their use in supporting both catalytic activity and the formation of Lewis acidic species was explored.

REFERENCES

- (1) (a) Trotus, I-T.; Zimmermann, T.; Schüth, F. *Chem. Rev.* **2014**, 114, 1761-1782. (b) Corma, A.; Navas, J.; Sabater, N. J. *Chem. Rev.* **2018**, 118, 1410-1459. (c) Solomon, E. I.; Stahl, S. S. *Chem. Rev.* **2018**, 118, 2299-2301.
- (2) *Metal-Ligand Interactions: Structure and Reactivity*; Russo, N.; Salahub, D. R, Eds.; Kluwer Academic Publishers: The Netherlands, 1996.
- (3) *The Organometallic Chemistry of the Transition Metals*; Crabtree, R. H., Ed.: Wiley: Hoboken, New Jersey, 2014.
- (4) *Transition Metal Complexes of Phosphorus, Arsenic and Antimony Ligands*; McAuliffe, C. A., Ed.: MacMillan Publishers Limited: Palgrave, London, 1973.
- (5) (a) Bazzicalupi, C.; Bencini, A.; Ciattini, S.; Giorgi, C.; Masotti, A.; Paoletti, P.; Valtancoli, B.; Navon, N.; Meyerstein, D. *J. Chem. Soc., Dalton Trans.* **2000**, 0, 2383-2391. (b) Acar, M. H.; Becer, C. R.; Ondur, H. A.; İnceoğlu, S. *ACS Symposium Series* **2006**, 944, 98-110.
- (6) (a) Zeitler, H. E.; Kaminsky, W. A.; Goldber, K. I. *Organometallics* **2018**, 37, 3644-3648. (b) Grice, K. A.; Goldberg, K. I. *Organometallics* **2009**, 28, 953-955.
- (7) (a) Lam, W. H.; Lin, Z. *Organometallics* **2003**, 22, 473-480. (b) Terabayashi, T.; Kajiwara, T.; Yamashita, M.; Nozaki, K. *J. Am. Chem. Soc.* **2009**, 131, 14162-14163. (c) Braunschweig, H.; Radacki, K.; Shang, R. *Chem. Commun.* **2013**, 49, 9905-9907.
- (8) (a) Yu, X.; Morton, L. A.; Xue, Z. -L. *Organometallics* **2004**, 23, 2210-2224. (b) Shelby, Q. D.; Lin, W.; Girolami, G. S. *Organometallics* **1999**, 18, 1904-1910. (c) Raza, A. L.;

- Panetier, J. A.; Teltewskoi, M.; Macgregor, S. A.; Braun, T. *Organometallics* **2013**, 32, 3795-3807. (d) McBee, J. L.; Tilley, T. D. *Organometallics* **2009**, 28, 5072-5081.
- (9) Mkhaliid, I. A. I.; Barnard, J. H.; Marder, T. B.; Murphy, J. M.; Hartwig, J. F. *Chem. Rev.* **2010**, 110, 890-931.
- (10) Moulton, C. J.; Shaw, B. L. *J. Chem. Soc. Dalton Trans.* **1976**, 1020-1024
- (11) Leis, W.; Mayer, H. A.; Kaska, W. C. *Coord. Chem. Rev.* **2008**, 252, 1787-1797.
- (12) Crocker, C.; Empsall, H. D.; Errington, R. J.; Hyde, E. M.; McDonald, W. S.; Markham, R.; Norton, M. C.; Shaw, B. L.; Weeks, B. *J. Chem. Soc., Dalton Trans.* **1982**, 1217.
- (13) Weng, W.; Parkin, S.; Ozerov, O. V. *Organometallics* **2006**, 25, 5345-5354.
- (14) Doyle, L.; Piers, W. E.; Bi, D. W. *Dalton Trans.* **2017**, 46, 4346-4354.
- (15) Comanescu, C. C.; Iluc, V. M. *Organometallics* **2014**, 33, 6059-6064.
- (16) Langbein, S.; Wadepohl, H.; Gade, L. H. *Organometallics* **2016**, 35, 809-815.
- (17) Murugesan, S.; Kirchner, K. *Dalton Trans.* **2016**, 45, 416-439.
- (18) Zhang, J.; Barakat, K. A.; Cundari, T. R.; Gunnoe, T. B.; Boyle, P. D.; Peterson, J. L.; Day, C. S. *Inorg. Chem.* **2005**, 44, 8379-8390.
- (19) Pell, C. J.; Ozerov, O. V. *Inorg. Chem. Front.* **2015**, 2, 720-724.
- (20) Ma, Q. -Q.; Liu, T.; Li, S.; Zhang, J.; Chen, X.; Guan, H. *Chem. Commun.* **2016**, 52, 14262-14265.
- (21) Bedford, R. B.; Draper, S. M.; Scully, P. N.; Welch, S. L.; *New J. Chem.* **2000**, 24, 745.
- (22) Pell, C. J.; Ozerov, O. V. *ACS Catal.* **2014**, 4, 3470-3480.
- (23) Timpa, S. D.; Fafard, C. M.; Herbert, D. E.; Ozerov, O. V. *Dalton Trans.* **2011**, 40, 5426-5429.

- (24) Timpa, S. D.; Pell, C. J.; Ozerov, O. V. *J. Am. Chem. Soc.* **2014**, 136, 14772-14779.
- (25) Connor, G.; Lease, N.; Casuras, A.; Goldman, A. S.; Holland, P. L.; Mayer, J. M. *Dalton Trans.* **2017**, 46, 14325-14330.
- (26) (a) Press, L. P.; Kosanovich, A. J.; McCulloch, B. J.; Ozerov, O. V. *J. Am. Chem. Soc.* **2016**, 138, 9487-9497. (b) Kosanovich, A. J.; Press, L. P.; Ozerov, O. V. *J. Organomet. Chem.* **2017**, 23, 19-24.
- (27) Gupta, M.; Hagen, C.; Flesher, R. J.; Kaska, W. C.; Jensen, C. M. *Chem. Commun.* **1996**, 2083-2084.
- (28) Kumar, A.; Bhatti, T. M.; Goldman, A. S. *Chem. Rev.* **2017**, 117, 12357-12384.
- (29) Goldman, A. S.; Roy, A. H.; Huang, Z.; Ahuja, R.; Schinski, W.; Brookhart, M. *Science* **2006**, 312, 257-261.
- (30) Rosenkoetter, K. E.; Wojnar, M. K.; Charette, B. J.; Ziller, J. W.; Heyduk, A. F. *Inorg. Chem.* **2018**, 57, 9728-9737.
- (31) Szigethy, G.; Heyduk, A. F. *Dalton Trans.* **2012**, 41, 8144-8152.
- (32) Davidson, J. J.; DeMott, J. C.; Douvris, C.; Fafard, C. M.; Bhuvanesh, N.; Chen, C.-H.; Herbert, D. E.; Lee, C.-I.; McCulloch, B. J.; Foxman, B. M.; Ozerov, O. V. *Inorg. Chem.* **2015**, 54, 2916-2935.
- (33) Kurogi, T.; Miehllick, M. E.; Halter, D.; Mindiola, D. J. *Organometallics* **2018**, 37, 165-167.
- (34) Masuda, J. D.; Jantunen, K. C.; Ozerov, O. V.; Noonan, K. J. T.; Gates, D. P.; Scott, B. L.; Kiplinger, J. L. *J. Am. Chem. Soc.* **2008**, 130, 2408-2409.
- (35) Zhu, Y.; Fan, L.; Chen, C. -H.; Finnell, S. R.; Foxman, B. M.; Ozerov, O. V. *Organometallics* **2007**, 26, 6701-6703.

- (36) Fan, L.; Foxman, B. M.; Ozerov, O. V. *Organometallics* **2004**, 23, 326-328.
- (37) Calimano, E.; Tilley, T. D. *J. Am. Chem. Soc.* **2009**, 131, 11161-11173.
- (38) Foley, B. J.; Zhou, J.; Bhuvanesh, N.; Ozerov, O. V. *manuscript in preparation*
- (39) Morrison, R. F.; Lipscomb, N.; Eldridge, R. B. *Ind. Eng. Chem. Res.* **2014**, 53, 19136-19144.
- (40) Du, G.; Fanwick, P. E.; Abu-Omar, M. M. *J. Am. Chem. Soc.* **2007**, 129, 5180-5187.
- (41) Wozniak, B.; Li, Y.; Tin, S.; de Vries, J. G. *Green Chem.* **2018**, 20, 4433-4437.
- (42) Wright, D. D.; Brown, S. N. *Inorg. Chem.* **2013**, 52, 7831-7833.
- (43) (a) Lambic, N. S.; Sommer, R. D.; Ison, E. A. *J. Am. Chem. Soc.* **2016**, 138, 4832-4842. (b) Robbins, L. K.; Lilly, C. P.; Smeltz, J. L.; Boyle, P. D.; Ison, E. A. *Organometallics* **2015**, 34, 3152-3158.
- (44) Ozerov, O. V.; Gerard, H. F.; Watson, L. A.; Huffman, J. C.; Caulton, K. G. *Inorg. Chem.* **2002**, 41, 5615-5625.
- (45) Ozerov, O. V.; Watson, L. A.; Pink, M.; Caulton, K. G. *J. Am. Chem. Soc.* **2007**, 129, 6003-6016.
- (46) Banert, K.; Heck, M.; Ihle, A.; Kronawitt, J.; Pester, T.; Shoker, T. *J. Org. Chem.* **2018**, 83, 5138-5148.
- (47) Bojan, V. R.; Fernandez, E. J.; Laguna, A.; Lopez-de-Luzuriaga, J. M.; Monge, M.; Olmos, M. E.; Puellas, R. C.; Silvestru, C. *Inorg. Chem.* **2010**, 49, 5530-5541.
- (48) Holmes, N. J.; Levason, W.; Webster, M. *J. Chem. Soc., Dalton Trans.* **1998**, 3457-3461
- (49) Ortmann, D. A.; Gevert, O.; Laubender, M.; Werner, H. *Organometallics* **2001**, 20, 1776-1782.

- (50) Reichl, K. D.; Dunn, N. L.; Fastuca, N. J.; Radosevich, A. T. *J. Am. Chem. Soc.* **2015**, *137*, 5292-5295.
- (51) Yang, H.; Gabbai, F. P. *J. Am. Chem. Soc.* **2014**, *136*, 10866-10869.
- (52) Sahu, S.; Gabbai, F. P. *J. Am. Chem. Soc.* **2017**, *139*, 5035-5038.
- (53) Breunig, H. J.; Kanig, W. *Phosphorous and Sulfur and Related Elements* **1982**, *2*, 149-159.
- (54) (a) Bentley, J. N.; Caputo, C. B. *Organometallics* **2018**, ASAP (b) Douvris, C.; Ozerov, O. *V. Science* **2008**, *321*, 1188-1190.
- (55) Yang, M.; Tofan, D.; Chen, C. -H.; Jack, K. M.; Gabbai, F. P. *Angew. Chem. Int. Ed.* **2018**, *57*, 13868-13872.
- (56) Yang, M.; Paiti, N.; Belanger-Chabot, G.; Hirai, M; Gabbai, F. P. *Dalton Trans* **2018**, *47*, 11843-11850.
- (57) (a) Hirai, M.; Gabbai, F. P. *Angew. Chem. Int. Ed.* **2015**, *54*, 1205-1209. (b) Chen, C.-H.; Gabbai, F. P. *Dalton Trans.* **2018**, *47*, 12075-12078.
- (58) Olah, G. A.; Schlosberg, R. H.; *J. Am. Chem. Soc.* **1968**, *90*, 2726-2727.
- (59) (a) *The Chemistry of Pincer Compounds*; Morales-Morales, D.; Jensen, C. M., Eds.; Elsevier: Amsterdam, 2007. (b) *Organometallic Pincer Chemistry*; Van Koten, G.; Milstein, D., Eds.; Springer: Heidelberg, 2013.
- (60) (a) Van der Boom, M. E.; Milstein, D. *Chem. Rev.* **2003**, *103*, 1759-1792. (b) Choi, J.; MacArthur, A. H. R.; Brookhart, M.; Goldman, A. S. *Chem. Rev.* **2011**, *111*, 1761-1779. (c) Selander, N.; Szabó, K. *J. Chem. Rev.* **2011**, *111*, 2048-2076.
- (61) Morales-Morales, D. *Rev. Soc. Quim. Méx.* **2004**, *48*, 338-346.

- (62) For a few seminal examples, see: (a) Gozin, M.; Weisman, A.; Ben-David, Y.; Milstein, D. *Nature* **1993**, *364*, 699-701. (c) Kumar, A.; Zhou, T.; Emge, T. J.; Mironov, O.; Saxton, R. J.; Krogh-Jespersen, K.; Goldman, A. S. *J. Am. Chem. Soc.* **2015**, *137*, 9894-9911.
- (63) (a) Vogt, M.; Nerush, A.; Iron, M. A.; Leitus, G.; Diskin-Posner, Y.; Shimon, L. L. W.; Ben-David, Y.; Milstein, D. *J. Am. Chem. Soc.* **2013**, *135*, 17004–17018. (b) Vogt, M.; Nerush, A.; Diskin-Posner, Y.; Ben-David, Y.; Milstein, D. *Chem. Sci.* **2014**, *5*, 2043–2051.
- (64) Korstanje, T. J.; Lutz, M.; Jastrzebski, J. T. B. H.; Gebbink, R. J. M. K. *Organometallics* **2014**, *33*, 2201-2209.
- (65) Lang, H.-F.; Fanwick, P. E.; Walton, R. A. *Inorg. Chim. Acta* **2002**, *329*, 1-8.
- (66) Porchia, M.; Tisato, F.; Refosco, F.; Bolzati, C.; Cavazza-Ceccato, M.; Bandoli, G.; Dolmella, A. *Inorg. Chem.* **2005**, *44*, 4766-4776.
- (67) Ozerov, O. V.; Watson, L. A.; Pink, M.; Caulton, K. G. *J. Am. Chem. Soc.* **2004**, *126*, 6363-6378.
- (68) Radosevich, A. T.; Melnick, J. G.; Stoian, S. A.; Bacciu, D.; Chen, C.-H.; Foxman, B. M.; Ozerov, O. V.; Nocera D. G. *Inorg. Chem.* **2009**, *48*, 9214-9221.
- (69) Choualeb, A.; Lough, A. J.; Gusev, D. G. *Organometallics* **2007**, *26*, 3509-3515.
- (70) Wanniarachchi, S.; Liddle, B. J.; Toussaint, J.; Lindeman, S. V.; Bennett, B.; Gardinier, J. R. *Dalton Trans.* **2010**, *39*, 3167-3169.
- (71) Klopsch, I.; Finger, M.; Wuertele, C.; Milde, B.; Werz, D. B.; Schneider, S. *J. Am. Chem. Soc.* **2014**, *136*, 6881-6883.
- (72) Aoki, T.; Crabtree, R. H. *Organometallics* **1993**, *12*, 294-298.
- (73) Chen, H.; Hartwig, J. F. *Angew. Chem. Int. Ed.* **1999**, *38*, 3391-3393.

- (74) Fryzuk, M. D.; MacNeil, P. A. *J. Am. Chem. Soc.* **1981**, *103*, 3592-3593.
- (75) Fryzuk, M. D. *Can. J. Chem.* **1992**, *70*, 2839-2845.
- (76) Kuninobu, Y.; Kawate, A.; Takai, K. *J. Am. Chem. Soc.* **2005**, *127*, 13498-13499.
- (77) All ORTEP plots were created using Ortep-3 for Windows. Farugia, L. *J. Appl. Crystallogr.* **1997**, *30*, 565.
- (78) Mayer, J. M. *Inorg. Chem.* **1988**, *27* (22), 3899-3903
- (79) Tatsumi, K.; Hoffmann, R. *Inorg. Chem.* **1980**, *19*, 2656-2658.
- (80) Matano, Y.; Northcutt, T. O.; Brugman, J.; Bennett, B. K.; Lovell, S.; Mayer, J. *Organometallics* **2000**, *19*, 2781-2790.
- (81) Ozerov, O. V.; Watson, L. A.; Pink, M.; Caulton, K. G. *J. Am. Chem. Soc.* **2003**, *125*, 9604-9605.
- (82) Luo, X.-L.; Crabtree, R. H. *J. Chem. Soc. Dalton Trans.* **1991**, 587-590.
- (83) Chatt, J.; Coffey, R. S. *J. Chem. Soc. A* **1969**, 1963-1972.
- (84) Wazio, J. A.; Jimenez, V.; Soparawalla, S.; John, S.; Moehring, G. A. *Inorg. Chim. Acta* **2009**, *362*, 159-165.
- (85) Gusev, D. G.; Nietlispach, D.; Vymenits, A. B.; Bakhmutov, V. I.; Berke, H. *Inorg. Chem.* **1993**, *32*, 3270-3276.
- (86) Hamilton, D. G.; Crabtree, R. H. *J. Am. Chem. Soc.* **1988**, *110*, 4126-4133.
- (87) Ortuno, M. A.; Vidossich, P.; Conejero, S.; Lledos, A. *Angew. Chem.* **2014**, *126*, 14382-14385.
- (88) Cotton, F. A.; Luck, R. L.; Root, D. R.; Walton, R. A. *Inorg. Chem.* **1990**, *29*, 43-47.

- (89) Romão, C. C. "Rhenium: Organometallic Chemistry," In *Encyclopedia of Inorganic Chemistry, 2nd Edition*; King, R. B., Ed; Wiley & Sons: Hoboken, NJ, 2006; pp 9-10.
- (90) Kim, Y.; Gallucci, J.; Wojcicki, A. *J. Am. Chem. Soc.* **1990**, *112*, 8600-8602.
- (91) Rudolph, R. N.; Strickler, S. J. *J. Am. Chem. Soc.* **1977**, *99*, 3872-3874.
- (92) For an example of a bridging PCP ligand in a dipalladium complex, see: Frech, C. M.; Shimon, L. J. W.; Milstein, D. *Angew. Chem. Int. Ed.* **2005**, *44*, 1709-1711.
- (93) Du, G.; Abu-Omar, M. M. *Organometallics* **2006**, *25*, 4920-4923.
- (94) Robbins, L. K.; Lilly, C. P.; Smeltz, J. L.; Boyle, P. D.; Ison, E. A. *Organometallics* **2015**, *34*, 3152-3158.
- (95) Shih, W.-C.; Ozerov, O. V. *Organometallics* **2015**, *34*, 4591-4597.
- (96) Fulmer, G. R.; Miller, A. J. M.; Sherden, N. H.; Gottlieb, H. E.; Nudelman, A.; Stoltz, B. M.; Bercaw, J. E.; Goldberg, K. I. *Organometallics* **2010**, *29*, 2176-2179.
- (97) *p*-Xylene could also be substituted with similar results.
- (98) Dolomanov, O.V.; Bourhis, L.J.; Gildea, R.J.; Howard, J.A.K.; Puschmann, H., *J. Appl. Cryst.* **2009**, *42*, 339-341.
- (99) Sheldrick, G.M., *Acta Cryst.* **2015**, A71, 3-8.
- (100) Sheldrick, G.M., *Acta Cryst.* **2008**, A64, 112-122.
- (101) For an introduction to the special issue on MOFs in *Chemical Reviews*, see: Zhou, H.-C.; Long, J. R.; Yaghi, O. M. *Chem. Rev.* **2012**, *112*, 673-674.
- (102) Furukawa, H.; Cordova, K. E.; O'Keeffe, M.; Yaghi, O. M. *Science* **2013**, *341*, 974-985.
- (103) Davies, D. L.; Macgregor, S. A.; McMullin, C. L. *Chem. Rev.* **2017**, *117*, 8649-8709.

- (104) Gray, A.; Tsybizova, A.; Rithova, J. *Chem. Sci.* **2015**, *6*, 5544-5553.
- (105) Ackermann, L. *Chem. Rev.* **2011**, *111*, 1315-1345.
- (106) Bedford, R. B.; Bowen, J. G.; Davidson, R. B.; Haddow, M. F.; Seymour-Julen, A. E.; Sparkes, H. A.; Webster, R. L. *Angew. Chem. Int. Ed.* **2015**, *54*, 6591-6594.
- (107) Kosanovich, A. J.; Reibenspies, J. H.; Ozerov, O. V. *Organometallics* **2016**, *35*, 513-519.
- (108) Johnson, N. P.; Lock, C. J. L.; Wilkinson, G. *J. Chem. Soc.* **1964**, 1054-1066.
- (109) (PCPiPr)ReO(OAc)₂ (**304a**) was also prepared as a blue, semi-crystalline solid of ca. 90% purity by treatment of **202** with AgOAc, followed by addition of Ac₂O.
- (110) In reaction with excess anhydrous NaOAc, though **303b** was not evident, a spectroscopically characterized intermediate putatively assigned as (PCPtBu)ReO(OAc)(Cl) was observed to slowly convert exclusively to **304b**.
- (111) Reddy, R. K.; Domingos, A.; Paulo, A.; Santos, I. *Inorg. Chem.* **1999**, *38*, 4278-4282.
- (112) (a) *The Chemistry of Pincer Compounds*; Morales-Morales, D.; Jensen, C. M., Eds.; Elsevier: Amsterdam, 2007. (b) *Organometallic Pincer Chemistry*; Van Koten, G.; Milstein, D. Eds.; Springer: Heidelberg, 2013.
- (113) (a) Van der Boom, M. E.; Milstein, D. *Chem. Rev.* **2003**, *103*, 1759-1792. (b) Selander, N.; Szabó, K. J. *Chem. Rev.* **2011**, *111*, 2048-2076. (c) Kumar, A.; Bhatti, T. M.; Goldman, A. S. *Chem. Rev.* **2017**, *117*, 12357-12384.
- (114) Sacco, A.; Vasapollo, G.; Nobile, C. F.; Piergiovanni, A.; Pellinghelli, M.; Lanfranchi, M. *J. Organomet. Chem.* **1988**, *356*, 397-409.

- (115) (a) Ben-Ari, E.; Leitus, G.; Shimon, L. J. W.; Milstein, D. *J. Am. Chem. Soc.* **2006**, *128*, 15390-15391. (b) Zhang, J.; Leitus, G.; Ben-David, Y.; Milstein, D. *Angew. Chem. Int. Ed.* **2006**, *45*, 1113-1115. (c) Xie, Y.; Ben-David, Y.; Shimon, L. J. W.; Milstein, D. *J. Am. Chem. Soc.* **2016**, *138*, 9077-9080. (d) Anaby, A.; Feller, M.; Ben-David, Y.; Leitus, G.; Diskin-Posner, Y.; Shimon, L. J. W.; Milstein, D. *J. Am. Chem. Soc.* **2016**, *138*, 9941-9950.
- (116) Gunanathan, C.; Milstein, D. *Chem. Rev.* **2014**, *114*, 12024-12087.
- (117) Dauth, A.; Gellrich, U.; Diskin-Posner, Y.; Ben-David, Y.; Milstein, D. *J. Am. Chem. Soc.* **2017**, *139*, 2799–2807.
- (118) Poverenov, E.; Milstein, D. *Top. Organomet. Chem.* **2013**, *40*, 21– 48.
- (119) (a) Gozin, M.; Weisman, A.; Ben-David, Y.; Milstein, D. *Nature* **1993**, *364*, 699-701. (c) Kumar, A.; Zhou, T.; Emge, T. J.; Mironov, O.; Saxton, R. J.; Krogh-Jespersen, K.; Goldman, A. S. *J. Am. Chem. Soc.* **2015**, *137*, 9894-9911.
- (120) For an example of dearomatization of Re complexes of PNP, see: Vogt, M.; Nerush, A.; Diskin-Posner, Y.; Ben-David, Y.; Milstein, D. *Chem. Sci.* **2014**, *5*, 2043-2051.
- (121) All complexes reported here are derived from the PCP ligand with $-P^tBu_2$ side donors. For brevity, we refer to these specific ligands in this chapter as “PCP” or “P*CP”
- (122) The asymmetric unit contains two independent molecules of **401**. However, the distances and angles under discussion are not significantly different in the two independent molecules. For the sake of brevity, we only use the values from one of the molecules in the text.

- (123) For examples of Re(V) alkylidenes see: (a) Cai, S.; Hoffman, D. M.; Wierda, D. A.; *J. Chem. Soc. Chem. Commun.* **1988**, 1489-1490. (b) Chen, J.; He, G.; Ho-Yung, S.; Williams, I. D.; Lin, Z.; Jia, G. *Organometallics* **2010**, 29, 2693-2701. (c) Ozerov, O. V.; Watson, L. A.; Pink, M.; Caulton, K. G. *J. Am. Chem. Soc.* **2003**, 125, 9604-9605
- (124) For an example of a Re(VII) alkylidene see: Toreki, R.; Schrock, R. R.; Davis, W. M. *J. Am. Chem. Soc.* **1992**, 114, 3367-3380.
- (125) For examples of Re(V) NHC complexes see: (a) Braband, H.; Zahn, T. I.; Abram, U. *Inorg. Chem.* **2003**, 42, 6160-6162. (b) Kückmann, T. I.; Abram, U. *Inorg. Chem.* **2004**, 43, 7068-7074. (c) Oehlke, E.; Kong, S.; Arciszewski, P.; Wiebalck, S.; Abram, U. *J. Am. Chem. Soc.* **2012**, 134, 9118-9121.
- (126) DFT optimization were performed with the B3LYP functional using the SDD basis set with an effective core potential for the rhenium atom and the 6-311G(d) basis set for all other atoms (B3LYP/BSI).
- (127) (a) Wiberg, K. B. *Tetrahedron* **1968**, 24, 1083. (b) NBO 6.0. Glendening, E. D.; Badenhoop, J. K.; Reed, A. E.; Carpenter, J. E.; Bohmann, J. A.; Morales, C. M.; Landis, C. R.; Weinhold, F. (Theoretical Chemistry Institute, University of Wisconsin, Madison, WI, 2013); <http://nbo6.chem.wisc.edu/>
- (128) (a) AIMAll (Version 17.11.14), Keith, T. A. TK Gristmill Software, Overland Park KS, USA, 2017 (aim.tkgristmill.com). (b) Bader, R. F. W.; Johnson, S.; Tang, T. -H.; Popelier, P. L. A. *J. Phys. Chem.* **1996**, 100, 15398-15415.
- (129) Vogt, M.; Gargir, M.; Iron, M. A.; Diskin-Posner, Y.; Ben-David, Y.; Milstein, D. *Chem.-Eur. J.* **2012**, 18, 9194-9197.

- (130) Huff, C. A.; Kampf, J. W.; Sanford, M. S. *Organometallics* **2012**, *31*, 4643–4645
- (131) Andrae, D.; Häußermann, U.; Dolg, M.; Stoll, H.; Preuß, H. *Theor. Chem. Acc.* **1990**, *77*, 123-141.
- (132) (a) Krishnan, R.; Binkley, J. S.; Seeger, R.; Pople, J. A. *J. Chem. Phys.* **1980**, *72*, 650. (b) McLean, A. D.; Chandler, G. S. *J. Chem. Phys.* **1980**, *72*, 5639.
- (133) Gaussian 16, Revision B.01, Frisch, M. J.; Trucks, G. W.; Schlegel, H. B.; Scuseria, G. E.; Robb, M. A.; Cheeseman, J. R.; Scalmani, G.; Barone, V.; Petersson, G. A.; Nakatsuji, H.; Li, X.; Caricato, M.; Marenich, A. V.; Bloino, J.; Janesko, B. G.; Gomperts, R.; Mennucci, B.; Hratchian, H. P.; Ortiz, J. V.; Izmaylov, A. F.; Sonnenberg, J. L.; Williams-Young, D.; Ding, F.; Lipparini, F.; Egidi, F.; Goings, J.; Peng, B.; Petrone, A.; Henderson, T.; Ranasinghe, D.; Zakrzewski, V. G.; Gao, J.; Rega, N.; Zheng, G.; Liang, W.; Hada, M.; Ehara, M.; Toyota, K.; Fukuda, R.; Hasegawa, J.; Ishida, M.; Nakajima, T.; Honda, Y.; Kitao, O.; Nakai, H.; Vreven, T.; Throssell, K.; Montgomery, J. A., Jr.; Peralta, J. E.; Ogliaro, F.; Bearpark, M. J.; Heyd, J. J.; Brothers, E. N.; Kudin, K. N.; Staroverov, V. N.; Keith, T. A.; Kobayashi, R.; Normand, J.; Raghavachari, K.; Rendell, A. P.; Burant, J. C.; Iyengar, S. S.; Tomasi, J.; Cossi, M.; Millam, J. M.; Klene, M.; Adamo, C.; Cammi, R.; Ochterski, J. W.; Martin, R. L.; Morokuma, K.; Farkas, O.; Foresman, J. B.; Fox, D. J. Gaussian, Inc., Wallingford CT, 2016.
- (134) NBO 6.0. Glendening, E. D.; Badenhoop, J. K.; Reed, A. E.; Carpenter, J. E.; Bohmann, J. A.; Morales, C. M.; Landis, C. R.; Weinhold, F. (Theoretical Chemistry Institute, University of Wisconsin, Madison, WI, 2013); <http://nbo6.chem.wisc.edu/>

- (135) (a) Romao, C. C.; Kuhn, F. E.; Hermann, W. A. *Chem. Rev.* **1997**, *97*, 3197-3246. (b) Toreki, R.; Schrock, R. R. *J. Am. Chem. Soc.* **1990**, *112*, 2448-2449. (c) Klopsch, I.; Finger, M.; Wurtele, C.; Milde, B.; Werz, D. B.; Schneider, S. *J. Am. Chem. Soc.* **2014**, *136*, 6881-6883. (d) Klopsch, I.; Kinauer, M.; Finger, M.; Wurtele, C.; Schneider, S. *Angew. Chem. Int. Ed.* **2016**, *55*, 4786-4789.
- (136) (a) Feng, Y.; Aponte, J.; Houseworth, P. J.; Boyle, P. D.; Ison, E. A. *Inorg. Chem.* **2009**, *48*, 11058-11066. (b) Smeltz, J. L.; Boyle, P. D.; Ison, E. A. *J. Am. Chem. Soc.* **2011**, *133*, 13288-13291. (c) Smeltz, J. L.; Webster, C. E.; Ison, E. A. *Organometallics* **2012**, *31*, 4055-4062. (d) Smeltz, J. L.; Lilly, C. P.; Boyle, P. D.; Ison, E. A. *J. Am. Chem. Soc.* **2013**, *135*, 9433-9441. (e) Robbins, L. K.; Lilly, C. P.; Smeltz, J. L.; Boyle, P. D.; Ison, E. A. *Organometallics* **2015**, *34*, 3152-3158.
- (137) (a) Cochran, F. V.; Bonitatebus Jr., P. J.; Schrock, R. R. *Organometallics* **2000**, *19*, 2414-2416. (b) Mosch-Zanetti, N. C.; Kopke, S.; Herbst-Irmer, R.; Hewitt, M. *Inorg. Chem.* **2002**, *41*, 3513-3520.
- (138) Botha, J. M.; Keisuke, U.; Sasaki, Y. *Inorg. Chem.* **1998**, *37*, 1609-1615.
- (139) Lindner, R.; van den Bosch, B.; Lutz, M.; Reek, J. N. H.; van der Vlugt, J. I. *Organometallics* **2011**, *30*, 499-510.
- (140) Wanniarachchi, S.; Liddle, B. J.; Toussaint, J.; Lindeman, S. V.; Bennett, B.; Gardinier, J. *R. Dalton Trans.* **2010**, *39*, 3167-3169.
- (141) Rossi, R.; Marchi, A.; Magon, L.; Casellato, U.; Tamburini, S.; Graziani, R. *J. Chem. Soc. Dalton Trans.* **1991**, 263-268.

- (142) To illustrate this inequivalence, one phosphorus is attached to the ring that is raised towards the oxo, while the other phosphorus is attached to the ring that is pivoted away from the oxo.
- (143) The 80 °C spectrum could also arise from isomerization to a C₂-symmetric isomer (oxo trans to Namido) with slow “flipping”, but that seems less likely. However, isomers with oxo *trans* and *cis* to the Namido for (PNP)ReOCl₂ have been observed in the work of Caulton et al. with Fryzuk’s disilylamido-based PNP ligands.
- (144) Herbert, D. E.; Ozerov, O. V. *Organometallics* **2011**, 30, 6641-6654.
- (145) DeMott, J. C.; Guo, C.; Foxman, B. M.; Yandulov, D. V.; Ozerov, O. V. *Mendeleev Commun.* **2007**, 17, 63-65.
- (146) Representing a racemic mixture of a pair of enantiomers.
- (147) Ozerov, O.V.; Watson, L. A.; Pink, M.; Caulton, K. G. *J. Am. Chem. Soc.* **2004**, 126, 6363-6378.
- (148) (a) Nolin, K. A.; Krumper, J. R.; Pluth, M. D.; Bergman, R. G.; Toste, D. F. *J. Am. Chem. Soc.* **2007**, 129, 14684-14696. (b) Du, G.; Fanwick, P. E.; Abu-Omar, M. M. *J. Am. Chem. Soc.* **2007**, 129, 5180-5187.
- (149) Addison, A. W.; Rao, T. N.; Reedijk, J.; van Rijn, J.; Verschoor, G. C. *J. Chem. Soc., Dalton Trans.* **1984**, 1349-1356.
- (150) Riehl, J. -F.; Jean, Y.; Eisenstein, O.; Pellissier, M. *Organometallics* **1992**, 11, 729-737.
- (151) Sueki, S.; Guo, Y.; Kanai, M.; Kuninobu, Y. *Angew. Chem. Int. Ed.* **2013**, 52, 11879-11883.

- (152) Sung, S.; Kumar, D.; Gil-Sepulcre, M.; Nippe, M. *J. Am. Chem. Soc.* **2017**, 139, 13993-13996.
- (153) Schneider, T.W.; Ertem, M. Z.; Muckerman, J. T.; Angeles-Boza, A. M. *ACS Catal.* **2016**, 6, 5473-5481.
- (154) Bernskoetter, W. H.; Schauer, C. K.; Goldberg, K. I.; Brookhart, M. *Science* **2009**, 306, 553-556.
- (155) Lambic, N. S.; Lilly, C. P.; Robbins, L. K.; Sommer, R. D.; Ison, E. A. *Organometallics* **2016**, 35, 2822-2829.
- (156) (a) Tondreau, A. M.; Boncella, J. M. *Organometallics* **2016**, 35, 2049-2052. (b) Tondreau, A. M.; Michalczyk, R.; Boncella, J. M. *Organometallics* **2017**, 36, 4179-4183. (c) Nguyen, D. H.; Trivelli, X.; Capet, F.; Paul, J. -F.; Dumeignil, F.; Gauvin, R. M. *ACS Catal.* **2017**, 7, 2022-2032. (d) Elangovan, S.; Neumann, J.; Sortais, J. -B.; Junge, K.; Darcel, C.; Beller, M. *Nature Commun.* **2016**, 7, 1-8. (e) Mukherjee, A.; Nerush, A.; Leitus, G.; Shimon, L. J. W.; Ben-David, Y.; Jalapa, N. A. E.; Milstein, D. *J. Am. Chem. Soc.* **2016**, 138, 4298-4301.
- (157) Li, H.; Wei, D.; Bruneau-Voisine, A.; Ducamp, M.; Henrion, M.; Roisnel, T.; Dorcet, V.; Darcel, C.; Carpentier, J. -F.; Soulé, J. -F.; Sortais, J. -B. *Organometallics* **2018**, 37, 1271-1279.
- (158) Zhu, Y.; Smith, D. A.; Herbert, D. E.; Gatard, S.; Ozerov, O. V. *Chem. Commun.* **2012**, 478, 218-220.
- (159) (a) Adhikary, A.; Guan, H. *ACS Catalysis* **2015**, 5, 6858-6873. (b) Poverenov, E.; Milstein, D. *Top. Organomet. Chem.* **2013**, 40, 21-48.

- (160) Shih, W. -C.; Ozerov, O. V. *J. Am. Chem. Soc.* **2017**, 139, 17297-17300.
- (161) (a) Burford, R. J.; Piers, W. E.; Ess, D. H.; Parvez, M. J. *J. Am. Chem. Soc.* **2014**, 136, 3256-3263. (b) Cui, P.; Iluc, V. M. *Chem. Sci.* **2015**, 6, 7343-7354.
- (162) (a) Korshin, E. E.; Leitus, G.; Shimon, L. J. W.; Konstantinovski, L.; Milstein, D. *Inorg. Chem.* **2008**, 47, 7177-7189. (b) MacInnis, M. C.; MacLean, D. F.; Lundgren, R. J.; McDonald, R.; Turculet, L. *Organometallics* **2007**, 26, 6522-6525. (c) Mitton, S. J.; McDonald, R.; Turculet, L. *Organometallics* **2009**, 28, 5122-5136. (d) Takaya, J.; Iwasawa, N. *J. Am. Chem. Soc.* **2008**, 130, 15254-15255. (e) Whited, M. T.; Deetz, A. M.; Boerma, J. W.; DeRosha, D. E.; Janzen, D. E. *Organometallics* **2014**, 33, 5070-5073.
- (163) (a) Kameo, H.; Ishii, S.; Nakazawa, H. *Dalton Trans.* **2012**, 41, 11386-11392. (b) Takaya, J.; Miyama, K.; Zhu, C.; Iwasawa, N. *Chem. Commun.* **2017**, 53, 3982-3985.
- (164) (a) Mankad, N. P.; Rivard, E.; Harkins, S. B.; Peters, J. C. *J. Am. Chem. Soc.* **2005**, 127, 16032-16033. (b) Amgoune, A.; Bourissou, D. *Chem. Commun.* **2011**, 47, 859-871.
- (165) (a) You, D.; Gabbaï, F. P. *J. Am. Chem. Soc.* **2017**, 139, 6843-6846. (b) Sahu, S.; Gabbaï, F. P. *J. Am. Chem. Soc.* **2017**, 139, 5035-5038.
- (166) Haibach, M. C.; Wang, D. Y.; Emge, T. J.; Krogh-Jespersen, K.; Goldman, A. S. *Chem. Sci.* **2013**, 4, 3683-3692.
- (167) Suess, D. L. M.; Peters, J. C. *Organometallics* **2012**, 31, 5213-5222.
- (168) Lee, C. -I.; Zhou, P. J.; Ozerov, O. V. *J. Am. Chem. Soc.* **2013**, 135, 3560-3566.
- (169) Charette, B. J.; Ritch, J. S. *Inorg. Chem.* **2016**, 55, 6344-6350.
- (170) Harkins, S. B.; Peters, J. C. *J. Am. Chem. Soc.* **2004**, 126, 2885-2893.

- (171) Locke, H.; Herrera, A.; Heinemann, F. W.; Linden, A.; Frieß, S.; Schmid, B.; Dorta, R. *Organometallics* **2015**, 34, 1925–193.
- (172) Levason, W.; Reid, G. *Coord. Chem. Rev.* **2006**, 250, 2565–2594.
- (173) Benjamin, S. L.; Reid, G. *Coord. Chem. Rev.* **2015**, 297, 168–180.
- (174) Landers, B. A. PhD thesis, University of Hawaii, 2015.
<https://scholarspace.manoa.hawaii.edu/handle/10125/51210> Accessed May 29, 2018.
- (175) Jones, J. S.; Wade, C. R.; Gabbai, F. P. *Organometallics* **2015**, 34, 2647–2654.
- (176) Jones, J. S.; Gabbai, F. P. *Acc. Chem. Res.* **2016**, 49, 857–867.
- (177) Lee, C. -I.; DeMott, J. C.; Pell, C. J.; Christopher, A.; Zhou, J.; Bhuvanesh, N.; Ozerov, O. V. *Chem. Sci.* **2015**, 6, 6572–6582.
- (178) Lamprecht, G. J.; Van Biljon, C. P.; Leipoldt, J. G. *Inorganica Chimica Acta* **1986**, 119, L1–L4.
- (179) Benjamin, S. L.; Levason, W.; Light, M. E.; Reid, G.; Rogers, S. M. *Organometallics* **2014**, 33, 2693–2695.
- (180) Lo, Y. H.; Gabbai, F. P. *Organometallics* **2018**, 37, 2500–2506.
- (181) Chen, C. H.; Gabbai, F. P. *Angew. Chem. Int. Ed.* **2017**, 56, 1799–1804.
- (182) Yang, M.; Tofan, D.; Chen, C. H.; Jack, K. M.; Gabbai, F. P. *Angew. Chem. Int. Ed.* **2018**, 57, 13868–13872.
- (183) You, D.; Yang, H.; Sen, S.; Gabbai, F. P. *J. Am. Chem. Soc.* **2018**, 140, 9644–9651.
- (184) Hirai, M.; Gabbai, F. P. *Angew. Chem. Int. Ed.* **2015**, 54, 1205–1209.
- (185) Kosanovich, A. J.; Jordan, A. M.; Bhuvanesh, N.; Ozerov, O. V. *Dalton Trans.* **2018**, 47, 11619–11624.

- (186) (a) Cherkasov, V. K.; Abakumov, G. A.; Grunova, E. V.; Poddel'sky, A. I.; Fukin, G. K.; Baranov, E. V.; Kurskii, Y. V.; Abakumova, L. G. *Chem. Eur. J.* **2006**, 12, 3916-3927.
- (b) Poddel'sky, A. I.; Smolyaninov, I. V.; Somov, N. V.; Berberova, N. T.; Cherkasov, V. K.; Abakumov, G. A. *J. Organomet. Chem.* **2010**, 695, 530-536.
- (187) Phillips, D. C.; Ahmed, F. R.; Barnes, W. H. *Acta. Cryst.* **1960**, 13, 365-377.
- (188) Ashe III, A. J.; *J. Am. Chem. Soc.* **1971**, 93, 6690-6691.
- (189) Plasseraud, L.; Catty, H. *C. R. Chimie* **2013**, 16, 613-620.
- (190) Ukai, T.; Kawazura, H.; Ishii, T. *J. Organomet. Chem.* **1974**, 65, 253.
- (191) Fulmer, G. R.; Miller, A. J. M.; Sherden, N. H., Gottlieb, H. E.; Nudelman, A.; Stoltz, B. M.; Bercaw, J. E., Goldberg, K. I. *Organometallics* **2010**, 29(9), 2176-2179.

APPENDIX A

LIST OF PUBLICATIONS RESULTING FROM PHD WORK

- (1) Kosanovich, A. J.; Reibenspies, J. H.; Ozerov, O. V. "Complexes of High-Valent Rhenium Supported by the PCP Pincer" *Organometallics* **2016**, 35, 513-519.
- (2) Press, L. P.; Kosanovich, A. J.; McCulloch, B. J.; Ozerov, O. V. "High Turnover Aromatic C-H Borylation Catalyzed by POCOP-type Pincer Complexes of Iridium" *J. Am. Chem. Soc.* **2016**, 138, 9487-9497.
- (3) Kosanovich, A. J.; Shih, W. -C.; Ramirez-Contreras, R.; Ozerov, O. V. "N-H Cleavage as a Route to New Pincer Complexes of High-Valent Rhenium" *Dalton Trans.* **2016**, 45, 18532-18540.
- (4) Kosanovich, A. J.; Press, L. P.; Ozerov, O. V. "Boryl Transfer Reactivity of a POCOP-Supported Ir-diboryl: Reduction of CO₂ to CO and Borylation of Other Small Molecules" *J. Organomet. Chem.* **2017**, 845, 19-24.
- (5) Zabula, A. V.; Qiao, Y.; Kosanovich, A. J.; Manor, B. C.; Carroll, P. J.; Ozerov, O. V.; Schelter, E. J. "Structure, Electronics and Reactivity of Ce(PNP) Complexes" *Chem. Eur. J.* **2017**, 23, 17923-17934.
- (6) Kosanovich, A. J.; Shih, W. -C.; Ozerov, O. V. "The Irreversible Hydrolysis of PCP-Supported Rhenium(V)-Acetates" *Inorg. Chem.* **2018**, 57, 545-547.
- (7) Kosanovich, A. J.; Komatsu, C. H.; Bhuvanesh, N.; Perez, L. M.; Ozerov, O. V. "Dearomatization of the PCP Pincer Ligand in a Re(V) Oxo Complex" *Chem. Eur. J.* **2018**, 24, 13754-13757.

- (8) Kosanovich, A. J.; Jordan, A. M.; Bhuvanesh, N.; Ozerov, O. V. "Synthesis and Characterization of a Diarylamido Based PNSb Pincer Ligand and its Complexes of Rhodium, Iridium, and Palladium" *Dalton Trans* **2018**, 47, 11619-11624.